73-Deoxychondropsin A
A Novel Inhibitor of Bone Resorption Sourced From a Great Barrier Reef Sponge

Dickson, Iain Gordon

Awarding institution:
King's College London

73-Deoxychondropsin A: A Novel Inhibitor of Bone Resorption Sourced From a Great Barrier Reef Sponge

Iain Gordon Dickson

A thesis submitted for the degree of Doctor of Philosophy at the University of London

2015

Declaration

No part of the work referred to in this thesis has been submitted in support of an application for other degrees or qualifications at this or any other university. All sources of information have been acknowledged.

Acknowledgements

I am greatly indebted to a number of people, first and foremost of which are my parents and girlfriend, who have provided invaluable support throughout my studies. I am extremely grateful for all the help, training and advice that was provided by my supervisors, Dr Paul Long and Professor Agi Grigoriadis. I also owe thanks to the BBSRC for funding my research. Additionally, I am also thankful for help given to me by Ranko Gacesa, Professor Tim Arnett, Dr. Sukhi Bansal, Dr. Anna Caldwell and Dr. Walt Dunlap.

Abstract

73-deoxychondropsin A (73-DOC), a natural product of the polyketide family sourced from the marine sponge *Ircinia ramosa*, has previously shown inhibition of vacuolar-type H^+-ATPases. This enzyme is crucial for osteoclastic bone resorption and is important in the pathogenesis of metabolic bone diseases, which affect both osteoclasts and the bone-forming osteoblasts. Following extraction of 73-DOC from *I. ramosa* tissues, *in vitro* experiments were performed to establish the differential effects of 73-DOC on primary osteoclast and osteoblast differentiation and function. Dose-response and time course analyses, as well as confocal microscopy assessments of cellular acidification, showed that 73-DOC inhibited mouse and human osteoclast resorption at concentrations 5-10-fold lower than those causing inhibition of osteoblast activity. The inhibition of bone resorption whilst maintaining bone formation demonstrates a novel application for 73-DOC and potential as a therapeutic for osteolytic diseases such as osteoporosis.

Symbiotic microorganisms have frequently been proposed as the true producers of sponge-sourced secondary metabolites. Whilst symbionts are typically resistant to culturing, metagenomic approaches allow for microbial biosynthetic genes from the sponge holobiome to be cloned and ultimately expressed in a heterologous host, leading to a sustainable supply of the compound. To clone and sequence the biosynthetic gene cluster responsible for 73-DOC, a metagenomic fosmid library was screened for conserved features of polyketide synthase biosynthesis. Metagenomic DNA was also directly sequenced and screened using *in silico* analysis tools, which led to the annotation of genes with putative partial involvement in 73-DOC biosynthesis. Further work required to identify the remaining biosynthetic components was suggested.

Table of contents

List of figures

List of tables

List of abbreviations

The following are abbreviations used in this thesis that are not found in the standard abbreviations and acronyms list from the Journal of Medicinal Chemistry (Guidelines for authors, 2015):

73-DOC	73-deoxychondropsin A
ACP	Acyl carrier protein
ADO	Autosomal dominant osteopetrosis
ALP	Alkaline phosphatase
ARNO	ADP-ribosylation factor nucleotide site opener
ARO	Autosomal recessive osteopetrosis
AT	Acyltransferase
BLAST	Basic local alignment search tool
BMM	Bone marrow macrophage
BMU	Basic multicellular unit
BSP	Bone sialoprotein
CAII	Carbonic anhydrase II
cAMP	Cyclic adenosine monophosphate
CFU-M	Macrophage colony-forming units
ClC-7	Chloride channel 7
Col1a	Collagen 1a
CTHRC1	Collagen triple helix repeat containing 1
CTR	Calcitonin receptor
DC-STAMP	Dendritic cell-specific transmembrane protein
DEBS	6-Deoxyerythronolide B synthase

DH	3-Hydroxyacyl-ACP dehydratase
Dlx5	Distal-less homeobox 5
ECM	Extracellular matrix
EMBOSS	European molecular biology open software suite
ER	Enoyl-ACP reductase
ERK	Extracellular signal-related kinase
FACS	Fluorescent-activated cell sorting
FBS	Fetal bovine serum
F-ATPase	F-Type adenosine triphosphatase
GEF	GDP/GTP exchange factor
GTPase	Guanosine triphosphatase
HSC	Hematopoeitic stem cell
IARO	Intermediate autosomal recessive osteopetrosis
IGF	Insulin-like growth factor
IKK	IκB kinase
IL	Interleukin
IMO	Infantile malignant osteopetrosis
JNK	c-Jun N-terminal kinases
KR	β-keto reductase
KS	β-ketoacyl-ACP synthase
LB	Lysogeny broth
LC3	Microtubule-associated protein light chain 3
M-CSF	Macrophage colony stimulating factor
MEF2	Myocyte enhancer factor-2
MITF	Micropthalmia-associated transcription factor
MMP	Matrix metalloproteinase

MNC	Multinucleated cell
MSC	Mesenchymal stem cell
Msx2	Muscle segment homeobox homologue-2
mTOR	Mammalian target of rapamycin
mTORC1	Mammalian target of rapamycin complex 1
MTS	(3-(4,5-dimethylthiazol-2-yl)-5-(3-carboxymethoxyphenyl)-2-(4-sulfophenyl)-2H-tetrazolium)
mWGS	Metagenomic whole genome shotgun sequencing
Na^+/K^+ ATPase	Sodium-potassium adenosine triphosphatase
NCI	National cancer institute
NFATc1	Nuclear factor of activated T cells, calcineurin dependent 1
NF-κB	Nuclear factor κ-light-chain-enhancer of activated B cells
NGS	Next generation sequencing
NRPS	Nonribosomal peptide synthetase
OPG	Osteoprotegerin
Osx	Osterix
OUT	Operational taxonomic unit
PBMC	Peripheral blood mononuclear cell
PI3K	Phosphatidylinositol 3-kinase
PKS	Polyketide synthase
PLEKHM1	Pleckstrin homology domain containing, family member 1
Ppant	Phosphopantetheine
PTH	Parathyroid hormone
PTHrP	Parathyroid hormone-related protein
RANK	Receptor activator of nuclear factor κB
RANKL	Receptor activator of nuclear factor κB ligand

ROV	Remote operated vehicle
Runx2	Runt-related transcription factor 2
rRNA	Ribosomal ribonucleic acid
sAC	Soluble adenylyl cyclase
SCUBA	Self-contained underwater breathing apparatus
SERMS	Selective estrogen receptor modulators
SNARE	Soluble N-ethylmaleimide-sensitive factor attachment protein receptor
SPE	Solid phase extraction
SQSTM1	Sequestosome 1
TNFR	Tumor necrosis factor receptor
TRAF	TNFR-associated cytoplasmic factors
TFEB	Transcription factor EB
TRAP	Tartrate-resistant acid phosphatase
TE	Thioesterase
V-ATPase	Vacuolar-type H^+-ATPases

Chapter 1: Introduction

1.1 Marine natural products

The marine environment represents a rich source of novel bioactive compounds, with more than 20,000 discovered since the 1960s and 1,241 discovered in 2012 alone (Blunt et al., 2014, Martins et al., 2014). These compounds are known as natural products and are typically produced by living organisms as secondary metabolites with no direct involvement in primary metabolic pathways such as growth, development or reproduction (Dewick, 2002). Instead, secondary metabolites have a broad range of functions including pheromones, signalling molecules, transport chaperones as well as in the chemical defence of an organism (Demain and Fang, 2000). With this latter role in particular, many secondary metabolites have potent antibacterial, antiviral or cytotoxic activities that offer exciting potential in developing pharmaceutical leads for treating human disease. Over a 30 year period between 1981 and 2010, 1355 new active substances were approved for therapeutic use and 55 % of these are considered natural products, or derived from natural products (Newman and Cragg, 2012). Additionally, 60-70 % of current anticancer and anti-infective drugs in current clinical use are also believed to be derived from natural products (Cragg and Newman, 2013). The need for new drugs certainly exists due to the occurrence of various cancers and neurodegenerative diseases that cannot be effectively treated, as well as the growing problem of antibiotic resistance in many bacterial pathogens (Hill and Fenical, 2010).

Marine natural products are typically discovered from marine invertebrates including sponges, coelenterates, echinoderms, tunicates, molluscs and bryozoans, but microorganisms plus macro- and microalgae are also major sources (Blunt et al., 2004, Bhatnagar and Kim, 2010). The majority of these invertebrates are sessile or slow-

moving, and when faced with a predator or competitor, the release of stored cytotoxic secondary metabolites are thought to be relied upon to act as toxins or feeding deterrents (Proksch, 1994, Pawlik et al., 2002, Haefner, 2003). However, most marine invertebrates harbour microorganisms within host tissues that include bacteria, cyanobacteria, fungi and algae, and many of the natural products discovered from marine invertebrates show structural homology with known metabolites of a microbial origin. This has led to speculation that the true producers of many marine invertebrate-associated natural products are actually microbes living in symbiosis with the host animal (Kobayashi and Ishibashi, 1993, Hildebrand et al., 2004, Dunlap et al., 2006, Piel, 2006, Simmons et al., 2008, Leal et al., 2012). As an example, the natural product trabectadin **(1)**, sourced from the marine tunicate *Ecteinascidia turbinata*, shows structural similarity with cyanosafracin B **(2)**, produced by the bacterium *Pseudomonas fluorescens* (Figure 1.1).

Marine natural product research was stimulated in the 1950s following the discovery of the nucleosides, spongothymidine **(3)** and spongouridine **(4)**, from the marine sponge *Tethya crypta* (Bergmann and Burke, 1955). These discoveries resulted in development of cytarabine **(5)** and vidarabine **(6)**, which were subsequently approved for human use as anticancer and antiviral compounds respectively. Following the advancement of diving techniques including SCUBA (1970s), manned submersibles (1980s) and remote operated vehicles (1990s), exploration of the marine environment significantly expanded, leading to the rapid discovery of novel marine natural products and necessitating annual reviews started by Faulkner (1986). Currently, there are 7 marine derived natural products approved for use in humans, with an additional 25 compounds in various stages of clinical trials (Table 1.1) (Mayer, 2014). The structures of some of the compounds listed in Table 1.1 as well as other important marine natural products referenced in this section are shown in Figure 1.2.

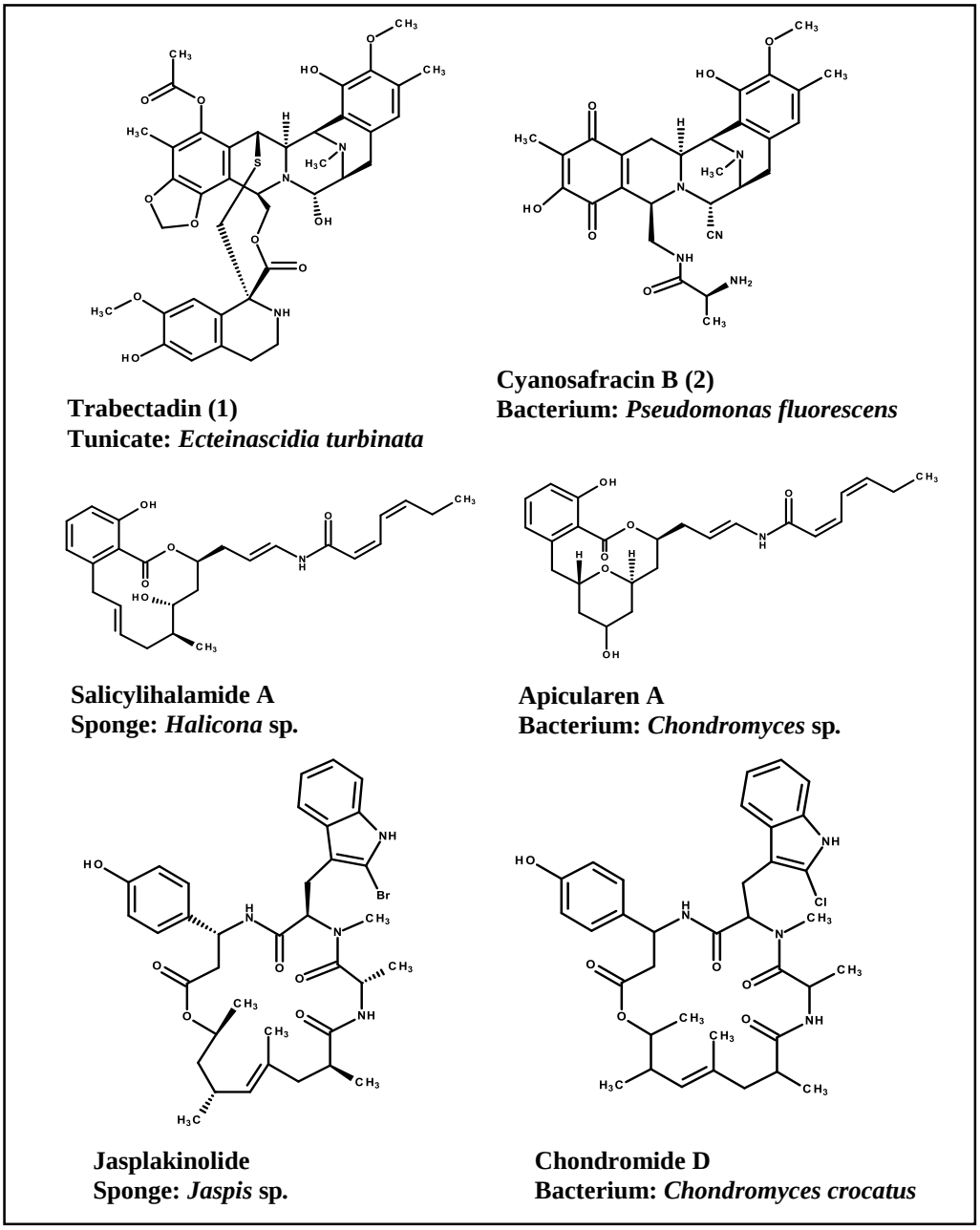

Figure 1.1 Examples of structural similarity between marine invertebrate-derived natural products and those sourced from prokaryotes. Natural products sourced from marine invertebrates are shown on the left with their prokaryote analogues shown on the right. Compounds with numbers in brackets are referred to in the text. Adapted from Piel (2006).

Interest in the biochemistry of the marine environment stems from the enormous biodiversity present in the oceans and the fact that much of it is largely unexplored (Costello et al., 2010, Appeltans et al., 2012). There is also the suggestion that the marine environment is a superior source of natural products than the terrestrial environment, demonstrated by the discovery of totally novel chemical classes (Cragg and Newman,

Compound	Compound derivative trademark	Marine organism	Molecular target	Function	Status
Trabectadin **(1)** (ET-743)	Yondelis	Tunicate	Minor Groove of DNA	Anticancer	EU Approved
Cytarabine **(5)**	Cytosar-U	Sponge	DNA Polymerase	Anticancer	FDA Approved
Vidarabine **(6)**	Vira-A	Sponge	Nucleoside	Antiviral	FDA Approved
Ziconotide **(8)**	Prialt	Cone Snail	N-Type Calcium Channel	Severe Pain	FDA Approved
Eribulin Mesylate **(9)**	Halaven	Sponge	Microtubules	Anticancer	FDA Approved
Omega-3-acid ethyl esters	Lovaza	Fish	Trigliceride synthesizing enzymes	Hypertri-glyceridemia	FDA Approved
Brentuximab vedotin	Adcetris	Mollusc/ Cyanobacteria	Microtubules	Anticancer	FDA Approved

Table 1.1 Marine natural products approved for human use (Mayer 2015).

2013), as well as a greater incidence of significant bioactivity amongst compounds from marine organisms (Munro et al., 1999). As marine organisms often have to cope with extreme environmental conditions such as high salt, low nutrients, low oxygen, as well as high pressures and limited sunlight in deep sea environments, adaptations for such conditions ultimately lead to differences between the biochemistry of terrestrial and marine organisms (Montaser and Luesch, 2011, Trincone, 2011). Due to the diluting effects of the aqueous environment within which marine natural products are released, marine compounds are also often found to be far more potent than similar compounds from the terrestrial environment (Hughes and Fenical, 2010). For example, the marine

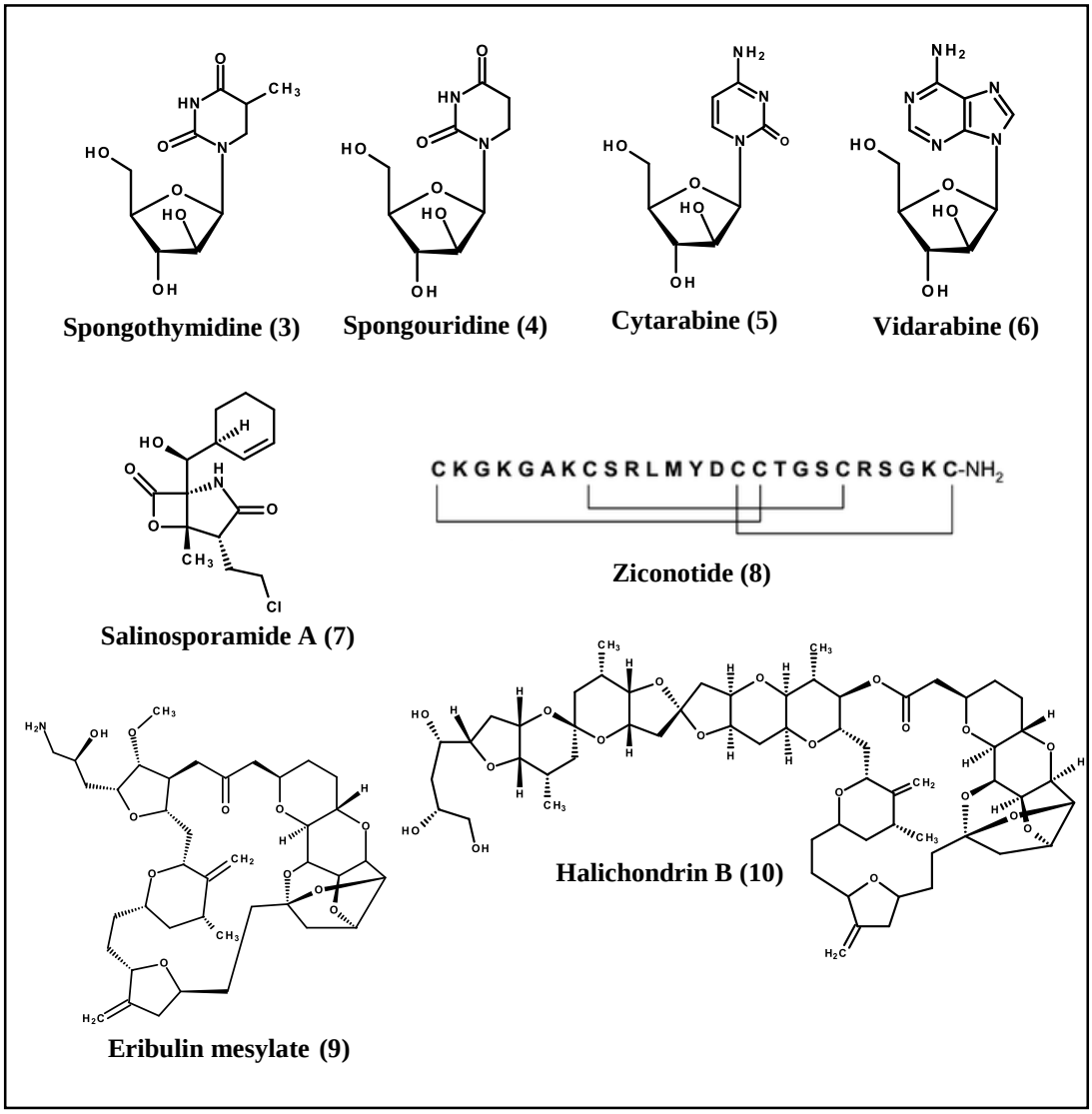

Figure 1.2 Examples of marine natural products. Chemical structures for marine natural product are shown with numbers in brackets used to refer to the compounds in the text. Ziconotide is a peptide and so the amino acid sequence has been provided in place of chemical structure.

actinomycete-derived salinosporamide A **(7)** is one of the most potent known proteasome inhibitors (Fenical et al., 2009), and ziconotide **(8)**, a synthetic derivative of a toxin produced by marine cone snails to treat severe and chronic pain in humans, is known to be 1000-fold more potent than that of morphine (Olivera, 2000).

The case of ziconotide **(8)** highlights another benefit of studying natural products, the fact that many possess completely novel mechanisms of action. The analgesic effect of ziconotide is mediated via the reversible blocking of N-type calcium channels which does not result in the development of addiction or tolerance, as

experienced by patients using opioids (Terlau and Olivera, 2004). This discovery subsequently validated N-type calcium channels as drugable targets and stimulated research into other drugs for this target (McGivern, 2006, Clark et al., 2012). A further example can be found with another marine natural product success story, the anticancer drug trabectadin **(1)**. This compound, isolated from the colonial tunicate *Ecteinascidia turbinata*, and subsequently approved for the treatment of human sarcomas by the European Commission in 2007, induces apoptosis in cancer cells by binding with the minor groove of the DNA double helix (D'Incalci and Galmarini, 2010).

Accelerated research into marine natural products by the pharmaceutical industry is currently underway due to the success of the compounds mentioned above, the demonstrated broad range of bioactivities and the large volume of novel compounds discovered on an annual basis (Hu et al., 2011, Martins et al., 2014). In the marine environment, there is one group of animals that has been responsible for the discovery of more natural products than any other source, and that is the sponges (Lane and Moore, 2011). Contributing to 3 out of the 7 human approved marine natural compounds, sponges have enormous potential in the field of drug discovery, earning a reputation as the "drugstore of the sea" (Blunt et al., 2009, Mehbub et al., 2014).

1.2 Marine sponges and their natural product potential

Sponges (phylum: Porifera) are sessile filter-feeding organisms and the most ancient of extant metazoan animals, with fossil records estimating their appearance almost 630 million years ago (Maloof et al., 2010). Through the act of pumping and filtering large quantities of water, sponges actively remove microscopic particles such as bacteria, microalgae, viruses and organic/inorganic detritus from the surrounding environment. Once captured, the majority of these particles are phagocytosed as food

items, but a large number of microorganisms are known to remain in the sponge tissue existing as sponge-specific symbionts, including members of the Bacteria, Archaea as well as the Eukarya (Wilkinson et al., 1984, Taylor et al., 2007b). In some species, known as high-microbial-abundance sponges, microbial symbionts can account for as much 40 % of the total sponge volume, with bacterial population densities of 10^8-10^{10} bacteria per gram of sponge wet weight (Vacelet and Donadey, 1977, Hentschel et al., 2006). However, the environmental, metabolic and biosynthetic relationships that exist between the host and the complex symbiont assemblages are currently poorly understood.

A total of 4851 novel compounds have been discovered from sponges, represented by a diverse range of chemical classes including terpenoids, alkaloids, peptides and polyketides (Taylor et al., 2007b, Mehbub et al., 2014). A large proportion have demonstrated antimicrobial, antifungal and cytotoxic activities that suggest defensive functions for these compounds (Blunt et al., 2005, Mehbub et al., 2014), also confirmed in some cases by ecological studies (Paul et al., 2011). The presence of bioactive natural products in sponges is therefore considered to be an adaptation that has been shaped by millions of years of evolution, contributing to the ecological success of these animals (Proksch et al., 2003a).

The occurrence of invertebrate-derived natural products with structural similarities to known bacterial metabolites has led to speculation of a microbial origin. In the sponges, this is particularly evident in the pederin **(11)**/mycalamide **(12)** family, where the structure of mycalamide A **(12)**, discovered from the sponge *Mycale hentscheli* (Perry et al., 1988), is almost identical to pederin **(11)**, a toxin isolated from a bacterial symbiont of the beetle species *Paederus fuscipes* (Kellner and Dettner, 1996) (Figure 1.3). The structures of other sponge-sourced natural products such as psymberrin **(13)**, theopederin A **(14)** and onnamide A **(15)** also share structural similarities with

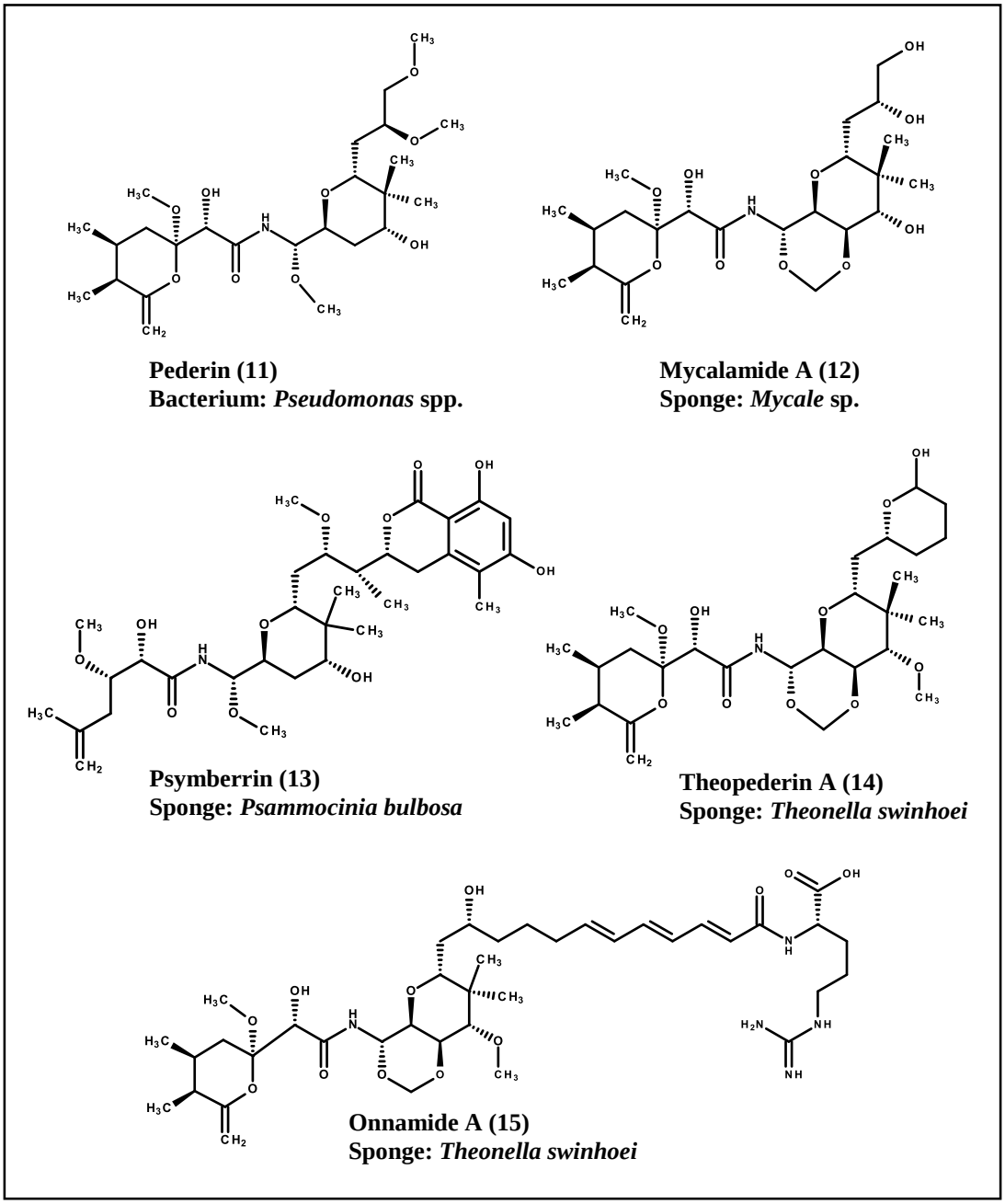

Figure 1.3 Structures of the pederin/mycalamide family. The chemical structures and source of each member of the pederin/mycalamide family are shown. Numbers in brackets are used to refer to the compounds in the text.

pederin (Figure 1.3). Structural homology in compounds from unrelated organisms such as a sponge and beetle, suggests the compounds are produced by commensal organisms with a common ancestry, implicating the involvement of bacterial symbionts in producing some of the sponge-associated natural products (Newman and Hill, 2006, Piel, 2006).

The first genetic evidence for the bacterial origin of a sponge-derived natural product came from the work of Piel et al. (2004), where metagenomic approaches (see Section 1.3.1) were used to clone the biosynthetic gene cluster involved in the production of onnamide A**(15)**/theopederin A **(14)** from the sponge *Theonella swinhoei*, showing that the gene sequences contained features indicative of a prokaryotic origin. Further recent work by Piel and colleagues, using single-cell genomic analyses, provided conclusive proof for the exact biogenic origin of onnamide A **(15)** and theopederin A **(14)**, in addition to other structurally similar compounds found from the sponge *T. swinhoei*. Biosynthetic genes for these compounds were all encoded by the genomes of one bacterial phylotype, the candidate genus *Entotheonella*, which was proposed as belonging to a novel candidate phylum named the Tectomicrobia (Wilson et al., 2014). A total of 28 biosynthetic gene clusters were found from the 9 Mb genomes of two representatives of *Entotheonella* spp., including 14 that encoded unknown products. These discoveries show that the Tectomicrobia represent a new biosynthetically rich phylum and, given that the authors also detected *Entotheonella* in 28 sponge species from geographically distant regions, these results will likely have significant implications for future drug discovery in sponges.

The sponge-derived compounds mentioned above have all demonstrated significant *in vitro* antitumour activity and additionally, are all classed as hybrid polyketide/nonribosomal peptides (Burres and Clement, 1989, Fusetani et al., 1992, Kobayashi et al., 1993, Cichewicz et al., 2004). Polyketides, nonribosomal peptides, and hybrids of the two, are a diverse class of secondary metabolites, and include many of the pharmacologically most promising natural products discovered from sponges (Hochmuth and Piel, 2009a). These compounds, described further in Section 1.4, are almost exclusively produced by bacteria, fungi and algae, supporting a role for microbial symbionts as the biogenic origin of some sponge-associated natural products. The

implication of a microbial origin for a particular compound is of great interest to drug discovery due to the potential offered in overcoming the principle impedance to natural product research, that of generating a sustainable supply.

1.3 The supply problem and solutions

Natural products show great potential for discovering and inspiring novel drug leads, but the issue of ensuring continuous large-scale production for a global market presents significant obstacles in the development of many exciting compounds. The requirements of a compound to progress to the advanced stages of preclinical candidates include determining mechanism and site of action, development of structure-activity relationships, evaluation of *in vivo* performance in animal models for toxicity and efficacy, as well as characterisation of pharmacokinetic parameters and pharmaceutical properties (Gerwick and Moore, 2012). An abundant supply of the test compound is therefore crucial for the advancement of a therapeutic candidate, but due to the fact that most marine natural products are found at low concentrations, or are from organisms whose abundance in the environment is site-specific or patchy, harvesting stocks of a compound from natural sources is often considered unsound or insufficient for producing the yields required (Proksch et al., 2003b, Dunlap et al., 2006).

Examples of this problem can be seen with the promising anticancer agent, trabectadin **(1)**, and the powerful cytostatic compound halichondrin B **(10)**. In order to obtain approximately 1 g of trabectadin **(1)**, close to 1 metric tonne of the tunicate *E. turbinata* had to be collected and extracted (Proksch et al., 2002), whilst 1 metric tonne of the sponge *Lissodendoryx* sp., a source of halichondrin B **(10)**, only yielded 300 mg of the compound (Jackson et al., 2009). If, for example, halichondrin B (**10)** was successfully launched as a drug for the treatment of cancer, it is estimated that the annual

requirement of halichondrin B **(10)** would be between 1-5 kg, corresponding to 3,000-16,000 metric tonnes of sponge material per year (Proksch et al., 2003b). Harvesting such quantities from the wild for a global market is ethically unsound and is therefore typically limited to preclinical investigations only (Munro et al., 1999).

In the case of halichondrin B **(10)**, the testing of hundreds of structurally simpler analogues eventually led to the discovery of eribulin mesylate (E7389) **(9),** and almost 25 years after the discovery of halichondrin B **(10)**, this synthetic analogue was finally approved by the FDA in 2010 for treating metastatic breast cancer in humans (Towle et al., 2001, Seletsky et al., 2004, Cortes et al., 2011, Huyck et al., 2011). For other natural products, such as trabectadin **(1)**, chemical synthesis is found to be an economically unviable option (Corey et al., 1996). This exemplifies the need for alternative biosynthetic strategies such as that demonstrated by Cuevas et al. (2000), where large-scale fermentation of *P. fluorescens* is used to produce cyanosafracin B **(2)**, which is used as starting material for the semi synthesis of the trabectadin **(1)**.

The possibility of a microbial origin for many marine invertebrate-derived natural products presents significant opportunities for solving the supply problem through the cloning of biosynthetic genes and expression in fermentable heterologous hosts. The heterologous expression of natural product biosynthetic genes represents an elegant and efficient solution to the supply problem as it capitalises on the pre-existing biosynthetic machinery of Nature, leading to a cheap, reliable and potentially limitless source of a compound. But there can be significant challenges to this solution such as the impeded expression of foreign genes by host codon preferences, incompatible gene promoter recognition and transcription factors, a lack of correct biosynthetic precursors, improper protein folding due to absent post-translational machinery and the toxicity of foreign gene products to the host cell (Wenzel and Muller, 2005, Ekkers et al., 2012).

Such challenges are not insurmountable, however, and there have already been previous successes. The cloning and successful heterologous expression of patellamide, for example, a marine natural product produced by a cyanobacterial symbiont of the ascidian *Lissoclinum patella*, has been achieved by two independent groups (Long et al., 2005, Schmidt et al., 2005). The study by Long et al. (2005) showed that genes from a cyanobacterium could be successfully expressed in *Escherichia coli* using bacterial artificial chromosome shuttle vectors. This strategy allowed for whole isolated biosynthetic pathways to be shuttled between various hosts such as the genetically amenable *E. coli*, or the physiologically more flexible *Streptomyces*, which increased the chances of successfully overcoming transcription and translation barriers. The application of novel shuttle vectors that expand the range of potential hosts, as well as the engineering of *E. coli* to improve heterologous expression of foreign genes have also improved opportunities for transferring biosynthetic genes across taxonomically distant organisms (Martinez et al., 2004, Sørensen and Mortensen, 2005). More recent achievements with marine natural products include the expression of the cyanobacterial compound, barbamide, in a terrestrial *Streptomyces* sp. (Kim et al., 2012), the marine actinomycete product, enterocin, was also expressed in *Streptomyces* (Bonet et al., 2014), and alterochromide, a product from a marine pseudoalteronomad, was successfully expressed in *E. coli* (Ross et al., 2014).

Heterologous expression of a sponge-derived natural product is thus a worthwhile strategy for ensuring large scale production of a therapeutic candidate and represents a logical example of how knowledge obtained from studying terrestrial molecular biology can be applied to marine organisms. In order to attempt this approach, the biosynthetic genes for a natural product of interest must first be identified and cloned, requiring an examination of complex microbial communities that can prove challenging. Of crucial importance to the study of sponge symbionts is that the majority are not amenable to

culturing. For example, in a study by Webster and Hill (2001) on the Australian sponge species, *Rhopaloeides odorabile*, only 0.1-0.23 % of the total bacterial community were reported as culturable. Despite improvements in culturing techniques, the majority of sponge symbionts are still resistant to culturing, likely due to the necessity of the host environment in providing growth signals which cannot be simulated by standard microbiological approaches (Joint et al., 2010). Considering this, the most feasible approach to solving the supply problem of sponge-sourced natural products lies with the development of modern -omic tools and methods such as metagenomics, which are often referred to as culture independent approaches.

1.3.1 Metagenomic solutions to the supply problem

The –omics, which include genomics, proteomics, metabolomics and transcriptomics, are tools that can overcome the limitations encountered with traditional cultivation studies by exploring the biosynthesis of natural products at the genetic level (Schofield and Sherman, 2013). These approaches have become particularly prevalent over the last 15 years, driven by increases in speed and decreases in the cost of DNA sequencing, as well as the expansion of publicly available bioinformatic databases which contain vast amounts of gene and protein information (Kircher and Kelso, 2010).

Metagenomics represents another culture independent technique, a term first coined by Handelsman et al. (1998) in describing the collective genomes of a soil sample, but which is now used to refer to the study of multiple genomes acquired from any environmental sample or organism. Over recent years metagenomics has emerged as a highly promising tool for studying the genes of complex communities in both terrestrial and aquatic environments (Rondon et al., 2000, Tringe et al., 2005). For example, sequencing of a metagenome from the Sargasso Sea resulted in the discovery

of 1.2 million new genes and 148 novel microbial species, demonstrating the potential offered by metagenomics in accessing uncharacterised metabolic pathways, particularly amongst unculturable species (Venter et al., 2004). In terms of natural product discovery from a sponge metagenome, or holobiome, two potential approaches to metagenomic studies are illustrated in Figure 1.4.

The first approach involves directly sequencing metagenomic DNA, an approach that has become possible due to the advent of next generation sequencing (NGS) technologies and the improved potential for sequencing large genomes and metagenomes (Hall, 2007). This approach has the advantage of circumventing the need to construct and screen clone libraries and instead uses genome mining and *in silico* bioinformatic techniques to search for biosynthetic genes from large sequence datasets. For example, pyrosequencing was recently employed by Kwan et al. (2012) to reveal the biosynthetic pathway of the patellazoles from a tunicate metagenome, and a combination of metagenomic and metaproteomic strategies was used by Rath et al. (2011) to elucidate the biosynthetic pathway of trabectadin **(1)** from an ascidian metagenome. The application of computer programs such as ClustScan (Starcevic et al., 2008) and antiSMASH (Blin et al., 2013), which use profiles derived from hidden Markov models (HMM) to recognise protein domains and predict the catalytic functions of biosynthetic genes from DNA sequences, has greatly facilitated the direct sequencing approach to metagenomic studies.

The second, indirect approach to metagenomic studies typically involves the generation and screening of large-insert DNA libraries in bacterial hosts using either function based or sequence based screening strategies. Once a DNA library has been constructed, one option is to look for the functional expression of encoded biosynthetic genes that result in detectable phenotypes of *E. coli* growing on plates (Rondon et al., 2000, Wang et al., 2000, Gillespie et al., 2002). Another variant of the functional

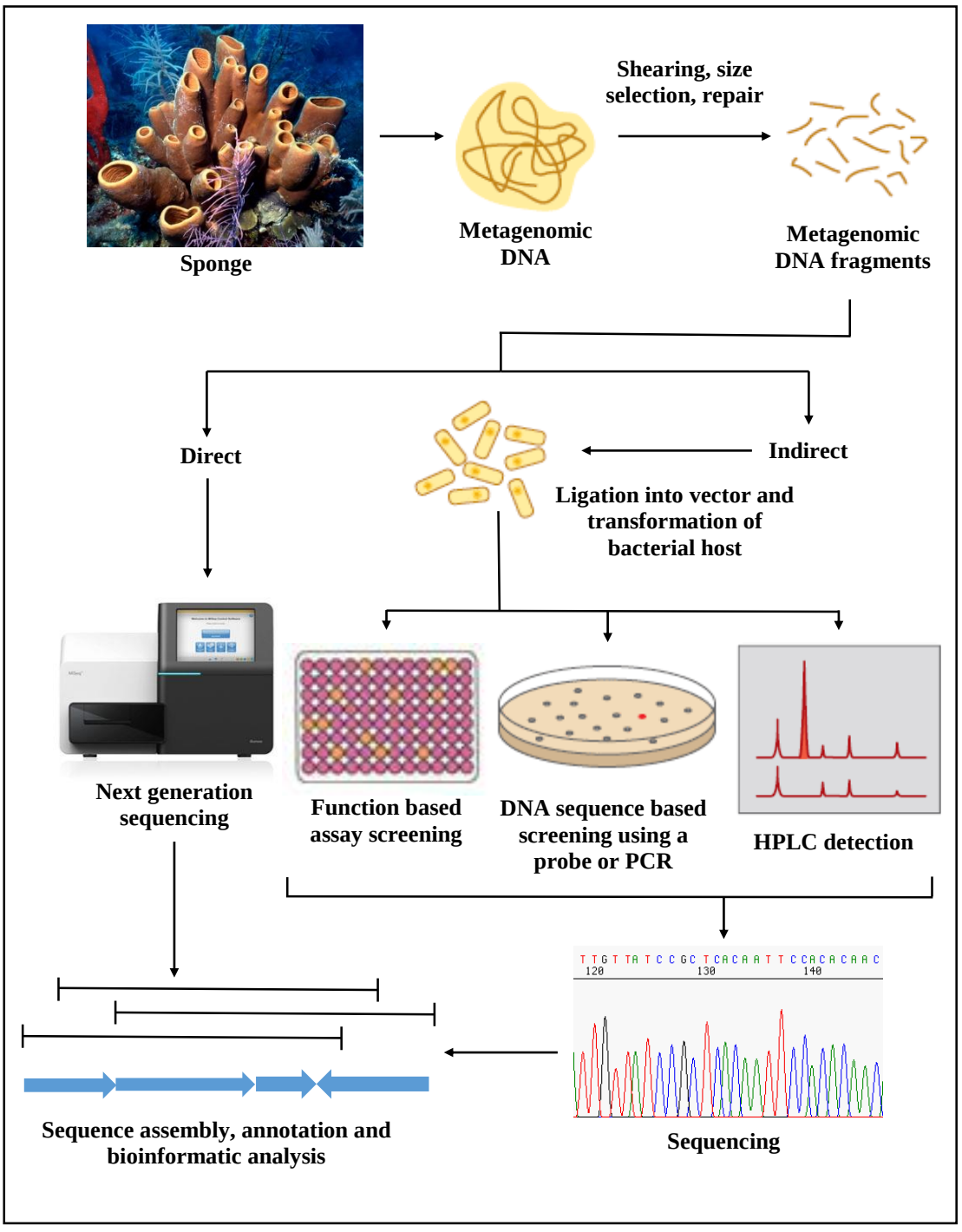

Figure 1.4 Metagenomic strategies for isolating biosynthetic genes from sponges. Isolating biosynthetic genes from the metagenomes of sponges can be approached directly through the use of NGS technologies, which allow for the capture of large volumes of sequence data which can then be mined for biosynthetic genes of interest. Alternatively, an indirect approach would involve construction of a metagenomic DNA library in a bacterial host, which can then be screened via the various options shown, ultimately sequencing clones of interest. Both direct and indirect strategies will end with assembling sequence data and using bioinformatic analyses to annotate and characterise the results. Adapted from Piel (2011).

screen relevant to natural product discovery is the use of chemical analyses, such as high performance liquid chromatography (HPLC) or mass spectrometry (MS), to detect the biosynthetic products of clones. Such an approach was successfully utilised by Long et al. (2005) to isolate and express the gene cluster involved in patellamide biosynthesis. Alternatively, libraries can be screened based on the detection of DNA sequences which has the advantage of enabling natural product pathways to be identified even if they are not expressed in the host, or kept silenced under laboratory conditions. This approach is particularly suitable for well characterised biosynthetic pathways as the strategy relies upon targeting features of biosynthesis that are highly conserved, permitting the use of degenerate PCR primers designed from consensus sequences or the hybridisation of oligonucleotide probes based on homology.

Much of the biotechnological research into marine natural product production has focused on the study of polyketides or nonribosomal peptides, which are diverse chemical families that contain nearly two thirds of all antitumour therapeutic candidates (Newman and Cragg, 2004). These clinically important compounds are particularly well suited to metagenomic and heterologous expression studies as all known bacterial genes encoding the producing enzymes are found in gene clusters, a feature that facilitates both the isolation and expression of complete biosynthetic pathways (Rodriguez et al., 2009). Additionally, the producing enzymes are cytosolic systems and do not require any specialised cellular substructures for activity, and despite their diverse structural complexity, polyketides and nonribosomal peptides are all formed from common organic molecules (Rodriguez et al., 2009). Further interest from a biotechnology standpoint is fuelled by the potential of manipulating the biosynthetic enzyme-producing genes in order to generate novel structural analogues of bioactive compounds. How this is accomplished is related to the modular architecture of both the biosynthetic genes and

the enzymes that assemble polyketides and nonribosomal peptides, which are explored in the following section.

1.4 Polyketides and nonribosomal peptides

Polyketides have given rise to many medically important compounds including the antibiotic erythromycin **(16)**, the immunosuppressant rapamycin **(17)** and the anticancer epithilone B **(18)** (Figure 1.5) (Kwan and Schulz, 2011). Polyketides are synthesised by large, multimodular proteins called polyketide synthases (PKS) using simple carboxylic acid monomers. These enzymes are organised into coordinated groups of active sites or domains, arranged into modules with each module responsible for the catalysis of one cycle of polyketide chain elongation and any associated functional group modifications (Staunton and Weissman, 2001, Fischbach and Walsh, 2006). The broad range of biological activities found with polyketides is attributed to the diverse range of structures seen within this family, a feature related to the mechanism of biosynthesis which is highly similar to the process of fatty acid synthesis by fatty acid synthases (FAS) (Smith and Tsai, 2007).

Nonribosomal peptides are an equally diverse family of secondary metabolites that include notable medically important examples such as cyclosporine A **(19)**, bleomycin **(20)** and vancomycin **(21)** (Figure 1.5). The biosynthesis of nonribosomal peptides is remarkably similar to that of polyketides, but instead of carboxylic acid derived starter and extender units, the non-ribosomal peptide is assembled from amino acids by multimodular enzymes called nonribosomal peptide synthetases (NRPS) (Finking and Marahiel, 2004).

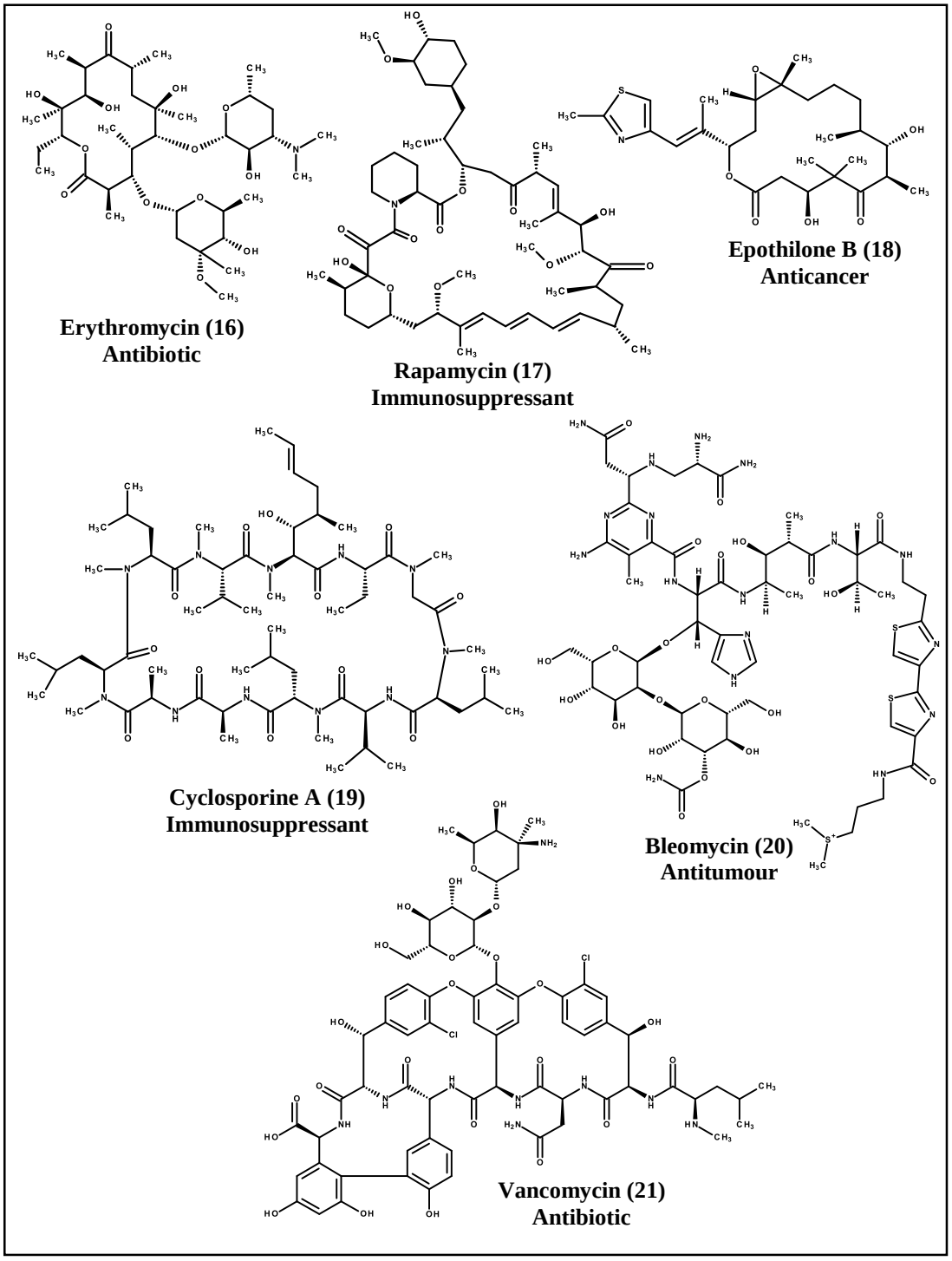

Figure 1.5 Examples of medically important polyketides and nonribosomal peptides with their applications. Chemical structures and applications are shown with the numbers in brackets used to refer to the compound in the text.

1.4.1 The biosynthesis of fatty acids, polyketides and nonribosomal peptides

The PKS, FAS and NRPS enzymes all use modular biosynthetic logic to assemble products from simple monomers (Fischbach and Walsh, 2006, Meier and Burkart, 2009). Between FAS and PKS, there are further similarities such as the utilisation of common precursors, as well as similar overall chemistry, structure and domain architecture (Smith and Tsai, 2007). On the basis of domain architecture and relationships to previously characterised FAS enzymes, PKSs have been classified into 3 different categories, type I-III (Hertweck, 2009): Type I refers to linearly arranged and covalently fused catalytic domains within large, multifunctional enzymes that may act in an iterative or non-iterative way; where a set of domains may be used repeatedly or only once. These are similar to the type I FAS of fungi and animals. Type II indicates a PKS complex composed of discrete mono-functional enzymes that act in an iterative fashion to produce aromatic compounds that to date, are only found in bacteria and show similarity with the type II FAS found in bacteria and plants. Type III PKSs produce the simplest polyketide products, also in an iterative way, but are typically associated with the chalcone and stilbene synthases which produce organic compounds almost exclusively found in higher plants.

Both polyketide and fatty acid synthesis share a common pool of precursors that are used to assemble products, namely acetyl co-enzyme A (CoA) or malonyl-CoA, and both carry out chain extension through repetitive decarboxylative condensations of acyl starter units and then CoA derived extender units (Rawlings, 1998, Hertweck, 2009, Meier and Burkart, 2009). However, PKSs also typically use methylmalonyl-CoA extender units, as well as other acetyl starter units such as propionyl-, benzoyl-, malonamyl- or methoxymalonyl-CoA (Moore and Hertweck, 2002, Fischbach and Walsh, 2006). The extension reaction in both processes is performed by a β-ketoacyl-

ACP synthase (KS) domain, with the building blocks and intermediate products covalently bound to acyl carrier proteins (ACP), and extender units selected and transferred to the ACP by acyltransferase (AT) domains. The KS and ACP domains both have thiol groups which are used to bind to the carboxy groups of the extender units and intermediate products via a thioester linkage. The thiol group of the ACP is found on the phosphopantetheine, a prosthetic group of the ACP that acts as an arm to swing the growing product between domains (Keatinge-Clay, 2012). Typical chain extension in a type I PKS module is shown in Figure 1.6.

In fatty acid biosynthesis, the intermediate products are fully reduced by the actions of a β-ketoreductase (KR) domain, a dehydratase (DH) domain and an enoylreductase (ER) domain, before another round of chain elongation takes place using the same domains. However, in type I modular polyketide synthesis, the reductive modifications to the β-position of the polyketide backbone are optional and so an intermediate following chain extension can be partly or fully reduced before the growing polyketide is further extended by successive modules, with the final product released from the final ACP by a thioesterase (TE) domain, also found in type I FAS (Figure 1.6) (Smith and Tsai, 2007). In any module of a type I PKS, there are therefore a set of domains that are always present, the KS, ACP and AT, whilst some or all of the KR, DH and ER domains may or may not be present. The variable combinations of reductive domains, in addition to the incorporation of different types of starter and extender units is what gives rise to the structural and functional diversity seen amongst polyketides.

In addition to reductive domain use, a further major difference between modular polyketide synthesis and the iterative actions of the type I FAS concerns the AT domain. Whilst only one type of AT domain is found in FAS, with dual specificities for either the primer acetyl unit or the malonyl-CoA extender units, in the modular type I PKS the loading of primer or extender units is carried out by separate dedicated AT domains with

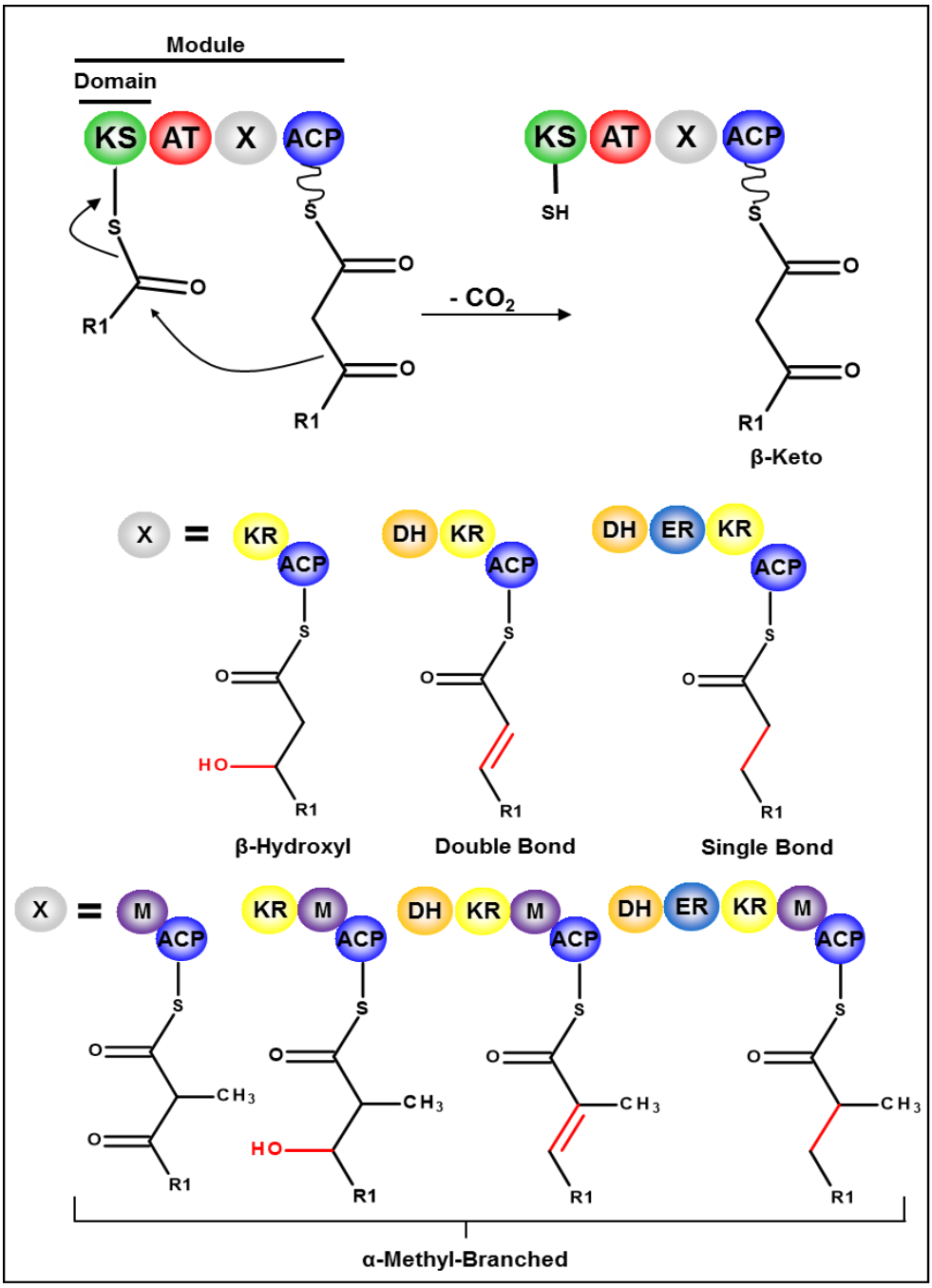

Figure 1.6 General biosynthetic steps during a round of polyketide extension in a single type I *cis*-AT PKS module. A typical *cis*-AT PKS module is shown, where the acyltransferase (AT) domain is integrated in each module. A malonyl-CoA extension unit has been loaded to the phosphopantetheinyl arm (Ppant) of the acyl carrier protein (ACP) via the AT domain. The charged ACP then docks with the ketosynthase (KS) domain, which catalyses the chain extension via decarboxylative condensation, before the ACP transfers the polyketide to a downstream module. The X domain is variable and can be filled by the shown combinations of ketoreductase (KR), dehydratase (DH), enoylreductase (ER) or methyltransferase (M) domains. The biosynthetic products for these domain sets are shown below each combination. *Cis*-AT PKSs can also introduce α-methyl-branched groups by AT-directed incorporation of methylmalonyl-CoA extension units. Adapted from Nguyen et al. (2008)

the potential for utilising different extender substrates during each elongation step. Whilst the AT domain responsible for loading the PKS starter substrate has relaxed specificity, like the FAS AT domains, the AT domains for PKS chain extension typically exhibit specificity for either malonyl or methylmalonyl-CoA (Khosla et al., 1999, Liou et al., 2003). The use of methyl-branched extender units in modular PKS systems allows for the generation of methyl-branched polyketides, but PKS-incorporated methyltransferase domains may also be utilised for this function (Figure 1.6) (Nguyen et al., 2008).

The domains of the modular type I PKS enzyme can therefore be considered as a molecular assembly line, with biosynthesis following co-linearity principles where the number of condensation reactions dictate the chain length of the final product, each module is used only once, and the structures of intermediates directly correspond to the PKS module domain architecture. This enables polyketide structures to be predicted from PKS domain architecture and vice versa (Staunton and Weissman, 2001, Weissman and Leadlay, 2005, Hertweck, 2009, Cummings et al., 2014). However, these canonical rules for polyketide biosynthesis are only applied to a subclass of modular PKSs called the *cis*-AT PKS, where the AT domain is present in every module and connected to the KS domain via a subdomain also found in the mammalian FAS (Tang et al., 2006, Maier et al., 2008). The classic example of a *cis*-AT PKS is the 6-deoxyerythronolide B synthase, which produces an intermediate of the antibiotic erythromycin **(16)** and is the most studied type I modular PKS (Khosla et al., 2007). However, there are also non-canonical PKSs, such as in the evolutionary distinct *trans*-AT systems, where the AT domain is not integrated into the assembly line and is instead expressed as a free-standing enzyme. These discrete AT domains typically transfer malonyl-CoA extender units to multiple ACP domains within a PKS (Piel, 2010). Other examples of non-canonical polyketide biosynthesis include broken or split modules, as well as module or

domain skipping or stuttering during chain extension (Katz, 2009).

Nonribosomal peptide biosynthesis by NRPSs use a strategy that is very similar to that of modular PKSs, with the final compound arising out of linear, modular biosynthetic assemblies of amino acid extender units. As with polyketides, a remarkable structural and functional diversity is seen with nonribosomal peptides, due to a large pool of potential building blocks that include 20 proteinogenic amino acids as well as a large variety of nonproteinogenic amino and aryl acids (Marahiel and Essen, 2009). Domains of NRPSs are also arranged into modules, where the order and number of the modules in an NRPS system dictate the sequence and number of extender units in the resulting product (Cane and Walsh, 1999, Finking and Marahiel, 2004, Fischbach and Walsh, 2006). In a typical NRPS module there are at least three domains: An adenylation domain, responsible for the activation and incorporation of a particular amino acid or building block, a thiolation domain for the thioesterification of the activated amino acid, and a condensation domain to form an amide bond between the amino acid units (Cane et al., 1998, Du et al., 2001). Typical chain extension in an NRPS module in shown in Figure 1.7. Initiation of the process occurs via a module lacking a condensation domain, and a TE domain ultimately releases the completed polypeptide chain from the thiolation domain of the previous module (Finking and Marahiel, 2004). Like the KR, DH and ER domains of PKSs, NRPSs may also contain tailoring domains such as cyclisation domains or epimerization domains which catalyse the heterocyclisation of serine, threronine or cysteine residues, or epimerise amino acids into the D-configuration, respectively (Cane and Walsh, 1999, Finking and Marahiel, 2004).

PKS and NRPS modules also occur in hybrid assembly lines that contain both types of modules (Du et al., 2001). These complexes may be referred to as hybrid PKS/NRPSs or NRPS/PKSs depending on the order of modules in the system. For the former, a ketide chain formed by an upstream PKS module is accepted by the C-domain

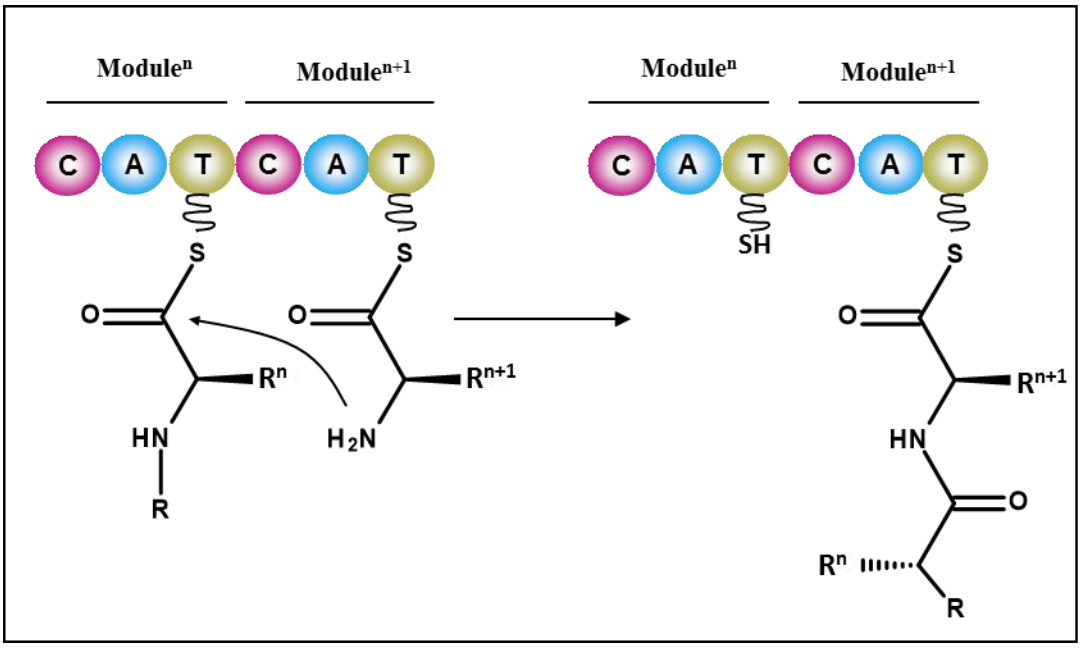

Figure 1.7 Bond formation in nonribosomal peptides. In the NRPS system, a dedicated adenylation domain (A) activates an amino acid extension unit as an aminoacyl adenylate which is then transferred to the thiolation domain (T). The condensation domain (C) then catalyses nucleophilic attack of the amino nitrogen of the downstream aminoacyl group on the electrophilic carbonyl carbon of the upstream acyl group. Adapted from Du et al. (2001).

of a downstream NRPS module which subsequently mediates a C-N bond formation, elongating the polyketide chain with an amino acid. With NRPS/PKS hybrids, the KS domain accepts an upstream peptide chain rather than a ketide chain and catalyses the formation of a C-C bond, elongating the peptide chain with a short carboxylic acid (Figure 1.7 C) (Du et al., 2001). Characterised examples of such systems include rapamycin **(17)** (Aparicio et al., 1996) and bleomycin **(20)** (Shen et al., 1999).

The biosynthesis of type I polyketides and nonribosomal peptides are modular at many levels. At the genetic level the biosynthetic genes are typically located in clusters, encoding the PKS/NRPS, any tailoring enzymes that may be involved in cyclisation or dimerisation of the final product, as well as regulatory and resistance genes (Cummings et al., 2014). Once transcribed and translated, the enzymes themselves also show modularity. Considering this, there is therefore potential to alter the end product and generate structural analogues through addition, removal and substitution of domains or

modules, either at the genetic or protein level using combinatorial biosynthesis (Menzella et al., 2005, Weissman and Leadlay, 2005). Consequently there is great interest from a pharmaceutical perspective in examining the PKS/NRPS systems of natural products with a view to generate novel products of therapeutic value, or even rationally engineering a predefined product if domains or modules can be successfully stitched together (Kennedy, 2008, Walsh and Fischbach, 2010, Williams, 2013, Cummings et al., 2014). Biosynthetic characterisation of a sponge-derived natural product is thus worthwhile for not only solving the supply problem of potential pharmaceutical leads, but also for the exciting potential in generating new leads. One example of a sponge natural product with a predicted, but uncharacterised type I PKS/NRPS mode of biosynthesis is found with the chondropsins, a group of macrolide lactams with demonstrated potent antiproliferative activity and the potential for pharmaceutical exploitation.

1.5 The Chondropsins

Chondropsin A **(23)** and B **(25)** were originally described by Cantrell et al. (2000), whilst chondropsin D **(26)** was subsequently reported by Rashid et al. (2001a), but all were found in a *Chondropsis* sp. sponge. A further two members of the chondropsin family, chondropsin C **(24)** and 73-deoxychondropsin A (73-DOC) **(22)**, were also discovered from sponges, but from a Philippine *Ircinia* sp. and the Australian species, *Ircinia ramosa*, respectively (Rashid et al., 2001b) (Figure 1.8). All the chondropsins were observed to have structural patterns of oxygenation, alkylation and dehydration that indicate a polyketide biosynthetic origin but the absolute stereochemistry of the compounds has not yet been resolved. Additionally, the structures all contain amide linkages with side chains that suggest the incorporation of amino acid

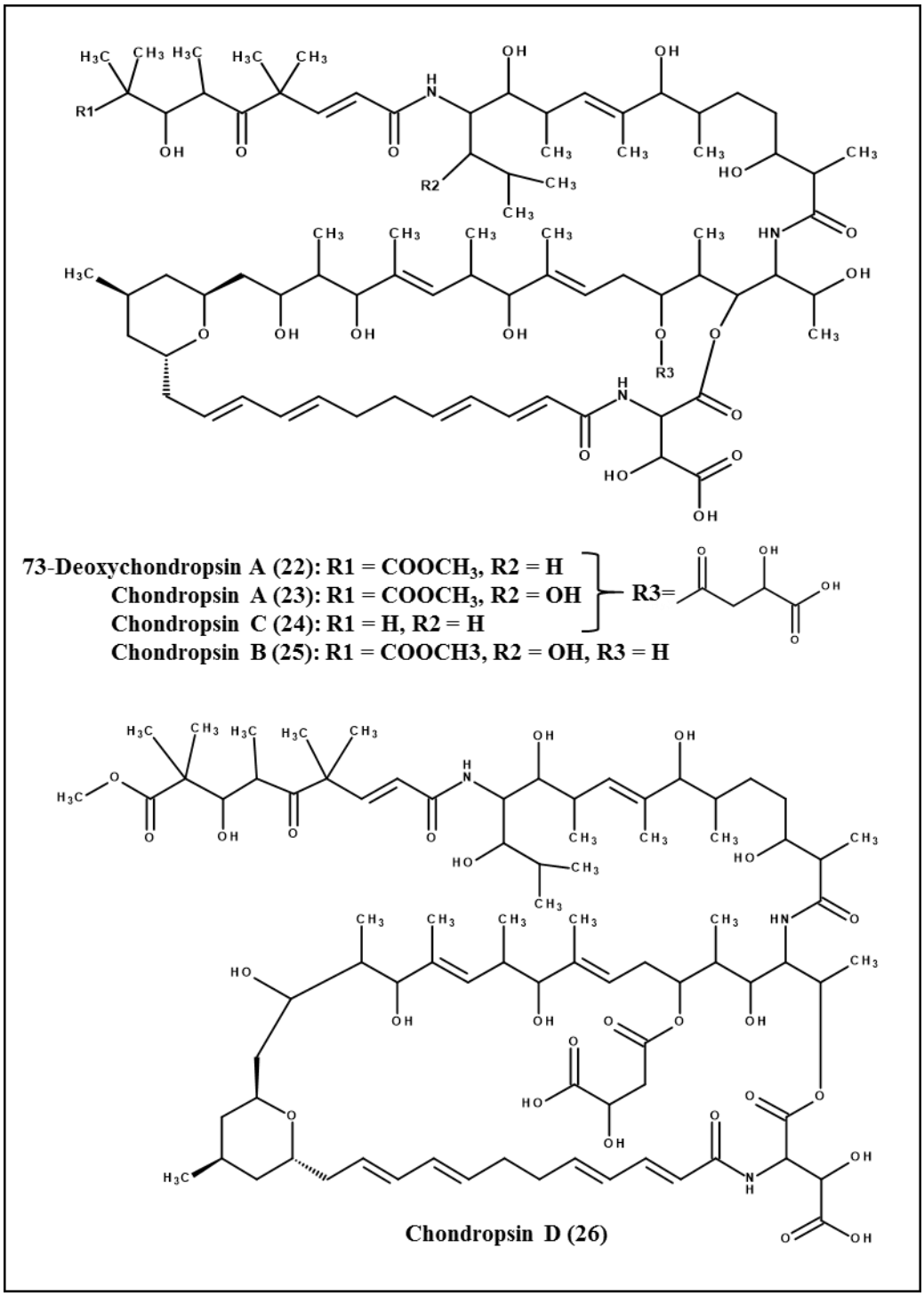

Figure 1.8 Chemical structures of the chondropsins. Numbers in brackets are used to refer to the compounds in the text

units. The route of chondropsin biosynthesis is therefore predicted to occur via a type I hybrid PKS/NRPS. The fact that chondropsins have been found across two orders of metazoans, coupled with a predicted polyketide biosynthetic origin, suggests these compounds are produced by a microbial sponge-specific symbiont (Cantrell et al., 2000,

Rashid et al., 2001b, Dunlap et al., 2007). However, whilst previous studies with *I. ramosa* have confirmed the presence of monophyletic cyanobacteria (Dunlap et al., 2007) as well as many other microbial species (Webster et al., 2010), the biosynthetic origin of 73-DOC **(22)** and the other chondropsins has not yet been investigated.

The biological activities of many natural products were established following screening by the US National Cancer Institute (NCI) using a panel of 60 human antitumour cell lines, where antiproliferative activity in response to test extracts was assessed using cellular viability assays (Shoemaker, 2006). Since 1989, over 75,000 crude samples from the natural environment have been screened by the NCI in this way, typically followed up by bioassay-guided isolation of novel bioactive compounds (Shoemaker, 2006). Following the discovery of chondropsin A **(23)**, this compound was tested in the NCI 60-cell antitumour screen, and showed potent (low nanomolar) differential growth inhibition with a profile distinct from other conventional antitumour agents at that time (Cantrell et al., 2000). Chondropsins C **(24)**, D **(25)** and 73-DOC **(22)** were also found to be cytotoxic towards melanoma and leukaemia cell lines and the chondropsin family were indicated as a class of compounds worthy of exploitation due to their potential as anticancer therapeutics by the NCI Developmental Therapeutics Program (NCI registry numbers (https://dtp.cancer.gov/): 719165, 719166, 720964, 722377, 720963 for chondropsin A-D and 73-DOC, respectively) (Rashid et al., 2001a, Rashid et al., 2001b).

A subsequent study by Bowman et al. (2003) used the NCI data to compare the profile of cellular response generated in the 60-cell screen from chondropsin A **(23)** to the profiles generated by other test compounds using the COMPARE pattern recognition algorithm (Boyd and Paull, 1995). The theory behind this analysis was that compounds that highly correlate through their activity in the NCI screen would be expected to share a molecular target or mechanism of action, even if different in structure. The authors

found that the profile for chondropsin A **(23)** exhibited a high correlation with profiles generated by the plecomacrolide compounds bafilomycin A_1 **(27)** and concanamycin A **(28)**, which are known to be potent inhibitors of vacuolar H^+-ATPases (V-ATPases) (Figure 1.9) (Bowman et al., 1988, Huss et al., 2002). The V-ATPases are further discussed in Section 1.6.

Bowman et al. (2003) subsequently investigated the inhibitory effects of the chondropsins on fungal V-ATPases from the vacuolar membranes of *Neurospora crassa* and mammalian V-ATPases from chromaffin granule membranes of *Bos taurus*. Using a biochemical assay for specific V-ATPase activity, which involved quantifying the liberation of inorganic phosphate and inhibitors of other membrane-bound ATPases (F-type, P-type) to discriminate ATPase activity, the authors presented compelling

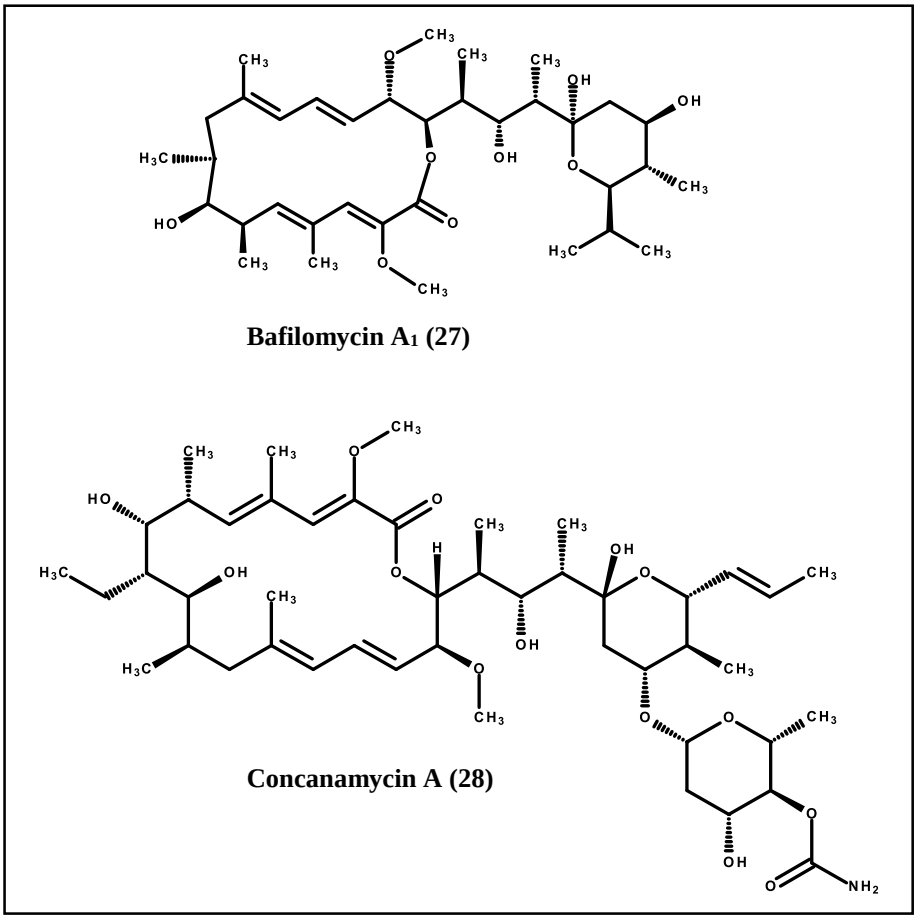

Figure 1.9 Structures of plecomacrolides bafilomycin A1 and concanamycin A. Numbers in brackets are used to refer to the compounds in the text.

evidence that the chondropsins were excellent V-ATPase inhibitors with a preference for inhibiting the fungal type over the mammalian type (Bowman and Bowman, 1988, Bowman et al., 2003). However, whilst the authors also stated that chondropsin B **(25)** and 73-DOC **(22)** were inactive against other membrane ATPases including the mitochondrial F-ATPase, the plasma membrane H^+-ATPase from *N. crassa* and the Na^+/K^+ ATPase from canine kidney cells, the data for these experiments were not shown. Interestingly, these reported effects contrast with the activity of bafilomycin **(27)** and concanamycin **(28)** which are known to inhibit other membrane ATPases, potentially causing off-target effects when used *in vivo* which would limit their use as therapeutics (Bowman et al., 1988, Droese et al., 1993, Keeling et al., 1998).

The fact that 73-DOC **(22)** showed selective V-ATPase inhibition, with a magnitude of differential activity greater than the other chondropsins, as well as a possible lack of inhibitory activity towards other ATPases, implies that this particular member of the chondropsin family could represent a novel V-ATPase inhibitor that does not induce *in vivo* systemic toxicity. As V-ATPase subunit structure is known to show both ubiquitous and cell-specific compositions (see Section 1.6.1), the inhibitory activity of 73-DOC **(22)** has effectively only been examined using two specific types of V-ATPases. As such, questions remain regarding what effects this compound has on other mammalian V-ATPases, or other targets, and whether it can be used as a selective therapeutic to treat diseases caused by V-ATPase dysfunction.

1.6 V-ATPases

The V-ATPases are a ubiquitous class of proton pumps in eukaryotic cells that function to regulate intracellular pH and generate electrochemical gradients across membranes (Nishi and Forgac, 2002). Due to involvement in a diverse set of

physiological processes, as well as a wide range of diseases including tumour metastasis, sensorineural deafness, distal renal tubule acidosis and osteopetrosis (see Section 1.7), V-ATPases have been highlighted as attractive targets for therapeutics (Bowman and Bowman, 2005, Hinton et al., 2009, Huss and Wieczorek, 2009). Typically V-ATPases are found associated with components of the endomembrane system such as the Golgi apparatus, endosomes, lysosomes and secretory vesicles (Bowman and Bowman, 2005). However, some V-ATPases are involved in more specialised roles where they may be targeted to the plasma membrane to carry out extracellular acidification. This is known to occur in the renal intercalated cells of the kidney for the task of urine acidification (Brown et al., 2009), in epididymal clear cells where luminal acidification is critical for sperm maturation (Shum et al., 2009), and in osteoclast bone cells where the V-ATPase is crucial in generating an acidic local environment that leads to bone resorption (Frattini et al., 2000) (see Section 1.7.1.2). V-ATPases are also found on the plasma membranes of tumour cells where they are thought to generate an acidic extracellular environment which aids metastasis (Sennoune et al., 2004).

However, V-ATPases also have physiological roles that extend beyond their ability to regulate pH and are now recognised as protein complexes critically involved in cellular signalling cascades. Studies have related V-ATPase activity to Wnt (Cruciat et al., 2010), Notch (Vaccari et al., 2010), Insulin-like growth factor (IGF-I) (O'Callaghan et al., 2010) and EGFR/ErbB signalling (Xu et al., 2012), thereby implicating the V-ATPase in all the physiological and pathophysiological processes associated with those pathways such as embryonic tissue development, proliferation, apoptosis, metabolism and cancer.

1.6.1 Structure and mechanism

The V-ATPase is composed of two large complexes containing at least 14 subunits organised into two domains, the 650 kDa V_1 domain and the 260 kDa V_0 domain (Figure 1.10). Together, these domains form a complex that functions as a molecular motor, where the energy generated from ATP hydrolysis on the cytoplasmic-facing V_1 domain is used to drive protons through an ion channel embedded within the membrane-bound V_0 domain. The V-ATPases operate by a rotary mechanism, demonstrated when a gold bead was attached to subunits of the V_1 complex and rotation coupled to ATP hydrolysis was observed (Imamura et al., 2003). The structure and function of the V-ATPase is similar to that of the F-ATP synthase found in the inner mitochondrial membranes of eukaryotes, but V-ATPases function in reverse, using ATP to translocate protons rather than using proton electrochemical gradients to generate ATP (Forgac, 2007).

The V_1 domain contains 8 different subunits (*A-H*), some of which are present in multiple copies. There are 3 copies of *A* and *B*, which are arranged in alternating positions of a 400 kDa hexamer with the catalytic sites of ATP hydrolysis located at the interface of these subunits (Nishi and Forgac, 2002). The rest of the V_1 subunits form two types of stalk, peripheral or central, that connect the V_1 and V_0 domains. During rotation, hydrolysis of ATP induces conformational changes that drive clockwise rotation of the *A/B* hexamer. The central stalk couples the rotation of the V_1 to the V_0 domain, whilst the peripheral stalks act as stators, maintaining the complex position during rotation (Forgac, 2007).

The V_0 domain of higher eukaryotes contains 7 different subunits designated *a*, *d*, *e*, *c*, *c"* and the accessory subunits, *Ac45* and *M8*. There are 4-5 copies of subunit *c* and a single copy of *c"*. Both *c* and *c"* are proteolipid subunits formed of highly

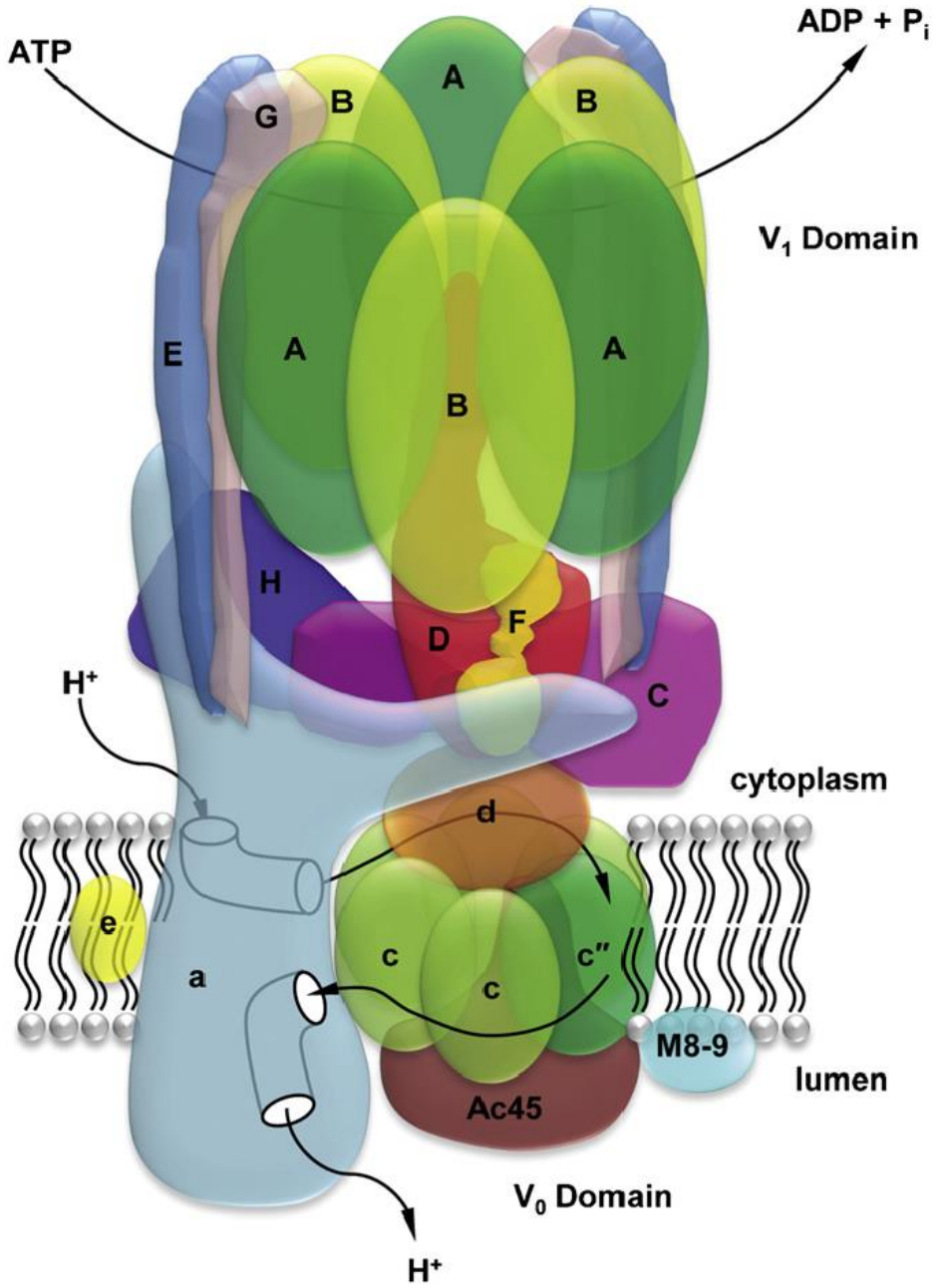

Figure 1.10 Structural model of the mammalian V-ATPase. The complex is composed of at least 14 subunits which are organised into two distinct domains: The peripherally orientated V_1 domain, which contains the site of ATP hydrolysis and is made up of subunits *A-H*; and the membrane-embedded proton-translocating V_0 domain, which is formed by subunits *a*, *c*, *c"*, *d* and *e*. There are also two accessory subunits, *Ac45* and *M8-9*, associated with the V_0 domain. Proton transport across membranes via hemi-channels in subunit *a* and the proteolipid *c*/*c"* ring is also shown. Taken from Qin et al. (2012b).

hydrophobic proteins arranged in a ring, with each containing a single glutamic acid residue that undergoes reversible protonation (Wilkens and Forgac, 2001, Nishi and Forgac, 2002). Subunit *d*, located on top of the proteolipid ring, provides a connection

between V_1 and V_0 and participates in controlling the reversible assembly/disassembly of the V_1 and V_0 domains, a fundamental feature exclusive to the V-ATPases (Forgac, 2007, Marshansky et al., 2014). The V_0 domain also contains the 100 kDa subunit *a* that contains a hydrophilic N-terminal domain and a C-terminal containing 8 or 9 transmembrane helices, one of which contains an arginine residue shown to be crucial for proton transport (Kawasaki-Nishi et al., 2001b). Subunit *a* provides entry and exit routes for protons via two hemi-channels that enable proton translocation. Protons enter one channel and are forcibly bound to the glutamic acid residues of the proteolipid ring subunits by the hydrophobic environment (Junge and Nelson, 2005, Marshansky et al., 2014). Rotation of the stalk from ATP hydrolysis is coupled to rotation of the proteolipid ring relative to the subunit *a*, and on reaching the luminal hemi-channel, deprotonation of the buried glutamic acid residues occurs, induced by the crucial interaction with the arginine residue of subunit *a* (Junge and Nelson, 2005, Forgac, 2007). Rotation of the proteolipid ring relative to subunit *a* thus results in active transport of protons across membranes (Figure 1.10).

In mammalian cells, almost all V-ATPase subunits exist as two or more isoforms that, to a certain extent, display tissue specific expression or differential membrane targeting (Table 1.2). In higher animals there are ubiquitous and tissue/cell-specific isoforms, the latter particularly associated with a subset of V-ATPases with specialised roles at the plasma membranes of cells, but which typically contain ubiquitous isoforms as well (Holliday, 2014). Mammalian cells contain four isoforms of subunit *a* (*a1*, *a2*, *a3* and *a4*) of the V_0 domain, with the *a4* isoform almost exclusively expressed in the apical membranes of epididymal clear cells and renal intercalated cells, where the V-ATPase is responsible for acid balance and sperm maturation, respectively (Toei et al., 2010). Mutations in this particular isoform have been shown to cause defective acid secretion, resulting in renal tubular acidosis (Smith et al., 2000). There are other

Subunit	Gene Name	Isoform (expression)	Proposed Function
V_1 Domain			
A	ATP6V1A	-	Catalytic ATP binding site
B	ATP6V1B1	B1 (renal, epididymis, olfactory epithelium	Non-catalytic ATP binding site; actin binding; osteoclast actin ring and ruffled border formation
	ATP6V1B2	B2 (ubiquitous)	
C	ATP6V1C1	C1 (ubiquitous)	Peripheral stator; actin binding; osteoclast actin ring formation
		C2a, b (lung, renal, epididymis)	
D	ATP6V1D	-	Central rotor
E	ATP6V1E1	E1 (epididymis, olfactory epithelium)	Peripheral stator; binds aldolase
	ATP6V1E2	E2 (ubiquitous)	
F	ATP6V1F	-	Central rotor
G	ATP6V1G1	G1 (ubiquitous)	Peripheral stator
	ATP6V1G2	G2 (neural)	
	ATP6V1G3	G3 (renal, epididymis)	
H	ATP6V1H	-	Peripheral stator
V_0 Domain			
a	ATP6V0A1	a1 (ubiquitous, neural)	Peripheral stator; proton translocation; targeting; a3 is important for osteoclast resorption
	ATP6V0A2	a2 (ubiquitous, endothelial)	
	TCIRG1	a3 (ubiquitous, osteoclasts, pancreas)	
	ATP6V0A4	a4 (renal, epididymis, optic)	
c	ATP6V0C	-	Proton translocation
c”	ATP6V0B	-	Proton translocation
d	ATP6V0D1	d1 (ubiquitous)	Coupling ATP hydrolysis and proton translocation; d2 important for pre-osteoclast fusion, maturation and bone resorption
	ATP6V0D2	d2 (renal, epididymis, osteoclasts, dendritic cells)	
e	ATP6V0E1	e1	Function unknown
	ATPV0E2	e2	
Accessory			
Ac45	ATP6AP1	-	Regulate secretory pathway; osteoclast bone resorption
M8-9	ATP6AP2	-	Proposed in assembly and function of V-ATPase

Table 1.2 Mammalian V-ATPase subunits, isoforms and proposed functions. Adapted from Forgac (2007) and (Cantrell et al., 2000), Qin et al. (2012b).

isoforms such as *C2*, *G3* and *d2*, that are also shared between renal and epididymal cell types, suggesting the formation of V-ATPase complexes with unique subunit combinations in these and possibly other cell types (Nishi and Forgac, 2002, Smith et al., 2002, Pietrement et al., 2006).

Localisations of isoforms can also be compartment-specific. In mouse kidney proximal tubes, all isoforms of *a* are expressed, but while *a1*, *a3* and *a4* are targeted to the plasma membrane *a2* is targeted to early endosomes (Hurtado-Lorenzo et al., 2006). A further example can be seen with osteoclasts, where the *a3* isoform is highly expressed and re-localised from lysosomes to the plasma membrane during bone resorption, whilst the *a1* and *a2* isoforms are localised at the Golgi complex (Toyomura et al., 2000, Toyomura et al., 2003). Mutations in the *a3* subunit are shown to cause a defective bone resorption phenotype associated with osteopetrosis, which is characterised by excessive, dense bone formation (see Section 1.7.4) (Frattini et al., 2000). It is generally accepted that subunit *a* is crucial for trafficking and specific targeting of the V-ATPase complex in mammalian cells, which is also known from yeast and protists, but the underlying mechanisms are currently unresolved (Kawasaki-Nishi et al., 2001a, Wassmer et al., 2006).

1.6.2 Assembly and regulation

Knockdown studies with the yeast V-ATPase have shown that all subunits of the V-ATPase are required for correct assembly and function (Kane and Parra, 2000, Graham et al., 2003). In yeast, the V_0 domain is assembled in the endoplasmic reticulum and is dependent on a set of dedicated chaperones (Graham et al., 2003, Forgac, 2007). Assembly with either almost fully assembled V_1 domains, or individual V_1 subunits, occurs in the Golgi (Graham et al., 2003, Malkus et al., 2004). However, there are

alternative pathways to V-ATPase assembly in yeast that are still being resolved, including the role of RAVE (regulator of H+-ATPase of vacuolar and endosomal membranes), which is involved with yeast V-ATPase assembly, and possibly differential targeting, as well as the reversible disassembly of V-ATPase complexes (Kane, 2006, Smardon et al., 2014). Homologues for RAVE are also known from higher eukaryotes and implicated in defective organelle acidification, but V-ATPase assembly in mammals is otherwise understudied (Yan et al., 2009, Sethi et al., 2010, Einhorn et al., 2012).

The reversible disassembly of the V-ATPase complex is one mechanism controlling the regulation of V-ATPase activity, and is known to occur for energy conservation in yeast in response to glucose depletion (Kane, 1995), as well as insects during moulting (Beyenbach and Wieczorek, 2006). Dissociation of the V-ATPase in yeast and humans is thought to be controlled by the direct interaction of the complex with cytosolic aldolase, an enzyme of the glycolytic pathway, which might be the glucose sensor that signals for V-ATPase dissociation (Lu et al., 2004). Whilst glucose was the paradigm signal for reversible V-ATPase disassembly, other signals such as pH are now indicated but there are likely to be other uncharacterised signals that also influence assembly/disassembly of the complex (Dechant et al., 2010, Diakov and Kane, 2010).

Modulation of V-ATPase activity can also occur through changes in the coupling efficiency between proton transport and ATP hydrolysis. In yeast, this is achieved through variations in the C-terminal domains of subunit *a* isoforms (Kawasaki-Nishi et al., 2001a). For example, the yeast V-ATPase complex found in the Golgi, has a much lower coupling efficiency than that found in the vacuole, and this is attributed to the different subunit *a* isoforms (Kawasaki-Nishi et al., 2001c). In mammals, mutations in other subunits, including *d* (Owegi et al., 2006), *A* (Shao et al., 2003), *E* (Sun-Wada et

al., 2002) and *C* (Sun-Wada et al., 2003) have all been proposed to have roles in regulating coupling efficiency.

In cell types that have V-ATPase complexes targeted to the plasma membrane, the density of pumps at the cell surface is controlled through reversible exo- and endocytosis of intracellular vesicles which contain high densities of V-ATPases (Forgac, 2007). In epididymal clear cells (Pastor-Soler et al., 2003), and possibly other secretory cells such as renal intercalated and osteoclasts (Geng et al., 2005, Geng et al., 2009), the recycling of V-ATPases to and from the plasma membrane is controlled by a novel soluble adenylyl cyclase (sAC), sensitive to cytoplasmic levels of bicarbonate. As bicarbonate and pH increase, sAC is activated, giving rise to increases in cyclic adenosine monophosphate (cAMP) that increase exocytosis and/or decrease endocytosis of V-ATPases via a currently unknown mechanism (Pastor-Soler et al., 2003).

In most cells, V-ATPases are located only in membranes of acidic intracellular compartments such as lysosomes or vacuoles, where transcriptional control involves TATA-less, GC-rich regulatory regions containing multiple Sp1 or AP-2-like binding sites, as found with other housekeeping enzymes (Lee et al., 1997, Holliday, 2014). Expression of other cell-specific isoforms are controlled by transcription factors such as Foxi1 in kidney, epididymal and inner ear cells (Jouret et al., 2005, Blomqvist et al., 2006, Vidarsson et al., 2009). In osteoclasts, the *a3* isoform is induced by the receptor activator of NF-κB ligand (RANKL), a master regulator for osteoclast differentiation (see Section 1.7.2), with the *d2* subunit also showing positive regulation by nuclear factor of activated T-cells, cytoplasmic 1 **(**NFATc1), in conjunction with microphthalmia-associated transcription factor (MITF) and myocyte enhancer factor 2 (MEF2) (Lacey et al., 1998, Kim et al., 2008, Feng et al., 2009a). Beyond these examples, however, very little is known about V-ATPase transcriptional regulation.

1.6.3 Function

The classical role of the V-ATPase is in pH homeostasis of intracellular compartments, but during the last two decades unconventional roles of V-ATPases in other cellular processes have also been described.

1.6.3.1 The endocytotic pathway

One of the most important roles concerning the V-ATPases is in the regulation of signalling, trafficking and degradation of cellular receptors and signalling molecules through the endocytotic pathway. Endocytosis is a fundamental cellular process that is used by all eukaryotic cells to communicate between the intra and extracellular environments and is responsible for internalising signalling molecules, nutrients, hormones, plasma membrane proteins, as well as cellular receptors via clathrin-dependent endocytosis. The endocytotic pathway is a network of endosomes which, following internalisation of molecules, results in recycling them back to the surface membrane or to be sorted and degraded in late endosomes or lysosomes.

There are two aspects to the endocytotic pathway that are known to be dependent on low endosomal pH: The dissociation of receptor-ligand complexes during recycling and the degradation of molecules in lysosomes (Mellman, 1992, Marshansky et al., 2002, Forgac, 2007, Marshansky and Futai, 2008). V-ATPases are responsible for the generation of the required low endosomal pH, and additionally, across the pathway from early endosomes to lysosomes there exists a finely regulated, decreasing pH gradient generated by the actions of the V-ATPases which if disturbed using V-ATPase inhibitors results in improper endocytotic functioning (Clague et al., 1994, Xu et al., 2003, Hurtado-Lorenzo et al., 2006).

1.6.3.2 The exocytotic pathway

Vesicular trafficking of the exocytotic pathway is essential for communication between organelles and involves a combination of two steps: The budding of vesicles from a donor and subsequent fusion with an acceptor compartment/membrane (Bonifacino and Glick, 2004). Studies in yeast have suggested that V-ATPases may be involved in fusion events where a direct role of the *c*-subunits of the V_0 domain has been proposed (Peters et al., 2001). In this model, fusion pores were proposed to assemble from V_0 domains in opposing membranes that pair, associated with SNARE (soluble N-ethylmaleimide-sensitive factor attachment protein receptor) complexes (Strasser et al., 2011).

The process in yeast was regulated by a homologue of a subunit *a* isoform of the V-ATPase, which has also been observed in other organisms. In *Drosophilia melanogaster*, for example, the neuron-specific *a1* isoform interacts with SNARE and loss-of-function mutations were shown to block synaptic vesicle fusion with the presynaptic membrane (Hiesinger et al., 2005). In mammals, V-ATPases are believed to control the exocytotic trafficking and secretion of hormones, where knockout mice lacking the *a3* isoform, which is highly expressed in endocrine tissues, show defective insulin secretion with no concordant alteration in the pH of the secretory cells (Sun-Wada et al., 2006, Sun-Wada et al., 2007). This suggests that V-ATPases may have a role in membrane fusion that is independent of acidification.

1.6.4 Inhibitors

The involvement of the V-ATPase in numerous aspects of cellular physiology has led to efforts to identify and develop novel V-ATPase inhibitors for therapeutic purposes (Huss and Wieczorek, 2009). The bafilomycins (A_1 **(27)**, B_1, C_1, D_1) were the first such

inhibitors discovered. These macrolide antibiotics were isolated from *Streptomyces* spp. (Werner et al., 1984) and bafilomycin A_1 **(27)** was subsequently shown to inhibit V-ATPases (Bowman et al., 1988). Concanamycin **(28)**, another member of the same chemical family (plecomacrolides), was found to have similar activity and several groups have since identified subunit *c* of the V_0 domain as being the primary binding site for the plecomacrolides, though there is some evidence that subunit *a* might also be involved (Kinashi et al., 1984, Bowman and Bowman, 2002, Huss et al., 2002, Bowman et al., 2006). These inhibitors function by perturbing the mechanical rotation of the V_0 domain proteolipid ring.

Whilst other V-ATPase inhibitors such as archazolid (Huss et al., 2005), and salicylihalamide A (Boyd et al., 2001, Xie et al., 2004) have since been discovered, due to the ubiquitous occurrence of V-ATPases, inhibitors such as bafilomycin **(27)** and concanamycin **(28)** are found to cause off-target effects and systemic toxicity that impede use as therapeutics (Keeling et al., 1998). However, V-ATPases that perform specialist functions are known to contain distinct subunit isoforms, or combinations of subunits, that may permit specific pharmacological targeting. One example of this is the osteoclast where the plasma membrane V-ATPase is crucial to the function of bone resorption. The following sections introduce the processes involved in bone remodelling, in addition to further details regarding the osteoclast V-ATPase and its unique role in treating osteolytic diseases.

1.7 Bone: Structure and cells

Bone tissue is a porous, mineralised structure made up of an organic component (~25 %) consisting of a collagenous matrix (90 % type I collagen) plus cells and vessels, and an inorganic component (~75 %) containing hydroxyapatite crystals

($Ca_{10}(PO_4)_6(OH)_2$). At the macroscopic level, there are two types of bone found in the adult human skeleton, cortical and trabecular (Figure 1.11). At the microscopic level, there are also two types of bone that are characterised by the orientation of their collagen fibres, lamellar or woven. Woven bone is laid down quickly in response to fracture or pathological states of high turnover, and is characterised by the disordered and random organisation of collagen fibres and hydroxyapatite crystals. This type of bone is ultimately replaced by lamellar bone, which has an organised structure of collagen and hydroxyapatite arranged in parallel or concentric sheets around blood vessels (Figure 1.11) (Martini and Martini, 1992, Seeman and Delmas, 2006).

Bone is a dynamic tissue that is constantly broken down and reformed in response to damage, as well as changes in mechanical loading and serum calcium levels (Sims and Gooi, 2008). The process by which this is achieved is known as bone remodeling, where 5-10 % of the skeleton is annually renewed with the equivalence of the entire adult human skeleton replaced in 10 years (Parfitt, 1982). Bone remodeling (see Section 1.7.3) is primarily carried out by the actions of osteoclasts and osteoblasts but there are also other important cellular components of bone, including osteocytes and bone lining cells, which are members of the osteoblast lineage.

1.7.1 Osteoclasts

1.7.1.1 Osteoclastogenesis

Osteoclasts are large multinucleated cells derived from hematopoietic stem cells (HSC) of the monocyte/macrophage lineage. These cells carry out bone resorption, and are usually found in contact with the bone surface within a resorption pit, or lacuna, created as a result of their resorptive activity (Hadjidakis and Androulakis, 2006).

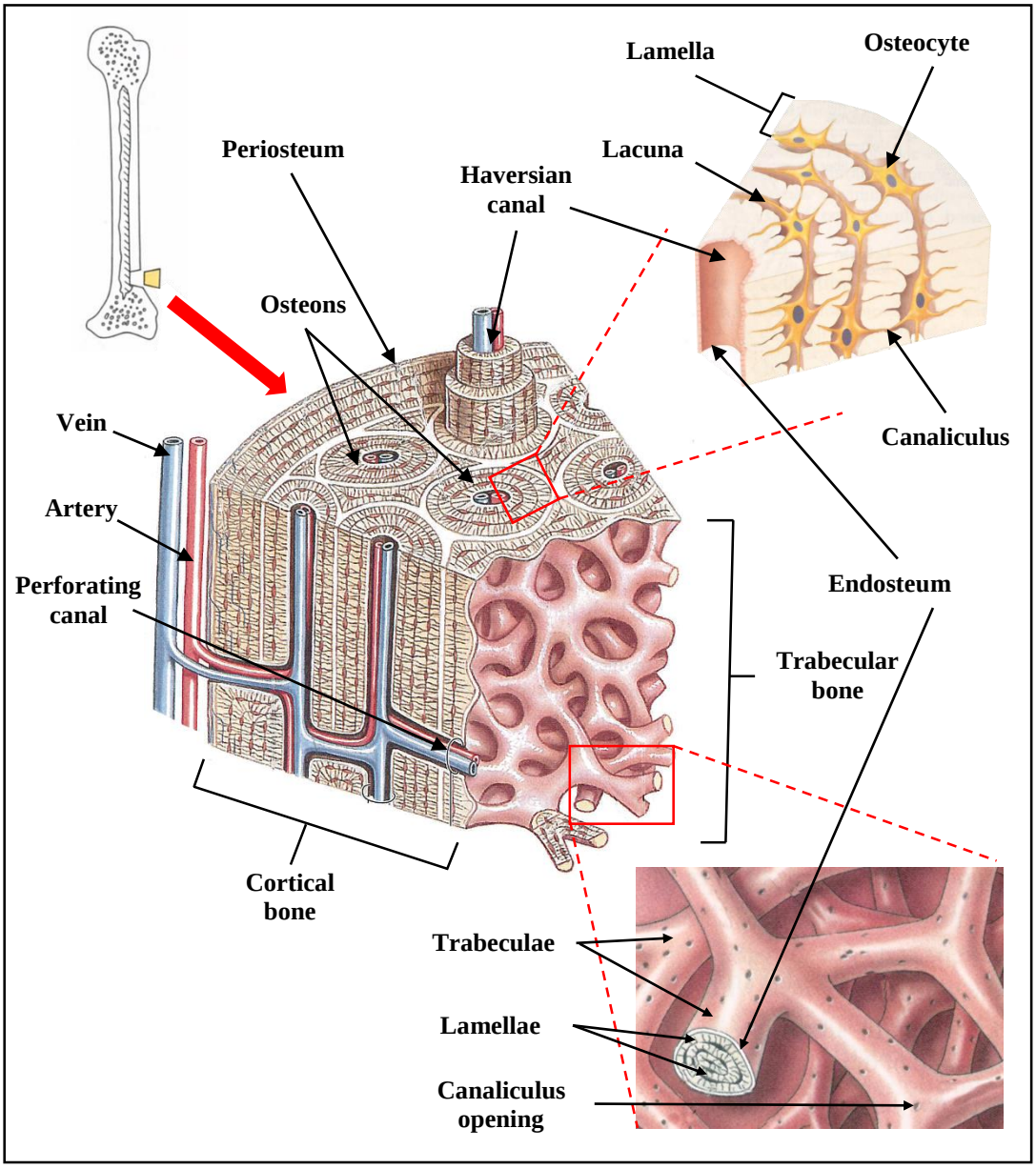

Figure 1.11 The structure of bone. A segment of bone from the wall of the humerus is shown, revealing the organisation of cortical and trabecular bone. Cortical bone comprises 80% of the skeleton and forms the outer part of all skeletal structures. It is dense and compact and functions to provide mechanical strength. The basic functional unit of cortical bone is the osteon, in which osteocytes are arranged and embedded in concentric layers (lamellae) of matrix around a central canal, called the Haversian canal. These canals contains one or more blood vessels carrying blood to and from the osteon and there are also perforating canals that extend perpendicular to the surface. Trabecular bone represents less of the skeletal mass but accounts for 80% of the bone surface area, typically found at and within the ends of long bones, and within the interior of vertebrae. This type of bone is more elastic and vascular, with a higher turnover rate than cortical bone. In this type of bone, lamellae are not arranged in osteons but instead the bone matrix forms interconnecting struts and plates called trabeculae within which lies the bone marrow. Adapted from Martini and Martini (1992) and Marieb et al. (2014).

Osteoclastogenesis begins when HSCs residing in the bone marrow or circulating peripheral blood mononuclear cells (PBMC) are committed to the monocyte/macrophage lineage, regulated by the myeloid and B cell transcription factor PU.1 (Figure 1.12). These cells (specifically cluster of differentiation (CD)14^+, $CD11b^+$ and $CD61^+$ cells) are the progenitors of osteoclasts and mice lacking PU.1 lack myeloid cells and exhibit osteopetrosis, attributed to a lack of osteoclasts (Tondravi et al., 1997, Tolar et al., 2004, Husheem et al., 2005).

Studies on the naturally occurring osteopetrotic *op*/*op* mouse model led to the identification of other key factors in osteoclastogenesis, including macrophage colony stimulating factor (M-CSF), which is mutated in *op/op* mice. M-CSF binds to the colony-stimulating factor 1 receptor (c-Fms) on monocytes/macrophages and is essential in the generation of common progenitors for macrophages and osteoclasts (macrophage colony forming units or CFU-M), as well as an essential microenvironment factor for mature osteoclast generation (Wiktor-Jedrzejczak et al., 1990, Yoshida et al., 1990, Mossadegh-Keller et al., 2013). As such, during the first stage of osteoclast differentiation, M-CSF induces the proliferation and survival of osteoclast precursors (CFU-M), and also the expression of receptor activator of nuclear factor κB (RANK), which is a prerequisite for osteoclast precursors (Arai et al., 1999, Dougall et al., 1999). Other key molecules during this stage are the transcription factor MITF and the anti-apoptotic protein Bcl-2, which are both downstream of M-CSF signalling and result in osteopetrosis and a lack of macrophages if targeted *in vivo* (Weilbaecher et al., 2001, McGill et al., 2002) (Figure 1.12).

During the final stage of osteoclastogenesis, further molecular signalling result in the fusion of osteoclast precursors at the site of bone resorption to produce a mature multinucleated osteoclast, or polykaryon. This is mainly induced by RANKL, a member of the tumour-necrosis factor family that is essential for mature osteoclast differentiation

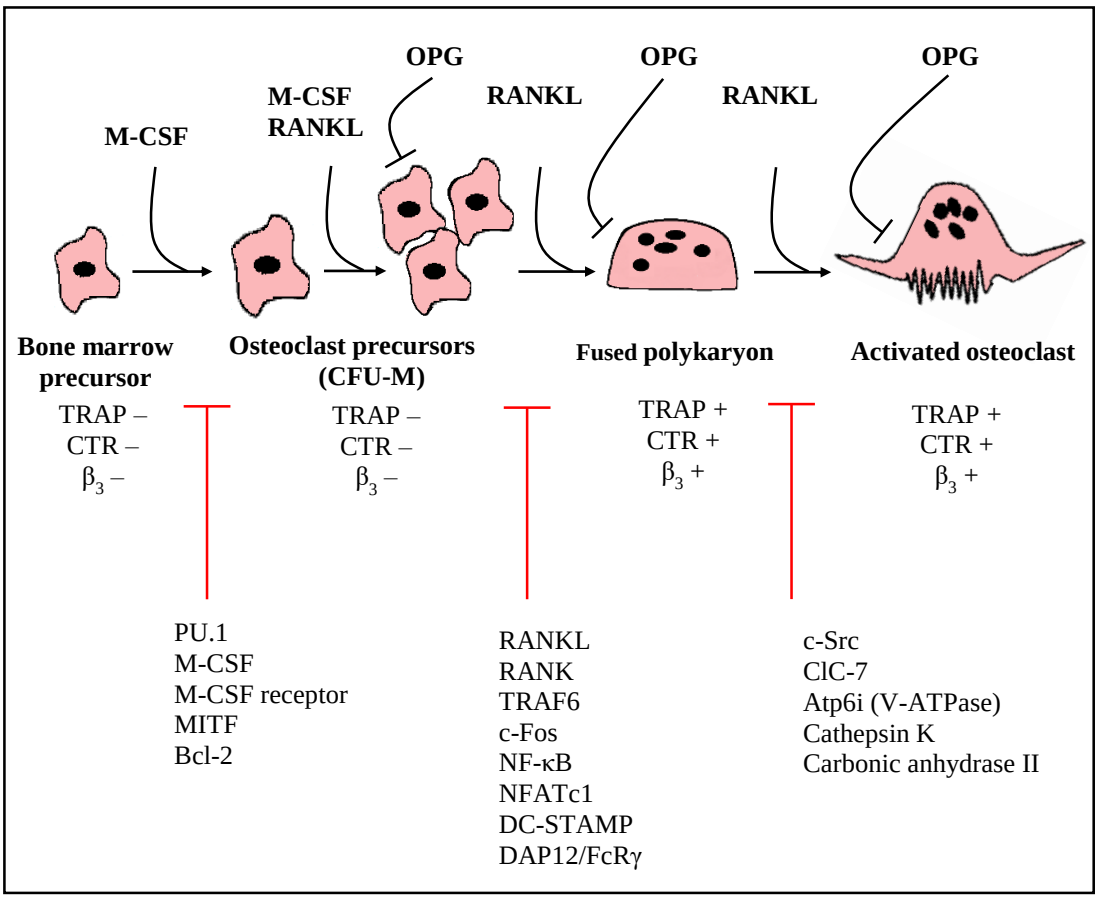

Figure 1.12 Osteoclastogenesis. A schematic illustrating the differentiation of haematopoietic precursor cells into activated osteoclasts is shown, with the expressed traits of the monocyte/macrophage/osteoclast lineage shown below each stage. These include tartrate-resistant acid phosphatase (TRAP), calcitonin receptor (CTR) and the β_3 integrin. M-CSF and RANKL are essential for osteoclastogenesis, and their involvement during differentiation is shown at the top of the figure. Osteoprotegerin (OPG) can bind RANKL and negatively regulate differentiation and activation of osteoclasts (see Section 1.7.3). Shown below are the key molecules needed for osteoclastogenesis and osteoclast activation. The first group induce differentiation of HSCs into macrophage colony-forming units (CFU-M). Defects in these molecules result in a lack of osteoclasts and macrophages. The second group induce the cellular fusion of precursors and the differentiation of multinucleated osteoclasts, mainly via RANKL. Defects here result in a lack of multinucleated osteoclasts. The third group induce the activation of osteoclasts and the commencement of bone resorption. Defects here result in non-functional, multinucleated osteoclasts. Adapted from Boyle et al. (2003) and Asagiri and Takayanagi (2007).

and survival, with co-stimulation by the adaptor proteins DAP12 and FcRγ (Anderson et al., 1997, Lacey et al., 1998, Yasuda et al., 1998, Humphrey et al., 2005). Deficiency in RANK (Li et al., 2000) or RANKL (Kong et al., 1999), as well as downstream molecules including TRAF6 (Lomaga et al., 1999, Kobayashi et al., 2001), c-Fos (Wang et al., 1992, Grigoriadis et al., 1994), NFATc1 (Ishida et al., 2002, Takayanagi et al.,

2002) and DC-STAMP (Kukita et al., 2004, Yagi et al., 2005), have all been shown to cause osteopetrosis due to a lack of multinucleated osteoclasts, despite normal or increased numbers of monocyte/macrophages (Asagiri and Takayanagi, 2007) (Figure 1.12).

A third set of key molecules determine the activation of mature osteoclasts, and the commencement of bone resorption. These include c-Src, a non-receptor tyrosine kinase, as well as ClC-7 (chloride channel), cathepsin K (protease) and *Atp6i* (V-ATPase), which are directly involved with the bone resorption process (see Section 1.7.1.2). Mice deficient in these molecules have severe osteopetrosis caused by non-functioning osteoclasts (Soriano et al., 1991, Gowen et al., 1999, Li et al., 1999, Kornak et al., 2001). Both M-CSF and RANKL are now known to be necessary, and sufficient, to induce expression of genes that typify the osteoclast lineage, including tartrate-resistant acid-phosphatase (TRAP), calcitonin receptor (CTR) and the β_3-integrin (Lee et al., 1995, Lacey et al., 1998, Boyle et al., 2003) (Figure 1.12).

Signalling is transduced via RANK through recruiting adaptor molecules such as the TRAF family (Inoue et al., 2000). Through knockout studies mentioned above, TRAF6 was identified as the major essential adaptor molecule, where the RANKL-induced binding of TRAF6 to RANK induces the activation of upstream pathways that activate NF-κB, NFATc1 and AP-1, as well as mitogen-activated protein kinases (MAPK) ERK1/2, JNK1/2 and p38, and other protein kinases such as IKK, c-Src and AKT (Boyle et al., 2003, Teitelbaum and Ross, 2003, Asagiri and Takayanagi, 2007). Whilst RANKL is generally considered as the factor that directly controls osteoclastogenesis, M-CSF is also important for later differentiation stages through activation of AKT, ERK, c-Fos, and c-Src pathways (Ross and Teitelbaum, 2005). Activation of these important signalling cascades are thought to be crucial for osteoclast differentiation, survival, activation and function, though some require *in vivo* evidence

of involvement, and many other details of RANKL/M-CSF-induced signalling cascades are still under investigation.

1.7.1.2 Osteoclast function

Mature osteoclasts are polarised cells with specialised membrane domains including the sealing zone, ruffled border and the basolateral (upper) membrane which also contains the functional secretory domain (Väänänen and Laitala-Leinonen, 2008) (Figure 1.13 A). The sealing zone is a circular attachment of the plasma membrane to the underlying mineralised bone substrate, initiated and facilitated by the integrin receptors, such as $\alpha_v\beta_3$, which bind to amino acid motifs in bone matrix proteins (Nesbitt et al., 1993, McHugh et al., 2000).

Bone resorption by osteoclasts involves the extracellular acidification of the sealing zone compartment adjacent to the substrate surface, which leads to the demineralisation and subsequent degradation of the bone matrix. Osteoclasts undergo several cycles of resorption before apoptosis, with each cycle lasting several hours, observed by monitoring phalloidin-stained actin ring formation and disappearance *in vitro* (Lakkakorpi et al., 1989, Lakkakorpi and Väänänen, 1996). During these cycles, the cytoskeleton undergoes dynamic rearrangement with the F-actin ring following the shape of the sealing zone during resorption. The sealing zone is initially marked by a belt of adhesion structures called podosomes, consisting of a core of F-actin bundles, covered by a vinculin-talin-β-integrin complex which anchors actin filaments to the membrane (Marchisio et al., 1988, Kanehisa et al., 1990). The function of the sealing zone is to form a tight seal between the substrate and the cell in order to isolate the resorptive space and prevent the loss of cellular secretory products during resorption (Lakkakorpi and Väänänen, 1996). The basolateral membrane is the non-bone-facing

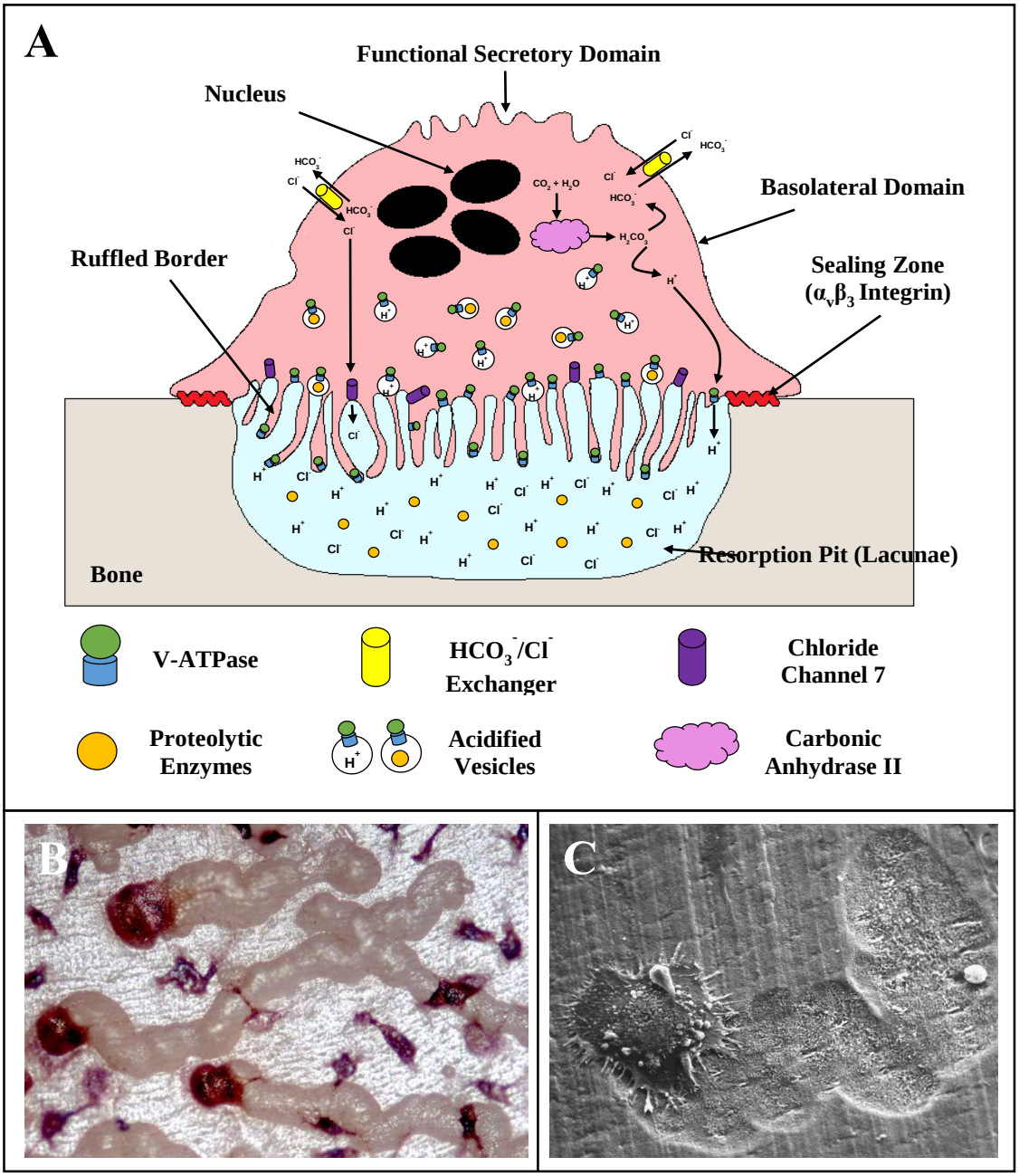

Figure 1.13 Overview of the activated osteoclast. A schematic cross-section of a polarised, resorbing osteoclast and the specialised membrane domains are shown **(A)**. Initiation of bone resorption is dependent on the attachment of the osteoclast to the bone surface and the formation of a sealing zone which isolates the underlying resorption space. The ruffled border forms from the fusion of acidified vesicles containing V-ATPases and proteolytic enzymes. The V-ATPases pump protons into the resorption space, generated by the activity of carbonic anhydrase II. Chloride ions, imported via HCO_3^-/Cl^- exchangers in the basolateral domain, are also pumped into the resorption space through ClC-7, thereby maintaining intracellular pH. The degradation of the mineralised component of bone by the acidic pH in the resorption space occurs alongside proteolytic degradation of the organic component of bone, ultimately leaving a resorption pit. Tartrate-resistant acid phosphatase (TRAP) stained mature osteoclasts are imaged on a substrate of dentin, with tailing tracks showing the result of their resorption activity (photo courtesy of Prof Tim Arnett) **(B)**. Scanned electron micrograph of an osteoclast carrying out bone resorption (image courtesy of Prof Alan Boyde) **(C)**.

plasma membrane and contains the functional secretory domain, which has a slightly ruffled morphology and serves for the secretion of the digested bone matrix following transcytosis (Nesbitt and Horton, 1997, Salo et al., 1997). The basolateral membrane also contains a bicarbonate HCO_3/Cl^- exchanger which is important in maintaining intracellular electron neutrality during bone resorption (Teti et al., 1989).

The ruffled border is the most prominent feature of a resorbing osteoclast and serves two purposes: The secretion of protons and proteases to digest the bone matrix, and the endocytosis of digested material to be trancytosed across the cell and released at the functional secretory domain. It forms within the sealing zone of the osteoclast from the result of fusion with targeted transport vesicles, and is composed of numerous extensions and invaginations of the plasma membrane, giving it a ruffled appearance (Väänänen et al., 1990, Palokangas et al., 1997).

The secretion of protons across the ruffled border and into the sealed extracellular space between the bone surface and the cell is carried out by the actions of V-ATPases localised to the ruffled border (Blair et al., 1989, Väänänen et al., 1990). Osteoclasts are the only cells with the ability to resorb bone and the osteoclast V-ATPase is crucial to this function. This was demonstrated by disruption of the osteoclast V-ATPase by antisense DNA and small interfering RNAs, or by mutations in genes encoding specific V-ATPase subunits, all of which resulted in reduced resorption activity leading to osteopetrosis in both mice and humans (Laitala-Leinonen and Vaananen, 1999, Li et al., 1999, Frattini et al., 2000, Scimeca et al., 2000, Michigami et al., 2002, Hu et al., 2005b, Lee et al., 2006). Furthermore, bafilomycin **(27)**, an established non-specific V-ATPase inhibitor, has been shown to reduce bone resorption *in vitro*, highlighting the potential of pharmacologically inhibiting the osteoclast V-ATPase in order to treat osteolytic diseases characterised by excessive resorption (see Section 1.7.4) (Sundquist et al., 1990, Sundquist and Marks, 1994, Yuan et al., 2010).

Osteoclasts require a high efflux of protons across their plasma membranes during resorption, involving high densities of V-ATPases localised at the ruffled border. This is thought to be achieved by insertion of fully assembled V-ATPases derived from specialised populations of intracellular vesicles (Blair et al., 1989, Väänänen et al., 1990, Palokangas et al., 1997). Intracellular vesicles containing the V-ATPases are targeted to the ruffled border during resorption and then endocytosed during periods when resorption is not taking place, though the precise mechanisms regulating V-ATPase recycling have yet to be determined (Qin et al., 2012b). However, modulation of the actin cytoskeleton is thought to play an important role, as both isoforms of V-ATPase subunit *B* (*B1*, *B2*) have been shown to directly bind to actin in an association that is thought to facilitate recruitment of V-ATPases to the ruffled border, directed by PI3K signalling (Holliday et al., 2000, Chen et al., 2004, Zuo et al., 2006).

The pool of cytoplasmic protons used for extracellular acidification are generated by carbonic anhydrases (Hall and Kenny, 1987) with the subsequent bicarbonate accumulation counteracted by bicarbonate/chloride exchangers on the basolateral domain (Teti et al., 1989). Also located at the ruffled border is the chloride channel, ClC-7, which enable a concurrent chloride ion flow alongside the protons, allowing for electroneutral secretion (Kornak et al., 2001). The resulting proton and chloride ions in the extracellular resorptive space form hydrochloric acid (HCl), producing an acidic pH of ~4.5, which dissolves the hydroxyapatite component the bone matrix, exposing the organic collagenous component (Qin et al., 2012b). This is then digested enzymatically by secreted cathepsin K and matrix metalloproteinases (MMPs) such as MMP-9 or MMP-13 (Nakamura et al., 2004, Everts et al., 2006). Osteoclasts also express and secrete TRAP (Figure 1.13 B), a marker for mature osteoclasts which is thought to be involved in dephosphorylating bone matrix proteins such as bone sialoprotein, a necessary step for integrin binding and generating reactive oxygen

species involved in matrix degradation (Halleen et al., 1999, Hayman and Cox, 2003, Vääräniemi et al., 2004). The combined actions of matrix demineralisation and degradation cause bone resorption leaving a resorption lacuna (Figure 1.13 C).

1.7.2 Osteoblasts

1.7.2.1 Osteoblastogenesis

Osteoblasts secrete the organic bone matrix that subsequently becomes mineralised. Osteoblasts are mature, cuboidal-shaped cells derived from mesenchymal stem cells (MSCs) that terminally differentiate to bone-lining cells and osteocytes(Figure 1.14). As the major bone-forming cells, osteoblasts produce a unique

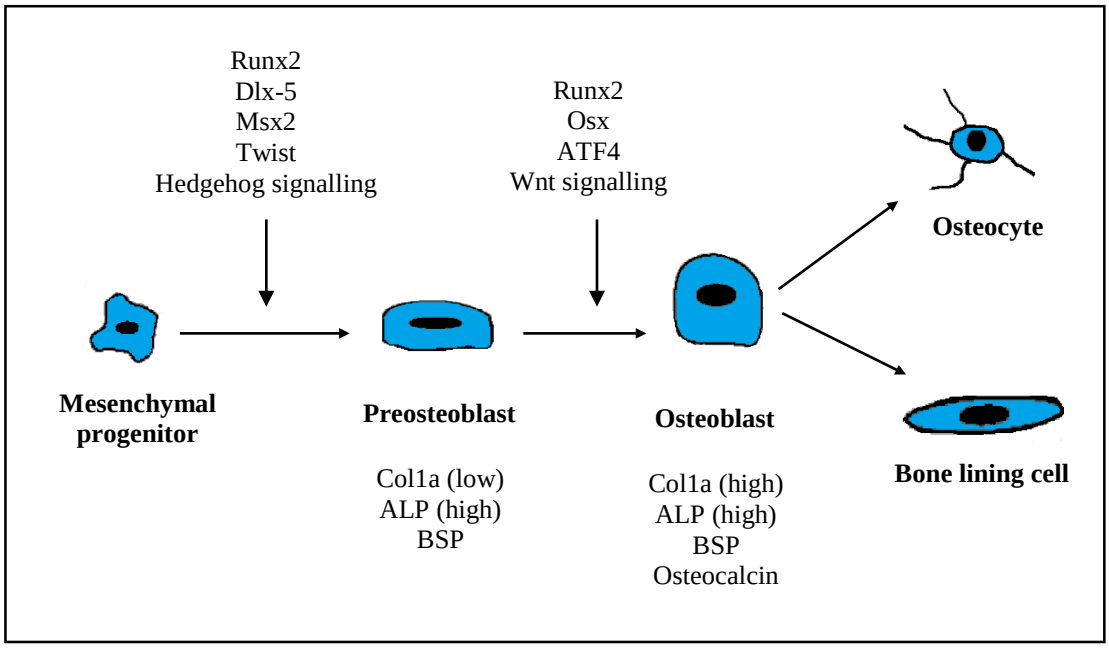

Figure 1.14 Osteoblastogenesis. A schematic illustrating the differentiation of osteoblasts from mesenchymal progenitors is shown. The process starts with the differentiation of preosteoblasts from MSCs, in which Runx2 plays an essential role. In the next step, preosteoblasts differentiate into osteoblasts, in which Osx is critical. Key inducers of osteoblast differentiation are shown above black arrows for each stage. The marker genes expressed by preosteoblasts and osteoblasts are shown below. These include collagen 1a (Col1a), alkaline phosphatase (ALP), bone sialoprotein (BSP) and osteocalcin. The terminally differentiated osteocytes and bone lining cells are also shown. Adapted from Zhang (2010) and Robling et al. (2006).

combination of extracellular proteins such as osteocalcin, alkaline phosphatase (ALP) and type I collagen, which aid in their identification. Osteoblasts deposit osteoid, the organic, unmineralised extracellular matrix composed mainly of type I collagen, which is subsequently mineralised through the precipitation of hydroxyapatite crystals (see Section 1.7.2.2). Contrary to osteoblasts, the identities and molecular markers for the mesenchymal progenitors and preosteoblasts are less well defined and understood, as the heterogeneous preosteoblasts are represented by all cells transitioning from progenitors to mature osteoblasts (Long, 2012).

Following bone-forming activity, a subset of osteoblasts can become embedded in the bone matrix as osteocytes. Osteocytes function as mechanosensors and are important regulators of osteoclasts and osteoblasts, responding to damage, hormonal signals, and changes in mechanical loading through the formation of an extensive network of cytoplasmic processes that extend throughout the bone matrix in tiny canals called canaliculi (Martini and Martini, 1992, Heino et al., 2002, Galli et al., 2010, Bonewald, 2011) (Figure 1.11). Osteocytes secrete sclerostin, a negative regulator of osteoblast activity, which is also used as a marker for this cell type (Poole et al., 2005). Other osteoblasts undergo apoptosis or become the quiescent bone-lining cells that are found on the surfaces of newly formed bone structures, exhibiting a flattened and elongated morphology (Miller et al., 1989, Bonewald, 2011). Bone-lining cells are thought to have roles coupling bone resorption to bone formation (Everts et al., 2002, Andersen et al., 2009) (see Section 1.7.3).

Osteoblast differentiation begins with the local proliferation of MSCs residing in the marrow forming osteoblast progenitors (Robling et al., 2006). Only 15% of MSCs have the capacity to form bone (Wu et al., 2000) and they are directed towards the osteoblast phenotype, and away from adipocyte, myocyte and chondrocyte lineages by expression of the runt-related transcription factor-2 (Runx2) (Ducy et al., 1997). Mice

deficient in Runx2 lack osteoblasts and show skeletal abnormalities, demonstrating the importance of this factor in osteoblastogenesis (Komori et al., 1997, Otto et al., 1997). Further gene deletion studies have shown that the Runx2 pathway involves additional transcription factors, including distal-less homeobox-5 (Dlx5), muscle segment homeobox homologue-2 (Msx2) and basic helix-loop-helix transcription factors (Twist proteins) (Bendall and Abate-Shen, 2000, Robledo et al., 2002, Bialek et al., 2004). At this point the preosteoblasts express type I collagen and bone sialoprotein with further differentiation into a mature, bone-forming phenotype requiring the sustained expression of Runx2 as well as osterix (Osx), a zinc finger-containing transcription factor that is essential for osteoblast differentiation and bone formation, and activating transcription factor 4 (ATF4) (Nakashima et al., 2002, Yang et al., 2004) (Figure 1.14).

Osteoblast differentiation is also indirectly modulated by components of the Wnt/β-catenin pathway, where a high level of β-catenin commits progenitors to osteoblast differentiation whilst low expression is important for chondrogenesis (Hu et al., 2005a, Milat and Ng, 2009). Other important factors for osteoblast differentiation are bone morphometric protein (BMP) signalling (Bandyopadhyay et al., 2006), Hedgehog signalling (Long et al., 2004), Notch signalling (Hilton et al., 2008) and fibroblast growth factors (FGF) (Montero et al., 2000). Once mature, osteoblasts express type I collagen and osteocalcin, as well as alkaline phosphatase (ALP), a key enzyme in the mineralisation process (Robling et al., 2006).

1.7.2.2 Osteoblast function

Osteoblasts have abundant mitochondria, enlarged Golgi and extensive endoplasmic reticulum, all of which are consistent with the capacity to synthesise collagen and other extracellular matrix (ECM) proteins. These cells are also rich in

secretory vesicles containing the ECM proteins which form osteoid. Mineralisation of the osteoid occurs after a time lag of approximately 10 days and begins with nucleation, the formation of an initial hydroxyapatite crystal. The exact mechanisms of this process are still not clear with three modes of nucleation having been proposed. One theory suggests that crystals are actively nucleated from solution by charge proteins in the collagen gap zones without any intervention from cellular processes (Glimcher and Muir, 1984). Another theory suggests that initial nucleation takes place in the 100 nm-wide extracellular matrix vesicles that bud from the plasma membrane of osteoblasts and are seeded within the ECM. Initial crystals are generated inside the vesicles, controlled by alkaline phosphatase (ALP) and calcium binding proteins (Ali et al., 1970), before the breakdown of the vesicular membrane and further crystal proliferation is governed by extracellular conditions (Anderson, 1995).

A more recent theory suggests that disordered calcium phosphate material is formed in matrix vesicles intracellularly before being exocytosed and deposited in the collagen gap zones where it crystallises, a strategy known to be employed in the formation of fish fin-bones and by various invertebrates (Mahamid et al., 2011). Several proteins secreted by osteoblasts are required for proper mineralisation, including ALP and osteocalcin, the ablation of which results in hypomineralisation of the skeleton (Tesch et al., 2003) and impaired mineral maturation (Boskey et al., 1998) respectively. ALP and osteocalcin are therefore used as markers for osteoblastic activity.

1.7.3 Bone remodeling and coupling factors

Bone remodeling is carried out by the coordinated actions of osteoclasts and osteoblasts, together known as the “Basic Multicellular Unit” (BMU). Bone remodeling takes place asynchronously throughout the skeleton with resorption activity in an adult

BMU taking approximately 3 weeks, and the formation response 3 to 4 months (Sims and Martin, 2014). The dynamics of bone remodelling were first described by Frost (1964) over 50 years ago, in which the BMU was thought to consist of two cell types, osteoclasts and osteoblasts, that act in close apposition and regulate the function of each other through production of inhibitory and stimulatory factors. The different processes of bone remodeling in cortical and trabecular bone are shown in Figure 1.15.

The coupling of a BMU is tightly controlled, coordinated by signalling cross-talk between the relevant cell types via local factors, as well as matrix-derived signals and systemic hormones, which together ensure that the removal of old bone is always followed by the formation of new bone (Parfitt, 2000, Sims and Gooi, 2008). In healthy individuals, coupling is a finely balanced process but any disruptions to this balance can lead to metabolic bone diseases characterised either by low bone mass such as osteoporosis, attributed to excessive resorption by osteoclasts leading to increased fracture risk, or by high bone mass such as osteosclerosis or osteopetrosis, attributed to a net imbalance favouring bone formation (Zaidi, 2007).

The application of an *in vitro* method of osteoclast generation involving the co-culture of bone marrow cells with osteoblasts demonstrated the importance of cellular contact between osteoclast precursor cells and osteoblasts, and led to the identification of RANKL (Jimi et al., 1996, Suda et al., 1999). The discovery of RANKL represented a major advance in bone biology and has greatly facilitated *in vitro* osteoclastogenesis, where it is now well established that cells of the monocyte/macrophage lineage, obtained from bone marrow or peripheral blood, can be differentiated into mature, functional osteoclasts by adding recombinant M-CSF and RANKL to the culture medium (Yasuda et al., 1998, Suda et al., 1999). Both M-CSF and RANKL are primarily produced by osteoblast lineage cells, meaning that the cell lineage that performs bone formation also

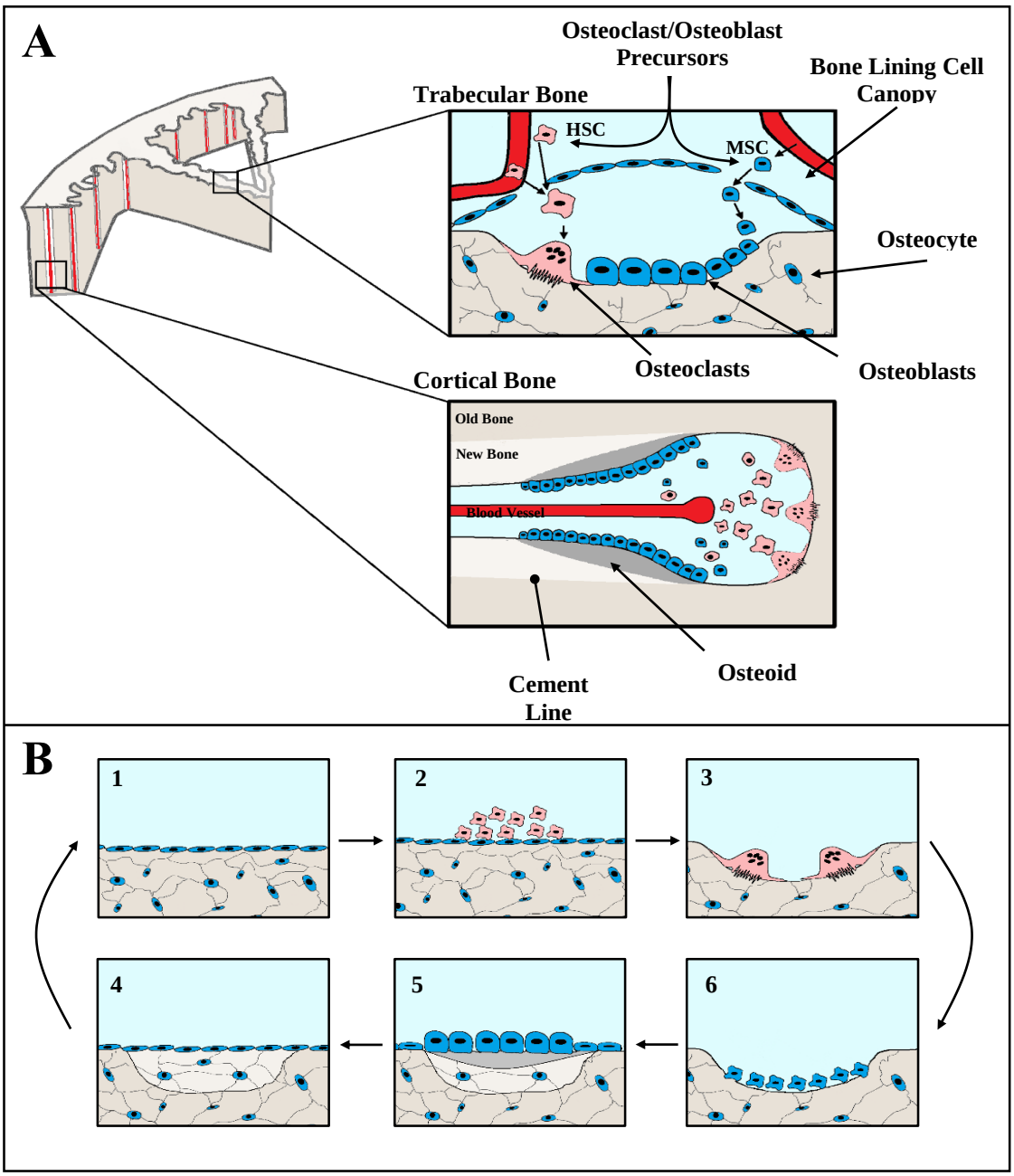

Figure 1.15 Cells of basic multicellular units (BMU) during bone remodeling. Bone remodeling is initiated beneath a canopy of bone lining cells in trabecular bone (upper panel) and within cortical bone Haversian canals (lower panel) **(A)**. Osteoclasts are derived from hematopoietic stem cells (HSC), osteoblasts are derived from mesenchymal stem cells (MSC), both via the marrow and blood. Lining cells may also differentiate into active osteoblasts and vice versa. A scheme representing the bone remodeling cycle is also shown **(B)**: 1. Bone lining cells cover the quiescent surface of bone. 2. Upon signals derived from apoptotic osteocytes, preosteoclasts are recruited to the bone surface. 3. Mature osteoclasts form and perform bone resorption. 4. A group on mononuclear cells, believed part of the osteoblast lineage, line the resorptive cavity during the reversal phase. The exact function of these cells is unknown but may smooth the cavity in preparation for the deposition of new bone matrix. 5. Osteoblasts secrete matrix proteins in the form of osteoid which subsequently mineralises to become new bone. 6. Osteoblasts become apoptotic or differentiate into osteocytes or bone lining cells and the bone surface is again quiescent. Adapted from Sims and Martin (2014) and Burr and Allen (2013).

stimulates osteoclast differentiation (Wiktor-Jedrzejczak et al., 1990, Kong et al., 1999, Pixley and Stanley, 2004, Nakashima et al., 2011). At the same time RANKL was discovered, the soluble decoy receptor osteoprotegerin (OPG) was also found to be produced by osteoblastic cells, which inhibits osteoclastogenesis by competitively binding to RANKL preventing the induction of RANK-signalling in osteoclasts (Simonet et al., 1997, Yasuda et al., 1998). Bone remodeling is thus coordinated by RANKL:OPG expression in osteoblastic cells, stimulating osteoclastogenesis and bone resorption by increasing RANKL expression and decreasing OPG, which is then closely followed by local osteoblast-mediated bone formation (Boyle et al., 2003) (Figure 1.16).

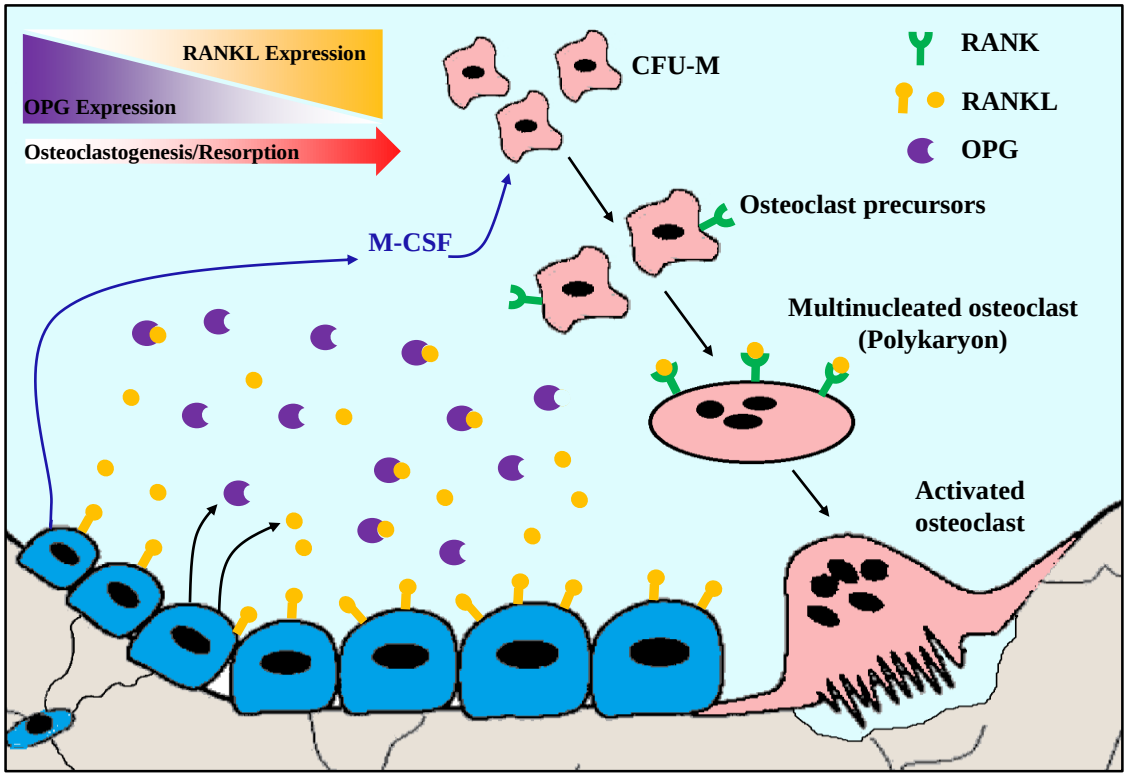

Figure 1.16 Regulation of osteoclast differentiation by the osteoblast lineage. The release of M-CSF by osteoblastic cells stimulates osteoclast precursors to express RANK. RANKL is also secreted by osteoblastic cells and can either bind to RANK on the surface of osteoclast precursors to promote osteoclast differentiation, or it can bind to the decoy receptor OPG, impeding osteoclast differentiation. OPG is also secreted by cells of the osteoblast lineage and so the ratio of RANKL to OPG is critical for determining *in vivo* osteoclast numbers and bone resorption, as shown by the schematic in the top left corner. Adapted from Sims and Martin (2014)

Various local and systemic factors, including cytokines and paracrine signals, exhibit an effect on bone remodeling via signals to the osteoblast/stromal cell, which are then transduced into the appropriate ratio of RANKL:OPG (Hofbauer et al., 2000, Martin, 2004). Parathyroid hormone (PTH), for example, is classically regarded as a hormone that stimulates bone resorption, mediated by the ability to induce production of RANKL by the osteoblast lineage (Fu et al., 2002). Other factors that have been shown to upregulate RANKL-induced bone resorption include TNF-α, vitamin D_3, PTH-related peptide (PTHrP), glucocorticoids, prostaglandin E_2, insulin-like growth hormone 1 (IGF-1) and interleukins (IL), such as IL-1, IL-6 and IL-17 (Hofbauer et al., 1999, Li et al., 2000, Ma et al., 2001, Liu et al., 2005, Lee et al., 2008). Conversely, oestrogen negatively regulates bone resorption by increasing OPG and decreasing RANKL expression in osteoblastic cells, as well as reducing osteoclast survival and stimulating osteoblast proliferation (Kameda et al., 1997, Saika et al., 2001, Srivastava et al., 2001, Eghbali-Fatourechi et al., 2003, Nakamura et al., 2007). The loss of oestrogen in postmenopausal women therefore results in increased osteoclast survival and resorption, ultimately leading to osteoporosis. Another negative regulator of bone resorption is calcitonin, which directly inhibits resorption through specific receptors on the osteoclasts (Zaidi et al., 2002).

However, in contrast to the catabolic effect of PTH, intermittent administration of PTH can be used therapeutically to increase bone formation and bone mass in menopausal women (Neer et al., 2001). This is due to the direct effects of PTH on the osteoblast lineage where it promotes osteoblast differentiation (Dobnig and Turner, 1995), inhibits osteoblast apoptosis (Jilka et al., 1999, Stanislaus et al., 2000) and reduces the production of the bone formation inhibitor sclerostin (Keller and Kneissel, 2005). As PTH appears to stimulate both bone formation and resorption, it has been suggested that the anabolic effect of PTH is dependent on the ability to stimulate

osteoclast activity, implying that osteoclasts are an essential intermediate for the anabolic effect (Koh et al., 2005). Furthermore, the anabolic effect of intermittent PTH therapy was reduced when bisphosphonates were used concomitantly, also indicating the required presence of osteoclasts for the anabolic effect of PTH (Delmas et al., 1995, Coxon et al., 2006). The anabolic effects of intermittent PTH therapy therefore suggest the involvement of osteoclast-derived coupling factors that function to stimulate bone formation. Work by Karsdal et al. (2008) and Henriksen et al. (2012a) also presented compelling evidence for the existence of an osteoclast-derived coupling factor, as conditioned media from human osteoclasts, cultured on either bone or plastic, led to a dose dependent increase in bone nodule formation by primary osteoblasts, indicating the presence of stimulatory factor(s) produced by the osteoclasts independent of bone resorption.

Whilst the major osteoblast-derived coupling factors have been understood for many years now, in recent years there has been great interest in identifying the putative osteoclast-derived coupling factors. Such candidates have included factors that are released from the bone matrix during bone resorption such as IGF-1 or TGFβ (Hayden et al., 1995, Tang et al., 2009), as well as other factors secreted by both inactive and active osteoclasts which are shown to have positive effects on osteoblasts. These include cardiotrophin-1 (Walker et al., 2008), ephrinB ligands (Zhao et al., 2006, Sims, 2010), sphingosine-1-phosphate, BMP6 and Wnt10b (Ryu et al., 2006, Pederson et al., 2008, Ishii et al., 2009), collagen triple helix repeat containing 1 (CTHRC1) (Takeshita et al., 2013) and semaphorin 4D (Negishi-Koga et al., 2011). None of these are exclusively expressed by osteoclasts and further *in vivo* studies are needed to determine their roles as coupling factors. However, the implication of an osteoclast-derived coupling factor has significant consequences for treating imbalances in bone remodeling and for developing novel effective therapeutics, as discussed in the following section.

1.7.4 Osteolytic bone diseases and the osteoclast V-ATPase

Osteolytic bone diseases are caused by disturbances to bone remodeling in the form of enhanced osteoclast activity, leading to increased bone resorption, hypercalcemia and a loss of bone mass. This activity is observed in osteopathic disorders such as osteoporosis, Paget's disease, primary bone tumours, multiple myeloma as well as lytic bone metastases (Goltzman, 2001, Heymann et al., 2005, Guise et al., 2006, Chamoux et al., 2009). Osteoporosis, specifically, represents a serious worldwide health problem, as the consequent increase in bone fragility leads to increased risk of fracture, particularly in the hip, wrist and vertebrae (Seeman, 2003, Johnell and Kanis, 2005). In the UK, the lifetime risk of an osteoporotic fracture at age 50 is 53 % and 21 % for women and men respectively, with the increased risk of hip fracture a major concern due to the associated high morbidity, mortality and loss in quality of life (Van Staa et al., 2001). Global estimates suggest there are 1.25 million osteoporotic hip fractures each year, predicted to increase by 310 % in men and 240 % in women due to the aging of the population, and leading to predicted costs of $131.5 billion by 2050 (Gullberg et al., 1997, Johnell, 1997). It is thus worthwhile and important to prevent osteoporotic fractures, and treating high risk osteoporotic patients with drugs known as antiresorptives has been shown to be a cost-effective solution (Johnell and Kanis, 2005).

Currently the most widely used treatments for osteolytic diseases are the bisphosphonates, such as alendronate and zoledronate (Chen and Sambrook, 2012). Bisphosphonates are synthetic analogues of inorganic pyrophosphate and bind to bone mineral surfaces *in vivo*. Upon release following bone resorption, bisphosphonates inhibit the formation, activity and survival of osteoclasts through disruption of key enzymes involved in the isoprenylation of small GTPases, which are required for osteoclast polarisation and vesicular trafficking (Coxon et al., 2006). In addition to

bisphosphonates, there are also other antiresorptive compounds such as selective oestrogen receptor modulators (SERMS), denosumab (monoclonal antibody to RANKL) and calcitonin (Chen and Sambrook, 2012). However, whilst all of these treatments have been shown to be effective inhibitors of bone resorption, a common secondary effect is the suppression of bone turnover and a decrease in bone formation that can lead to atypical bone fractures and osteonecrosis (Ott et al., 2002, Odvina et al., 2005, McClung et al., 2006, Karsdal et al., 2007, Lenart et al., 2008). The cause of reduced bone formation is likely a result of the inhibitory mechanisms of the antiresorptives, which involve eliminating or reducing the number of osteoclasts leading to decreased bone formation due to coupling with osteoblasts (Karsdal et al., 2007, Henriksen et al., 2011a).

An ideal treatment for osteolytic diseases is the use of an antiresorptive that uncouples bone remodeling so that bone formation can occur independently of bone resorption, leading to a net gain in bone tissue (Thudium et al., 2012). Analyses of the phenotypic characteristics of osteopetrosis mutations in humans has indicated that the osteoclast ruffled border V-ATPase may be a promising target to uncouple bone resorption from bone formation. Osteopetrosis is divided into three groups based on severity: Autosomal dominant osteopetrosis (ADO), where the phenotype ranges from mild to asymptomatic; autosomal recessive osteopetrosis (ARO), the most severe group; and intermediate autosomal recessive osteopetrosis (IARO). ADO is caused by dominant negative mutations in ClC-7, the chloride ion-proton antiporter that ensures ion homeostasis in resorbing osteoclasts (Cleiren et al., 2001, Del Fattore et al., 2008). ARO on the other hand is caused by homozygous mutations in either CIC-7 (Kornak et al., 2001, Frattini et al., 2003), RANK/RANKL (Sobacchi et al., 2007, Guerrini et al., 2008) or the *a3* subunit of the V-ATPase (Frattini et al., 2000, Kornak et al., 2000). Of all the mutations causing osteopetrosis, mutations in the *a3* isoform gene (TCIRG1) are

responsible for approximately 50% of cases of malignant osteopetrosis, resulting in symptoms that include high bone density, propensity to fractures and no marrow cavity (Frattini et al., 2000, Michigami et al., 2002).

Interestingly, mutations of the *a3* V-ATPase subunit or ClC-7, were found to cause uncoupling of bone remodelling, where resorption was inhibited but bone formation was normal or increased. Observations at the cellular level showed that patients with defects in acid secretion had high numbers of osteoclasts that showed normal polarisation and interaction with the bone surface, but no bone resorption due to inhibited extracellular acidification (Flanagan et al., 2000, Frattini et al., 2000, Del Fattore et al., 2006). These patients were also found to have correlating numbers of osteoblasts resulting in normal or increased bone formation, demonstrating the uncoupling of bone remodeling (Bollerslev et al., 1993, Del Fattore et al., 2006, Karsdal et al., 2007). In contrast to the osteoclast-rich osteopetrosis models are the osteoclast-poor osteopetrosis models where mutations in RANK/RANKL, or M-CSF lead to low numbers of osteoclasts, causing patients to have both lowered bone resorption and formation with no uncoupling of bone remodeling (Dobbins et al., 2002, Dai et al., 2004, Sakagami et al., 2005, Segovia-Silvestre et al., 2009).

These observations support the evidence that osteoclasts mediate anabolic signals to osteoblasts, emphasising the importance of sustaining osteoclast populations during treatment of bone remodeling disorders. Additionally, they suggest that attenuating the acid secretion machinery of osteoclasts is a way to uncouple bone resorption from bone formation, providing the ideal therapeutic scenario for osteolytic diseases. This uncoupling was observed in the *oc/oc* mice, which have a natural mutation in the *a3* subunit of the V-ATPase, and *in vitro* effects mimicking the phenotype of osteoclast-rich osteopetroses have also been observed using inhibitors of V-ATPases (Li et al., 1999, Karsdal et al., 2005, Sorensen et al., 2007). It was also shown that if

osteopetrosis was induced in wild-type mice using fetal liver-derived HSCs from the *oc/oc* mice, bone formation and bone strength were increased, confirming that attenuation of acid secretion through targeting the V-ATPase can lead to uncoupling and anabolic activity (Henriksen et al., 2011b).

Interestingly, *ex vivo*-generated osteoclasts from *a3*-mutant mice, as well as osteoclasts with siRNA mediated knockdown of *a3* had defective extracellular acidification but showed normal osteoclastogenesis and normal intracellular pH homeostasis, suggesting that the *a3* isoform is not involved in the latter processes (Li et al., 1999, Hu et al., 2005b). Whilst osteoclasts are known to contain subunit isoforms *a1*, *a2* and *a3*, only *a3* has been shown to be crucial for osteoclast resorption despite also being expressed in other tissues, as this isoform is dramatically upregulated during osteoclastogenesis and re-localised from lysosomes to the ruffled border during osteoclast activation (Scott and Chapman, 1998, Li et al., 1999, Manolson et al., 2003, Toyomura et al., 2003).

Other V-ATPase subunits of importance in the osteoclast are *B2, C1*, *d2* and the accessory subunit *Ac45*. There are two isoforms of subunit *d* found in humans but *d2* is expressed 5-fold higher that *d1* in human osteoclasts (Smith et al., 2005, Lee et al., 2006, Wu et al., 2009a) and like *a3*, expression is highly induced by RANKL (Feng et al., 2009b, Wu et al., 2009a). Ablation of the *d2* gene in mice was found to cause osteopetrosis, with osteoclasts from those mice showing defects in the formation of fused multinucleated cells suggesting a role for this subunit in pre-osteoclast fusion (Lee et al., 2006). The subunit isoform *C1* is also highly induced by RANKL, with a role that is thought to involve actin-binding to facilitate the recruitment of V-ATPases at the ruffled border, also attributed to the *B2* subunit. In osteoclasts, both *C1* and *B2* are expressed exclusively and localised to intracellular vesicles and the ruffled border (Bartkiewicz et al., 1995, Lee et al., 1996, Feng et al., 2009b), and depletion of *C1* caused

impaired osteoclast resorption and disrupted actin ring formation but otherwise normal differentiation (Feng et al., 2009b). The precise physiological role of *Ac45* is still unclear, though studies have shown that this subunit is essential for osteoclast-mediated bone resorption as well as osteoclast formation and maturation (Feng et al., 2008, Qin et al., 2011, Yang et al., 2012). In summary, there are specific V-ATPase subunits expressed in osteoclasts (*a3*, *B2*, *C1*, *d2*, *Ac45*), which have all been shown to localise at the ruffled border. Whilst *a3, B2* and *C1* have been shown to have roles in osteoclast activation and resorption only, *d2* and *Ac45* have shown dual roles, involved in both osteoclast differentiation and activation.

The crucial and specific involvement of the *a3* isoform in the function of bone resorption, coupled with the knowledge that certain other subunit isoforms are highly expressed and localised to the ruffled border, has led to the suggestion that the osteoclast ruffled border V-ATPase is structurally distinct from V-ATPases involved in other cellular processes. This permits the intriguing possibility of specifically targeting subunits of the ruffled border V-ATPase with inhibitors in order to attenuate osteoclast function without causing off-target effects. As seen with the osteoclast-rich osteopetroses, this should then lead to the uncoupling of bone remodeling and a net gain in bone density. As such, examination of the effects of uncharacterised V-ATPase inhibitors on osteoclasts is thus a worthwhile endeavour in the search for novel osteolytic therapeutics.

1.8 Research aims

This thesis addressed two general aims concerning the study of the sponge-derived compound 73-DOC **(22)**. The V-ATPase is crucial to the bone resorptive function of osteoclasts as well as the pathogenesis of osteolytic diseases such as osteoporosis, which is characterised by effects on both osteoclasts and osteoblasts. Previous work with 73-DOC **(22)** demonstrated V-ATPase inhibitory activity, but the effects of the compound on osteoclasts and osteoblasts have never been investigated.

Using the hypothesis that 73-DOC **(22)** will cause specific V-ATPase-mediated inhibition of osteoclastic bone resorption, the first aim of this thesis was to evaluate 73-DOC **(22)** as a novel bone resorption inhibitor and to characterise differential activity between osteoclasts and osteoblasts. This was achieved by:

- Extracting a stock of 73-DOC **(22)** from the sponge *I. ramosa* for *in vitro* testing and establishing biological activity against an osteoblastic cell line (Chapter 3).
- Determining the effects of 73-DOC **(22)** on primary osteoclast/osteoblast precursor proliferation, differentiation and mature cell viability (Chapter 4).
- Examining the effects of 73-DOC **(22)** on osteoclast activation, bone resorption and osteoblast mineralised bone nodule formation (Chapter 5).

The second aim of this thesis sought to provide a long-term solution to the supply problem of natural products alongside *in vitro* experimentation with 73-DOC **(22)**. Using the hypothesis that 73-DOC **(22)** biosynthesis involves a type I hybrid PKS/NRPS, which implies that the cloned biosynthetic genes may ultimately be expressed in a fermentable bacterial species, the second aim was to clone and sequence the PKS/NRPS gene cluster responsible for 73-DOC **(22)** biosynthesis from the sponge *I. ramosa*. This was achieved by:

- Screening a metagenomic clone library for conserved features of PKS/NRPS biosynthesis, in addition to direct sequencing of sponge-derived metagenomic DNA (Chapter 6).
- Comparison of annotated PKS sequences with a predicted model of 73-DOC **(22)** biosynthesis (Chapter 6).

Chapter 2: Materials and Methods

2.1 Extraction of 73-deoxychondropsin A

2.1.1 Materials

Samples of *I. ramosa* were collected from the central region of the Great Barrier Reef by AIMS by scuba diving at a depth of approximately 15 m. Immediately after collection, the sponges were either flash-frozen in liquid nitrogen, stored and shipped to KCL at -80 °C for DNA extractions described in Section 2.3.3, or freeze-dried for the extraction of 73-DOC and shipped at -80 °C with the flash-frozen samples. All specimens were verified to contain 73-DOC by AIMS using published methods (Rashid et al. 2001b). A 2.5 mg authentic sample of 73-DOC was also supplied by AIMS, prepared by Dr. M. Freckelton and Dr. C. Motti from the Bio-Analytical Facility, and shipped as a dry residue. The concentration was estimated with UV spectroscopy as detailed in Section 2.1.4. All solvents were sourced from Fisher Scientific (Loughborough, UK).

2.1.2 Preparation of semi-crude extract

Preparation of the semi-crude extract was carried out according to procedures previously optimised by Dr. Walt Dunlap of AIMS. Freeze-dried whole *I. ramosa* tissue (10 g) was cut up into small pieces using a disposable scalpel. The tissue was placed into 50 ml tubes and extracted with 20 % methanol for 2 hours using mild sonication. This was repeated using the same tissue 4 times, with the extracts combined after removing gross particulates by centrifugation at 4000 x *g*. The extract was then filtered through a

glass-fibre filter with a 1.5 cm bed of celite. A C18-E solid phase extraction (SPE) column from Phenomenex (Macclesfield, UK) was prepared by washing with 1 volume (50 ml) of 100 % methanol followed by water. The celite filtered extract was then applied to the column followed by 2x 50 ml washes of water and then eluted successively with 3 volumes of 90% methanol. The eluate was dried using a rotary evaporator and the residue was resuspended in 50 ml 20 % methanol. Another SPE column was prepared with 1 volume of 100 % methanol followed by 20 % methanol, before the resuspended sample was applied to the new column. This column was washed with 1 volume of 20 % methanol and then eluted with 2 volumes of 90 % methanol. This eluate represented the semi-crude 73-DOC extract and was dried using a rotary evaporator.

2.1.3 Chromatography procedures

Reversed-phase high performance liquid chromatography (HPLC) was carried out using an Agilent Technologies system (Stockport, UK). The HPLC system involves the interaction of the analyte with the stationary phase and the mobile phase, constituted of a mixture of solvents. Reversed-phase HPLC has a non-polar stationary phase and an aqueous, moderately polar mobile phase. A Phenomenex C18 Jupiter column (300Å, 5 µm, 150 x 2 mm) was used for the analytical work, using a flow rate of 0.2 ml/min and a 30 minute gradient of 10-90 % acetonitrile in water. Both the acetonitrile and water were supplemented with 0.1 % trifluoroacetic acid. Samples (10 µl) were auto-injected into the system and the UV signal was monitored at 216, 226 and 261 nm using a diode array detector and Agilent's ChemStation software, based on spectral data reported by Rashid et al. (2001b). Preparative reversed-phase HPLC was performed using the same equipment but with a preparative Whatman Partisil (GE Healthcare, Little Chalfront, UK) C18 column (10 µm, 500 x 9.4 mm) and a flow rate of 5 ml/min. Semi-crude 73-

DOC was resuspended in 10 ml of 10 % acetonitrile at a concentration of 10 mg/ml, and injected manually. The gradient and detection conditions were the same as for the analytical column, the UV signals (216, 226 and 261 nm) were monitored during each run and the relevant peak corresponding to 73-DOC was collected in 15 ml tubes. The solvents were then removed using a freeze-drier, leaving a white powder.

Liquid chromatography-mass spectrometry (LC-MS) was performed using a Thermo Accela LC system interfaced directly to a Thermo LTQ XL linear ion trap mass spectrometer, running in full scan positive ion electrospray mode (ThermoFisher Scientific, Massachusetts, USA). The chromatography column was a Hypersil Gold (1.9 µm, 50 x 2.1 mm) from Phenomenex and a flow rate of 0.2 ml/min was used. 1 mg of material was resuspended in 1 ml of 50 % methanol which was further diluted to 0.1 mg/ml before injection.

2.1.4 Spectrometry and spectroscopy procedures

Nuclear magnetic resonance spectra were recorded using a Brucker Advance DPX-400 spectrometer (Coventry, UK). The spectra were obtained from 2.5 mg of 73-DOC resuspended in deuterated methanol at 400 MHz.

UV spectroscopy was used to determine the concentration of 73-DOC. Dried 73-DOC was resuspended in 1 ml methanol, loaded into a Hellma-Analytics (Müllheim, Germany) quartz cuvette, and the absorbance of the solution at 261 nm was obtained using a spectrophotometer. Using the absorbance value and the coefficient of extinction ($\varepsilon = 36308$) reported by Rashid et al. (2001b) for 73-DOC at 261 nm, the concentration of the sample was calculated using the formula:

$$A = \varepsilon L c$$

Where A is absorbance, ε is the coefficient of extinction, L is the light path length through the cuvette (10 mm) and *c* is the concentration of the sample in mol/L. The solution of 73-DOC in methanol was then dried down and the compound was resuspended in 1 ml sterile water, aliquoted at concentrations of 1-10 µM and stored at -20 °C.

High resolution mass spectrometry (HRMS) was performed using an Exactive™ Plus Orbitrap Mass Spectrometer (ThermoFisher Scientific) running in full scan positive ion electrospray mode. The sample was delivered by direct infusion at a concentration of 1 µg/ml. Mass error estimates in parts per million (ppm) were calculated using the formula:

$$\text{Ppm} = 10^6 \times \frac{\text{measured mass} - \text{theoretical mass}}{\text{theoretical mass}}$$

2.2 *In vitro* studies with 73-deoxychondropsin A

2.2.1 Materials

All cells were cultured in minimum essential medium, alpha modification (α-MEM) (Lonza, Basel, Switzerland), supplied with ribonucleosides, deoxyribonucleosides and 2 mM L-glutamine. Cells were cultured in α-MEM containing 100 U penicillin and 100 µg/ml streptomycin from Sigma-Aldrich (Gillingham, UK), and 10 % heat-inactivated fetal bovine serum (FBS) (Lonza), batch-tested for osteoclast and osteoblast differentiation (complete culture medium). Murine recombinant RANKL and human recombinant M-CSF were purchased from R&D Systems (Bio-Techne, Abingdon, Oxford, UK). All cells were cultured at 37 °C in 5 % CO_2 in air, and media were replaced every 2-3 days.

Acridine orange was obtained from Fisher Scientific. Enzymes including trypsin, dispase and collagenase A were all obtained from Roche (Basel, Switzerland). Bafilomycin (bafilomycin A_1 - Sigma-Aldrich) was resuspended in dimethyl sulfoxide (DMSO) and stored at -20 °C in 5 µM aliquots.

All mice used were from the CD-1 strain and were housed and maintained in accordance with Home Office guidelines. Human peripheral blood was obtained from healthy adult male volunteers with approval from the KCL ethics committee (Dr Valerie Corrigall, Rheumatology, Centre for Molecular & Cellular Biology of Inflammation (CMCBI)).

Dentin slices were obtained from elephant ivory (HM Customs and Excise, Heathrow, London, UK). The ivory was cut into 250 µm-thick wafers using a diamond coated wafering blade (Buehler, Coventry, UK) and a standard hole-punch was used to produce 5 mm-diameter discs of dentin which could fit into 96-well culture plates. The dentin discs were sonicated in multiple changes of deionised water for a minimum of 3 hours before being washed in ethanol and dried in a laminar-flow cabinet.

2.2.2 MG-63 culture

The human osteosarcoma cell line, MG-63, was obtained from the American Type Culture Collection, and was used to determine the antiproliferative activity of the newly prepared 73-DOC stock using the MTS (3-(4,5-dimethylthiazol-2-yl)-5-(3-carboxymethoxyphenyl)-2-(4-sulfophenyl)-2H-tetrazolium) assay (see Section 2.2.11). MG-63 cells were maintained in 75 cm^2 culture flasks using α-MEM and 10 % FBS, and were passaged at confluence every 2-3 days.

2.2.3 Osteoclast culture

2.2.3.1 Murine osteoclast culture

Murine primary osteoclast precursors were obtained from bone marrow macrophages (BMMs) of 6-8 week old male mice as described by Orriss and Arnett (2012). Mice were killed by cervical dislocation with the femora and tibiae dissected and scraped cleaned of adherent tissue. Under sterile conditions, a 25-gauge needle was used to bore into the ends of each bone. The bone marrow of all bones was flushed out into 1 ml of α-MEM with 10 % FBS to create a single-cell suspension, and cultured overnight in complete culture medium containing 50 ng/ml M-CSF in a 75 cm^2 flask. The following day, non-adherent cells were poured through a 40 µm cell strainer and counted using a heamocytometer. These precursor cells were then either used in proliferation assays (see Section 2.2.11) or to generate mature osteoclasts.

For osteoclast differentiation, M-CSF-dependent done marrow cells were plated at 150,000 cells/cm^2 either on tissue culture plastic or directly on dentin discs in complete culture medium containing 50 ng/ml M-CSF. After 2 days, medium was changed to contain M-CSF (25 ng/ml) and RANKL (5 ng/ml). Media were replaced every 2-3 days and multinucleated osteoclasts typically formed within 3-4 days following the addition of RANKL.

For resorption analysis of mature osteoclasts, M-CSF-dependent bone marrow precursors were cultured in 24-well plates as described above. Once multinucleated osteoclasts were present, the cells were detached using Accutase® (Sigma-Aldrich) and seeded onto pre-soaked dentin discs in 100 µl of complete culture medium containing M-CSF (25 ng/ml) and RANKL (5 ng/ml), at an average of 1 well to 2 discs with treatment groups arranged in triplicate. The cells were left to adhere for 2-3 hours before

test compounds were added in an additional 100 µl of medium at 2x the desired final concentration. The cells were cultured for a further 48 hours before the experiment was terminated.

2.2.3.2 Human osteoclast culture

Human peripheral blood mononuclear cells (PBMCs) obtained from male volunteer donors were used to generate human osteoclasts using procedures similar to those described by Henriksen et al. (2012b). To isolate mononuclear cells from peripheral blood, the density gradient medium, Lymphoprep™, from Axis-Shield (Oslo, Norway) was used. Undiluted blood from a healthy volunteer was carefully layered over 20 ml of Lymphoprep™ in 4 x 50 ml tubes. The tubes were centrifuged for 20 minutes at 800 x *g* with no stopping brake. The mononuclear cell layer was removed from the Lymphoprep™/plasma interface, combined, and washed with PBS before being centrifuged at 250 x *g* for 10 minutes. This washing step was then repeated. In order to produce a more homogenous population of monocyte cells and to remove other contaminating cell types such as red blood cells, the PBMCs were sorted for CD14+ monocytes using a Dynabeads® Untouched™ Human Monocytes Kit from Life Technologies (California, USA). The kit protocol was followed, monocytes following isolation were resuspended in 10 ml of isolation buffer (PBS, 0.1% BSA and 2 mM EDTA).

The purified monocytes were then counted using a haemocytometer and cultured in 75 cm^2 flasks at a concentration of 3 x 10^6 cells/flask in complete culture medium containing 50 ng/ml M-CSF. After 2-4 days in culture, the M-CSF concentration was reduced to 25 ng/ml and RANKL was added at a concentration of 10 ng/ml. Culturing continued until mature osteoclasts were observed, usually after 7-10 days in culture.

Once present the cells were detached from the flasks using Accutase®, counted, and re-pated onto pre-soaked dentin discs in 100 µl of complete culture medium containing M-CSF (25 ng/ml) and RANKL (10 ng/ml), at a concentration of approximately 80,000 cells per disc. The cells were left to adhere for 2-3 hours before test compounds were added in an additional 100 µl of medium at 2x the desired final concentration. The cells were cultured for a further 72 hours before the experiment was terminated.

2.2.4 TRAP staining

Osteoclasts were fixed in 4 % paraformaldehyde and stained for Tartrate-Resistant Acid Phosphatase (TRAP) using the Acid Phosphatase, Leukocyte Kit (387A; Sigma-Aldrich), in the presence of 50 mM sodium-tartrate. Mature osteoclasts, defined as TRAP-positive cells with more than 3 nuclei, were either counted using bright-field microscopy with a graticule, or from images acquired using a stereomicroscope followed by ImageJ (http://imagej.nih.gov/ij/) quantification. All cell counts were made from triplicate wells in each treatment group, expressed as a percentage of the control group.

2.2.5 Actin staining

Staining of actin rings using phalloidin-TRITC (Sigma-Aldrich) was used for quantifying human osteoclasts cells. Following fixation with 4 % paraformaldehyde, cells were permeabilised with 0.1 % Triton X-100 in PBS for 5 minutes and stained with phalloidin-TRITC (1 µg/ml in PBS) for 30 minutes. Cells were visualised and imaged using a Leica fluorescence microscope (Wetzlar, Germany) with a TRTIC filter, set for emission wavelengths of 570 nm. Actin ring morphology was also used to quantify the activation state of mature osteoclasts during resorption. The number of osteoclasts

showing the actin ring morphology characteristic of resorbing osteoclasts were counted and expressed as a proportion of the total number of actin ring-positive cells (Lakkakorpi and Väänänen, 1996).

2.2.6 Acridine orange staining

Acridine orange was used to examine the extent of cellular acidification of osteoclasts in response to test conditions. Murine osteoclasts were cultured on dentin discs as described in Section 2.2.3.1 in the absence or presence of test compounds for a period of 24 hours. Thirty minutes before analysis, the culture medium was supplemented with 15 µg/ml of acridine orange, after which slices were washed and mounted on concave microscope slides for visualisation. Live cells were imaged using a Leica confocal microscope (Wetzlar, Germany), using a 63x lens and an excitation of 480 nm. Emissions in two channels set to 525 nm (green) and 650 nm (red) were captured. Image stacks were obtained for randomly chosen fields from duplicate test slices in each test group, with microscope settings maintained between test groups. The ImageJ software was then used to combine channels and produce final images.

2.2.7 Osteoclast resorption quantification

Following TRAP staining of osteoclasts, the cells were removed from the dentin discs using sonication and light brushing with a toothbrush. The dentin discs were then stained for 1 minute using a 1 % (w/v) toluidine blue in 1 % (w/v) sodium borate solution to aid visualisation. Resorption pits were imaged across the entire surface of the dentin disc using reflected light microscopy and a point-counting method was used to quantify the surface area of resorption pits (Orriss and Arnett, 2012). Resorption area estimations

were made from triplicate dentin discs for each treatment group with the data expressed as an average of total surface area or, by using matched cell count data, as an average of resorption area per cell.

The depth of resorption pits was also estimated using reflected light microscopy using the fine focus wheel of the microscope which was calibrated in microns. The maximum depth of an individual resorption pit could therefore be estimated by quantifying the distance in focus between the surface of the dentin disc and the bottom of the resorption pit. Ten randomly chosen pits per disc from triplicate samples were quantified.

2.2.8 Osteoblast culture

Primary murine osteoblast precursors were obtained from the calvaria of 4-5 day old CD-1 mice of mixed sex, as previously described Harmey et al. (2004). For each isolation, a whole litter of pups was used. Following cervical dislocation, the calvaria (frontal and parietal bones) were carefully dissected from the skulls of the mice and cleaned of any adherent tissue. The calvaria were then combined and subjected to successive enzymatic digestions of trypsin (1 mg/ml; 10 minutes), dispase (2 mg/ml; 20 minutes) and 3 successive rounds of collagenase A (2 mg/ml; 30 minutes each). All enzymes were resuspended in 5 ml pre-warmed Tyrode's solution and the digestions took place in a shaking water bath at 150 rpm and 37°C.

Cells harvested from the dispase and the three collagenase digestions were each centrifuged at 250 x *g* for 5 minutes, and cultured separately overnight in complete culture medium. The following day, the dispase population was discarded and the three collagenase populations were combined, passed through a 70 µm cell strainer and counted using a haemocytometer. These cells would then either be used in MTS

proliferation assays (see Section 2.2.11) or differentiation assays to yield mature osteoblasts capable of forming mineralised bone nodules.

For differentiation assays, precursor cells were seeded in 24-well plates at 10,000 cells/well in complete medium containing 50 µg/ml ascorbic acid and 10 mM β-glycerophosphate (βGP). Triplicate wells were used for each test group and culturing continued until the presence of mineralised bone nodules were evident in control wells, usually within 14-21 days. Test compounds were added and maintained in the culture medium at two different stages: at the time of the first media change (day 2-3), or once precursor cells were confluent (day 7-10).

2.2.9 Alkaline phosphatase (ALP) staining

Osteoblasts differentiation cultures were stained for ALP activity, a marker of osteoblast differentiation. Cells were fixed with 4 % paraformaldehyde. The ALP staining solution consisted of 0.1 M Tris-HCl (pH 8.3), 5 mg naphthol AS-MX phosphate, dissolved in 200 µl of dimethylformamide, and 30 mg red violet LB salt. The solution was filtered and then added to cells. Once developed, the stain was removed and cells were washed with water and stored dry. Stained cultures were imaged using a stereomicroscope and the area of positive red ALP staining per well was quantified using ImageJ. All ALP area measurements were obtained from triplicate wells.

2.2.10 Von Kossa staining

To visualise mineralised bone nodules, von Kossa staining was used. Following ALP staining, osteoblast differentiation cultures were washed with water and incubated in 2.5 % (w/v) silver nitrate in the dark at room temperature for 30 minutes. The silver

nitrate was removed and the cells were washed. The stain was developed in a sodium carbonate formaldehyde solution (0.05 g/ml sodium carbonate, 20 % formaldehye in water) for 2 minutes. Cells were washed with water and black areas corresponding to mineralised bone nodules were visualised and imaged using a stereomicroscope. The total von Kossa-positive area was quantified by ImageJ from triplicate wells for each group.

2.2.11 MTS Assay for proliferation

To measure cell proliferation, the MTS assay was used, which measures cellular metabolic activity (CellTiter 96®AQ_{ueous} One Solution Cell Proliferation kit, Promega, Southampton, UK). MG-63 cells (30,000 cells/cm^2), osteoclast bone marrow precursors (150,000 cell/cm^2) and osteoblast calvarial precursors (30,000 cells/cm^2) were seeded into 96-well plates and treated the following day with test compounds as indicated. After 48 hours, the tetrazolium compound was added to each well for 3 hours, according to the manufacturer's instructions. The resulting absorbance at 490 nm was then measured using a Multiskan 96-well plate reader (ThermoFisher Scientific). Absorbance values were averaged from triplicate readings and expressed as a percentage of control values.

2.2.12 Statistics

All data are expressed as a percentage of control values, shown using standard error of the mean (SEM) error bars for when $n = 3$ and standard deviation (SD) error bars for when $n = 1$. All statistics shown are the results of one-way ANOVAs, calculated using the statistics software, SPSS (IBM, New York, USA). All data were confirmed to be normally distributed and with equal variances before the test was run. The Tukey's

post-hoc test was used to determine any significant differences between test groups and the control group.

2.3 Cloning and sequencing of the 73-deoxychondropsin A gene cluster

2.3.1 Materials

Samples of frozen *I. ramosa* tissue for DNA extractions were obtained as described in Section 2.1.1. Genomic DNA samples of *E. coli* (JM109), *Nostoc* sp. (PCC 7120) and *Streptomyces rimosus* were provided by Dr Edward Spence (KCL). All culturing reagents, standard laboratory chemicals and solvents were sourced from Fisher Scientific unless otherwise stated. The CopyControl™ Fosmid Library Production Kit from Epicentre (Cambridge, UK) was used for fosmid library construction. This included the pCC2FOS vector and the host *E. coli* strain EPI300™-T1^{R} (genotype: *F- mcrA Δ(mrr-hsdRMS-mcrBC) Φ80dlacZΔM15 ΔlacX74 recA1 endA1 araD139 Δ(ara, leu)7697 galU galK λ- rpsL (Str^{R}) nupG trfA tonA*). The pGEM®-T Easy vector from Promega (Southampton, UK) was used for TA cloning of PCR products with the K12 JM109 strain of *E. coli* (genotype: *end*A1, *rec*A1, *gyr*A96, *thi, hsd*R17 (r_k^-, m_k^+), *rel*A1, *sup*E44, Δ(*lac-pro*AB), [F´ *tra*D36, *pro*AB, *laq*I^{q}ZΔM15]), also from Promega.

2.3.2 Microbiological culturing

Microbiological culturing of *E. coli* was performed in lysogeny broth (LB; 10g NaCl, 10g tryptone, 5 g yeast extract, per litre water), either in liquid cultures or supplemented with 12 g/l agar for plate cultures. For EPI300™-T1^{R} cells containing

fosmids, all culture media was additionally supplemented with 12.5 µg/ml chloramphenicol. For JM109 cells containing the pGEM®-T Easy vector, the culture medium was supplemented with 100 µg/ml ampicillin. Liquid cultures were incubated at 37 °C using a shaking incubator set to 150 rpm. Plate cultures were incubated statically at 37 °C. All media and consumables were autoclaved at 120 °C for 15 minutes prior to use and standard aseptic techniques were used to prevent contamination of cultures. Overnight cultures of fosmid or plasmid containing *E. coli* colonies were generated by inoculating 10 ml of LB media with either single colonies from plates using sterile pipette tips, or from frozen aliquots of cultures using a sterile inoculation loop.

In order to ensure high cloning efficiency and maintain stability of inserted sequences, clones transformed using the pCC2FOS vector were initially grown at single copy. However, for colony blot hybridisation screening and when positive clones were identified, fosmids were induced to high copy number in order to increase DNA yield. This was carried out using the CopyControl™ Fosmid Autoinduction Solution from Epicentre, which was added to overnight liquid or plate cultures at a 1x concentration.

Electrocompetent *E. coli* JM109 cells were generated from a 50 ml culture with an optical density of 0.4, measured using a spectrophotometer set to 600 nm and then immediately placed and kept on ice. The culture was then centrifuged at 4,000 x *g*, the supernatant was removed and the cell pellet was resuspended in 10 ml of ice-cold 10 % (v/v) glycerol in water. This process was repeated a further three times. After the final wash, the supernatant was removed and the cells were resuspended in 0.5 ml 10 % glycerol and kept on ice prior to transformation using electroporation (see Section 2.3.7).

2.3.3 DNA extraction

The metagenomic DNA used for KS cloning and fosmid library construction was extracted using a protocol from Dunlap et al. (2007). Whole sponge material (1 g), stored at -80 °C, was ground to a powder in a mortar and pestle under liquid nitrogen. The powder was transferred to a 15 ml tube and 10 ml of lysis buffer containing 100 mM Tris, 100 mM EDTA, 100 mM NaCl, 2 % sodium dodecyl sulphate (SDS) and 400 µg/ml proteinase k was added. The solution was incubated at 55 °C for two hours before particulate material was pelleted under centrifugation and the supernatant removed. DNA was purified from the supernatant with 2 rounds of phenol-chloroform extraction, where an equal volume of phenol/chloroform/isoamyl (25:24:1 v/v, pH 8) was added to the aqueous supernatant from the previous step. The mixture was inverted several times and centrifuged at 12,000 x *g*. The aqueous upper phase was removed and the process was repeated once more. DNA was then precipitated from solution using an equal volume of isopropanol at room temperature. The precipitated DNA was removed using a wide-bore pipette, washed in 70 % ethanol, dried and resuspended in TE buffer (10 mM Tris, 1 mM EDTA). The concentration of DNA was estimated using a NanoDrop spectrophotometer (Fisher Scientific) and aliquoted at 100 ng/µl. All DNA was kept at 4 °C when in regular use and -20 °C for long term storage.

The extraction of metagenomic DNA used for next generation sequencing involved a cell separation step to reduce the presence of sponge cells and enrich for microbial symbionts from Thomas et al. (2010). Whole frozen sponge tissue (1 g) was ground to a powder in a mortar and pestle under liquid nitrogen. To release embedded symbionts from sponge tissue, the powder was transferred to a 50 ml tube and incubated at 37 °C for 30 minutes, plus agitation at 150 rpm, in a solution of calcium, magnesium free seawater (CMFSW; 25 g NaCl, 0.8 g KCl, 1 g Na_2SO_4, 0.04 g $NaHCO_3$ per litre)

with 500 µg/ml collagenase A (Roche). The supernatant was then passed through a 40 µm cell strainer then centrifuged at 100 x *g* for 20 minutes to remove the heavier sponge cells. The new supernatant was then centrifuged at 4000 x *g* to pellet all remaining cells. Metagenomic DNA was extracted from the cell pellet using the same protocol detailed above, re-suspending the dried DNA in 10 mM Tris buffer, quantifying, aliquoting and storing as described above.

Plasmid and fosmid DNA were extracted from overnight liquid cultures using the PureYield™ Plasmid MiniPrep System (Promega), according the manufacturer's instructions. Extracted fosmid DNA was further purified by incubating with Plasmid-Safe™ (Epicentre), an ATP-dependant DNase that digests contaminating host chromosomal DNA from fosmid extractions, leaving circular DNA untouched. Fosmid DNA was incubated with the enzyme at 37 °C according to the manufacturer's instructions.

2.3.4 Agarose gel electrophoresis

Metagenomic sponge DNA, fosmid DNA and PCR products were visualised and sized using agarose gel electrophoresis. For metagenomic and fosmid DNA, 0.8 % (w/v) agarose was dissolved by boiling in 1x TBE (Tris/Borate/EDTA) buffer and supplemented with 0.5 µg/ml ethidium bromide. For PCR products, 1.6 % agarose gels were used. Once loaded with DNA dyes and 100 bp or 1 kb Plus DNA ladders from ThermoFisher Scientific, the gels were run at a voltage of 150 V and a UV light from a transilluminator was used to visualise bands.

2.3.5 Fosmid library construction

Fosmid vectors can accommodate 30-40 kbp sized inserts and contain an F-plasmid origin of replication which enables the fosmid to be maintained at single-copy levels in *E. coli* (Kim et al., 1992). Metagenomic sponge DNA was used to generate a fosmid clone library using the CopyControl™ HTP Fosmid Library Production Kit from Epicentre, according to the manufacturer's instructions. Briefly, metagenomic DNA was blunt-ended and size selected to 30-40 kbp using agarose gel electrophoresis and kit reagents. Once gel-purified, the DNA was ligated into the pCC2FOS vector in an overnight reaction and packaged using MaxPlax Lambda packaging extracts, according to the manufacturer's instructions. Packaged phage particles were then used to transform EPI300™-T1^{R} *E. coli* cells by incubating together at 37 °C. The titer of the fosmid-containing phage particles was determined through transforming *E. coli* cells with serial dilutions of the packaged phage and counting the colonies that grew overnight on LB agar plates supplemented with 12.5 µg/ml chloramphenicol. To confirm fosmid library construction, a selection of single colonies were induced to high copy number overnight (see Section 2.3.2) before fosmid DNA was extracted (see Section 2.3.3). A restriction enzyme digest was performed using the BamHI enzyme (Promega) and fosmid DNA, according to the manufacturer's instructions. This enzyme released the inserted sequence from pCC2FOS producing an expected band pattern consisting of a ~8 kbp vector fragment and fragments representing the 30-40 kbp insert, which were confirmed for the selected clones using agarose gel electrophoresis (see Section 2.3.4).

2.3.6 Polymerase chain reaction (PCR)

To amplify type I KS domains from metagenomic sponge DNA using PCR, the

degenerate primers KSDPQQF (5'-MGNGARGCNNWNSMNATGGAYCCNCARC-ANMG-3') and KSHGTGR (5'-GGRTCNCCNARNSWNGTNCCNGTNCCRTG-3') were used, designed from universally conserved motifs of KS domains (Piel, 2002). To amplify adenylation domains from fosmid DNA using PCR, the degenerate primers NP1 (5'-CCTAATTCAATACGAAAACCACGAADYTTNAYYTG-3') and NP2 (5'-TGTATGTTATTTATACTTCTGGTTCTACTGGTMRNCCANARGG-3') were used (Zhang et al., 2009). Typical PCR volumes of 25 μl for both primer sets contained 100 ng of DNA, 0.4 μM of each primer, 0.2 mM deoxynucleotide triphosphates, 6 mM magnesium chloride, 5 % DMSO and 2 U of a Hot-start *Taq* DNA polymerase. All PCR reagents were obtained from Promega. Thermal cycling conditions consisted of 5 minutes at 95°C followed by 35 cycles of 30 seconds at 95°C, 60 seconds at annealing temperature and 60 seconds at 72°C, with a final step of 5 minutes at 72°C. Annealing temperatures (55 °C for KS and 52 °C for adenylation domains) were determined using gradient PCR, where positive control DNA (*S. rimosus* for KS domains, *Nostoc* sp. for adenylation domains) was used in 12 identical PCRs and the annealing temperature was varied for each within the range of 48 to 58 °C using a specialised PCR program. The annealing temperature producing the optimum band at the expected size was then used in subsequent test PCRs. All PCR products were checked and sized using agarose gel electrophoresis (see Section 2.3.3).

2.3.7 TA cloning of PCR products

TA cloning is a useful method for cloning PCR products where, during PCR, the single nucleotide A is naturally added to the 3' end of a PCR product, resulting in an A' overhang terminus that hybridises with the 3'-T overhangs of the pGEM®-T Easy vector. Plasmids are then transferred to host *E. coli* cells using electroporation. KS and

adenylation domain PCR fragments of approximately 700 and 850 bp in length, respectively, were excised from agarose gels following electrophoresis and purified using the QIAquick Gel Extraction Kit from Qiagen (Manchester, UK). The PCR products were then ligated into pGEM®-T Easy in an overnight reaction according to the manufacturer's instructions. A 50 µl aliquot of electrocompetent JM109 cells on ice was mixed with 10 µl of the vector ligation reaction and transferred to an ice-cold electroporation cuvette. Electroporation was performed using an electroporator set at 2.5 kV for 6 ms. Immediately after electroporation, 1 ml of LB medium was added to the cuvette and then transferred to a 1.5 ml tube. The cells were incubated at 37 °C with shaking at 150 rpm for 1 hour. The cells were then pelleted using centrifugation (11,000 x *g*) and then resuspended in 100 µl LB medium and spread onto agar plates containing 100 µg/ml ampicillin, 0.1 mM Isopropyl β-D-1-thiogalactopyranoside **(**IPTG) and 40 µg/ml X-gal. Following an overnight incubation at 37 °C, white colonies indicating successful transformation by plasmids containing an inserted sequence were identified. Overnight cultures of 5-20 white colonies per PCR product were performed before plasmid DNA was extracted as described in Section 2.3.3. To check the size of inserted PCR product sequences, samples of plasmid DNA were digested with the EcoRI enzyme (Promega), according to the manufacturer's instructions. This digestion released the inserted sequence from the pGEM®-T Easy vector, the size of the insert was estimated using agarose gel electrophoresis (see Section 2.3.4).

2.3.8 Colony blot hybridisation screening of fosmid library

All reagents and materials for this task were obtained in kits from Roche unless stated otherwise. A DIG-labelled KS probe was first produced using the PCR DIG Probe Synthesis Kit according to the manufacturer's instructions. Plasmid DNA (100 ng)

encoding a KS sequence was used as a template in a PCR reaction along with a nucleotide mixture containing DIG-dUTP (0.2 mM), kit buffer plus 6 mM magnesium chloride, 3 U of the kit's high fidelity *Taq* DNA polymerase and 0.4 µM each of the KSDPQQF and KSHGTGR primers. The PCR conditions were the same as described in Section 2.3.6. Following the reaction, the DIG-labelled PCR product was stored at -20°C until needed.

Transformed fosmid-containing *E. coli* were induced to high copy number in patches on LB agar plates. A total of 1200 individual colonies were prepared in this way on large plates at approximately 80-100 colony patches per plate. Colony patches were blotted onto large nylon membranes for 1 minute. As a positive control for the hybridisation process, *E. coli* cells containing the plasmid used as a template for the DIG probe were also scratched onto the top of the membranes in a cross shape using a sterile pipette tip. The membranes were then incubated successively at room temperature in a denaturation solution (0.5 M NaOH, 1.5M NaCl), a neutralisation solution (1.5 M NaCl, 1 M Tris-HCl, pH 7.4) and 2x SSC (30 mM saline-sodium citrate, pH 7.0, 0.3 M NaCl), each for 15 minutes with blotting on Whatman 3MM filter paper between each step. The DNA was then crosslinked to the membrane by illuminating the disc with UV light (UVA, 1.8 mW cm^{-2}, Philips TL-20/05 lamps) for 90 seconds. Cell debris was removed from the membranes by incubating with proteinase K (140 mg/ml) diluted in 2x SSC for 1 hour at 37 °C, followed by blotting onto Whatman 3MM paper soaked in sterile water.

Hybridisation of the KS DIG probe to the nylon membranes was carried out using a hybridisation oven (GE Healthcare, Little Chalfont, UK) with single membranes placed in bottles on a rotisserie. A standard hybridisation buffer was used consisting of 5x SSC, 0.1 % (w/v) N-lauroylsarcosine, 0.02 % (w/v) sodium dodecyl sulphate (SDS) and 1 % (v/v) blocking solution from the Roche DIG Wash and Block Buffer Set. The

hybridisation temperature (T_{hyb}) was calculated to be 80.6 °C using formulas from the DIG Application Manual for Filter Hybridisation (Roche-https://lifescience.roche.com):

$$T_{hyb} = T_m - 25°C$$

$$T_m = 16.6 \log [\text{Mol. Na+}] + 0.41(\%GC) + 81.5$$

Where [Mol. Na+] for 5x SSC is 0.75 and the GC content of the probe was determined to be 64%.

The DIG-labelled probe was first denatured by boiling at 95 °C for 5 minutes and then placed immediately on ice, after which it was diluted to approximately 25 ng/ml in hybridisation buffer. The membranes were initially incubated with 60 ml hybridisation buffer for 1 hour at 81 °C. The buffer was then poured away before being quickly replaced with 15 ml per tube of pre-warmed hybridisation buffer containing the DIG labelled probe. The membranes were then left overnight at 81 °C with gentle rotation.

The following day the probe was removed and stored at -20 °C to be re-used for up to 4 additional rounds of hybridisation. The membranes were washed twice for 5 minutes with gentle shaking at room temperature using 2x SSC plus 0.1 % sodium dodecyl sulphate (SDS). Two high stringency washes were then performed using 0.1x SSC plus 0. 1% SDS at 68°C with gentle shaking for 15 minutes each. Detection of probe-target hybrids was then immediately performed on wet membranes using buffers and solutions from the DIG Wash and Block Buffer Set.

The membranes were first washed for 5 minutes with a washing buffer containing maleic acid and 0.3 % (v/v) tween 20, and then blocked for 30 minutes using a kit blocking solution. The membranes were then incubated for 30 minutes at room temperature with an anti-DIG-AP conjugate antibody, diluted 1:10,000 in blocking solution. Two washes for 15 minutes each with washing buffer were then performed before the membranes were equilibrated with detection buffer (100 mM Tris-HCl, pH

9.5, 100 mM NaCl) for 5 minutes at room temperature. Each membrane was then covered with a solution containing 34 µl of NBT (100 mg/ml 4-nitroblue tetrazolium chloride in 70 % DMF) and 35 µl of BCIP (50 mg/ml 5-bromo-4-chloro-3-indolyl phosphate in DMF) in 10 ml of detection buffer. The membranes were incubated at room temperature in the dark for 5-6 hours until hybridisation signals from the control were evident. The reaction was then stopped by incubating the membranes in TE buffer (10 mM Tris-HCl, 1 mM EDTA, pH 8.0). The membranes were then dried and stored.

Colonies producing strong, positive hits were identified back to their original low copy number colony and then cultured overnight both at low and high copy numbers (see Section 2.3.2). Fosmid DNA was extracted from overnight, high copy number liquid cultures (see Section 2.3.3), whilst 1 ml aliquots were taken from the low copy number cultures, diluted with glycerol to achieve a final concentration of 20 % (v/v) and stored at -80°C.

2.3.9 Sequencing

PCR products amplified from metagenomic sponge DNA, or subcloned from fosmid DNA were sequenced from pGEM®-T Easy vectors using the M13 binding site. This was carried out by Source Bioscience (Nottingham, UK) using the method of chain-terminating dideoxynucleotides (Sanger et al., 1977). Source Bioscience were also used to partially sequence fosmid DNA using primer-walking, where initial insert sequence was obtained using the forward sequencing primer binding site on the pCC2FOS vector, which was then used to design a new primer in order to extend the sequence.

Next generation sequencing of microbially enriched metagenomic DNA from *I. ramosa* and fosmid DNA was carried out using the Nextera DNA Sample Preparation Kit and the MiSeq platform from Illumina (California, USA), according to the

manufacturer's instructions. First, DNA was accurately quantified using a Qubit dsDNA HS Assay and the Qubit 2.0 fluorometer (Life Technologies, California, USA). The DNA was then enzymatically 'tagmented' (tagged and fragmented) into 300 bp fragements using kit reagents. A clean-up procedure was followed before sequencing primers and indexers were then appended to the sequences in a PCR amplification step. The kit consisted of 6 unique indexers, 1 was assigned to the metagenomic sponge DNA, the other 5 to fosmid libraries. A further clean-up step was performed before the sequencing libraries were size-validated using an Agilent Technologies 2100 Bioanalyzer and a High Sensitivity DNA chip (California, USA). The sequencing libraries were also quantified using Qubit. Once sequencing libraries for the fosmids and metagenomic DNA were validated and quantified, the libraries were pooled so that 94 % consisted of the metagenomic sponge DNA, 1 % for each of 5 fosmid libraries and 1 % for the PhiX control library supplied with the kits. The final library was denatured using 0.2 M NaOH before hybridisation buffer was used to dilute the library to a concentration of 16 pM, according to the manufacturer's advice. This library was loaded onto a standard MiSeq flow cell before 300 bp paired-end sequencing was carried out using MiSeq platform and 600 cycles of the v.3 MiSeq sequencing reagents.

2.3.10 Sequence assembly

Primer-walking sequences for fosmid DNA were assembled using pair-wise alignments and the MEGA software, version 6.06 (Tamura et al., 2013). Following the MiSeq run, all data was instantly uploaded to Illumina's cloud-based, genomics computing environment, BaseSpace (https://BaseSpace.Illumina.com). This platform contains numerous applications and tools for the analysis and management of NGS data. Assembly of all the fosmid reads was carried out using an automated, integrated

sequence assembly program on BaseSpace called DNASTAR SeqMan NGen (Wisconsin, USA). This program successfully assembled the sequencing reads from each fosmid sample into a single contiguous sequence (contig) representing the complete pCC2FOS vector and inserted sequence. The fosmid vector sequences were then removed to leave only the insert sequence using the MEGA software.

For the sequencing reads obtained from the metagenomic sponge DNA sample, metagenomic *de novo* assembly was carried out by Ranko Gacesa using the software, Velvet (Zerbino and Birney, 2008). The sequencing reads were first assessed for quality using the FastQC tool. This provided an overview of the quality of the sequencing reads, showing any regions of the reads that have recurrent drops in phred quality scores. Phred quality scores are logarithmically related to the base-calling error probabilities, so that a score of 10 means a 1 in 10 probability of an incorrect base call, a score of 20 means a 1 in 100 probability, a score of 30 means a 1 in 1000 probability. The FASTX-Toolkit was then employed to pre-process the sequencing reads before assembly was attempted, which removed all reads less than 100 bp as well as any detectable artefacts in the sequencing reads. The FASTX-Toolkit was also used to trim the first 20 base pairs from the start and end of every sequence as these were found to have phred quality scores below the commonly used threshold of 20. The processed reads were then assembled using the Velvet software, which is an algorithm package designed to deal with *de novo* assembly from short read sequences. The program takes all the sequencing reads and forms strings of sequences of length *k*, called *k*-mers. The algorithm then uses de Bruijn graphs to analyse and assemble the overlapping regions of *k*-mers, ultimately leading to assembled sequence data. The assembly of the metagenomic sponge DNA reads was carried out by running the Velvet algorithm, varying the length of *k*-mers used until an optimum was reached based on the proportion of sequences assembled and the length and number of contigs generated.

2.3.11 Sequence annotation

KS and adenylation domain nucleotide sequences were identified using the Basic Local Alignment Search Tool (BLAST - http://blast.ncbi.nlm.nih.gov/Blast.cgi) (Camacho et al., 2009), searching against the non-redundant database with default parameters. Nucleotide sequences were translated into amino acid sequences in all 6 reading frames using the European Molecular Biology Open Software Suite (EMBOSS) Transeq tool (Rice et al., 2000). Translated amino acid sequences were identified using BLAST or Pfam (http://pfam.xfam.org/) searches against non-redundant databases and default parameters. Pfam contains a large collection of protein families represented by sequence alignments and HMMs (Finn et al., 2011). Multiple sequence alignments of amino acid sequences were performed and used to construct phylogenetic trees using the MEGA software, version 6.06, and the ClustalW algorithm (Larkin et al., 2007). Other reference KS sequences used in the alignments were obtained from the National Center for Biotechnology Information (NCBI) GenBank database (http://www.ncbi.nlm.nih.gov/genbank/) (Benson et al., 2013). The Neighbour-Joining method (Saitou and Nei, 1987) was used for phylogenetic tree construction with the evolutionary distances estimated using the Poisson correction method (Zuckerkandl and Pauling, 1965) and robustness estimated using the bootstrap test (Felsenstein, 1985).

To predict the substrate specificity of adenylation domains from their nucleotide sequences, a web-based program designed by Baranasic et al. (2014) was used. This program detects adenylation domain binding pockets from amino acid sequences based on an alignment to a hidden markov model (HMM) of adenylation domains. The software then analyses the binding pocket residues with a latent semantic indexing model and provides predictions of amino acid substrate specificity along with a precision score showing the quality of the prediction.

Assembled NGS contigs from fosmid and metagenomic sponge DNA were automatically screened for the presence of secondary metabolite biosynthetic genes using the Antibiotics & Secondary Metabolite Analysis Shell software (antiSMASH 2.0) (Blin et al., 2013). This program allows the rapid genome-wide identification, annotation and analysis of secondary metabolite gene clusters from nucleotide sequences and integrates common bioinformatic tools such as NCBI's BLAST, Glimmer (Delcher et al., 2007), Muscle (Edgar, 2004) and HMMer (Finn et al., 2011) to identify biosynthetic genes and align identified regions with nearest relatives from databases containing all other known gene clusters. The program also integrates a suite of *in silico* secondary metabolite analysis tools such as PKS/NRPS domain detection using ClustScan (Starcevic et al., 2008) and CLUSEAN (Weber et al., 2009). The annotation of detected PKS genes by antiSMASH was also manually confirmed using ClustScan. This program annotates the domain architecture of PKS genes from nucleotide sequences, as well as the activity of reductive domains (ER/KR/DH), through comparative alignments with HMM profiles of individual domains. A prediction of AT domain specificity is also determined by HMM alignment, with the diagnostic amino acid residues extracted and compared with fingerprints corresponding to different specificities or activities (Starcevic et al., 2008).

Chapter 3: The Extraction of 73-Deoxychondropsin A

3.1 Introduction

The first aim of this thesis was to investigate *in vitro* effects of 73-DOC on the bone remodeling cell types, osteoclasts and osteoblasts. However, in order to achieve this aim, a stock of 73-DOC was first needed. Once a purified sample of 73-DOC was obtained, the biological activity of the compound also needed confirming before commencement of *in vitro* testing with bone cells. The objectives for this chapter were therefore: To extract a stock of 73-DOC for *in vitro* testing; and confirm biological activity of the new extract.

The only examples of 73-DOC extraction in the scientific literature are that of Rashid et al. (2001b), following the original discovery of the compound and Chevallier et al. (2004). 73-DOC was originally discovered in the Australian sponge species, *I. ramosa*, samples of which were also found to contain chondropsin A (Cantrell et al., 2000), which has a chemical structure almost identical to 73-DOC, but differs by a single oxygen atom (Figure 3.1). The extraction procedures detailed by Rashid et al. (2001b) showed that 73-DOC could be isolated through fractionation of an aqueous sponge tissue extract on a C18 chromatography column, using reverse-phase HPLC. As well as guiding extracting procedures used in this chapter, Rashid et al. (2001b) also provided spectral characteristics of 73-DOC, such as UV absorbance peaks, that will enable detection of the compound during HPLC-based fractionation, as well as quantification of the isolated compound using UV spectroscopy.

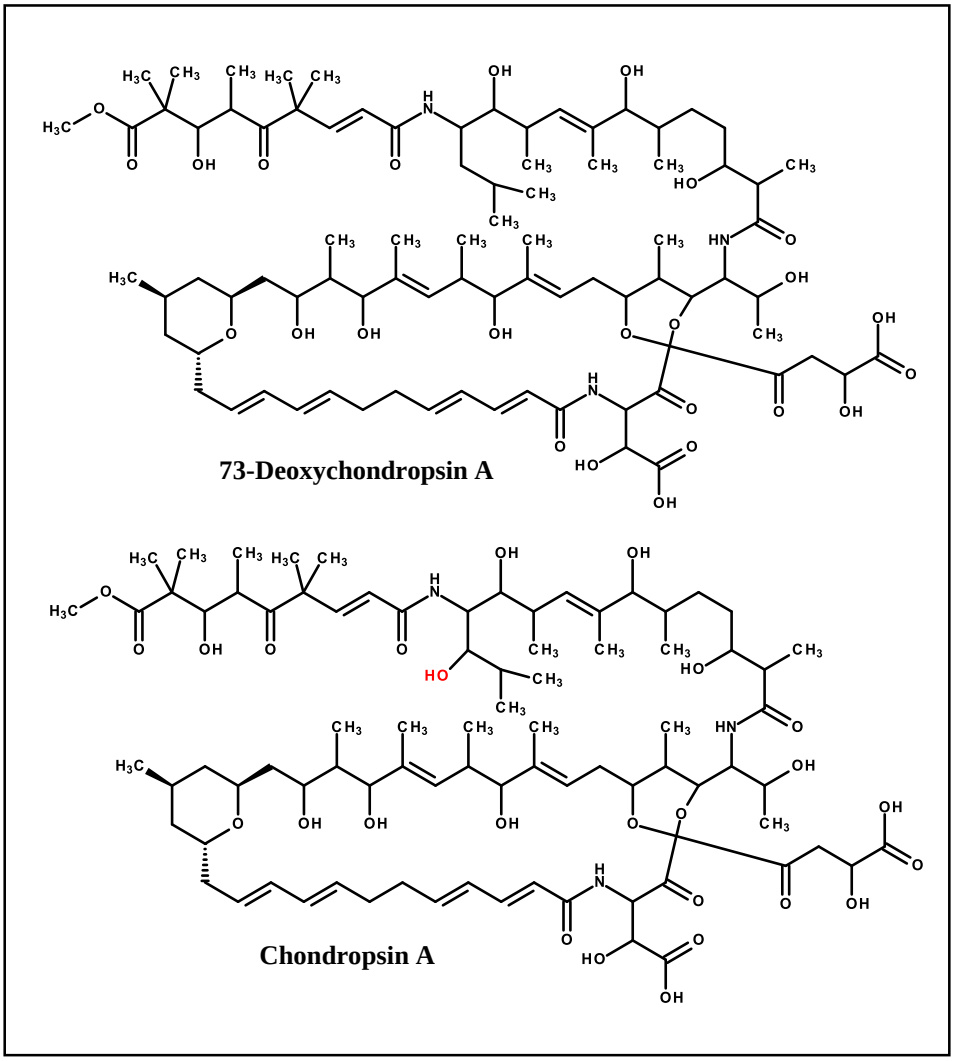

Figure 3.1 Chondropsin metabolites present in *I. ramosa*. The chemical structures of 73-DOC and chondropsin A are shown, as reported by Rashid et al. (2001b) and Cantrell et al., (2000), respectively. The additional oxygen present in chondropsin A is highlighted in red.

Samples of *I. ramosa*, from which 73-DOC could be extracted, were collected by Dr Paul Long (KCL) and Dr Walt Dunlap (AIMS) from the Great Barrier Reef with the support of AIMS. These were freeze-dried and shipped frozen to KCL along with an authentic sample of 73-DOC, prepared by Dr Marnie Freckelton and Dr Cherie Motti at AIMS, which was provided for comparison with the newly extracted material. Dr Walt Dunlap also assisted with work in this chapter by optimising the procedures for obtaining the semi-crude extract of 73-DOC, as described in the next section. Work presented in this chapter was also assisted by Miss Priyanka Rajeevkumar (KCL masters student).

See Sections 2.1 and 2.2 for specific details on the materials and procedures used in this chapter.

3.2 Results

3.2.1 Extraction of semi-crude 73-deoxychondropsin A

Freeze-dried samples of *I. ramosa*, collected from the Great Barrier Reef, were confirmed by Dr Walt Dunlap at AIMS to test positive for the presence of both 73-DOC and chondropsin A using LC-MS according to published procedures (Rashid et al., 2001b). A protocol for producing a semi-crude extract of 73-DOC was followed, using disposable SPE columns which separate compounds in an aqueous mixture according to their physiochemical properties. This protocol was optimised to produce a mixture that retains 73-DOC, as well as chondropsin A and other unwanted compounds, but which is much less heterogeneous than the raw extract. The semi-crude extract is thus more suitable for the improved accuracy and resolution offered by HPLC partitioning, which operates using the same physiochemical principles as SPE columns.

Images showing the procedures used for obtaining the semi-crude extract of 73-DOC from *I. ramosa* are shown in Figure 3.2. The protocol started with 4 successive rounds of extraction from shredded sponge tissue using 20 % methanol and mild sonication. Each round lasted 2 hours producing an aqueous solution containing soluble compounds present in the sponge. The combined extracts were then passed over a bed of celite in order to remove fine impurities before being further purified by passing through a C-18 SPE column. Here, 73-DOC was retained on the column whilst unwanted, more polar impurities, were washed away with water. 73-DOC, along with

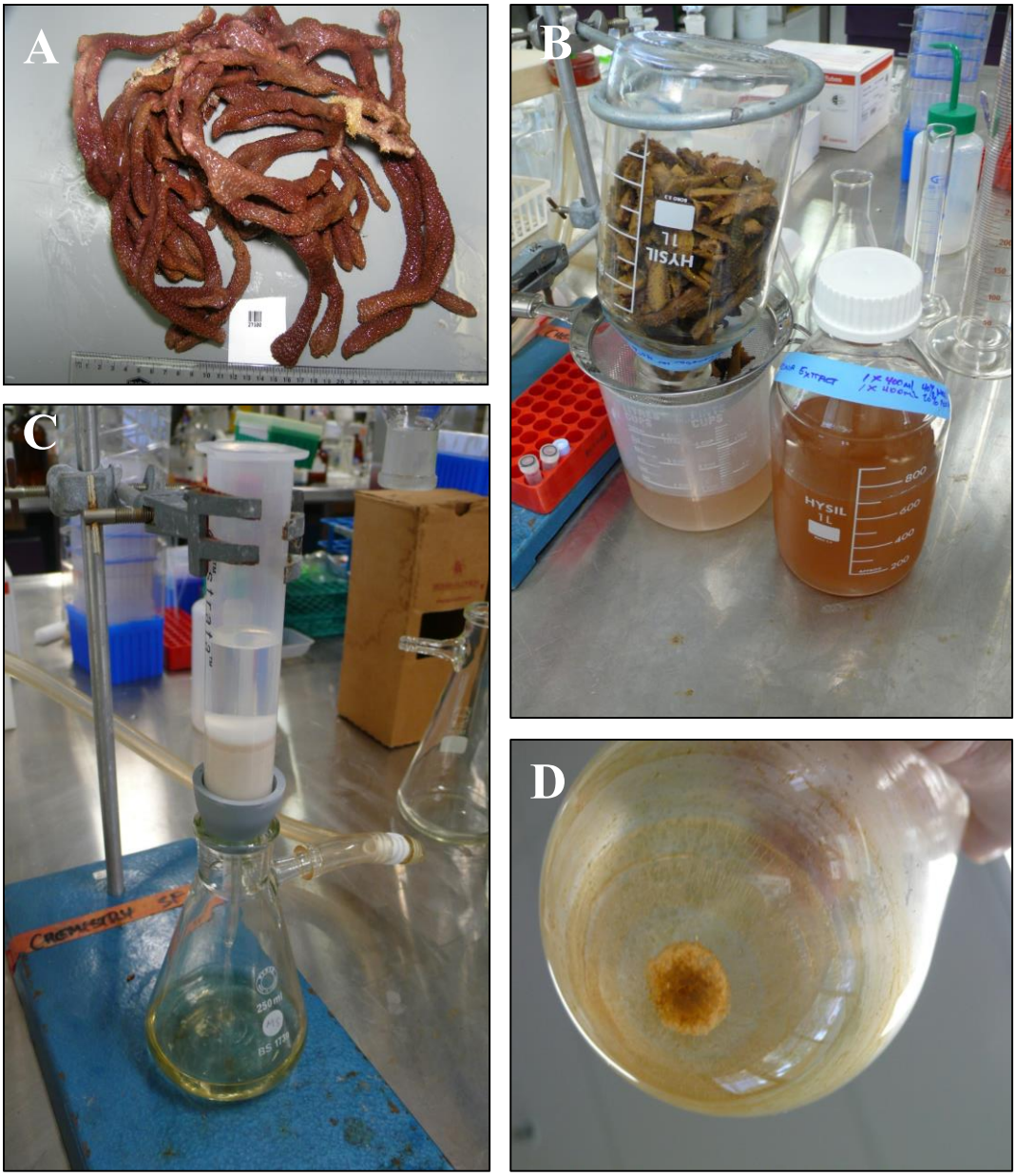

Figure 3.2 Images of procedures used to obtain semi-pure extract of 73-deoxychondropsin A. Images show the freeze-dried sample of *I. ramosa* used to extract 73-DOC **(A)**, the extraction of the semi-pure compound from shredded sponge tissue using methanol **(B)**, the purification of the methanol extract using a solid phase extraction column **(C)** and the final dried semi-pure extract of 73-DOC **(D)**.

other compounds of similar polarity, was then eluted from the column using 90 % methanol. This process was repeated, combining eluates and removing any solvents under vacuum, producing the semi-crude extract of 73-DOC (Figure 3.2 D). A total of 150 g of dried sponge tissue was processed in this way, producing 450 mg of a crystalline mixture containing 73-DOC.

3.2.2 Isolation of 73-deoxychondropsin A

In order to further purify the semi-crude extract, this was fractionated using analytical reversed-phase HPLC on a C18 column using a gradient of acetonitrile in water (10-90 % acetonitrile in 30 minutes). Based on the work of Rashid et al. (2001b) and advice given by Dr Walt Dunlap, 73-DOC was known to correspond to one of two prominent peaks found from the HPLC spectrum detected at 261 nm. Fractions corresponding to the two peaks, F1 and F2, were collected and subjected to MS analysis to determine which peak corresponded to 73-DOC based on the molecular mass of detected compounds (Figure 3.3).

The molecular formula for 73-DOC was reported as $C_{83}H_{133}N_3O_{25}$ with a molecular mass of 1571.92 by Rashid et al. (2001b). The MS data revealed that F2 corresponded to 73-DOC, assigning a mass of 1594.78 to the fraction, representing a sodium adduct $[M+Na]^+$ with a calculated molecular mass of 1594.91 (Figure 3.3 inset). F1 was assigned a mass of 1610.78, revealing this fraction corresponded to chondropsin A ($C_{83}H_{133}N_3O_{26}$), also detected as a sodium adduct with a calculated molecular mass of 1610.91 (Figure 3.3 inset) (Cantrell et al., 2000). Peak area analysis of the HPLC spectrum showed the semi-crude extract consisted of approximately 18 % 73-DOC at this stage.

Once the 73-DOC peak had been determined, the HPLC conditions used for fractionation of the semi-pure extract of 73-DOC were scaled up for use with a preparative HPLC column. Multiple runs using this column and the semi-crude extract were performed, collecting the relevant peak each time. All 450 mg of the semi-pure extract were processed in this way with each collected 73-DOC fraction dried down under vacuum leaving a white powder. A total of 19.5 mg of this material was obtained from 150 g of dried sponge tissue, equating to a yield of 0.13 mg g dry wt^{-1}.

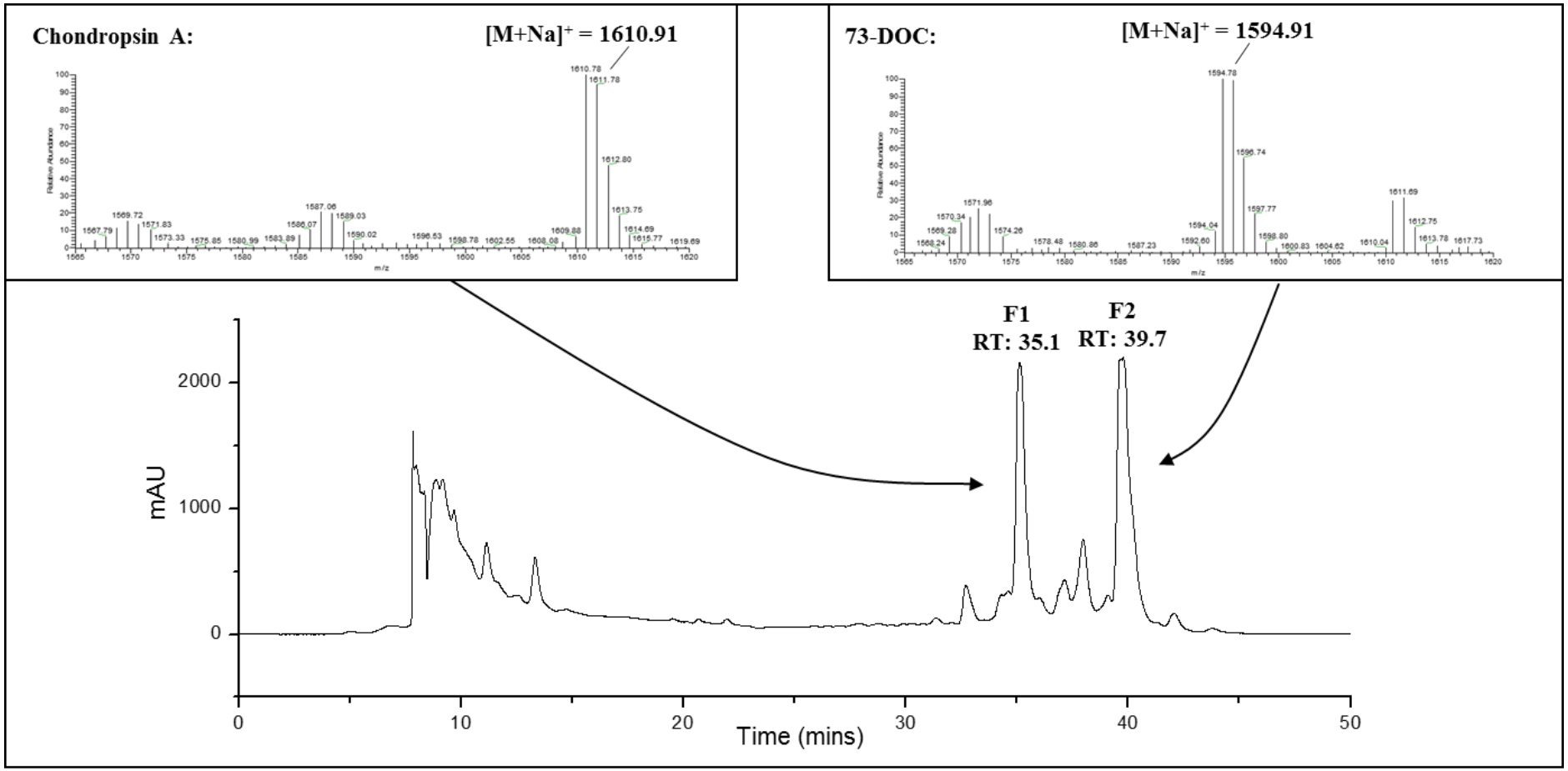

Figure 3.3 HPLC and MS analysis of semi-crude extract reveal peak corresponding to 73-DOC. A sample of the semi-crude extract obtained from *I. ramosa* was run on an analytical HPLC system. The resulting spectrum at 261 nm is shown, with the peaks collected for further MS analysis labelled F1 and F2, along with retention times (RT). MS spectra for F1 and F2 are shown in the insets above the HPLC spectrum. F1 shows the predominant presence of an ion corresponding to a sodium adduct of chondropsin A, where $[M+Na]^+ = 1610.91$ (Cantrell et al., 2000). The MS spectrum for F2 shows the predominant presence of an ion corresponding to a sodium adduct of 73-DOC, where $[M+Na]^+ = 1594.91$ (Rashid et al., 2001b).

3.2.3 Confirmation of the 73-deoxychondropsin A extraction

In order to confirm the success of the extraction procedures, the purified 73-DOC sample was re-analysed using the same analytical HPLC conditions along with additional LC-MS analysis (Figure 3.4). Both the HPLC and LC-MS chromatography spectra show the presence of a single peak that was also associated with a smaller, unknown shoulder peak. Attempts to further fractionate the sample with HPLC to remove the shoulder were performed but were not successful. Quantitative area analysis of the 73-DOC peak in Figure 3.4 A showed the sample consisted of 91 % 73-DOC following extraction.

The LC-MS data confirmed the sample to contain 73-DOC, showing prominent mass peaks corresponding to $[M+H]^+$ and $[M+Na]^+$ ions with calculated molecular masses of 1572.93 and 1595.91 respectively (Figure 3.4 B) (Rashid et al., 2001b). To provide an accurate mass estimation of the purified extract, a sample was also subjected to HRMS analysis. This data also showed two major peaks corresponding to 73-DOC in the form of $[M+H]^+$ and $[M+Na]^+$ ions, with measured masses of 1572.9320 and 1594.9139 respectively (Figure 3.5). These masses showed deviation from the calculated masses of 1572.9305 and 1594.9119, equal to mass errors of 0.95 and 1.25 ppm, respectively. Mass errors below 5 ppm are considered sufficient to support molecular formula assignment (Organic Letters, Guidelines for Authors, 2015). The HRMS data therefore unambiguously confirm the extract is 73-DOC with an elemental formula of $C_{83}H_{133}N_3O_{25}$.

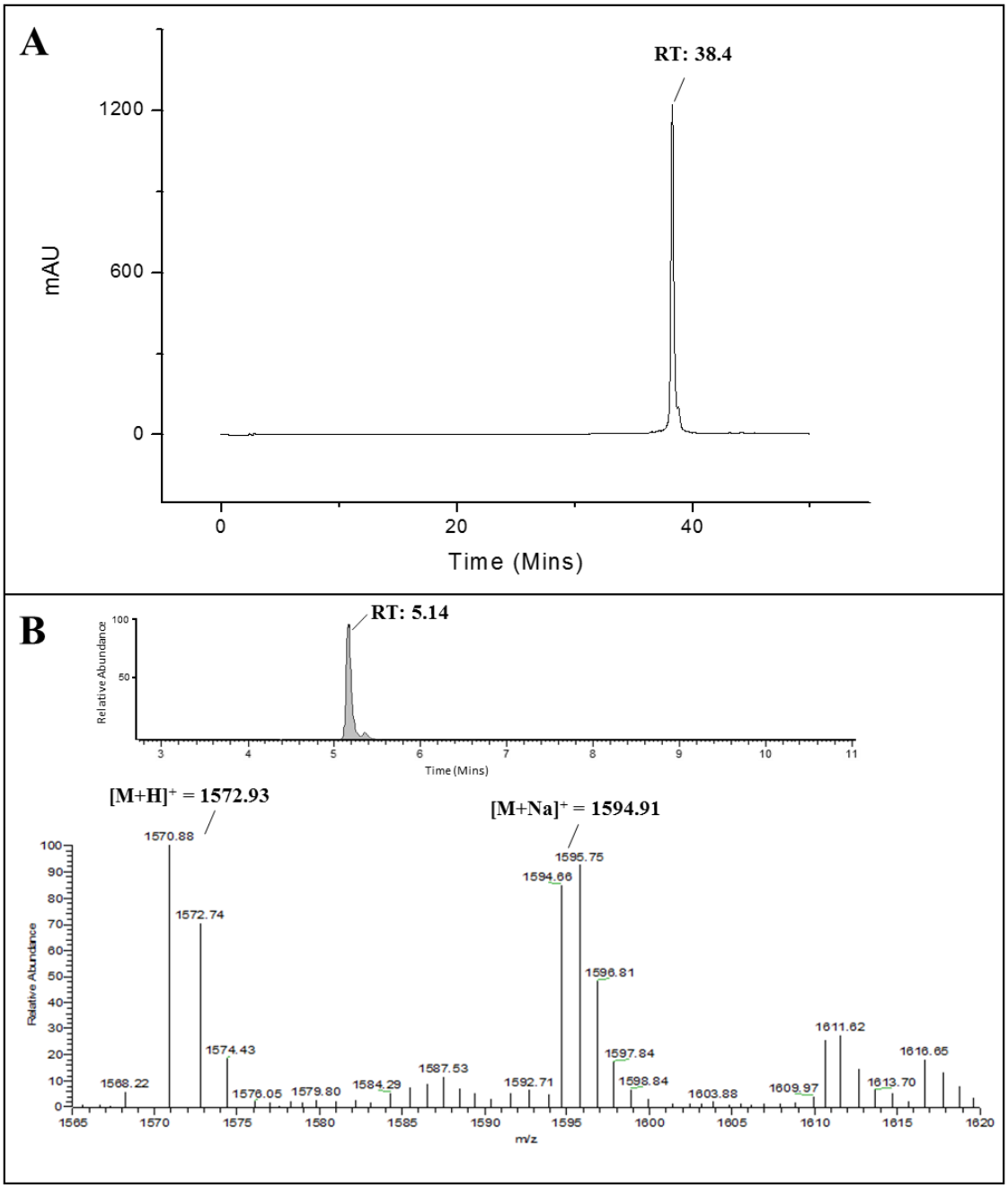

Figure 3.4 HPLC and LC-MS spectra confirms the identity of the isolated extract as 73-DOC. A sample of the purified 73-DOC extract was examined using an analytical HPLC column, with the spectrum obtained at 261 nm shown along with the retention time (RT) of the single peak detected **(A)**. The purified sample was additionally analysed using LC-MS, showing the total ion chromatogram spectrum with retention time (RT) above the MS spectrum for that peak **(B)**. Major MS peaks for ions corresponding to hydrogen and sodium adducts of 73-DOC were found where $[M+H]^+$ = 1572.93 and $[M+Na]^+$ = 1594.91 (Rashid et al., 2001b).

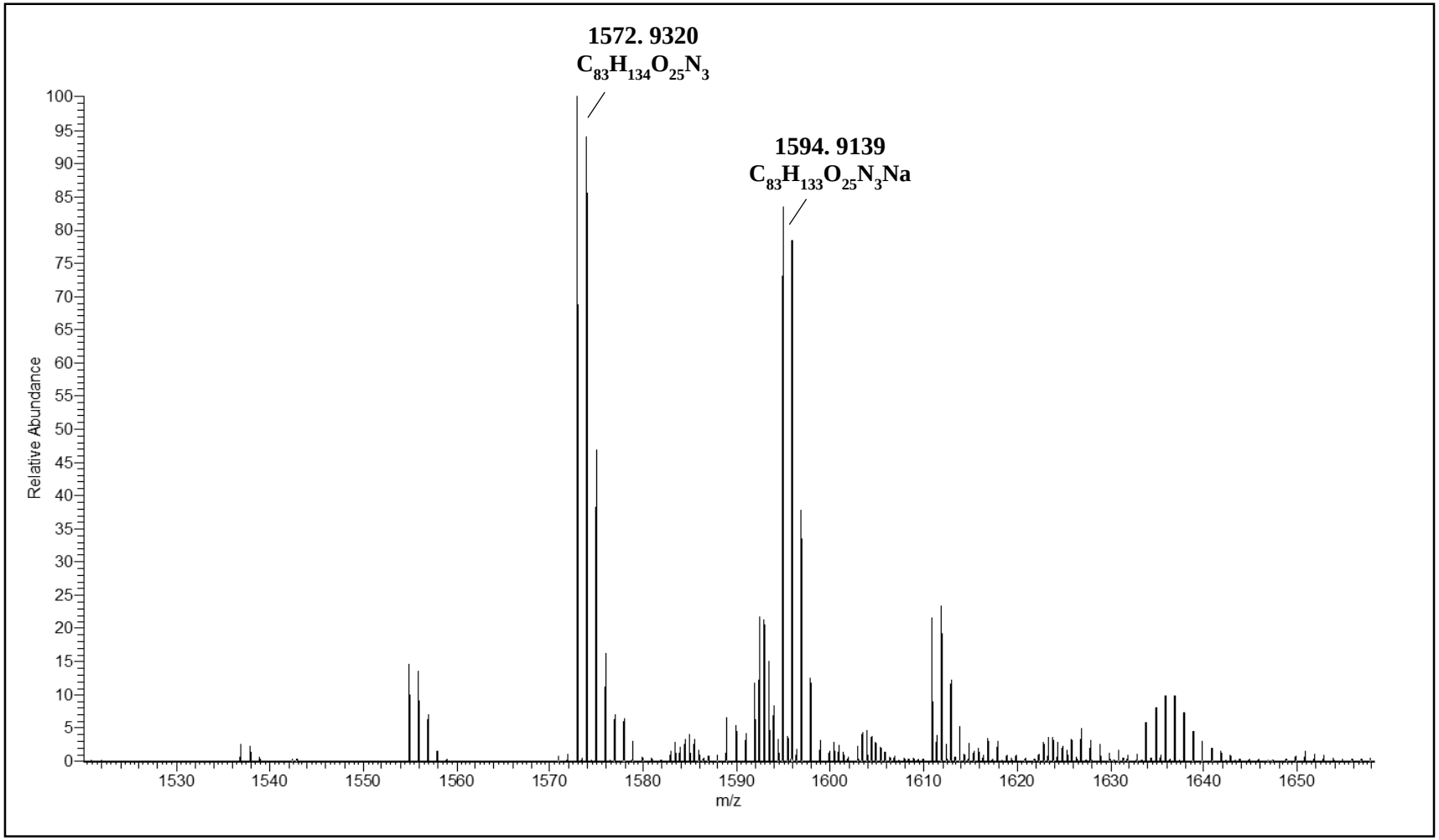

Figure 3.5 HRMS analysis of the isolated extract confirms the identity of 73-DOC. The spectrum shows two major peaks corresponding to ions, $[M+H]^+$ and $[M+Na]^+$. $[M+H]^+$, calculated for $C_{83}H_{134}O_{25}N_3$ = 1572.9305, measured at 1572.9320. $[M+Na]^+$, calculated for $C_{83}H_{133}O_{25}N_3Na$ = 1594.9119, measured at 1594.9139 (Rashid et al., 2001b).

A ^{1}H-NMR was also performed on a sample of the purified extract in order to confirm the chemical structure of the extracted material and determine any impurities. The spectrum obtained from the new extraction was compared with that of an authentic sample of 73-DOC prepared by AIMS. The spectrum from the current extraction had an enlarged water peak at 4.8 ppm caused by the hygroscopicity of the deuterated methanol in which the sample was analysed, but otherwise the profiles are identical (Figure 3.6).

Major peak values corresponding to chemical shifts from both spectra were compared with those reported by Rashid et al. (2001b) and assigned to the chemical structure of 73-DOC (Table 3.1). A total of 40 peaks were identified from spectra of the AIMS and current extractions. Data for the Rashid extraction were acquired from 73-DOC in deuterated dimethylformamide, whereas the data for the AIMS and current extractions were acquired from 73-DOC in deuterated methanol. Small deviations between chemical shift values are attributed to the different solvents used as well as inter-laboratory variables such as pH, temperature and concentration (Atta-ur-Rahman, 2000). Taken together, these data support both the high purity estimation of the current extraction, as well as the presence of structural features that confirm the identity of the extracted material as 73-DOC.

3.2.4 Biological activity of the 73-deoxychondropsin A extraction

Biological activity of 73-DOC was determined using the MTS assay for cell proliferation alongside the authentic sample of 73-DOC prepared by AIMS. The MTS assay is used for the quantification of viable cells in proliferation and cytotoxicity studies, and is detailed further in Section 2.2.8. The human osteosarcoma cell line, MG-63, was selected for the assay on the basis that previous work conducted by the NCI had established that chondropsin A has antiproliferative activity against this cell type

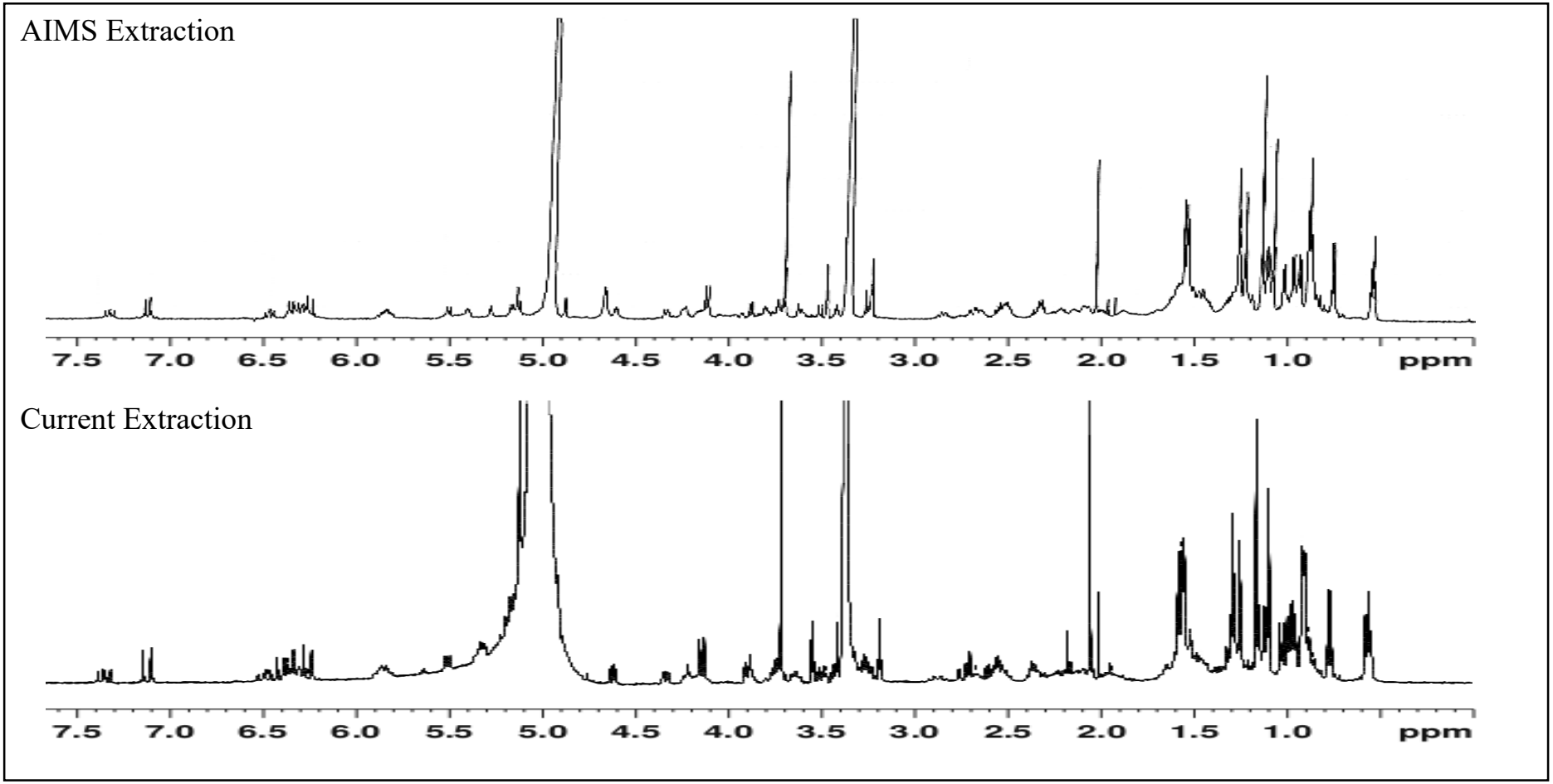

Figure 3.6 Comparison of ^{1}H-NMR spectra from the isolated material and an authentic sample confirm the extraction of 73-DOC. NMR spectra were obtained from a sample of the current extraction and from an authentic sample of 73-DOC produced by AIMS. Other than an enlarged water peak in the current extraction at 4.8 ppm, the two spectra have identical profiles, confirming the identity of 73-DOC in the current extraction**.** Both sets of spectra were obtained from 2.5 mg 73-DOC in deuterated methanol.

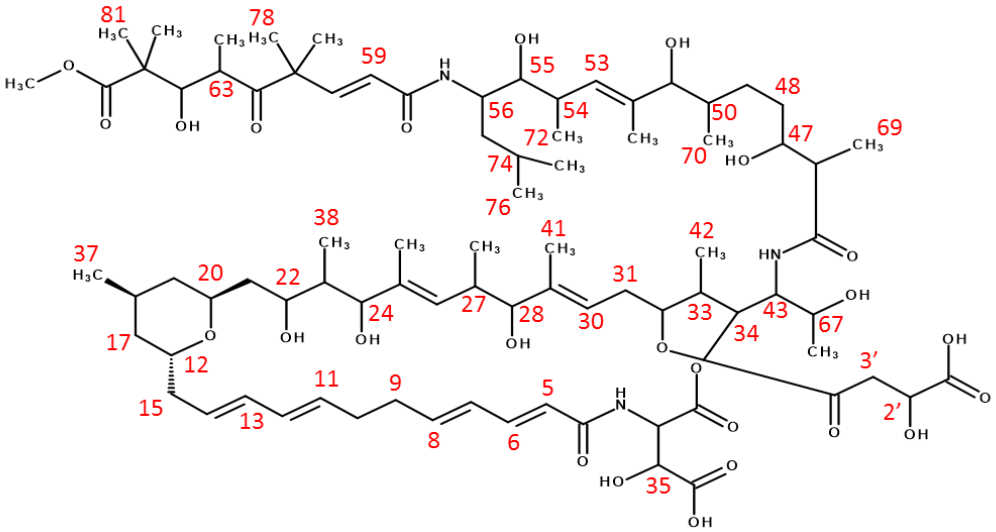

Position on Structure	Chemical Shifts (ppm) Rashid Extraction	AIMS Extraction	Current Extraction	Position on Structure	Chemical Shifts (ppm) Rashid Extraction	AIMS Extraction	Current Extraction
6	7.14	7.13	7.18	15	2.79	2.82	2.86
5/59	6.30/6.31	6.31	6.33	54/3’	2.64/2.63	2.64	2.66
13	6.17	6.17	6.23	27	2.54	2.5	2.54
8	6.12	6.12	6.13	9	2.29	2.32	2.37
11	5.70	5.70	5.73	31	2.05	2.03	2.02
53	5.42	5.38	5.40	15	2.03	1.98	1.99
30	5.22	5.28	5.23	33	2.00	1.94	1.95
34	5.10	5.05		50	1.57	1.58	1.59
35	4.82	4.77		74	1.56	1.57	1.58
2’	4.52	4.52	4.54	48	1.48	1.47	1.49
22	4.25	4.26	4.27	17	1.27	1.3	1.32
43	4.15	4.16	4.16	78	1.26	1.27	1.29
56	4.07	4.05	4.07	81	1.17	1.18	1.18
24	3.86	3.82	3.83	69	1.13	1.12	1.13
67	3.78	3.73	3.70	42	1.03	1.01	1.01
20	3.69	3.65	3.67	72	0.96	0.98	0.96
47	3.52	3.46	3.46	70	0.93	0.93	0.93
28	3.51	3.43	3.43	76	0.89	0.93	0.93
55	3.36	3.38	3.37	37	0.87	0.81	0.83
63	3.20	3.19	3.24	38	0.62	0.6	0.63

Table 3.1 ^{1}H NMR data for 73-DOC. Chemical shift values taken from NMR spectra are shown for the current extraction, the AIMS extraction and the published values reported by Rashid et al. (2001b). The corresponding positions on the 73-DOC chemical structure are also shown above for each identified shift, numbered as reported by Rashid et al. (2001b). Small deviations between chemical shift values are attributed to the different solvents used as well as pH, temperature and concentration variations (Atta-ur-Rahman, 2000).

(NCI, 2006, Dunlap et al., 2007), which thus allowed activity of the 73-DOC extraction to be compared with data from an almost identical compound.

The results of the MTS assays showed that both stocks of 73-DOC caused dose-dependent decreases in MG-63 cell numbers, leading to a 25-45 % decrease at 100 nM (Figure 3.7). The results for both stocks showed a similar trend of antiproliferative activity, though the second assay conducted with the AIMS extracted material showed cell viability was higher than the control at low concentrations, likely as a result of pipetting errors during the assay setup leading to low control measurements. The results

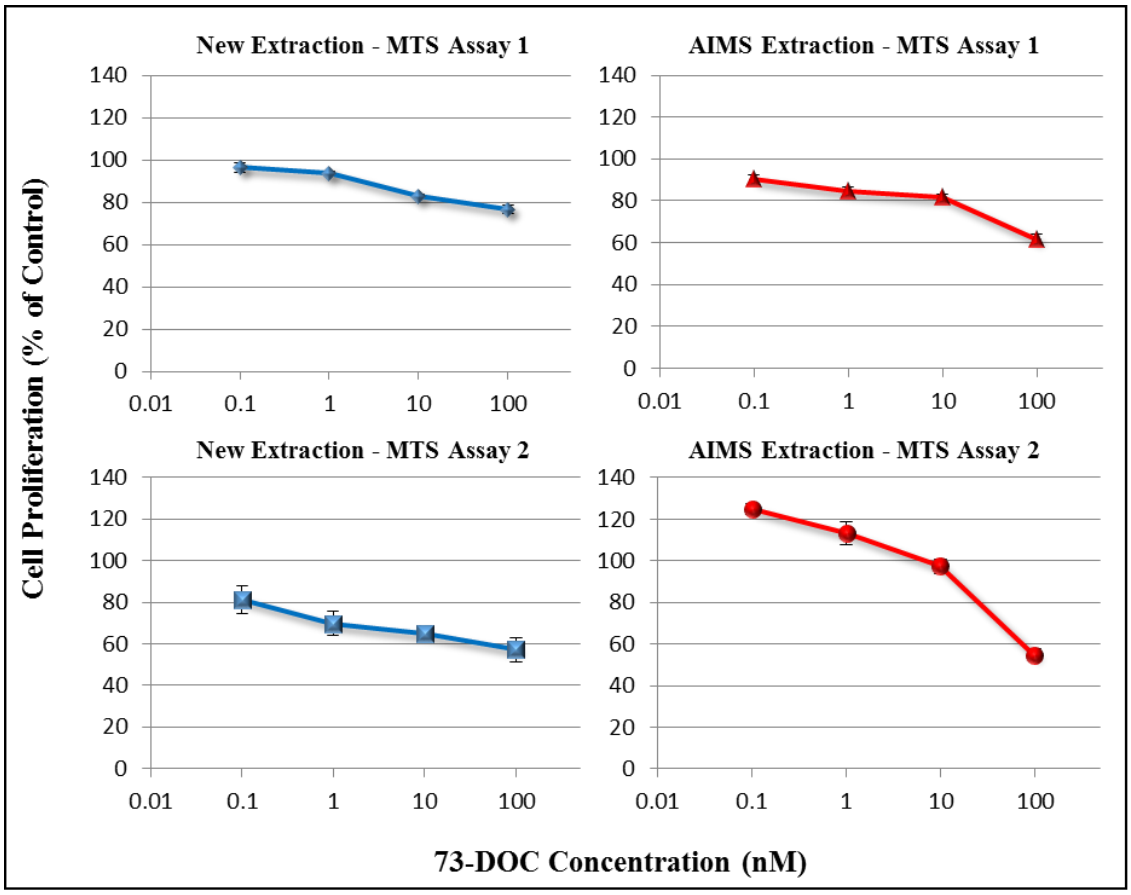

Figure 3.7 Comparison of the biological activities from two stock solutions demonstrate the antiproliferative effects of 73-DOC.

The MTS assay for cell proliferation was used to determine the antiproliferative activity of 73-DOC towards the MG-63 human osteosarcoma cell line. Cells were plated out in triplicate wells and exposed to 73-DOC for 48 hours before the MTS assay was performed. 2 experiments were performed with each of the stock solutions from the current extraction and that prepared by AIMS. Data are presented as a percentage of control values, error bars are ± SD.

show that the newly extracted stock of 73-DOC has antiproliferative activity toward the MG-63 cell-type, consistent with that of an authentic source of 73-DOC.

3.3 Discussion

The first objective of this chapter was to extract a stock of 73-DOC for *in vitro* testing. This objective was successfully met with approximately 20 mg of 73-DOC isolated from 150 g of *I. ramosa* tissue. A combination of analytical and preparative HPLC was used to identify and isolate solvent-partitioned material corresponding to 73-DOC, showing a demonstrated increase in purity estimation from 18 % of the semi-crude extract to 91 % of the final isolated material. As this stock will now be used for *in vitro* experimentation, the work presented in this chapter therefore sets a benchmark of purity that future preparations of 73-DOC must meet in order for biological data to be comparable with observations made using the current stock.

To confirm the extraction of 73-DOC, a variety of analytical spectrometry procedures were used, including LC-MS, HRMS, and ^{1}H-NMR. Based on molecular mass measurements, LC-MS and HRMS both consistently showed major peaks corresponding to ions that were consistent with that reported by Rashid et al. (2001b) and for 73-DOC, in which a molecular mass of 1571.92 was reported for the compound. In both sets of analyses presented here, other ionic species of less relative abundance were also observed due to fragmentation of the 73-DOC molecule during the electrospray ionisation process. Future work may therefore benefit from using a soft source of ionisation to accurately determine molecular mass, such as MALDI (matrix assisted laser desorption/ionisation). The HRMS data also accurately confirmed the assignment of the molecular formula, $C_{83}H_{133}N_3O_{25}$, identical to that reported by Rashid

et al. (2001b) but with greater accuracy as shown by the smaller mass error estimates (0.95 and 1.25 ppm versus 1.70 ppm).

A ^{1}H-NMR spectrum confirmed the structure of the isolated material, producing a profile almost identical to that obtained from an authentic sample of 73-DOC produced by AIMS, and showing chemical shift peaks that were consistent with the reported structure of 73-DOC (Rashid et al., 2001b). However, total assignment of all spectral peaks or all proton nuclei in the 73-DOC structure was not accomplished during the current work. Previous studies with chondropsin metabolites have shown that, in order to account for ambiguities arising from overlapping resonances, extensive interrogation of ^{1}H-NMR spectra in a variety of solvents are required for full structural elucidation (Cantrell et al., 2000). Such work was beyond the time limitations and aims of this thesis, but could be considered for future work alongside acquiring additional ^{13}C-NMR spectra, which would also aid in confirming the structure and purity of 73-DOC extractions.

Only two other extractions of 73-DOC from sponge tissue are found in the literature. A yield of 0.003 % g wet wt^{-1} from the sponge *Psammoclemma* sp. was reported by Chevallier et al. (2004), and a yield of 0.018 % g wet wt^{-1} from *I. ramosa* was calculated from the study by Rashid et al. (2001b). The yield of 73-DOC obtained from *I. ramosa* during the current extraction was equal to 0.013 % g dry wt^{-1} which, when converted to wet weight using data presented by Ricciardi and Bourget (1998), showed the current extraction was approximately 0.01 % g wet wt^{-1}. This enabled direct comparison with the other extractions of 73-DOC, as well as with other chondropsin metabolites (Table 3.2). These data showed that the current extraction yielded over 3 times the amount obtained by Chevallier et al. (2004) but almost half that obtained by Rashid et al. (2001b), though there is some uncertainty in the latter estimate as only the weight of the aqueous extract was shown, and not that of the original sponge tissue from

Sponge Species	Compound	Compound Concentration (mg kg wet wt^{-1})	Reference
Ircinia ramosa	73-DOC	100	This work
Ircinia ramosa	73-DOC	180	Rashid et al. 2001b*
Psammoclemma sp.	73-DOC	30	Chevallier et al. 2004
Psammoclemma sp.	Chondropsin A	30	Chevallier et al. 2004
Ircinia ramosa	Chondropsin A	40	Rashid et al. 2001b*
Chondropsis sp.	Chondropsin A	50	Cantrell et al. 2000
Chondropsis sp.	Chondropsin B	20	Cantrell et al. 2000
Ircinia sp.	Chondropsin C	130	Rashid et al. 2001b*
Chondropsis sp.	Chondropsin D	10	Rashid et al. 2001a

Table 3.2 Concentrations of chondropsin metabolites extracted from sponge tissues. * - Compound concentrations from this reference are likely over estimates as the weight of the original sponge tissue was not stated.

which the compound was extracted. The estimated tissue concentration from the Rashid et al. (2001b) study is likely an overestimate and closer to that of the current work.

As similar extraction methods were used by both Rashid et al. (2001b) and Chevallier et al. (2004), the difference seen in tissue concentrations from *I. ramosa* and *Psammoclemma* sp. likely reflect environmental variables that are known to influence the metabolite concentration in sponge tissues (Ruiz et al., 2013). If chondropsins are to be exploited for therapeutic development, the data shown in Table 3.2 imply that, out of all the chondropsin metabolites, 73-DOC from *I. ramosa* can be extracted in the highest yields, and would thus be the best option for using natural populations to supply small scale *in vitro* testing and possibly larger scale *in vivo* and preclinical trials. Yields equivalent or lower than those demonstrated in the current work have previously been shown to be sufficient for supplying other sponge-derived metabolites for such work (Munro et al., 1999, Hadas et al., 2005, Page et al., 2005, Sipkema et al., 2005, Ruiz et al., 2013).

However, extracting the amounts required for full commercial production using the method demonstrated in this chapter is likely to be economically unfeasible, as well as ethically unsound due to the amounts of sponges that would need to be harvested from

the natural environment. Despite finding that 73-DOC is present in *I. ramosa* at relatively high concentrations when compared with the other chondropsins, the overall small yield of the compound reiterates the supply problems typically associated with developing natural products for therapeutics, and reaffirms the need for an alternative method of 73-DOC supply if the compound is to meet global market demands. One ideal solution to this problem is the heterologous expression of the 73-DOC biosynthetic genes in a fermentable host. Work contributing to this solution is further explored in Chapter 6.

The final objective of this chapter was to confirm the biological activity of the 73-DOC extraction. The new stock of 73-DOC was compared alongside an authentic sample prepared by AIMS using a cell proliferation assay similar to those conducted for the NCI 60-cell antitumour screen (Boyd and Paull, 1995). Both stocks of 73-DOC were shown to have dose-dependent antiproliferative activity against the MG-63 human osteosarcoma cell line, comparable to previous work conducted by the NCI with chondropsin A, which showed a 50 % decrease in MG-63 cell proliferation at 40 nM (NCI, 2006, Dunlap et al., 2007). Chondropsin A, which was the only chondropsin metabolite evaluated in the NCI 60-cell screen, was also shown to cause 50 % growth inhibition at a mean concentration of 25 nM across a broad panel of cell lines (Cantrell et al., 2000). Similar, potent (low nanomolar) antitumour activity has also previously been demonstrated in melanoma and leukaemia tumour cell lines for 73-DOC/chondropsin C (Rashid et al., 2001b) and chondropsin D (Rashid et al., 2001a). Additionally, both 73-DOC and chondropsin A were shown to cause dose-dependent antitumour activity against a small panel of human tumour cell lines, where 50 % growth inhibition was reported at 2 nM and 0.3 nM for chondropsin A and 73-DOC respectively (Chevallier et al., 2004). Taken together, it is clear that the chondropsin metabolites are

effective *in vitro* antitumour compounds, and the work presented in this chapter with 73-DOC and the MG-63 cell line is consistent with that view.

In conclusion, the objectives of extracting a stock of 73-DOC and confirming biological activity were successfully met, as shown by the consistency with published chemical and biological data. As biological activity of the 73-DOC extract has been demonstrated, work in the next chapter sought to address what effects 73-DOC has on the cell types involved in bone remodeling, the osteoclasts and osteoblasts. Interestingly, osteosarcoma cells are osteoblastic in origin, so the effect of 73-DOC on the MG-63 cells suggests that the compound will have activity towards the osteoblast cell type. The type of activity, and the effects the compound has on osteoclasts and bone resorption are discussed in Chapters 4 and 5.

Chapter 4: The Effects of 73-Deoxychondropsin A on Osteoclast and Osteoblast Proliferation and Differentiation

4.1 Introduction

A major aim of this thesis was to evaluate 73-DOC as a bone resorption inhibitor with the goal of identifying osteoclasts and/or osteoblasts as potential target cells and ultimately providing insights into a novel therapeutic to treat diseases characterised by excessive bone resorption. Having shown in the previous chapter that the extracted 73-DOC had biological activity on MG-63 cells, the aim of this chapter was to now characterise specific *in vitro* effects of the compound on the cell types directly involved in bone remodeling, the osteoclasts and osteoblasts. As the inhibition of bone resorption can be achieved by targeting osteoclast differentiation as well as specifically inhibiting osteoclast function, the work presented in this chapter sought to initially characterise the effects of 73-DOC on the proliferation and differentiation of osteoclast precursors, as well as the viability of the mature cells. Similarly, the effects of 73-DOC on osteoblast precursor differentiation and viability were assessed, with a goal to establish an effective concentration range of 73-DOC for osteoclasts and osteoblasts.

4.2 Materials and methods

4.2.1 Materials

73-DOC was extracted as described in Chapter 3 and quantified as detailed in Section 2.1.4. As 73-DOC has been proposed as a V-ATPase inhibitor, the non-specific V-ATPase inhibitor, bafilomycin, was also used as a positive control in experiments.

4.2.2 Osteoclast cell culture

The effects of 73-DOC on different stages of osteoclast differentiation were investigated following the specific protocol summarised in Figure 4.1. Briefly,

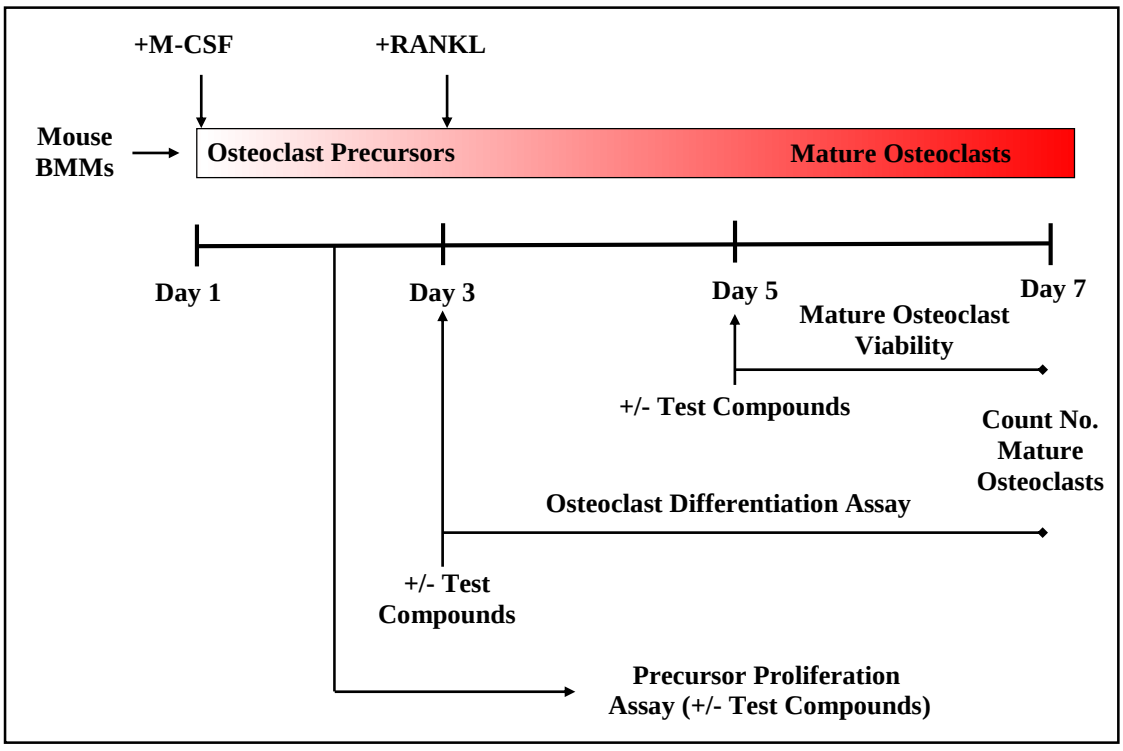

Figure 4.1 Schematic of *in vitro* osteoclast differentiation and experiments. Bone marrow macrophages (BMM) were directed to become osteoclast precursors through the addition of M-CSF to the culture medium on day 1. Precursors were either used in proliferation assays or directed to become mature osteoclasts through the addition of RANKL, which were then used to investigate the effects of test compounds on osteoclast differentiation and mature cell viability.

osteoclast precursors from murine BMMs, isolated as described in Chapter 2 (Section 2.2.3.1), were used either in proliferation assays or to generate mature osteoclasts. For proliferation experiments, the MTS assay was used as described in Section 2.2.11. Precursors were differentiated into mature osteoclasts through the addition of M-CSF and RANKL to the culture medium as indicated in Figure 4.1. Test compounds were added either with RANKL, to investigate the effects on differentiation, or once mature osteoclasts were formed, to determine effects on viability of the mature cell type. TRAP staining was used to quantify mature osteoclasts, as described in Section 2.2.4.

4.2.3 Osteoblast cell culture

A schematic summarising osteoblast culturing conditions and the experiments performed with 73-DOC in this chapter is shown in Figure 4.2. Briefly, primary murine osteoblast precursors were obtained following enzymatic digestions of mice calvaria as detailed in Section 2.2.8. These cells were then either used in proliferation assays (see Section 2.2.11) or cultured to produce mature osteoblasts through the addition of ascorbic acid and βGP to the culture medium. Test compounds were added at early or late stages of osteoblast differentiation as indicated in Figure 4.2. ALP activity was quantified as described in Section 2.2.9.

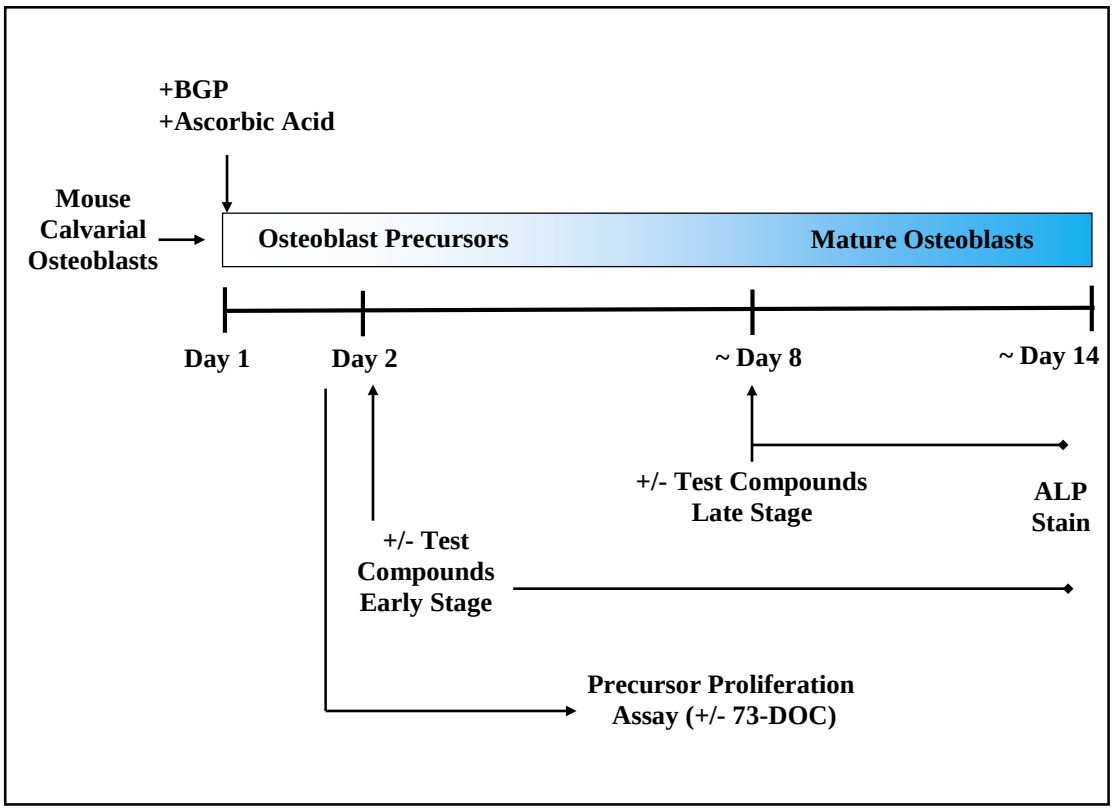

Figure 4.2 Schematic of *in vitro* osteoblast differentiation and experiments. Primary osteoblast precursors were isolated from the calvaria of neonatal mice and were either used in proliferation assays or cultured in the presence of βGP and ascorbic acid to stimulate the differentiation of mature osteoblasts, which were then used to investigate the effects of test compounds on osteoblast differentiation at early and late stages.

4.3 Results

4.3.1 73-Deoxychondropsin A inhibits the proliferation of osteoclast and osteoblast precursors

To establish the effects of 73-DOC on the proliferation of osteoclast and osteoblast precursors, the MTS assay was used. Following isolation and an initial period in either osteoclastogenic or osteogenic media, the precursors were exposed to varying concentrations of 73-DOC or bafilomycin for a period of 48 hours. The MTS assay was then performed. 73-DOC was found to cause a dose-dependent inhibition in both

osteoclast and osteoblast precursor cell number during the 48 hour exposure period, relative to untreated cells (Figure 4.3). A significant decrease in metabolically viable cell numbers was seen at 5 nM and 10 nM for osteoclasts and osteoblasts respectively (Figure 4.3 A, C). Interestingly, maximal doses of 73-DOC caused a ~70% decrease in total osteoclast precursor cell number, but only a 40% decrease in osteoblast number. Taken together, these results suggest that osteoclasts appear to be more sensitive to the antiproliferative effects of 73-DOC at the precursor stage. Bafilomycin was shown to cause similar effects but at higher concentrations (Figure 4.3 B, D).

4.3.2 73-Deoxychondropsin A inhibits the differentiation of osteoclasts

Once a suitable concentration range for 73-DOC was established for the two cell types, the effect of 73-DOC on the differentiation of murine osteoclast precursors was then investigated. To this end, M-CSF dependent precursor cells were cultured in 96-well plates on slices of dentin in the presence of the critical osteoclastogenic factors, M-CSF and RANKL, and mature osteoclasts were quantified after approximately 7 days. Culturing in the presence of 73-DOC was found to cause a significant dose-dependent decrease in the number of TRAP-positive MNCs formed, with a 40 % decrease at 2.5 nM and a 60 % decrease at 5 nM (Figure 4.4).

4.3.3 73-Deoxychondropsin A inhibits the viability of osteoclasts

In addition to characterising the effects of 73-DOC on osteoclast precursors, the response of mature osteoclasts to 73-DOC was also investigated. Osteoclast precursors were seeded on dentin slices as above and cultured until multinucleated osteoclasts were

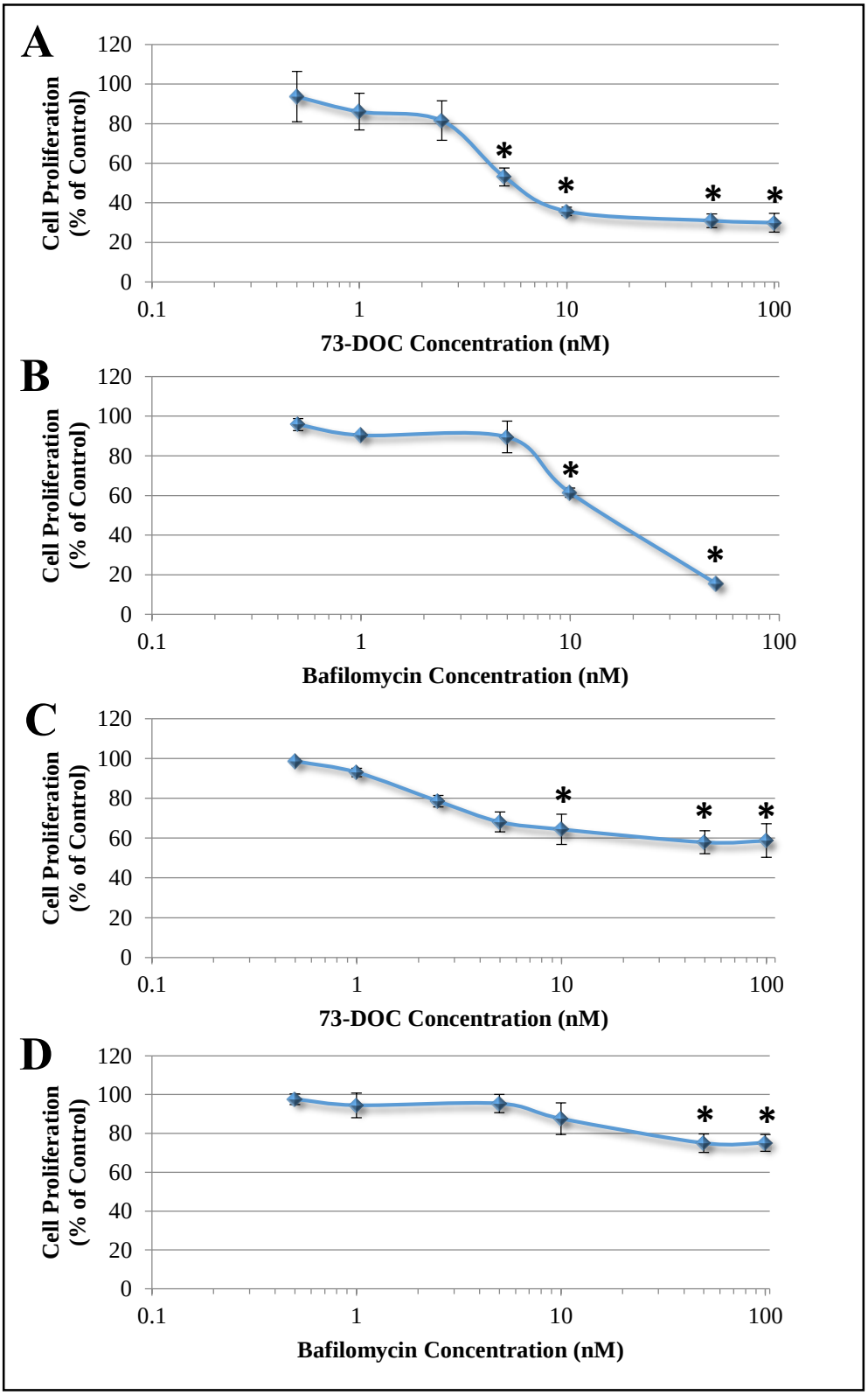

Figure 4.3 73-DOC inhibits the proliferation of osteoclast and osteoblast precursors. The MTS assay for cell proliferation was performed on osteoclast **(A, B)** and osteoblast **(C, D)** precursor cells following a 48 hour exposure to various concentrations of 73-DOC **(A, C)** or bafilomycin **(B, D)**. Assay measurements were made from triplicate wells and expressed as a percent of the control. For 73-DOC, graphs represent the mean ± SEM, $n = 3$. For bafilomycin, results from a single experiment are shown ± SD ($n = 2$). * = Significant change from lowest concentration tested, $p<0.05$.

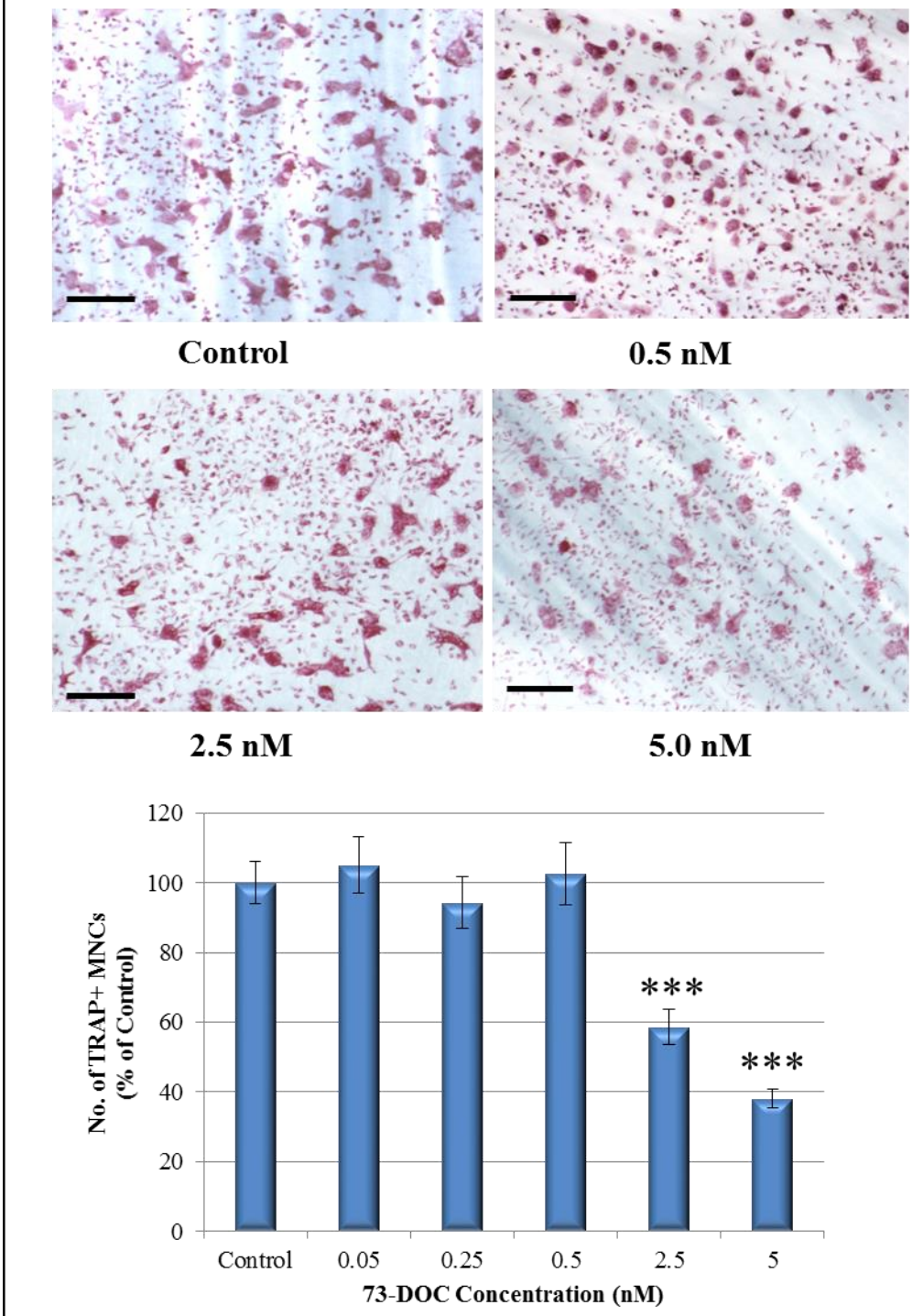

Figure 4.4 73-DOC inhibits the differentiation of murine osteoclasts. Osteoclast precursor cells were cultured on dentin slices. When RANKL was added to stimulate osteoclast differentiation, 73-DOC was also included in the culture medium of test groups and in all subsequent medium changes. Cells were fixed after 7 days and stained for TRAP. Representative images of TRAP stained cells at various concentrations are shown, scale bar = 200 µm. TRAP-positive MNCs (>3 nuclei) were counted from triplicate wells and expressed as a percentage of control counts. Bar graph shows mean data ± SEM, n = 3. *** = Significant change from control, p<0.001.

formed. 73-DOC or bafilomycin were then added at various concentrations for a further 48 hours and the number of TRAP-positive cells were quantified. 73-DOC caused a dose-dependent decrease in the number of mature osteoclasts, becoming significant at 25 nM (Figure 4.5). Interestingly, this concentration is 10-fold higher than that which caused similar significant effects on osteoclast precursors (Figure 4.4). Additionally, the cellular morphology of osteoclasts also appeared to be affected by high concentrations of 73-DOC, where the more common occurrence of larger, more vacuolated cells was observed that also showed a greater intensity of TRAP staining (Figure 4.5 A).

4.3.4 73-Deoxychondropsin A inhibits the differentiation of osteoblasts

The effect of 73-DOC on the differentiation of osteoblasts was next investigated. Osteoblast precursors were cultured in the presence or absence of 73-DOC or bafilomycin, added at two different stages, either early from the outset of culture, or late after the cells reached confluence during early bone nodule formation. The activity of the osteoblastic differentiation marker, ALP, was then compared between treatment groups. Histochemical staining for ALP showed that 73-DOC inhibited osteoblast differentiation, especially when added at an early stage (Figure 4.6 A). Quantification of the ALP stained area confirmed this observation, showing dose-dependent decreases in the area of ALP-positive staining, becoming significant at concentrations of 2.5 nM and higher (Figure 4.6 A). Late-stage addition of 73-DOC similarly inhibited ALP staining, although slightly higher concentrations were required (Figure 4.6 B). Bafilomycin also inhibited osteoblast differentiation, with significant decreases in ALP activity observed at 5 and 10 nM for early and late-stage addition, respectively (Figure 4.6 A, B). These data show that osteoblast differentiation is inhibited by both 73-DOC

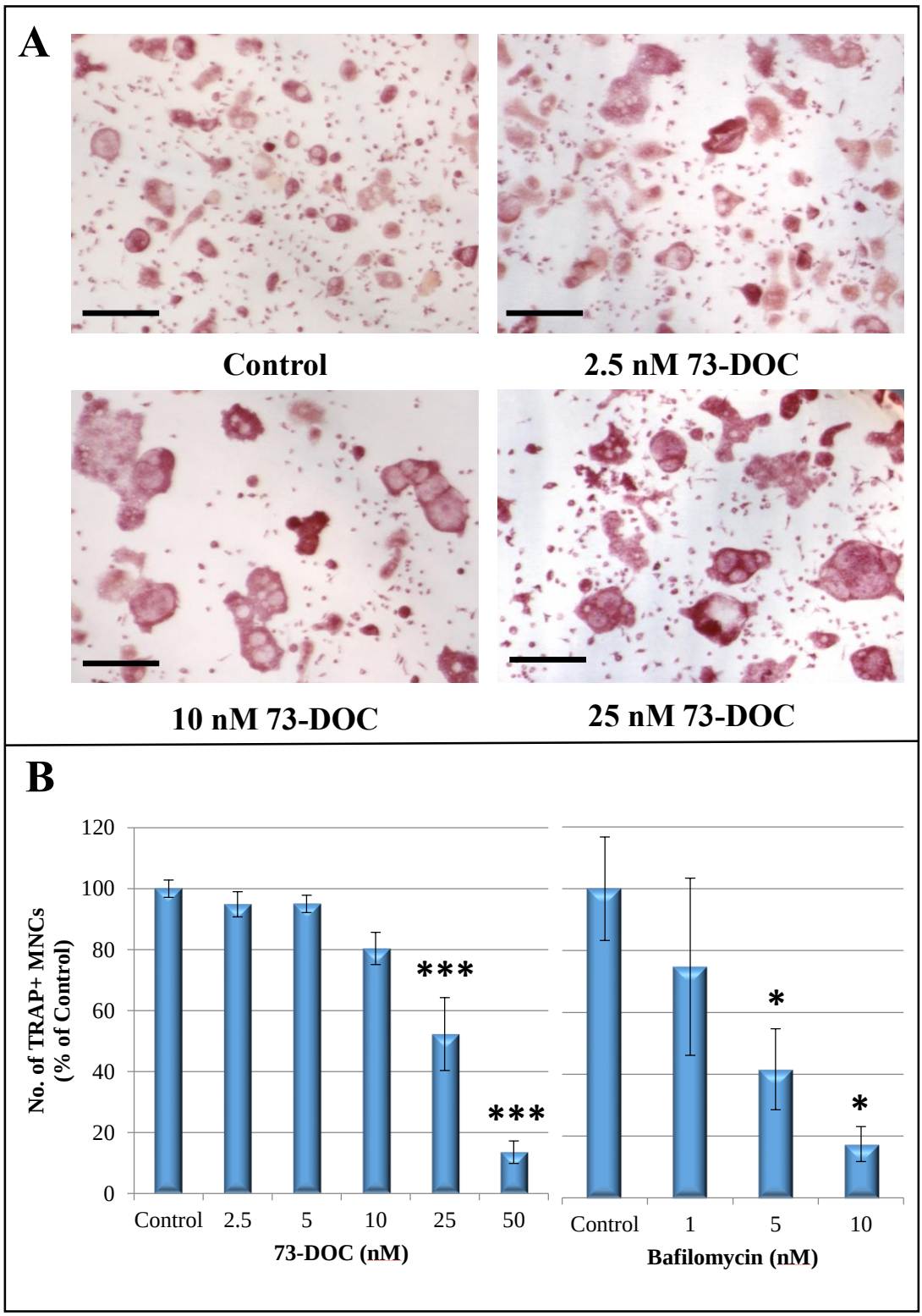

Figure 4.5 73-DOC inhibits the number of mature murine osteoclasts. Osteoclast precursors were cultured on dentin slices. Additional slices were monitored for the presence of mature osteoclasts and once observed, concentrations of 73-DOC and bafilomycin were added to the culture medium of test wells. Cells were fixed after 48 hours and stained with TRAP. Representative images are shown (scale bar = 200 µm) **(A)**. TRAP-positive MNCs (>3 nuclei) from triplicate wells were counted and expressed as a percentage of control counts. Bar graph for 73-DOC shows mean ± SEM, n = 3. For bafilomycin, results from a single experiment are shown ± SD (n = 2). Stars represent a significant change from control, *- p<0.05, ***- p<0.001.

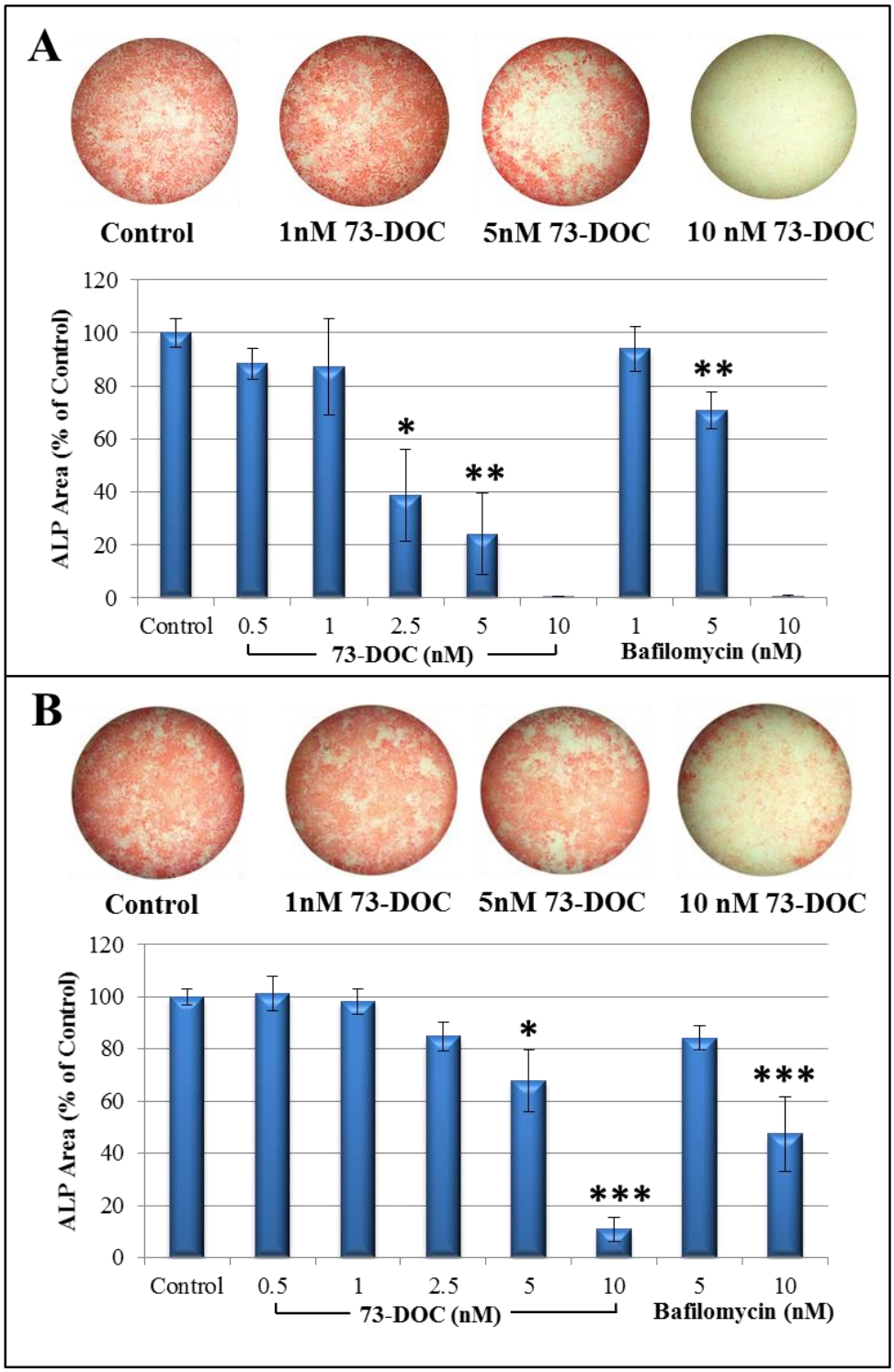

Figure 4.6 73-DOC inhibits the differentiation of murine osteoblasts. Osteoblast precursors were isolated from mouse calvaria and cultured in osteogenic media. 73-DOC and bafilomycin were added to the culture medium at an early stage on day 2 of culture **(A)** and at a late stage when the cells were confluent **(B)**. Cells were fixed when bone nodules were observed in control wells and stained for alkaline phosphatase (ALP) activity. Each plate well was imaged and the area of ALP-positive, red staining was quantified and expressed as a percentage of control values. Representative images of wells following staining are shown. Bar graphs show mean values ± SEM, n = 3. Stars represent significant change from control, *- p<0.05, **- p<0.01, ***- p<0.001

and bafilomycin, and that early precursors are more sensitive than mature cultures to their effects in addition to being more sensitive to 73-DOC than bafilomycin.

4.4 Discussion

In this chapter, the effects of 73-DOC on the viability and differentiation of osteoclasts and osteoblasts were characterised for the first time. This work was important in determining a concentration range in which 73-DOC is active towards the two cell types, in addition to examining what specific *in vitro* effects the compound has on the precursors and mature cells of osteoclasts and osteoblasts. The results showed that 73-DOC does have potent, low nanomolar activity towards these cell types. Proliferation of both osteoclasts and osteoblasts precursors were dose dependently inhibited by 73-DOC and significant inhibition of osteoclast and osteoblast differentiation was found to occur at the same concentration (2.5 nM) when 73-DOC was added at comparable stages. Additionally, mature osteoclast viability was shown to be inhibited by 73-DOC but at concentrations 10-fold higher than those causing effects in the precursor cells. The similarity in cellular response of both cell types between 73-DOC and bafilomycin suggest that they might share a common inhibitory mechanism, supporting the designation of 73-DOC as a V-ATPase inhibitor.

The inhibition of osteoblast precursor proliferation was not unexpected considering the inhibition of MG-63 osteosarcoma cell proliferation by 73-DOC (Chapter 3). However, the inhibition of osteoclast precursors by 73-DOC was a novel finding, consistent with other reported antiproliferative effects of V-ATPase interference in osteoclast precursors (Qin et al., 2011, Yang et al., 2012). Indeed, the proliferation of other non-bone cell types have also shown sensitivity to either 73-DOC, other chondropsin metabolites, as well as other V-ATPase inhibitors (Manabe et al., 1993,

Cantrell et al., 2000, Rashid et al., 2001a, Rashid et al., 2001b, Chevallier et al., 2004, Pérez-Sayáns et al., 2009, Rath et al., 2014). The mechanisms underlying the inhibition of osteoblast and osteoclast proliferation by 73-DOC are not yet known. However, other studies have shown that V-ATPase expression is upregulated during macrophage proliferation and that inhibition in other cell types can induce cell-cycle arrest leading to apoptosis, or can disturb intracellular trafficking and signalling events (Lee et al., 1997, McHenry et al., 2010, Rath et al., 2014). What effects 73-DOC has on the cell-cycle and apoptosis of osteoclasts and osteoblasts are currently unknown. Interestingly, it appears that proliferating cells are more susceptible to the effects of 73-DOC as both osteoclast and osteoblasts exhibit increased sensitivity when 73-DOC was added at a precursor stage in comparison to when added to differentiated cells. This observation is consistent with the reported effects of V-ATPase inhibition on the cell-cycle machinery, but future experiments characterising cell-cycle kinetics, or apoptotic signalling cascades would be worth examining to explain the potential mechanisms of osteoclast and osteoblast inhibition by 73-DOC.

Another possible explanation for decreased proliferation via V-ATPase inhibition might be found from a proposed novel function of the V-ATPase in mTOR signalling, which is responsible for regulating various cellular functions including proliferation, cell survival, amino acid sensing and autophagy (Weichhart, 2012). One theory linking the V-ATPase with mTOR signalling concerns cytoplasmic pH, as studies have shown that a lowered cytoplasmic pH correlates with inhibition of mTORC1 (mTOR complex 1) activity, attributed to impaired V-ATPase function (Balgi et al., 2011, Fonseca et al., 2012). Another model of mTOR signalling has proposed a more direct involvement of the V-ATPase in sensing amino acids, the lysosomal levels of which are known to be a crucial signal for mTOR (Jewell et al., 2013). Zoncu et al. (2011) proposed that amino acids interact with V-ATPases at the lysosome surface to regulate recruitment of Rag

guanosine triphosphates (GTPase), which activate mTORC1 following translocation to the lysosome. The V-ATPase was the first downstream target discovered in a putative amino acid sensing pathway, though other evidence has suggested the proton-assisted amino acid transporter, PAT1, or transcription factor EB (TFEB), may be the amino acid sensor with the V-ATPase acting as a key factor (Ögmundsdóttir et al., 2012, Settembre et al., 2012). Many questions regarding this model remain but the involvement of the V-ATPase in the mTOR signalling pathway seems clear, and components of the mTOR pathway are known to be expressed in osteoclasts (Indo et al., 2013). Disruption of this pathway by a V-ATPase inhibitor such as 73-DOC could therefore lead to inhibited cell growth and survival.

Other insights into the role of V-ATPase in proliferation and differentiation are provided by studies using genetic knockout *in* vivo, or *in vitro* knockdown of individual V-ATPase subunits. For example, mice with either the heterozygous or homozygous R740S mutation in the *a3* subunit isoform, as well as *a3*-knockout mice and *a3*-truncated mice, all had inactive osteoclasts due to a lack of a ruffled border or the uncoupling of proton pumping from ATP hydrolysis, but osteoclast numbers were normal or even increased (Nakamura et al., 1997, Li et al., 1999, Ochotny et al., 2011, Ochotny et al., 2013). Using a mouse knockout model of the *d2* subunit, Lee et al. (2006) showed that osteoclast differentiation was impaired, which was attributed to ineffective fusion of precursors, but the proliferation of osteoclast precursors was found to be unaffected by *d2* knockout. Finally, knockdown of the V-ATPase subunit *Ac45 in vitro* was shown to inhibit osteoclast differentiation via decreased precursor proliferation and fusion, due to down regulation of ERK, c-Fos and NFATc1, which suggest that *Ac45* acts upstream of osteoclastogenic signalling pathways (Yang et al., 2012). Similar effects on NF-κB and pERK pathways were also observed using the V-ATPase inhibitors saliphenylhalamide and bafilomycin (Qin et al., 2012a), and TRAF6, which mediates RANKL-induced

signalling, was shown to directly interact with V-ATPases suggesting a potential link with osteoclastogenesis (Ryu et al., 2005).

Interestingly, the V-ATPase inhibitor enoxacin, which targets the interaction between the *B2* V-ATPase subunits and actin microfilaments, was shown to directly inhibit osteoclastogenesis without inducing apoptosis (Toro et al., 2012b). The authors proposed that enoxacin was preventing the specific recruitment of *a3*-containing V-ATPase complexes to the ruffled border during differentiation, mediated by the actin-binding site on the *B2* subunit. The plasma membrane sorting of DC-STAMP, a protein involved in the fusion of osteoclast precursors, was also perturbed as were the trafficking of other proteins, suggesting effects downstream of V-ATPase-actin binding in regulating vesicular trafficking and sorting. A similar finding was reported by Voronov et al. (2013) where, contrary to other studies examining the *a3* subunit mentioned above, *in vitro* differentiation of osteoclasts from mice with the heterozygous R740S mutation was impaired, attributed to decreased NFATc1 translocation and elevated lysosomal pH. Currently the precise roles of lysosomal pH in osteoclastogenesis are unknown, however, there are other reports of inhibited signalling pathways in response to V-ATPase-mediated pH levels, such as Wnt/β-catenin (Cruciat et al., 2010) and notch (Yan et al., 2009). Intracellular pH is known to have a central role in transport along the endocytotic pathway as the activity of V-ATPases in different endocytotic compartments result in finely regulated pH gradients that are crucial for effective trafficking (Xu et al., 2003, Hurtado-Lorenzo et al., 2006, Marshansky and Futai, 2008). The effects seen by 73-DOC on osteoclastogenesis, as well as osteoblast differentiation, could therefore be attributed to disrupted endocytosis and trafficking of signalling molecules.

The direct effects of 73-DOC on V-ATPase subunits such as *a3*, *d2* or *Ac45* are currently unknown, but future molecular analyses determining the effects of 73-DOC on

the expression of these different subunits would help explain some of the observations made in this chapter. Similarly, examining 73-DOC-induced changes in osteoclastogenic signalling pathways such as NFATc1, c-Fos, NF-κB, pERK and TRAF6 in order to determine whether 73-DOC directly inhibits osteoclastogenesis. Regarding osteoblasts, very little is known about the role of V-ATPase in osteoblast differentiation, though knockout studies have shown that osteoblast parameters were unaffected by dysfunction of the *a3* and *d2* subunits (Li et al., 1999, Lee et al., 2006, Ochotny et al., 2013). In considering the role of V-ATPases in regulating trafficking and signalling, it is tempting to speculate that similar mechanisms are also affecting signalling cascades in osteoblasts, leading to the observed effects on differentiation. This hypothesis could be confirmed in the future by examining the expression of transcription factors that drive osteoblast differentiation in response to 73-DOC treatment, such as Runx2 or Osx.

A final explanation for the effects of 73-DOC may relate to autophagy (macroautophagy), a protein degradation pathway that functions to maintain cellular homeostasis. This process involves the encapsulation of damaged organelles, pathogens and protein aggregates by autophagosomes, which then fuse with lysosomes for enzymatic degradation of the contents. Crucial to this process is the V-ATPase-mediated acidification of lysosomes, as inhibition of V-ATPases by bafilomycin has been shown to block maturation of autophagosomes by inhibiting fusion with the lysosome, which may also be related to the effects of V-ATPase inhibition on endocytosis (Clague et al., 1994, Van Deurs et al., 1996, Yamamoto et al., 1998, Klionsky et al., 2008). Bafilomycin has since been used as a common tool to study autophagy and the importance of this process in bone cells and skeletal maintenance has also been recognised (Hocking et al., 2012).

In examining increased apoptosis in osteoclasts from mice with the homozygous R740S mutation in *a3,* Ochotny et al. (2013) found that the relative expression of the essential autophagy markers LC3-II and p62 were decreased and increased respectively, which led the authors to suggest that inhibition of autophagy as a result of ineffective intracellular acidification by V-ATPases caused increased sensitivity to toxic events, such as the accumulation of misfolded proteins that would typically be removed by the autophagy process. A similar mechanism has been reported in cancer cells, where V-ATPase inhibitors caused increased autophagy-related apoptosis (Wu et al., 2009b, Kallifatidis et al., 2013, von Schwarzenberg et al., 2013). Interestingly, Ochotny et al. (2013) also observed morphological defects in osteoclasts from mice with the *a3* mutation, including intense, mis-localised TRAP staining and the occurrence of large cytoplasmic vacuoles, consistent with the effects of high 73-DOC concentration on mature osteoclasts shown in this chapter. Similar morphological defects were also attributed to defective vesicular/endosomal trafficking in osteoclasts from osteopetrotic mice lacking either TRAP (Hollberg et al., 2002) or PLEKHM1 (Van Wesenbeeck et al., 2007), the latter of which has recently been shown to regulate fusion of autophagosomes with lysosomes (McEwan et al.). Inhibited late-stage autophagy often leads to the accumulation of autophagosomes due to impaired fusion with lysosomes, so it is possible the large vesicles seen in the 73-DOC-treated osteoclasts are indicators of inhibited autophagy, but electron microscopy would be required to identify the characteristic double membrane of autophagosomes.

Autophagy has also been directly implicated in osteoclastogenesis as Lin et al. (2013) showed that inhibiting autophagy by deletion of Atg7 decreased osteoclast differentiation, whereas inducing autophagy by overexpression of Beclin1 stimulated the production of mature osteoclasts. Also ERK phosphorylation was shown to be regulated by Atg5, Atg7 and LC3 (Martinez-Lopez et al., 2013), and hypoxia-induced

enhancement of osteoclast formation and precursor differentiation was found to be mediated by the upregulation of autophagy (Wang et al., 2011, Zhao et al., 2012). Additionally, pharmacological or genetic inhibition of autophagy has been shown to suppress the differentiation of MSCs to osteoblasts, providing a potential mechanism for the inhibitory effects of 73-DOC on osteoblasts (Pantovic et al., 2013). Conversely, there is evidence suggesting that induction of autophagy via mTOR inhibition may inhibit osteoclast formation. Rapamycin and other mTOR inhibitors have been reported to inhibit osteoclast formation and activity *in vitro* and *in vivo* in rodents and humans (Sanchez and He, 2009, Cejka et al., 2010, Smink et al., 2012). The above findings demonstrate that a mechanism related to autophagy could explain the observations of this chapter. Future experiments examining the expression of autophagy proteins such as Atg5, Atg7, LC3 and p62 in both osteoclasts and osteoblasts following 73-DOC treatment would help resolve this proposed mechanism of inhibition.

In conclusion, the studies in this chapter showed clear effects on osteoclast and osteoblast precursors. The mechanism of these effects may be related to the roles of V-ATPases in intracellular pH, endocytotic trafficking, mTOR signalling and autophagy, all of which are viable candidates for future experiments examining the effects of 73-DOC treatment. As the aim of this thesis was to evaluate 73-DOC as a resorption inhibitor, still to be determined is what effect the compound has on mature cell function. This was investigated in the next chapter.

Chapter 5: The Effects of 73-Deoxychondropsin A on Osteoclast and Osteoblast Function

5.1 Introduction

The previous chapter sought to investigate specific *in vitro* effects of 73-DOC on osteoclast and osteoblast precursor proliferation, viability and differentiation. This chapter will investigate the effects of 73-DOC on mature osteoclasts and osteoblasts, and whether there is differential responsiveness between these two cell types. The specific objectives were to investigate the effects of 73-DOC on the function of osteoclasts and osteoblasts through quantitative resorption and mineralised bone nodule formation assays, respectively, and to examine the effect of the compound on osteoclast cellular acidification, which is the putative primary function of V-ATPases in osteoclasts.

5.2 Materials and methods

5.2.1 Cell culture

Murine osteoclasts and osteoblasts were derived from primary cultures of BMMs and calvarial digests, respectively. Additionally, human osteoclasts were used in this chapter, derived from purified CD14+ PBMCs and cultured as detailed in Section 2.2.3.2.

5.2.2 Osteoclasts

For resorption assays, osteoclasts were cultured on tissue culture plastic before mature cells were detached and re-plated onto dentin in the presence of test compounds. Quantification of resorption pit surface area and depth was performed using reflected light microscopy as described in Section 2.2.7. Actin rings were fluorescently labelled using TRITC-phalloidin in mature human osteoclasts in order to quantify mature cell number, and the activation state of osteoclasts. For the analysis of cellular acidification, osteoclasts were fluorescently labelled with acridine orange and imaged using confocal microscopy as described in Section. 2.2.6

5.2.3 Osteoblasts

For quantification of mineralised bone nodule formation, experiments setup as described in Chapter 4 were examined using von Kossa staining, as detailed in Section 2.2.10.

5.3 Results

5.3.1 73-Deoxychondropsin A inhibits murine and human osteoclastic resorption

The effects of 73-DOC on the resorptive function of murine osteoclasts were first examined by quantifying resorption from cells cultured on dentin following exposure to the compound throughout RANKL-induced differentiation (Figure 4.4). The data show that 73-DOC caused a significant dose-dependent decrease in the surface area of resorption, with a 65 % and 90 % reduction at concentrations of 2.5 nM and 5 nM respectively (Figure 5.1 A). When resorption area was normalised to the number of

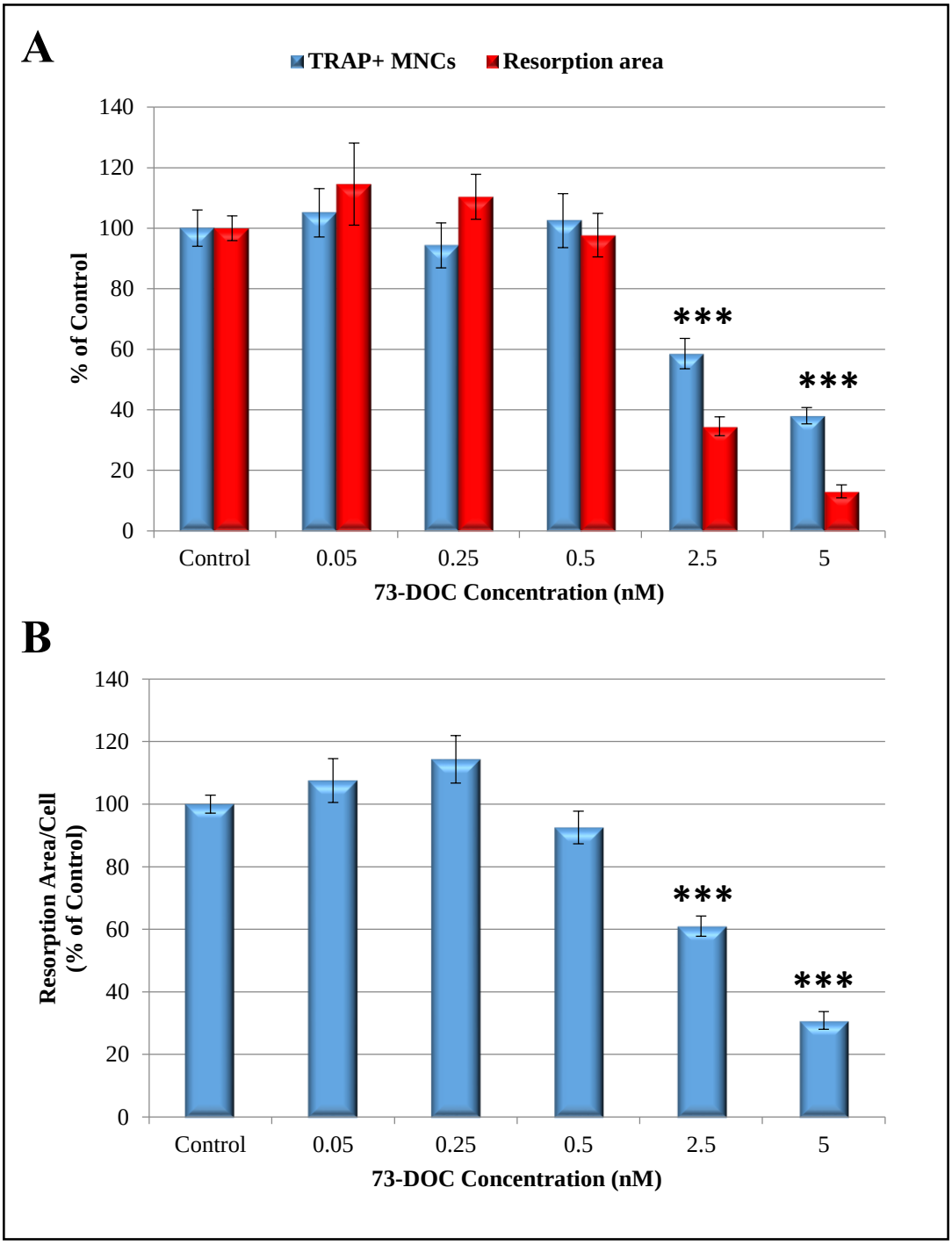

Figure 5.1 73-DOC inhibits the function of osteoclasts formed following continuous exposure during differentiation. Osteoclast precursor cells were cultured on dentin slices. When RANKL was added to stimulate osteoclast differentiation, 73-DOC was also included in the culture medium of test groups and in all subsequent medium changes. Cells were fixed after 7 days, stained for TRAP and counted (Figure 4.4). Cells were then removed from the dentin substrate and resorption surface area was quantified (red bars), shown alongside cell count data (blue bars) **(A)**. Resorption activity per cell was estimated using matched cell count data **(B)**. Bar graph shows mean data ± SEM, $n = 3$. *** = Significant change of all data from control, $p<0.001$.

mature TRAP-positive osteoclasts, a significant decrease in the amount of resorption per cell was seen at identical concentrations, suggesting that the decrease in resorption cannot be attributed to a decrease in cell number alone (Figure 5.1 B).

In order to further examine the specific resorptive function of murine osteoclasts, mature cells were re-seeded onto dentin before being exposed to varying concentrations of 73-DOC for a period of 48 hours. The data show that 73-DOC caused a significant dose-dependent decrease in the surface area of resorption, showing a 20 % decrease at concentrations as low as 0.5 nM 73-DOC, and a complete abolition of resorption at 25 nM (Figure 5.2 A-C, D). Normalisation of the resorption area to the number of mature TRAP-positive osteoclasts showed a similar significant dose-dependent decrease in the resorptive activity per cell (Figure 5.2 E). Measurement of resorption pit depth also revealed that 73-DOC caused a dose-dependent decrease in the depth of resorption pits, showing a significant 10 % decrease at 0.5 nM (Figure 5.2 F). Bafilomycin also caused a dose-dependent decrease in resorption as well as resorption per cell (Figure 5.2 D, E).

The effects of 73-DOC were next investigated on the function of human osteoclasts derived from purified PBMCs, cultured with M-CSF and RANKL. Similar to the procedure utilised with murine osteoclasts, mature human osteoclasts were generated on tissue culture plastic and then re-seeded onto dentin discs before exposure to 73-DOC for a period of 72 hours. TRAP staining of human osteoclasts was found to be highly variable and so actin ring staining was used to quantify osteoclasts before resorption surface area was assessed using reflected light microscopy (Figure 5.3 A-C). The results showed that, similarly to murine osteoclasts, 73-DOC caused a dose-dependent decrease in the number of human osteoclasts, leading to a significant 70 % decrease at 100 nM (Figure 5.3 D). 73-DOC also caused a significant dose-dependent decrease in the total surface area of resorption, showing a 30 % decrease at 1 nM and complete abolition at 30 nM (Figure 5.3 D). Normalising the resorptive activity per cell

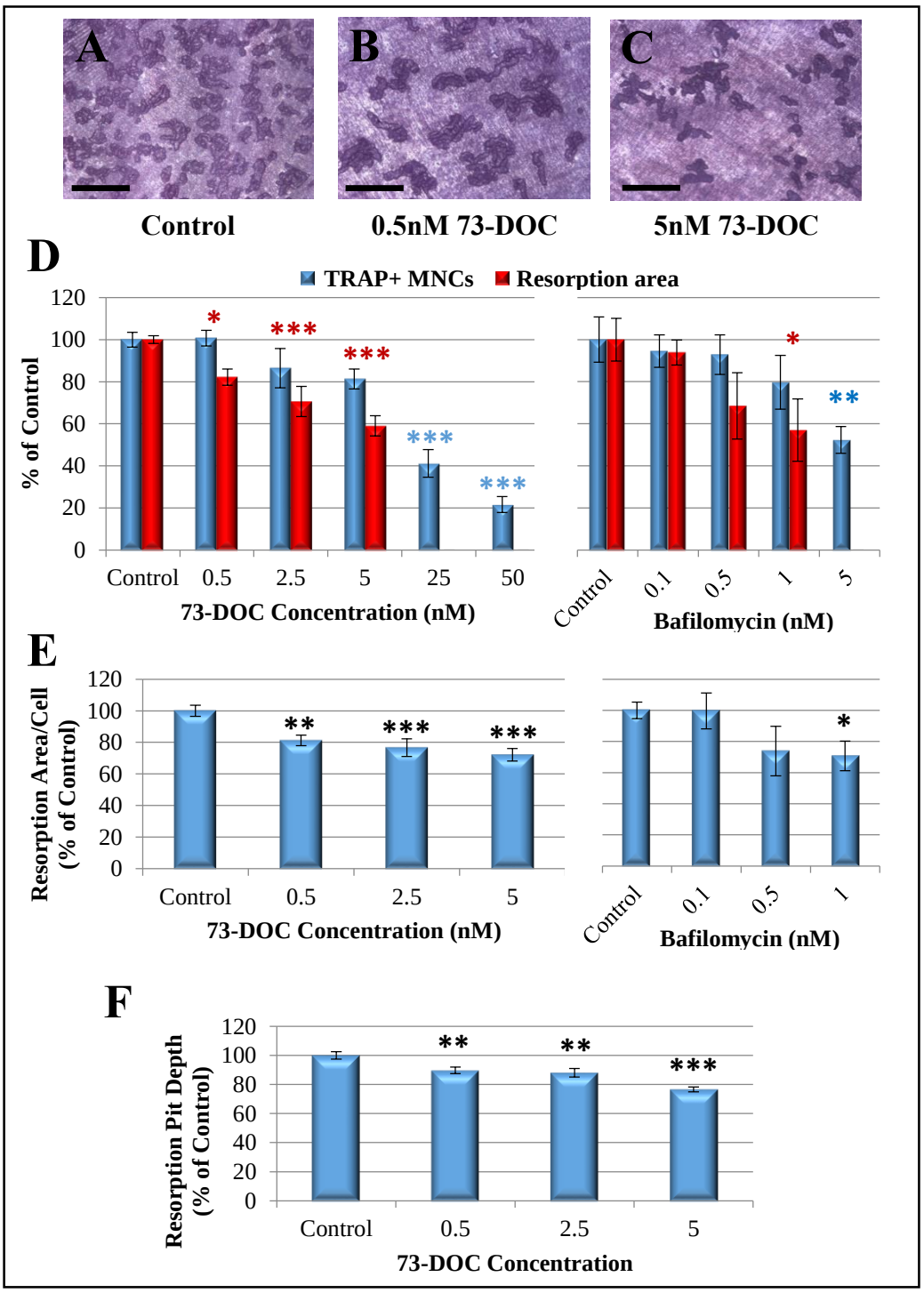

Figure 5.2 73-DOC inhibits the function of mature murine osteoclasts. Mature osteoclasts were re-seeded onto triplicate dentin slices and exposed to 73-DOC and bafilomycin for 48 hours. TRAP-positive MNCs were counted and removed before the dentin slices were stained with toluidine blue and resorption area was quantified using reflected light microscopy. Representative images of darkly stained resorbed areas are shown (scale bars = 400 µm) **(A-C)**. Resorption surface area over the whole dentin slice was estimated (red bars), shown alongside cell count data (blue bars) **(D)**, and then normalised to area per cell **(E)**. Resorption pit depths were also estimated **(F)**. Bar graphs for 73-DOC represent mean data (n = 3) ± SEM. Black or colour-coded stars represent a significant change from control values, *- p<0.05, **- p<0.01, ***- p< 0.001**.** Bafilomycin data from a single representative experiment are shown (n = 2), ± SD.

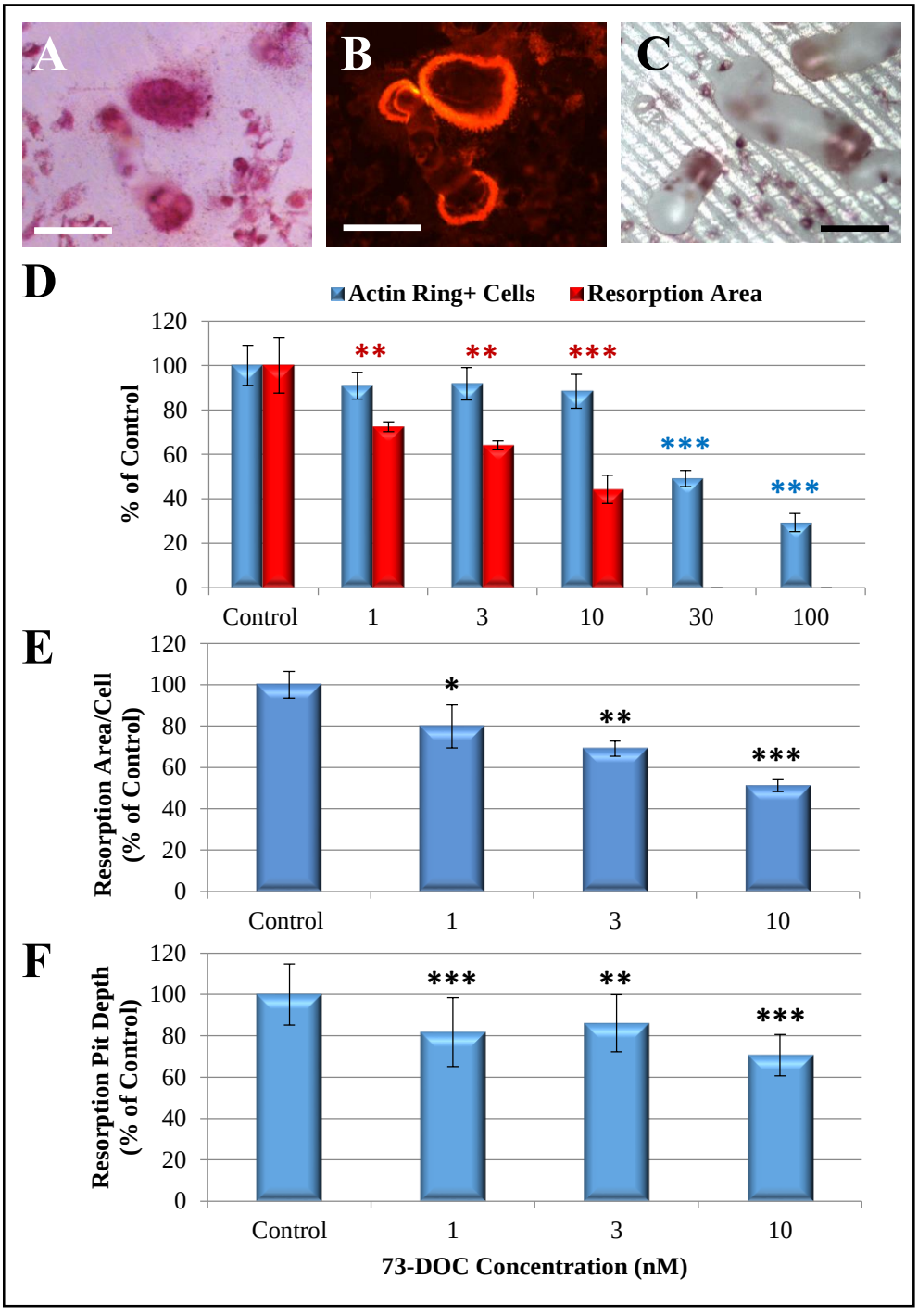

Figure 5.3 73-DOC inhibits the function of human osteoclasts. Human osteoclasts cultured from PBMCs were re-seeded onto dentin slices and exposed to 73-DOC for 72 hours. Typical TRAP **(A)** and matched fluorescent actin stained osteoclasts are shown **(B)**. A reflected light microscopy image of TRAP-stained osteoclasts within out-of-focus resorption pits is also shown **(C)** (all scale bars = 50µm). Actin ring-positive cells were quantified and then removed. Dentin slices were then stained with toluidine blue and the whole-slice surface area of resorption was estimated (red bars), shown alongside cell count data (blue bars) **(D)**, and then normalised to resorption per cell **(E)**. Resorption pit depth was also estimated **(F)**. Bar graphs show the mean values of triplicate data from 1 representative experiment (n = 2) ± S.D. Black or colour-coded stars represent a significant change from control values, *- p<0.05, **- p<0.01, ***- p< 0.001**.**

also showed a dose-dependent decrease, and resorption pit depth was decreased at all concentrations tested (Figure 5.3 D, E).

The inhibitory effect of 73-DOC on human osteoclasts was also confirmed by quantifying the number of osteoclasts that bear a characteristic crescent-shaped actin ring, as this is a hallmark of actively resorbing osteoclasts (Lakkakorpi et al., 1989, Lakkakorpi and Väänänen, 1996). Exposure of human osteoclasts to 73-DOC caused a dose-dependent decrease in the proportion of actively-resorbing osteoclasts, with a significant 65 % decrease at 10 nM, and the complete absence of active osteoclasts at 30 nM 73-DOC (Figure 5.4). Interestingly, significant reductions in resorbing osteoclasts were seen at concentrations that had no significant effect on the total number of actin ring-positive cells. Taken together, these results indicate that 73-DOC can inhibit the function of both mature murine and human osteoclasts.

5.3.2 73-Deoxychondropsin A inhibits osteoclast acidification

The decrease in the number of actively resorbing osteoclasts suggested that 73-DOC inhibits osteoclast function. This was further investigated by examining cellular acidification, which is essential for osteoclast function (Baron et al., 1985). To this end, acridine orange staining was used which fluoresces orange when protonated in regions of cellular acidification, and green in less acidic conditions when viewed using fluorescence microscopy. Confocal microscopy analysis following acridine orange staining of mature, actively-resorbing murine osteoclasts showed the expected orange fluorescence staining (Figure 5.5 A, B). Closer examination showed that the fluorescence was localised in putative intracellular vesicles, and significantly, to the

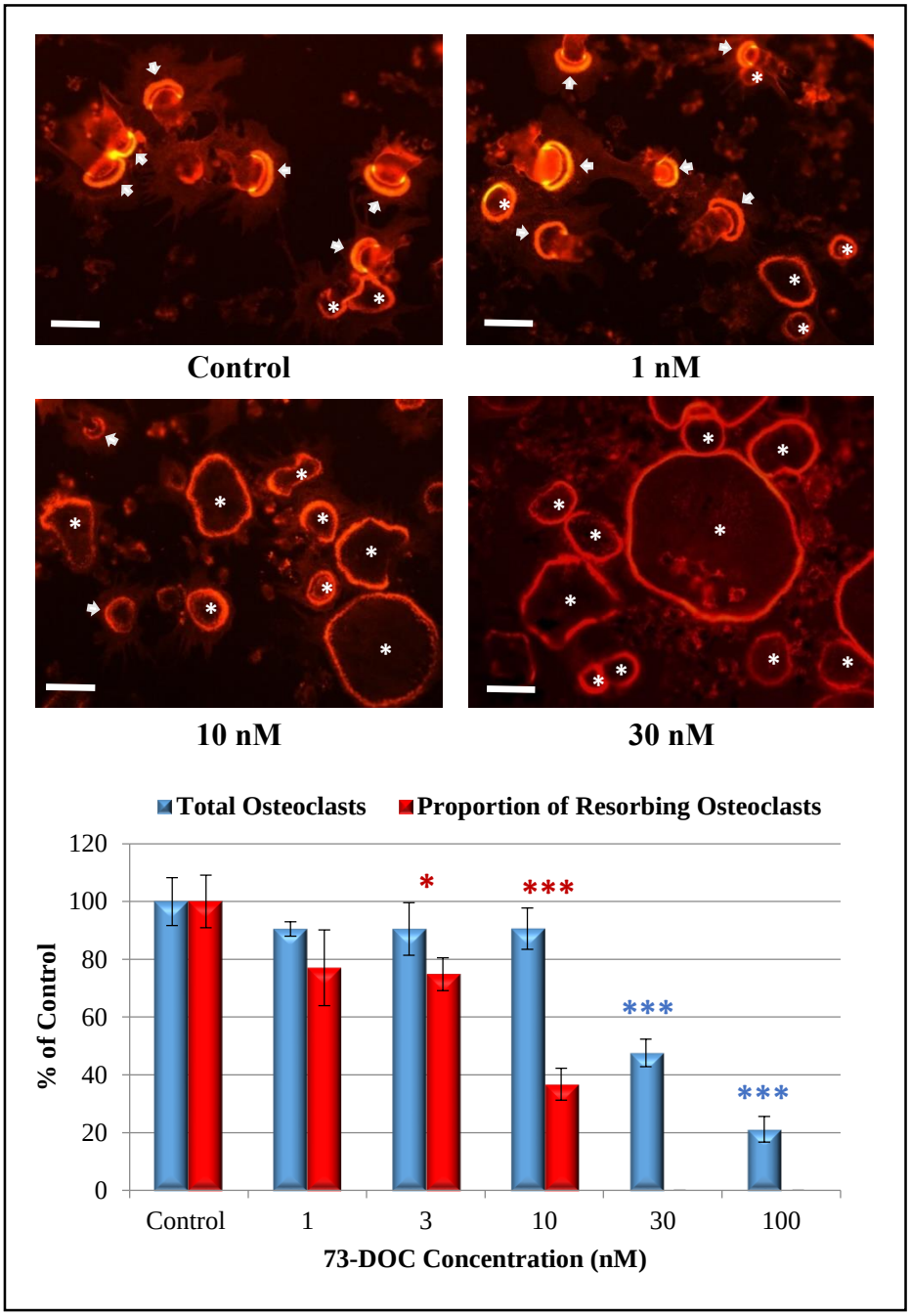

Figure 5.4 73-DOC inhibits the number of actively resorbing osteoclasts. Actin rings from human osteoclasts exposed to 73-DOC for 72 hours were fluorescently stained. Representative images are shown with white arrows indicating osteoclasts with the characteristic actin ring morphology of actively resorbing osteoclasts, and white stars indicating non-resorbing osteoclasts (scale bar = 50 µm). The number of actively resorbing osteoclasts were counted and expressed as a proportion of the total number of actin ring-positive osteoclasts (red bars). Total cell count data is also shown (blue bars). Bar graph shows the mean values of triplicate data from 1 representative experiment (n = 2) ± S.D. Colour-coded stars represent a significant change from control values, *- p<0.05, ***- p< 0.001**.**

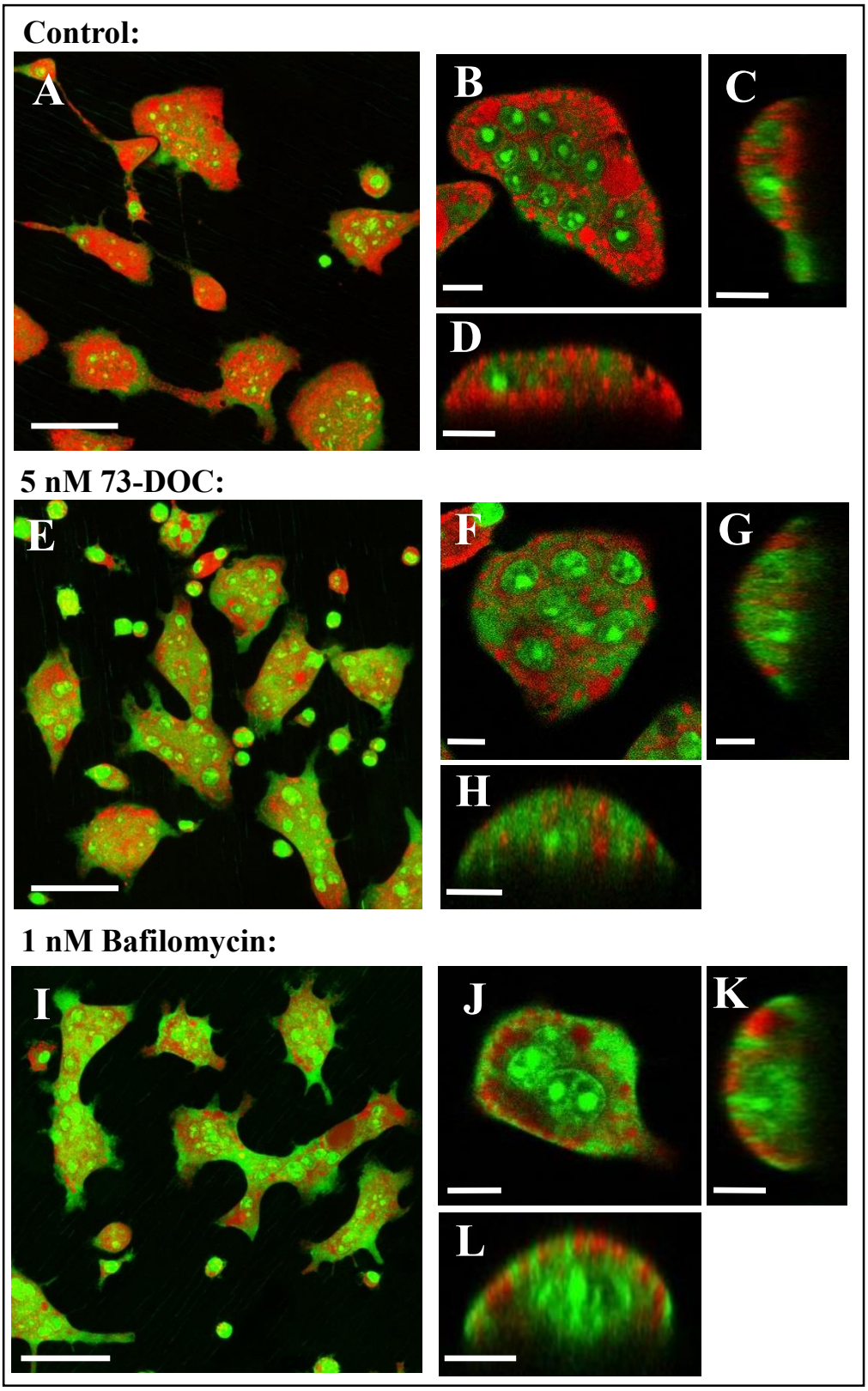

Figure 5.5 73-DOC inhibits cellular acidification in osteoclasts. Murine osteoclasts were cultured on dentin slices. 24 hours prior to imaging, 73-DOC (5 nM) and bafilomycin (1 nM) were added to test wells. Live untreated, **(A-D)**, 73-DOC-treated **(E-H)**, and bafilomycin-treated **(I-L)** cells were then imaged using confocal microscopy as described in Chapter 2. Images of z-stacks projections **(A, E, I)** and cross sections of individual cells **(B-D, F-H, J-L)** are shown. Scale bars: **A, E, I** = 50 µm; **B-D, F-H, J-L** = 10 µm.

ruffled border on the resorbing surface of the osteoclasts (Figure 5.5 C, D). Treatment with 73-DOC or bafilomycin for 24 hours showed a marked reduction in overall orange fluorescence (Figure 5.5 E-F, I-J) and significantly, there was reduced fluorescence localised at the resorbing surface of the osteoclasts (Figure 5.5 G-H, K-L). These results suggest that 73-DOC prevented acidification of the resorption lacunae, which would correlate with the inhibition of resorption activity.

5.3.3 73-Deoxychondropsin A inhibits murine osteoblast differentiation and matrix deposition

Finally, to further characterise the effects of 73-DOC on the differentiation of osteoblasts, bone nodule assays were performed using primary mouse osteoblasts. Varying concentrations of 73-DOC and bafilomycin were added to osteoblast differentiation cultures at two different stages (Figure 4.2), at early stages to investigate the effects on osteoblast precursors, and at later stages after nodule formation had started, to investigate the effects on nodule formation, matrix deposition and mineralisation.

Addition of 73-DOC to early stage cultures resulted in a dose-dependent decrease in bone nodule formation, with a ~60 % decrease in mineralised nodules at 2.5 nM and a complete inhibition at 5 nM 73-DOC (Figure 5.6 A). This correlated with the effects seen with ALP staining though the effect on mineralisation was marginally more sensitive (Figure 4.6 A). Addition of 73-DOC to late stage cultures after nodules had already started forming showed a 70 % decrease in mineralised bone nodule area at 5 nM with complete inhibition at 10 nM (Figure 5.6 B). Again, a similar effect was seen with ALP activity but the effect on mineralisation was more marked (Figure 4.6 B). Bafilomycin also caused a dose-dependent decrease in mineralised bone nodule

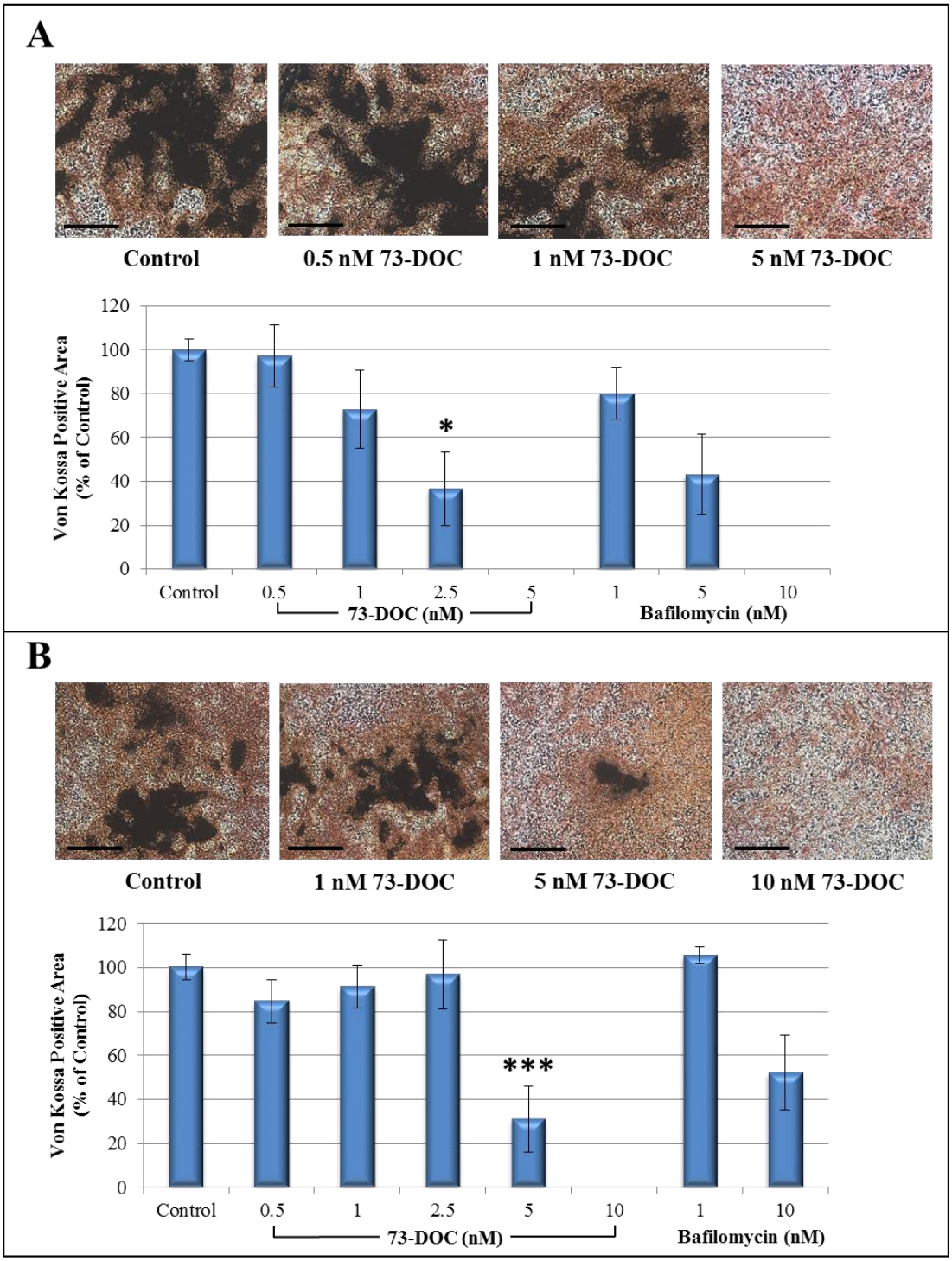

Figure 5.6 73-DOC inhibits the formation of mineralised bone nodules. Osteoblast precursors, isolated from mice calvaria, were cultured in osteogenic media. 73-DOC and bafilomycin were added to the culture medium of test groups at an early stage on day 2 of culture **(A)** and at a late stage when cells were confluent **(B)**. Cells were fixed when mineralised bone nodules were evident in control wells and, following ALP staining (Chapter 4, Figure 4.6), mineralised bone nodules were visualised using von Kossa staining and imaged. Representative images of stained cells are shown (scale bar = 500 µm). The area of von Kossa staining was quantified from each well and expressed as a percentage of control values. Bar graphs the mean values of mineralised bone nodule area ± SEM, $n = 3$. Stars represent significant change from control values, *- $p<0.05$, **- $p<0.01$.

formation at both time points but with increased sensitivity at an early stage (Figure 5.6 A, B). Interestingly, many unmineralised nodules were observed at concentrations where von Kossa staining was negative, implying that the process of mineralisation was inhibited whereas matrix deposition and nodule formation was still occurring. These results suggest that 73-DOC causes an overall inhibition of mineralisation of bone nodules and that osteoblast precursors are more sensitive to the effects than mature, differentiated osteoblasts.

5.4 Discussion

In this chapter, the effects of 73-DOC on osteoclasts and osteoblasts were demonstrated using functional assays. The inhibition of osteoclast function by 73-DOC was demonstrated in both mouse and human derived cells, showing significant inhibition of resorption at 0.5 and 1.0 nM respectively. This result is consistent with previous studies which showed that targeting the V-ATPase pharmacologically with inhibitors (Sundquist et al., 1990, Visentin et al., 2000, Niikura et al., 2004, Karsdal et al., 2005, Niikura et al., 2005, Niikura et al., 2007, Sorensen et al., 2007, Kartner et al., 2010, Qin et al., 2012a, Toro et al., 2012a, Crasto et al., 2013) or through knockdown/interference of the whole V-ATPase or its subunits (Laitala-Leinonen and Vaananen, 1999, Li et al., 1999, Hu et al., 2005b, Lee et al., 2006, Feng et al., 2009b, Yang et al., 2012, Ochotny et al., 2013), can lead to inhibition of osteoclast mediated bone resorption. Interestingly, the inhibition of osteoclast function was attained at concentrations that had no effects on the proliferation, differentiation and viability of osteoclasts, where such effects were seen at concentrations of 2.5 nM and above. To date, the most potent chemical inhibitor of *in vitro* osteoclast resorption has been bafilomycin, with half maximal inhibition reported at 0.625nM to 5nM (Karsdal et al., 2005, Qin et al., 2012a). In the current work,

although 73-DOC was found to be as potent as bafilomycin, mature osteoclasts appeared to be more tolerant of higher concentrations of 73-DOC than bafilomycin. As bafilomycin is generally considered unsuitable for therapeutic use due to off-target effects, this suggests that 73-DOC may represent an equally effective, but more therapeutically suitable V-ATPase inhibitor (Keeling et al., 1998).

The use of acridine orange staining showed that osteoclasts treated with 73-DOC were consistently found to have less overall cellular acidification, and in particular, less acidification localised at the ruffled border, than untreated cells. This result strongly implies that V-ATPase inhibition is indeed occurring and would provide one explanation for the inhibition of resorption by 73-DOC. That 73-DOC itself can inhibit V-ATPase activity was shown previously by Bowman et al. (2003) using a biochemical assay and isolations of membrane-bound V-ATPases from fungal and bovine sources. However, the results of this chapter demonstrated for the first time that 73-DOC inhibits human/murine V-ATPase-mediated osteoclast resorption. Furthermore, 73-DOC was found to elicit half maximal inhibition of osteoclast resorptive activity (~5 nM in mice) at concentrations 20- and 600-fold less than those causing similar inhibition of fungal (100 nM) and mammalian (3 μM) V-ATPase activity, respectively. These exciting findings demonstrate that 73-DOC has highly potent, novel activity in osteoclasts that provide further support for its potential application as a therapeutic. The inhibitory effects of 73-DOC on isolated human membrane V-ATPase activity have not yet been determined, but future experiments with differential V-ATPase-containing membrane fractions or microsomes, sourced from osteoclasts and other human cell types, would be of value in confirming specificity for the osteoclast V-ATPase. In this regard, the methods of either Bowman et al. (2003), or those involving spectroscopic *in vitro* measurements of acridine orange fluorescent quenching in response to ATP and test compounds (Wu et al., 2009a), could be applied.

The absence of acidic acridine orange staining at the ruffled border in 73-DOC-treated osteoclasts could suggest that the targeted localisation of V-ATPase-containing vesicles to the ruffled border is disrupted by 73-DOC. This would represent one exciting possible role of 73-DOC action, and is reminiscent of the proposed mechanism responsible for impaired bone resorption in osteoclasts depleted of the *Ac45* subunit, which showed disrupted localisation of fluorescently labelled V-ATPases in resorbing osteoclasts (Qin et al., 2011, Yang et al., 2012). However, the lack of acridine orange staining may also be explained by the lack of a ruffled bored. Indeed, osteoclasts treated with bafilomycin or from mice/humans lacking the *a3* V-ATPase subunit are not functional due to the absence of cell polarisation and ruffled border formation (Seifert and Marks, 1985, Nakamura et al., 1997, Bruder et al., 2003, Sahara et al., 2003, Ochotny et al., 2013). This cannot be ruled out at the present time, therefore electron microscopic analysis of 73-DOC-treated cells is one possible direction for future work.

Whilst it is clear that inhibition of specific V-ATPase subunits contribute to the loss of V-ATPase activity in osteoclasts, the putative binding site for 73-DOC remains to be resolved. In this regard, it is interesting to note that bafilomycin and concanamycin A have both been shown by two independent studies to bind to the *c* subunit of the V_0 V-ATPase domain (Bowman and Bowman, 2002, Huss et al., 2002) and that Bowman et al. (2003) also found that a mutated bafilomycin-resistant yeast strain exhibited decreased sensitivity to the effects of 73-DOC in comparison with wild-type yeast. Whether 73-DOC also binds directly to the *c* subunit, or to any other V-ATPase subunit is a very interesting question and remains a goal for future work (see Chapter 7) alongside characterising V-ATPase subunit transcription and expression in 73-DOC-treated osteoclasts.

Another possibility is that osteoclastic resorption in response to 73-DOC was inhibited due to the roles of V-ATPases in other cellular processes such as endosomal

trafficking. The role of the V-ATPase in maintaining intracellular pH for proper functioning of vesicular trafficking has been established previously, and it is known than trafficking of late endosomes/lysosomes is critical for the formation of the ruffled border and for bone resorption (Coxon and Taylor, 2008). Treatment of osteoclasts with bafilomycin has been shown by to interrupt endocytosis, vesicular trafficking as well as formation of a ruffled border (Sahara et al., 2003, Xu et al., 2003). Interestingly, osteoclasts treated with brefeldin A, a potent inhibitor of intracellular vesicular transport, also lacked ruffled borders and showed accumulation of extremely large vesicles consistent with the unusual osteoclast morphology observed following 73-DOC treatment (Sahara and Sasaki, 2001). Therefore, it is tempting to speculate that 73-DOC could be also be acting in a similar way, reducing resorptive activity through specific disrupted targeting of the ruffled border V-ATPase complex, or through dysfunctional endocytosis in general. This could be confirmed in the future by examining fluorescently labelled V-ATPase trafficking in response to 73-DOC treatment.

Disrupted endosomal pH is one indirect explanation to account for V-ATPase-mediated effects on intracellular trafficking but the crucial trafficking of late endosomes/lysosomes to the ruffled border is thought to also directly involve the V-ATPase and the microfilament cytoskeleton of the cell. F-actin binding domains have been found in the V-ATPase subunits *B* (Holliday et al., 2000) and *C* (Vitavska et al., 2003), with other studies demonstrating that the V-ATPase-actin interaction is essential for osteoclast activation (Lee et al., 1999), actin ring formation (Feng et al., 2009b) and proper ruffled border formation (Zuo et al., 2006). This led to the understanding that this interaction could mediate the tethering of V-ATPases to cortical actin following endosomal trafficking and prior to insertion at the ruffled border (Coxon and Taylor, 2008). This interaction also appears specific for *a3*-containing V-ATPases, as the V-ATPase fails to associate with the cytoskeleton in osteoclasts derived from *oc*/*oc* mice

(Nakamura et al., 1997) and actin-V-ATPase binding activity was specifically observed with the *a3* and not the *a1* subunit (Toro et al., 2012b).

Actin staining of 73-DOC-treated osteoclasts indeed showed that the proportion of actively resorbing osteoclasts was significantly reduced at levels greater than cortical actin ring formation, suggesting effects on the rearrangement of the cytoskeleton during osteoclast activation. This result could be explained by interference of the V-ATPase-actin interaction or by disrupted vesicular trafficking of the V-ATPase complex. Enoxacin, an inhibitor of the actin-V-ATPase interaction, was shown to inhibit osteoclast resorption and osteoclastogenesis similar to 73-DOC (Ostrov et al., 2009). However, the authors reported that actin ring formation was disrupted at concentrations that inhibited resorption, contradicting that found with 73-DOC. A similar situation was reported for *a3* siRNA interference (Hu et al., 2005b), though this was contradicted by Feng et al. (2009b) who showed that *C2* silencing disrupted actin ring formation but not *a3*. Knockdown of the *Ac45* V-ATPase subunit did not affect cortical actin ring formation (Yang et al., 2012).

Many processes involved with osteoclast polarisation and vesicular trafficking are regulated by small GTPases. In osteoclasts, the lysosomal GTPase Rab7 is particularly important in ruffled border formation and the targeted trafficking of V-ATPases, as shown by antisense knockdown studies (Zhao et al., 2001, Itzstein et al., 2011). An interesting result from the study by Yang et al. (2012) was that the *Ac45* subunit co-localised with Rab7 in resorbing osteoclasts and directly interacted with Rab7. This demonstrates an additional possible mechanism of V-ATPase inhibition leading to consequences for vesicular trafficking and ruffled border formation. The similarities between the effects of the 73-DOC and the *Ac45* knockdown would suggest that dysfunctional trafficking of the V-ATPase complex could be responsible for the observed decreases in resorption and osteoclast activation. The effects of 73-DOC on

the *Ac45* subunit or the Rab7 pathway also represent directions for future experiments alongside further examination of the osteoclast cytoskeleton and V-ATPase localisation in response to 73-DOC treatment.

A final mechanistic explanation for reduced osteoclast function following V-ATPase inhibition concerns autophagy. The bone remodelling disorder Paget's disease, characterised by excessive osteoclast numbers and activity, has been shown to be associated with mutations affecting the essential autophagy protein, SQSTM1, and indeed, autophagic protein degradation was found to be inhibited in osteoclasts with the *SQSTM1* (also known as p62) mutations (Helfrich and Hocking, 2008, Hocking et al., 2012). Further evidence of autophagy participating in osteoclast function comes from genetic knock-out studies of the key autophagosome proteins Atg5, Atg7, Atg4B and LC3. These were all shown using electron and immunofluorescence microscopy to be required for ruffled border formation and the function of osteoclasts *in vitro* and *in vivo* (DeSelm et al., 2011). Additionally, Rab7 localisation at the ruffled border was shown to be Atg5-dependent and lysosomal targeting to actin rings was disrupted by all the knockouts. These intriguing discoveries imply an important role for autophagy in lysosomal targeting and osteoclast function and may explain the observed effects of 73-DOC on osteoclast activity. Future experiments could confirm this hypothesis by examining Atg5, Atg7, Atg4B and LC3 expression and localisation in 73-DOC-treated osteoclasts.

A combination of the above mechanisms may also be occurring in osteoclasts, which may explain the 5-fold difference in magnitude between the concentration of 73-DOC needed to significantly affect osteoclast resorption versus differentiation. This observation may reflect the different levels of V-ATPase required by the relevant processes, as more complexes are required for resorption than for other endosomal/lysosomal-based intracellular functions, as shown by *a3* expression and

localisation relative to other *a* isoforms present in osteoclasts (Toyomura et al., 2000, Toyomura et al., 2003). This implies that resorption will be more sensitive to V-ATPase inhibition than other cellular processes. However, a compensatory mechanism may also be taking place with non-ruffled border V-ATPases leading to a higher tolerance of 73-DOC. Nyman and Vaananen (2010) demonstrated such a situation, showing that the V-ATPase subunit *a1* could compensate for *a3* inhibition in lysosomal V-ATPases, but not in the ruffled border V-ATPase. If 73-DOC is targeting a subunit that is present in both lysosomal and ruffled border V-ATPases, but that can be compensated for in the lysosome, this would explain the differential sensitivity between differentiation and resorption.

73-DOC was also shown to inhibit the formation of mineralised bone nodules by osteoblasts with osteoblast precursors being more sensitive than fully mature osteoblasts. However, when added after nodules started forming, 73-DOC appeared to have a greater inhibitory effect on mineralisation (~70 % decrease) than it did on differentiation (~30 % decrease). This was also evident by the persistence of unmineralised bone nodules at high concentrations of 73-DOC. This would suggest that 73-DOC regulates the processes of differentiation/matrix deposition and mineralisation via different mechanisms. Inhibition of mineralised nodule formation was also seen with bafilomycin but, as with osteoclasts, 73-DOC was found to be more potent. The role of V-ATPases in osteoblasts are scarcely studied and poorly understood. However, the effect of bafilomycin is consistent with that shown by Sorensen et al. (2007), where a 60 % decrease in bone nodule formation was seen at 10 nM bafilomycin. Interestingly, another V-ATPase inhibitor utilised in that study, diphyllin, was shown not to impair nodule formation despite inhibiting osteoclast resorption at comparable concentrations. Ostrov et al. (2009) also reported normal bone mineralisation despite impaired osteoclast function with enoxacin, suggesting that the V-ATPase-actin interaction or the *B2* subunit

is not critical in osteoblasts. In *d2* knockout mice, bone formation was actually found to be stimulated rather than inhibited but as *d2* is not expressed in osteoblasts, the effect was indirect (Lee et al., 2006). These results suggest that some V-ATPase subunit isoforms are not critical in osteoblasts but that some inhibitors, such as bafilomycin and 73-DOC, do have targets expressed in this cell type.

It is currently unknown what role the V-ATPase has in the bone mineralisation process of osteoblasts, however, it is possible that V-ATPase inhibition is modulating the secretory pathway of osteoblasts due to the effects on endosomal/vesicular trafficking. V-ATPases have indeed been shown to have a role in the mineralisation/demineralisation of epithelial cuticles in terrestrial isopods (woodlouse) during moulting, showing a contribution to the process of $CaCO_3$ deposition (Ziegler et al., 2004). The secretory processes of other cell types have been shown to be inhibited by V-ATPase targeting (Sun-Wada et al., 2006), so it is possible that the processes of matrix deposition and matrix vesicle exocytosis for bone formation may be similarly affected. Interestingly, autophagy appears to be an important process for other secretory cell-types including osteoblasts, where knockdown of autophagy genes has been shown to inhibit osteoblast mineralisation capacity *in vitro* and *in vivo*, and furthermore, autophagosomes have been implicated as vehicles for the secretion of apatite crystals (Nollet et al., 2014). Autophagy thus provides a mechanism that could explain the functional effects in both osteoclasts and osteoblasts following treatment with 73-DOC, suggesting an examination of autophagy proteins in both cell-types would be an important direction for future experiments. Characterisation of the subunit composition of osteoblast V-ATPases, with comparison to the osteoclast V-ATPase, would also be worthwhile to explain the mechanisms of 73-DOC inhibition.

In conclusion, the work presented clearly indicated that 73-DOC has potent inhibitory effects on osteoclast activity, whilst also exhibiting some inhibitory activity

on osteoblast function. Further characterisation of the mechanisms underlying these responses are necessary, with potential candidates including specific V-ATPase subunit expression, endosomal/vesicular trafficking and autophagy. Ultimately, characterisation of *in vivo* effects will also be crucial in clarifying any remaining questions regarding the efficacy of 73-DOC as a potential therapeutic (see Chapter 7). However, considering the supply problems of other commercially viable natural products, prior to investigating long-term mechanistic and *in vivo* studies, as critical way forward is to establish methodology that would allow for a sustainable and renewable supply of 73-DOC that would eliminate the need to harvest sponge stocks from the natural environment. Work presented in the next chapter was therefore performed in contribution to this goal.

Chapter 6: Partial Cloning and Sequencing of the 73-Deoxychondropsin A Biosynthetic Gene Cluster

6.1 Introduction

The final aim of this thesis was to isolate the gene products responsible for 73-DOC biosynthesis. Previous chapters have shown that 73-DOC has biological activity that requires future investigation, but many natural products are prevented from advancing as therapeutics due to issues of providing sufficient material to sustain a global market. This prompted an investigation into a potential solution for the sustainable supply of 73-DOC through cloning of the biosynthetic genes.

The chemical structures of 73-DOC and the other chondropsin metabolites indicate they are from polyketide family (Cantrell et al., 2000, Rashid et al., 2001a, Rashid et al., 2001b). As many marine sponges including *I. ramosa* are host to large communities of symbiotic microorganisms and given that the PKS enzymes responsible for polyketide biosynthesis are mainly produced by bacteria, fungi and plants, it is highly likely that 73-DOC is produced by a member of the *I. ramosa* microbial consortia (Taylor et al., 2007a, Webster et al., 2010). A compound with a microbial, polyketide origin has distinct benefits for overcoming the supply problem as the biosynthetic genes typically exist as gene clusters that facilitate the isolation of complete biosynthetic pathways using large-insert clone libraries, which might then also be directly shuttled into heterologous hosts. The first step in this ultimate goal was to clone and sequence the genes likely involved in the biosynthesis of 73-DOC.

Following the co-linearity principles of non-iterative type I PKS biosynthesis, where the number of modules dictate the chain length of the final product and the

structures of intermediates directly correspond to the PKS module domain architecture, such polyketide structures can be predicted from PKS domain architecture and vice versa (Staunton and Weissman, 2001, Weissman and Leadlay, 2005, Fischbach and Walsh, 2006). As the chemical structure for 73-DOC is already known (Rashid et al., 2001b), a putative model for the domain order of the PKS biosynthetic enzymes was predicted (Figure 6.1 A). A complete predictive model of 73-DOC biosynthesis was provided by Dr Paul Long (KCL) and Professor Barry Wilkinson (Department of Molecular Microbiology, John Innes Centre), showing a modular type I hybrid PKS/NRPS system consisting of a loading module and 26 extension modules, 3 of which were predicted as NRPS modules (modules 4, 10 and 26) that implied the incorporation of leucine, threonine and 3-hydroxyaspartic acid amino acids (Figure 6.1 B).

The likely domain architecture of each module, including enzymatic domains involved in acyl chain reduction and the type of extension units incorporated by each module, have also been predicted. Based on the presence of α-methyl branches in parts of the structure, the incorporation of methylmalonyl-CoA units (modules 1, 2, 6, 7, 9, 11, 13-16) was predicted, whilst malonyl-CoA extension units were putatively incorporated by modules corresponding to non-methyl branched parts of the structure (modules 3, 5, 8, 12 and 17-25). Chain release and the formation of the macrocycle is predicted to occur via a dedicated TE domain, similar to deoxerythronolide B synthase (DEBS), the PKS responsible for the biosynthesis of 6-deoxyerythronolide B (Staunton and Weissman, 2001). The starter unit used to initiate polyketide chain assembly by the putative loading module is unusual due to the presence of a geminal-dimethyl group, where two methyl groups are attached to one carbon atom (yellow moiety in Figure 6.1 A). One explanation for this is that the starter acid is methylmalonyl-CoA, or its ester, with a subsequent α-methylation step suggesting the presence of a methyltransferase domain in the loading module. A similar mechanism was also predicted in module 2.

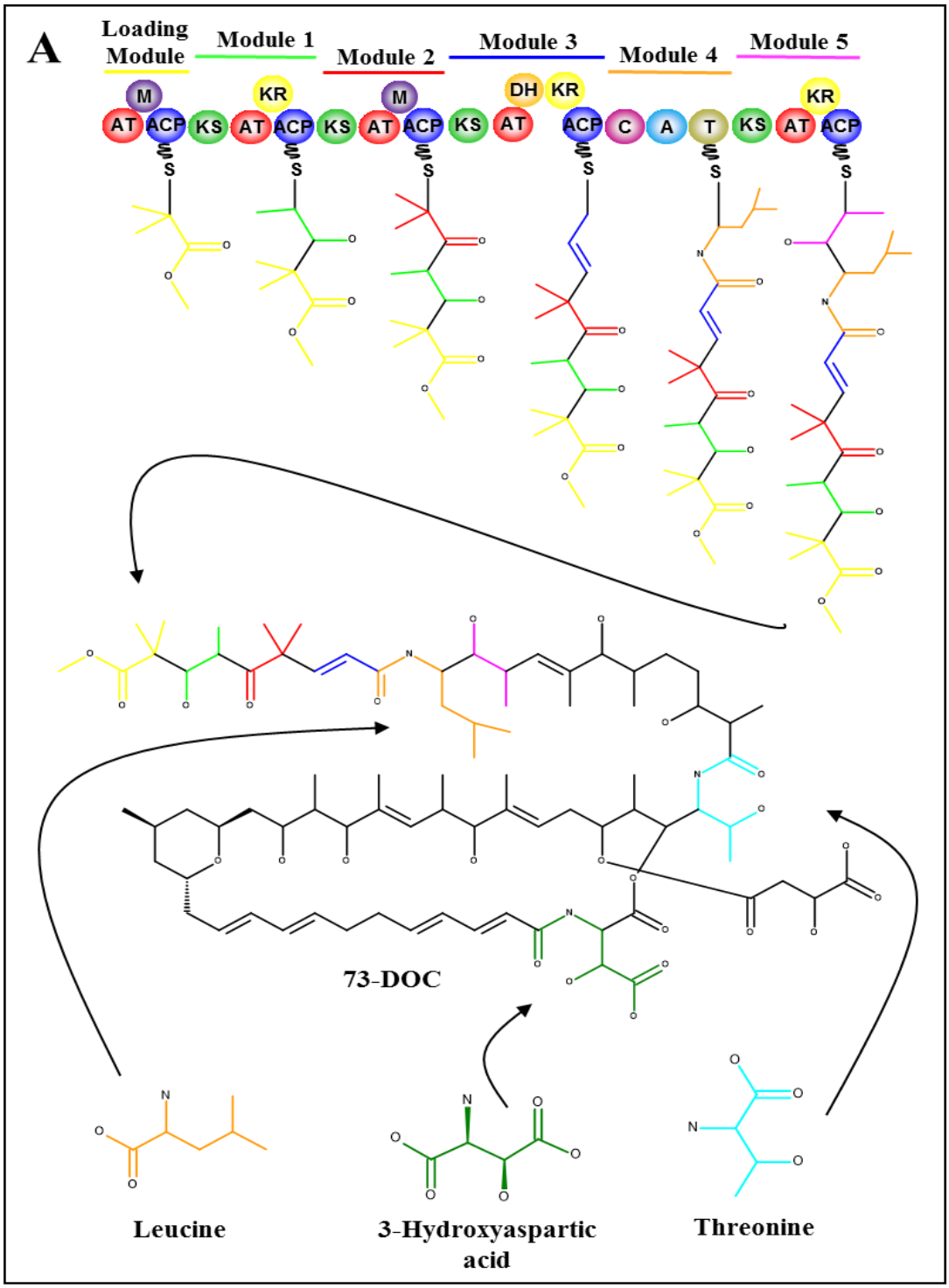

Figure 6.1 A putative model for 73-DOC biosynthesis. PKS and NRPS domain organisation of the first 5 modules from the predicted 73-DOC pathway is shown **(A)**. The products produced by each module are colour-coded to their location in the 73-DOC structure shown below. The colour-coded structures for the three amino acids putatively incorporated into 73-DOC are also shown. The complete predicted model of 73-DOC biosynthesis for all 26 modules is also shown **(B)**. The predicted extension unit selected by the acyl transferase (AT) domains of PKS modules are shown below each module, where mal is malonyl-CoA and methyl-mal is methylmalonyl-CoA. The substrate specificity of the adenylation (A) domains for each of the 3 NRPS modules are also shown below those modules.

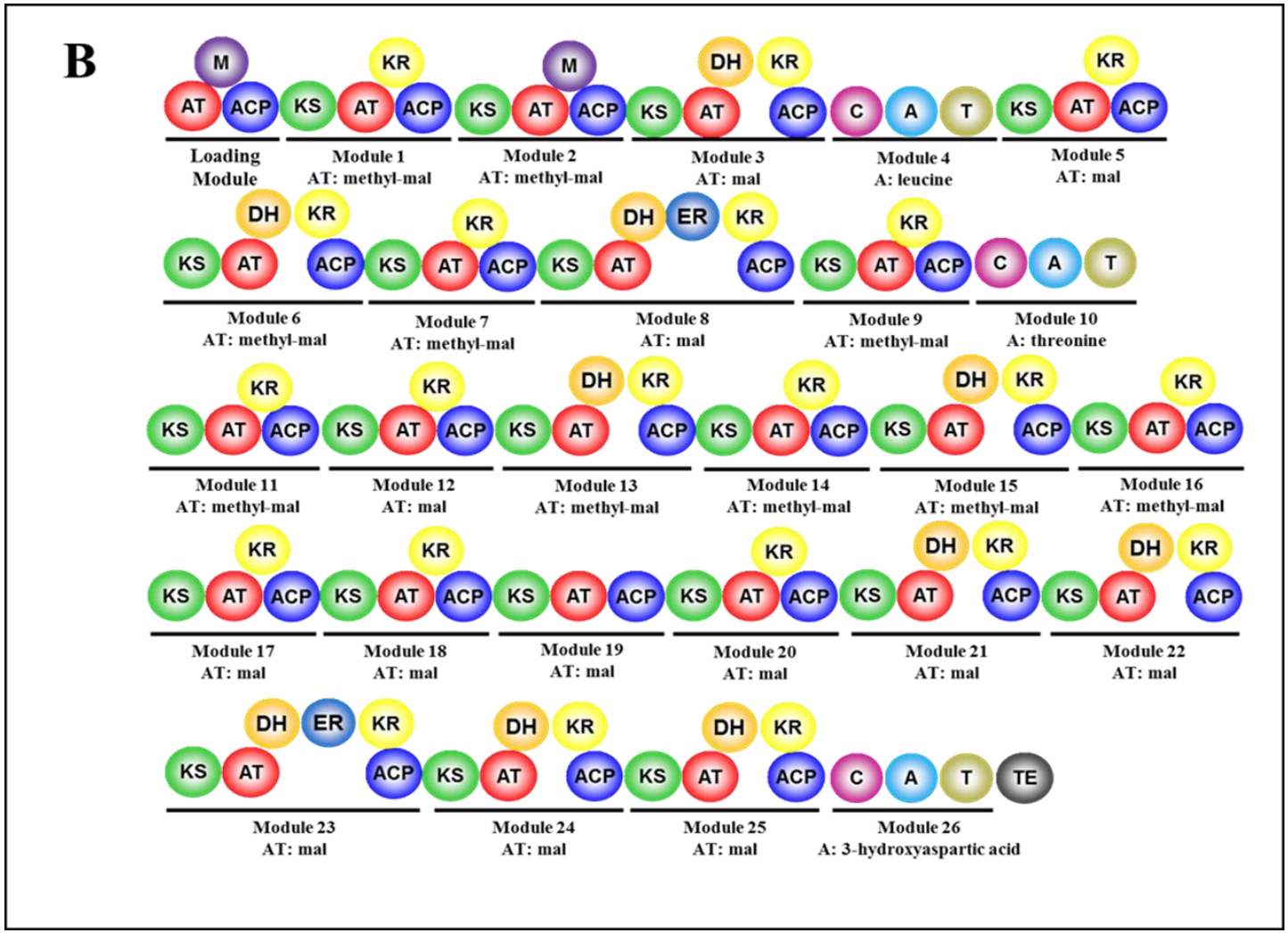
B
Loading Module
Module 1 AT: methyl-mal
Module 2 AT: methyl-mal
Module 3 AT: mal
Module 4 A: leucine
Module 5 AT: mal
Module 6 AT: methyl-mal
Module 7 AT: methyl-mal
Module 8 AT: mal
Module 9 AT: methyl-mal
Module 10 A: threonine
Module 11 AT: methyl-mal
Module 12 AT: mal
Module 13 AT: methyl-mal
Module 14 AT: methyl-mal
Module 15 AT: methyl-mal
Module 16 AT: methyl-mal
Module 17 AT: mal
Module 18 AT: mal
Module 19 AT: mal
Module 20 AT: mal
Module 21 AT: mal
Module 22 AT: mal
Module 23 AT: mal
Module 24 AT: mal
Module 25 AT: mal
Module 26 A: 3-hydroxyaspartic acid

Another possibility is that the unusual starter unit is a result of post-assembly carboxylation, as chondropsin C, which likely has similar biosynthesis, lacks the same starter group (Rashid et al., 2001b). Further post-assembly modifications could also be required for the biological activity of 73-DOC, performed by dedicated enzymes encoded in the gene cluster that may result in oxygenative tailoring, or group transfer reactions such as glycosylation and acylation (Fischbach and Walsh, 2006).

In order to isolate the genes involved in 73-DOC biosynthesis, suitable screening targets were required. Previous successful metagenomic strategies for cloning PKS genes from sponge holobiomes have typically relied upon targeting the KS domain from metagenomic DNA libraries (Piel et al., 2004, Schirmer et al., 2005, Fieseler et al., 2007, Fisch et al., 2009). These domains contain highly conserved structural motifs across multiple microbial phyla, which allows the use of degenerate primers, designed from consensus sequences, to amplify KS domains without prior knowledge of the producing organism (Piel, 2002, Moffitt and Neilan, 2003). Once sequenced, the degree of conservation amongst KS domains also allows for the phylogenetic classification of novel KS sequences into PKS groups by aligning and clustering the sequences with reference KS domains (Moffitt and Neilan, 2003). Target KS sequences can then be selected and used as screening targets.

The predicted involvement of NRPS-like domains in the biosynthesis of 73-DOC provides additional screening targets for 73-DOC biosynthetic components. Any clone from an *I. ramosa* metagenomic DNA library that was found to contain coding sequences for both PKS and NRPS domains would likely be a highly attractive candidate for containing part of the 73-DOC biosynthetic gene cluster. As with KS domain, the adenylation domain of NRPSs is known to be highly conserved at the amino acid level, enabling amplification using degenerate primers (Marahiel et al., 1997). The function of the adenylation domain in NRPS modules is to select and transfer the relevant amino

acid due to be incorporated into the molecule structure. Following the 3D structural resolution of the phenylalanine-activating adenylation domain of gramicidin synthetase, the amino acid residues responsible for substrate coordination in adenylation domains were identified and found to be highly conserved, forming 10 core binding pocket motifs based on alignments with other adenylation domains (Conti et al., 1997, Stachelhaus et al., 1999, Schwarzer et al., 2003). Software, such as that of Baranasic et al. (2014), was subsequently developed that can detect adenylation domain binding pockets from amino acid sequences and provide *in silico* prediction of substrate specificity. Such a tool could therefore be applied to facilitate the screening of adenylation domains by examining and comparing the substrate specificity with the predicted activities of the 73-DOC gene cluster.

The aim of this chapter was therefore to clone and sequence PKS genes from the metagenome of *I. ramosa* that encode proteins with domain architecture analogous to the predicted model of 73-DOC biosynthesis. To this end, the objectives were: Isolation of metagenomic DNA from *I. ramosa;* construction of a large-insert fosmid library; screening clones for nucleotide sequences indicative of type I hybrid PKS/NRPS biosynthesis using colony blot hybridisation; sequencing and annotating PKS/NRPS genes from candidate clones and metagenomic sponge DNA; and comparing PKS/NRPS translated peptides for homology to the predicted architectural domain model of 73-DOC biosynthesis.

6.2 Materials and methods

For specific details and parameters not mentioned below, see Section 2.3.

6.2.1 Fosmid library construction and screening

Metagenomic *I. ramosa* DNA was extracted and used to construct a fosmid clone library. Degenerate KS primers were used to amplify type I KS domains from metagenomic sponge DNA and a nucleotide sequence showing homology to a type I PKS/NRPS was used as template in generating a DIG-labelled probe. Transformed *E. coli* DNA was then screened using colony blot hybridisation and the DIG-labelled probe. A total of 1200 colonies were screened in this way, a number calculated to ensure 99 % probability of capturing a DNA sequence from a 10 Mb genome in a fosmid library containing 40 kbp inserts (Sambrook, 2001). Positive clones were then additionally screened for adenylation domains using degenerate primers. This work was assisted by Miss Urvi Shah, Miss Jaya Sanger and Miss Ptidya Boonvasit (all KCL undergraduate project students)

6.2.2 DNA sequencing

A chain termination method of sequencing was used for PCR products and primer-walking of fosmids. Next generation sequencing of fosmid DNA and microbial-enriched metagenomic DNA was performed using Illumina technologies. Metagenomic sequencing reads were assembled by Mr Ranko Garcesa (KCL) using the Velvet software (Zerbino and Birney, 2008).

6.2.3 Sequence annotation

Nucleotide and translated amino acid sequences were annotated using BLAST or Pfam searches using default parameters (Camacho et al., 2009, Finn et al., 2014). Multiple KS amino acid sequences were aligned using the MEGA software (Tamura et al., 2013). Alignments were used to construct phylogenetic trees using the Neighbour-Joining method (Saitou and Nei, 1987). Reference KS sequences from characterised PKS/FAS systems were also used in alignments, downloaded from the NCBI GenBank database (Benson et al., 2013). A web-based program designed by Baranasic et al. (2014) was used for *in silico* prediction of adenylation domain substrate specificity from the amino acid sequences. Contigs assembled from either fosmid or metagenomic sequence reads were automatically annotated for secondary metabolite biosynthetic genes using antiSMASH (Blin et al., 2013), with PKS domain organisation manually confirmed using ClustScan (Starcevic et al., 2008).

6.3 Results

6.3.1 Fosmid library construction

Metagenomic DNA was obtained from *I. ramosa* tissue using chemical lysis and ethanol precipitation. Gel electrophoresis was used to confirm the DNA was of high molecular weight and not excessively degraded, as evidenced by a lack of smearing in

the gel lane (Figure 6.2). A metagenomic fosmid library was generated from blunt-ended DNA fragments that were purified following gel electrophoresis, corresponding to a size of 30-40 kbp (Figure 6.2). The titer of the phage-packaged fosmids was determined, showing the library consisted of $2x10^6$ colony forming units, equal to 60-80 Gb of metagenomic DNA sequence.

6.3.2 Selection of the fosmid library screening probe

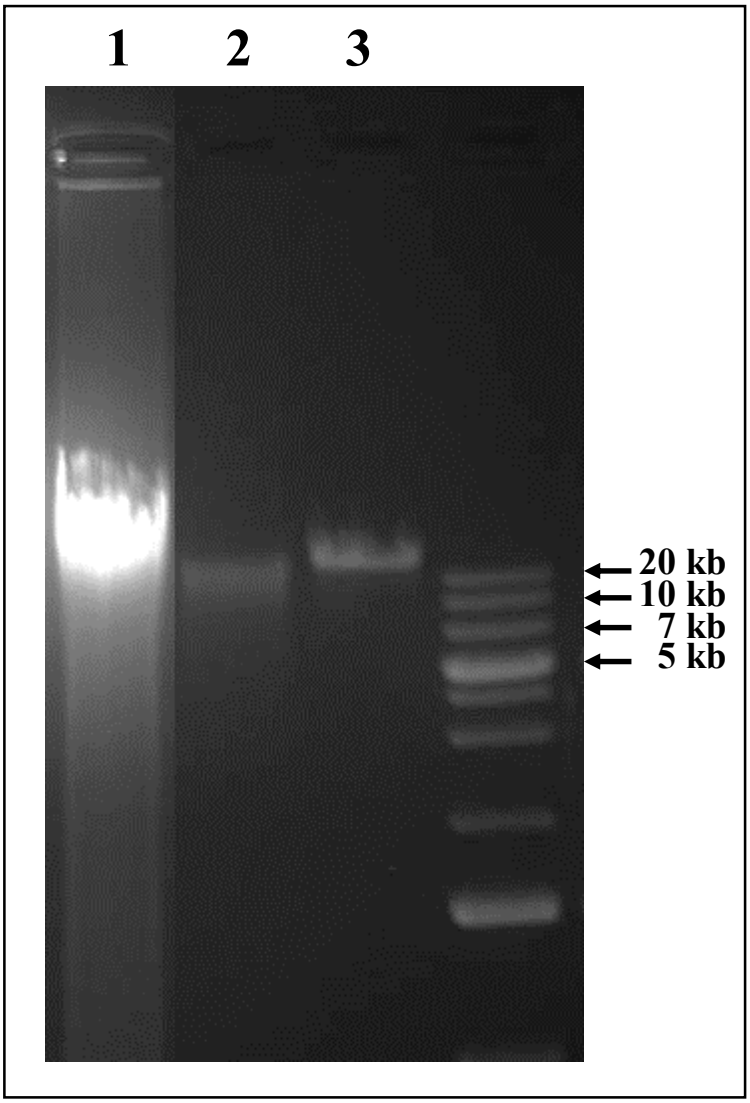

Figure 6.2 Agarose gel electrophoresis of metagenomic DNA used in fosmid library construction. A 0.8 % (w/v) agarose gel image. Lane 1: Total metagenomic DNA extracted from *I. ramosa*. Lane 2: Size-selected *I. ramosa* metagenomic DNA used in construction of the fosmid library. Lane 3: 40 kbp lambda control DNA supplied with kit.

To screen the fosmid library using colony blot hybridisation, a suitable oligonucleotide probe for the KS domains of type I PKSs was first required. A PCR using metagenomic *I. ramosa* DNA as a template and the degenerate KS primer set KSDPQQF/KSHGTGR (Piel, 2002) was performed, producing a band of the expected size (700 bp) (Figure 6.3). The 700 bp KS PCR products were purified following gel electrophoresis and cloned into *E. coli*. Correctly sized inserts were then sequenced from clones using the M13 forward sequencing primer. A total of 14 sequences were annotated as partial KS domains through comparison with the NCBI non-redundant nucleotide database using default parameters (BLASTn). The sequences showed high levels of identity (75-92 % across a coverage of 93-98 %) with partial KS sequences found from bacterial sponge symbionts (see Appendix, Table 1). Nucleotide KS sequences that shared less than 97 % similarity to each other were regarded as unique, resulting in 9 sequences which were each translated into the correct amino acid sequence.

To determine the phylogenetic classification of the uncharacterised KS domains from the current study, the amino acid sequences representing partial KS domains were aligned with truncated KS domains from modular type I PKS/FAS systems typically found from sponge metagenomes. The reference KS sequences were downloaded in FASTA format from the GenBank database. These included the *cis*-AT and *trans*-AT PKSs, as well as the hybrid PKS/NRPSs, which are all known to be involved in the biosynthesis of bioactive polyketides. Additionally, KS domains from the sponge-specific group of PKSs called *sup* (sponge symbiont ubiquitous PKS) were also included, as were the eukaryotic type I FAS group (Fieseler et al., 2007).

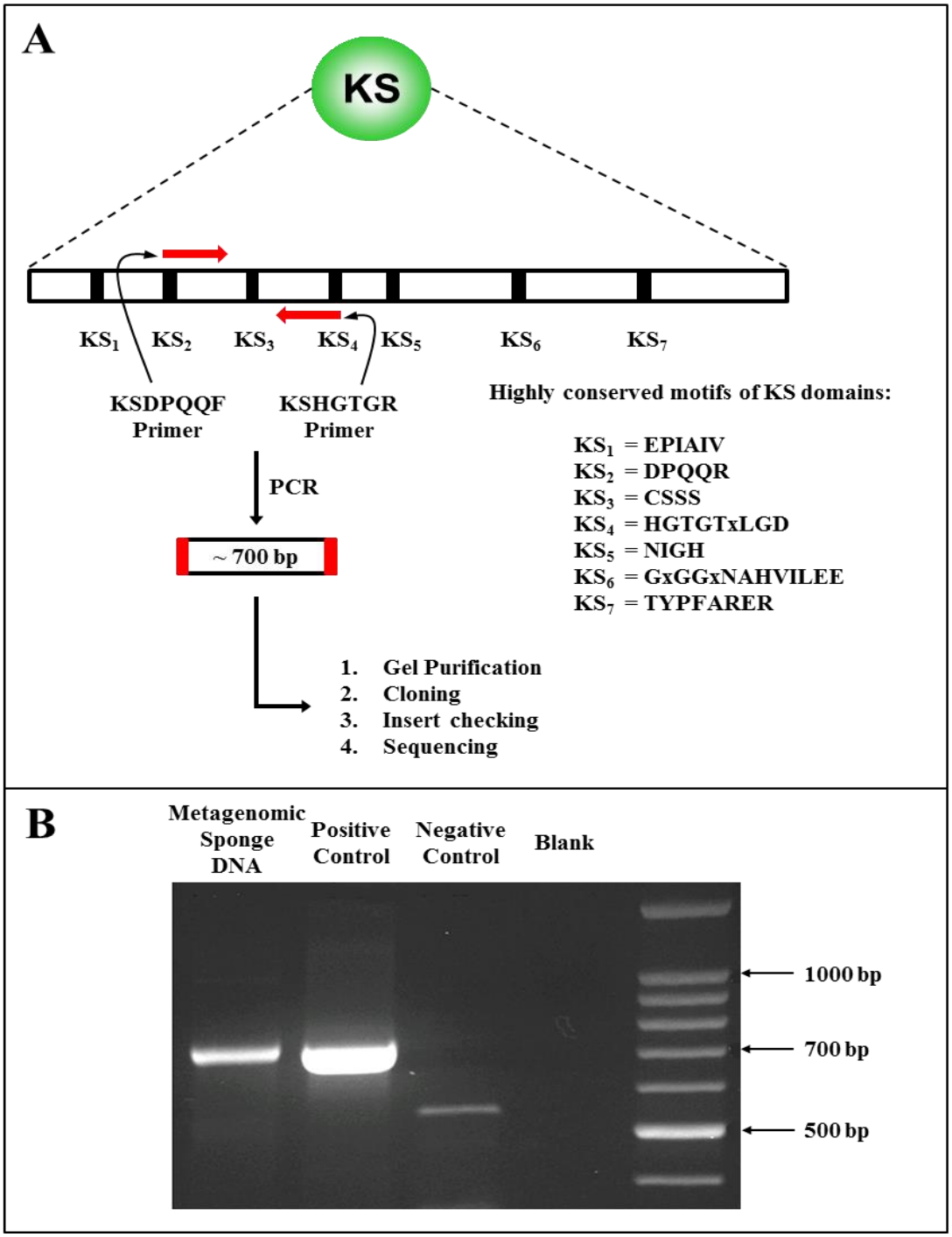

Figure 6.3 PCR amplification of KS domains from metagenomic sponge DNA using degenerate primers. A schematic of conserved KS structural motifs is shown along with the binding sites of the KSDPQQF/KSHGTGR primer pair and the procedure followed for sequencing the PCR products **(A)**. Agarose gel electrophoresis image of KS PCR products **(B)**. PCR products were run on a 1.6 % (w/v) agarose gel. The positive control was genomic *S. rimosus* DNA. The negative control was genomic *E. coli* DNA, strain K12 JM109.

A multiple alignment of the sequences was then performed (shown in Appendix, Figure 1), before a Neighbour-Joining phylogenetic tree was constructed, which group

sequences together by pairwise evolutionary distances, computed based on the number of amino acid changes at a particular site following alignment of the sequences (Saitou and Nei, 1987). This analysis showed that many (89 %) of the KS sequences amplified from *I. ramosa* clustered with the *sup* type of KS sequences, supported by high bootstrap values, which show the robustness of the inferred tree following iterative resampling or removal of alignment characters (Figure 6.4) (Felsenstein, 1985). However, a single sequence designated KS1 clustered with the hybrid PKS/NRPS reference sequences. As the 73-DOC gene cluster was predicted to encode a hybrid PKS/NRPS, the KS1 nucleotide sequence was chosen as a template for the oligonucleotide probe used to screen the metagenomic fosmid library.

6.3.3 Library screening

Fosmid clones were induced to high copy number in *E. coli* cells grown on agar plates before the colonies were blotted onto nylon membranes and screened using hybridisation with the KS1 probe. A total of 1200 colonies were screened, with positive colonies sub-cultured overnight before fosmid DNA was extracted. This screening procedure identified 118 KS positive colonies. To further reduce the number of candidate clones, a secondary screening procedure was performed targeting the adenylation domain of NRPS enzymes, as the structure of 73-DOC was predicted to incorporate 3 amino acids, corresponding to leucine, threonine and 3-hydroxyaspartic acid.

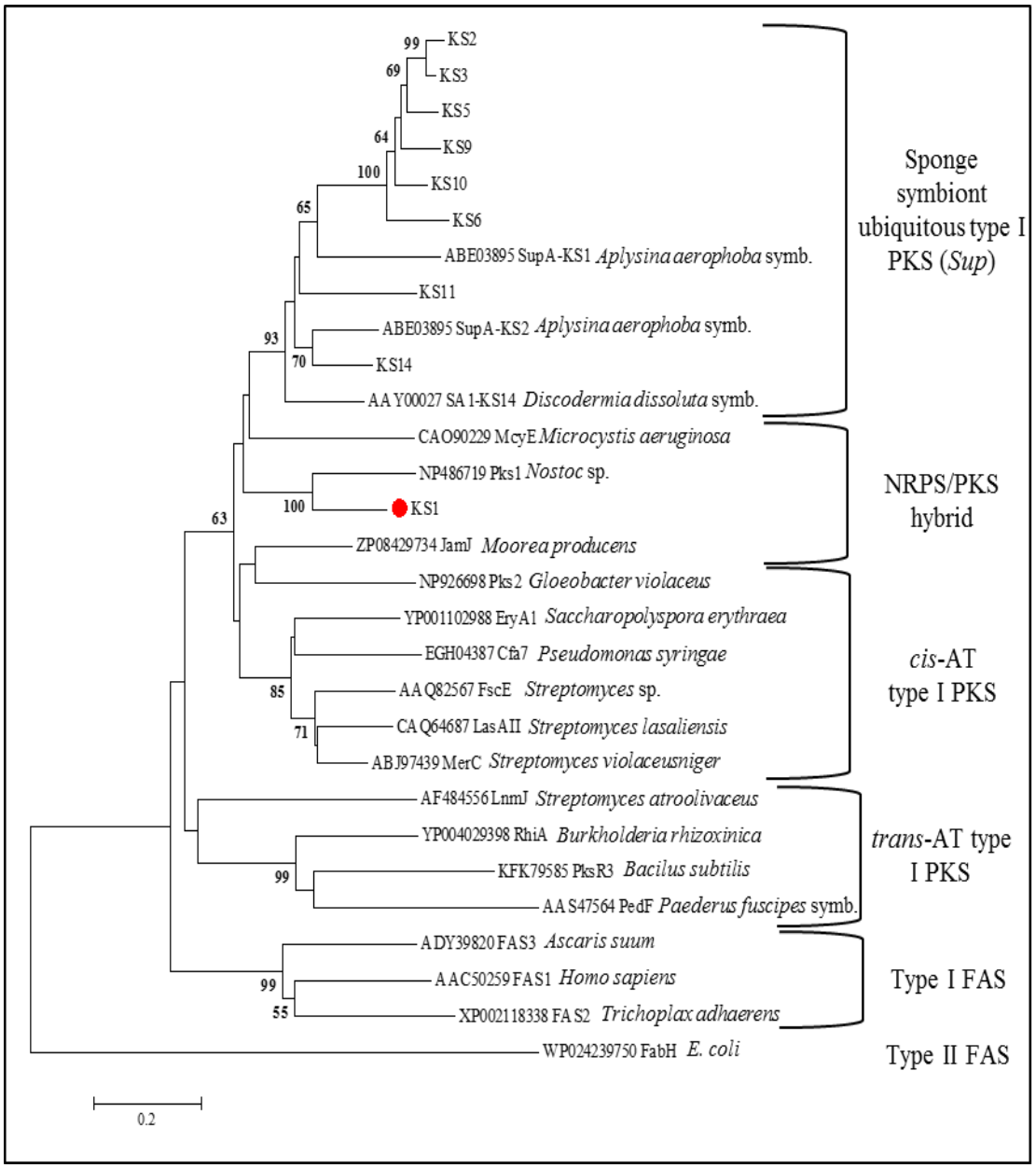

Figure 6.4 Phylogenetic analysis of KS amino acid sequences from *I. ramosa* shows KS1 to be a suitable fosmid library probe. Partial KS amino acid sequences amplified from *I. ramosa* were aligned with reference KS sequences before the Neighbour-Joining method was used to construct the tree shown (Saitou and Nei, 1987). The labels of reference KS sequences are shown with the GenBank accession numbers and the source organism. The PKS/FAS type enzymes from which they originated are labelled as groups on the far right. KS sequences amplified from *I. ramosa* are given the prefix KS- and the sequence chosen as a library screening probe is highlighted with a red circle. The percentage of replicate trees in which the associated sequences clustered together in the bootstrap test (1000 replicates) are shown next to the branches (Felsenstein, 1985). Only values over 50 % are shown. The evolutionary distances were computed using the Poisson correction method (Zuckerkandl and Pauling, 1965) and are in the units of the number of amino acid substitutions per site, also shown by the scale bar.

Fosmid DNA from the 118 KS-positive fosmids was then used as a template in a PCR using degenerate adenylation domains primers. A total of 6 fosmids (Fos114, Fos353, Fos441, Fos970 and Fos1118, Fos1207) were found to consistently produce a band of the expected size (~850 bp) (Figure 6.5). The 850 bp-sized PCR products from these 6 fosmids were sub-cloned into *E. coli* and sequenced. The nucleotide sequences were then translated into all 6 reading frames and analysed using the LSI tool for *in silico* prediction of adenylation domain substrate specificity (Baranasic et al., 2014). The HMM alignments (shown in Appendix, Figure 2) confirmed the presence of adenylation domain binding pockets in the PCR products amplified from the 6 fosmid templates. One fosmid, Fos1118, encoded two adenylation domain sequences whilst single domains were encoded by the 5 remaining fosmids. The results from the LSI predictor indicated that none of the substrate specificity predictions for the fosmid PCR product sequences matched the amino acids predicted in the 73-DOC structure (Table 6.1). As two putative adenylation domains were encoded by PCR products from the Fos1118 template, a decision was made to further investigate this fosmid further by partially sequencing the inserted sequence.

6.3.4 Sequencing of fosmids

Partial sequencing of the inserted sequence from Fos1118 was achieved using ten rounds of primer-walking, yielding approximately 9.5 kbp of fosmid insert DNA sequence. Annotation of this sequence was carried out using antiSMASH and revealed that there were no likely biosynthetic genes encoded by this sequence.

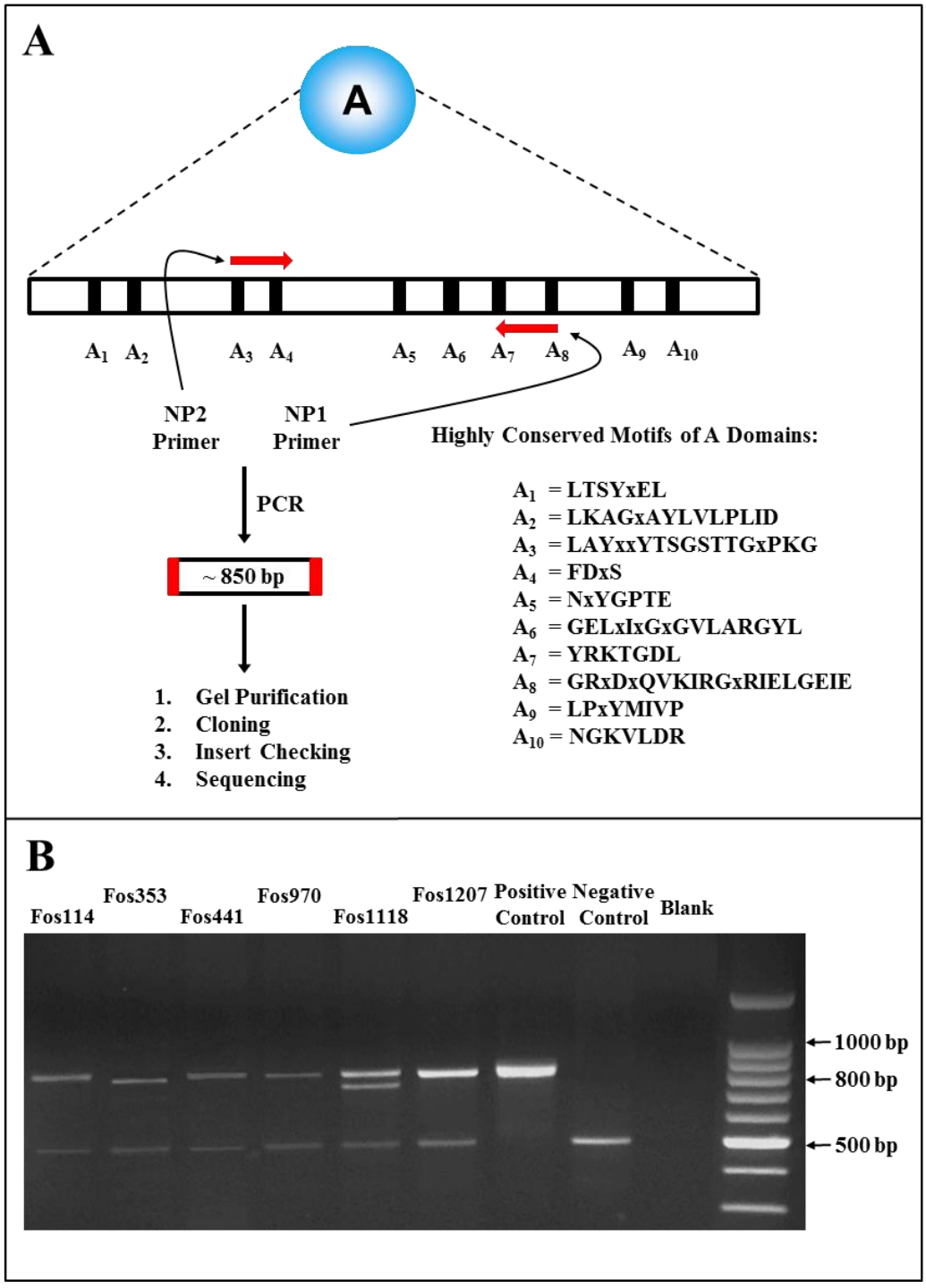

Figure 6.5 PCR amplification of adenylation domains from fosmid DNA using degenerate primers. A schematic of conserved adenylation domain structural motifs is shown along with the binding sites of the NP1/NP2 primer pair and the procedure followed for sequencing the PCR products **(A)**. Agarose gel electrophoresis image of PCR products from the 6 fosmids identified following a PCR screen for adenylation domains **(B)**. PCR products were run on a 1.6 % (w/v) agarose gel. The positive control was genomic *Nostoc* sp. DNA. The negative control was genomic *E. coli* DNA, strain K12 JM109.

HMM Alignment				
Sample	**Score**	**E-value**	**Substrate**	**Precision**
Fos114	94.5	$3.0x10^{-31}$	Phe	0.463
			Tyr	0.394
			Ser	0.388
Fos353	96.1	$9.4x10^{-32}$	Phe	0.463
			Tyr	0.394
			Ser	0.388
Fos441	92.9	$1.0 x10^{-21}$	Pro	0.493
			Ala	0.386
			Val	0.372
Fos970	94.0	$4.3x10^{-31}$	Pro	0.449
			Abu	0.434
			Tyr	0.414
Fos1118 (1/2)	66.8	$1.0x10^{-22}$	Pro	0.493
			Ala	0.386
			Val	0.372
Fos1118 (2/2)	94.5	$3.0x10^{-31}$	Phe	0.463
			Tyr	0.394
			Ser	0.388
Fos1207	94.9	$2.2x10^{-22}$	Phe	0.463
			Tyr	0.394
			Ser	0.388

Table 6.1 Output data from LSI tool shows adenylation domain substrate specificity. Adenylation domain amino acid sequences were analysed using the LSI tool (Baranasic et al., 2014). Binding pockets were detected through comparison with an adenylation domain HMM profile (Appendix I, Figure 2), showing the alignment score and E value for each. The top 3 LSI-based amino acid substrate predictions for each binding pocket are also shown along with precision scores ranging from 0 to 1.

In order to further annotate the proteins encoded by the Fos1118, the sequence was then searched against the Pfam database of protein families. The results confirmed that no PKS/NRPS domains could be detected from the Fos1118 insert sequence (Table 6.2).

Frame	Family	Description	E-Value
1	ADH N	Alcohol dehydrogenase-like domain	$1.4x10^{-20}$
1	ADH Zinc N	Zinc-binding dehydrogenase	$2.5x10^{-18}$
2	BsbC N	Disulfide bond isomerase protein N-terminus	$2.1x10^{-16}$
2	Thioredoxin 2	Thioredoxin-like domain	$5.8x10^{-16}$
2	FAD binding 2	Flavin adenine dinucleotide binding domain	$4.3x10^{-30}$
3	FAD binding 2	Flavin adenine dinucleotide binding domain	$2.2x10^{-25}$

Table 6.2 Table of Pfam matches found from the Fos1118 sequence. The DNA sequence obtained from primer walking Fos1118 was searched against the Pfam database. All matches are shown with the associated E-value. Alignments of these matches are shown in Appendix, Figure 3.

Due to time constraints, a decision was made to fully sequence all of the remaining candidate fosmids at once using NGS, alongside a sample of metagenomic DNA from *I. ramosa* (see Section 6.3.5). Sequencing libraries were made for each of the 6 candidate fosmids plus the metagenomic sponge DNA. However, due to technical limitations, only 6 samples in total could be sequenced simultaneously and so one fosmid (Fos1207) was dropped to be included on a future sequencing run. The sequencing run was performed, resulting in a total of 14.4 million, 300 bp-length reads. Following assembly of the sequencing reads, each of the fosmid samples were annotated using antiSMASH, which showed that none of the fosmid insert sequences were likely to have encoded homologs to PKS/NRPS domains. Further annotation using the Pfam database showed that various protein families were identified from the fosmid inserts. Whilst there were no predicted proteins common to all 5 of the fosmid sequences, 3 out of 5 were found to contain aminotransferase domains (Table 6.3).

In order to explain the results of the adenylation domain PCR screen, pairwise DNA alignments of the whole fosmid insert sequence and the PCR products amplified

Sample	Size	Top 3 Protein Family Hits	E-Value
Fosmid 1.14	38.3 Kb	Aldehyde dehydrogenase family	$6.0x10^{-150}$
		Prolyl oligopeptidase, N-terminal	$4.7x10^{-112}$
		Aminotransferase class-III	$1.8x10^{-97}$
Fosmid 3.53	33 Kb	Phage terminase subunit	$5.4x10^{-159}$
		Phage minor tail protein	$5.4x10^{-97}$
		Aminotransferase class-III	$1.9x10^{-50}$
Fosmid 4.41	35.8 Kb	CoA-transferase family III	$4.0x10^{-139}$
		Aminotransferase class-V	$1.9x10^{-50}$
		Bacterial secretion system protein	$1.3x10^{-37}$
Fosmid 9.70	36 Kb	tRNA synthetase class I	$2.3x10^{-193}$
		Tryptophan synthase alpha chain	$9.0x10^{-83}$
		Transposase	$2.7x10^{-67}$
Fosmid 1.118	34 Kb	Tripartite ATP-independent periplasmic transporter	$8.8x10^{-90}$
		Flavin adenine dinucleotide binding domain	$2.3x10^{-64}$
		Alcohol dehydrogenase-like domain	$7.5x10^{-50}$

Table 6.3 Table of top matches found following searches of the fosmid insert sequences against the Pfam database. Fosmid insert DNA sequences were translated into all 6 reading frames and searched against the Pfam database. The top 3 matches from each fosmid sequence are shown with the associated E-value. Alignments of these matches are shown in Appendix I, Figure 4.

from those fosmids were performed (see Appendix, Figure 5). These showed that none of the adenylation sequences aligned perfectly with their respective full sequence. Furthermore, the regions of the fosmid inserts that did align with the adenylation sequences, when searched against the Pfam database, showed no similarity in terms of the protein families found between each of the 5 fosmids. Similarly, pairwise alignments were constructed between the KS1 sequence that was used as a template for screening the fosmid library, and the sequenced fosmid inserts. The KS1 sequence was also found

to imperfectly align with the fosmid insert sequences. The aligned region of the fosmid insert with the KS1 sequence, when searched against the Pfam database, also showed no similarity in terms of the protein families found between each of the 5 sequence fosmids.

6.3.5 Metagenomic whole genome shotgun sequencing (mWGS) of Sponge DNA

After quality filtering, the metagenomic sponge DNA sample was sequenced with ~10 million, 300 bp-length reads, corresponding to 4.1 Gb of sequence. The optimum assembly resulted in 78 % of the sequencing reads assembling into contigs, which corresponded to a total of 152,650 sequences of varying size and a total of 174 Mb of assembled sequence. Following automatic annotation using antiSMASH, a total of 300 biosynthetic genes were annotated, 18 of which were annotated as type I PKS. No contigs were found to contain NRPS domains. The annotation of PKS domains was manually confirmed using ClustScan (see Appendix, Figure 7), which showed that each of the 18 sequences encoded 1 out of 2 types of consistent domain order (Table 6.4). Additionally, ClustScan predicted that the only active reductive domains in 14 of these sequences was the DH, whilst the remaining 3 had active DH, ER and KR domains and 1 partial sequence had no active reductive domains (Appendix, Figure 7). The AT substrate specificities were predicted as malonyl-CoA for 13 of the sequences, whilst the remaining sequences, and those with a second AT domain were non-predictable (Appendix, Figure 7).

An alignment of KS domains from each of the 18 sequences was constructed to include other reference KS domains (Appendix, Figure 8), in order to allow phylogenetic

Sequence	Size (kb)	PKS Cluster Domain Annotation
1318	15	KS AT DH M ER KR ACP KS
1506	50	KS AT DH M ER KR ACP KS AT
1836	65	KS AT DH M ER KR ACP KS AT
2482	43	KS AT DH M ER KR ACP KS AT
3054	50	KS AT DH M ER KR ACP KS
5079	32	KS AT DH M ER KR ACP KS AT
5439	20	KS AT DH M ER KR ACP KS AT
6648	50	KS AT DH M ER KR ACP KS AT
8429*	20	M ER KR ACP KS AT
9015	29	KS AT DH M ER KR ACP KS
10635	37	KS AT DH M ER KR ACP KS AT
15522	34	KS AT DH M ER KR ACP KS AT
25735*	28	KS AT DH M ER KR ACP
23	47	KS AT DH ER KR ACP
840*	25	KS AT DH ER KR
1020*	26	KS AT DH ER
21467	19	KS AT DH ER KR ACP
26257	21	KS AT DH ER KR ACP

Table 6.4 Summary of type I PKS domain annotation following screening of mWGS contigs with antiSMASH. Sequences detected as type I PKS were automatically annotated as shown. Annotation was manually confirmed using ClustScan (Appendix I, Figure 7). * indicates a partially recovered sequence.

classification of the mWGS PKS sequences. The reference KS sequences included were the same as those shown in Figure 6.4, with additional sequences representing another novel, sponge-specific type I PKS named *swf* (sponge symbiont widespread FAS), discovered from the sponge *Planktoris simplex* (Della Sala et al., 2013). The *swf* sequences were included as 5 of the mWGS PKS sequences (23, 840, 1020, 21467,

26257) showed common annotation of PKS domain architecture. A Neighbour-Joining phylogenetic tree constructed from the KS alignment showed that 13 (72 %) of the KS sequences clustered with *sup* sequences, whilst the remaining 5 sequences clustered with *swf* sequences (Figure 6.6).

To confirm the phylogenetic analysis, BLASTp searches of entire mWGS PKS sequences detected by antiSMASH were conducted. This showed that 13 of the mWGS PKS sequences had homology (55-80 % identity over at least 97 % sequence coverage) of SupA from either *T. swinhoei* or *A. aerophoba* (see Appendix, Figure 9). The remaining 5 PKS sequences showed homology (66-80 % identity over at least 96 % coverage) with SwfA from *P. simplex* (see Appendix, Figure 9). Additionally, 9 of the 13 *sup* sequences, and 3 of the 5 *swf* sequences, had regions flanking the PKS which showed homology with components in either the *sup* (Fieseler et al., 2007) or *swf* (Della Sala et al., 2013) operons, including SupB-E and SwfB-C (see Appendix, Figure 9). Furthermore, the C-terminal AT domains of PKS genes showing homology to SupA were found to include a characteristic serine to glycine substitution at a residue considered crucial for activity (Fieseler et al., 2007) (see Appendix, Figure 10), and the KS domains of PKS genes which showed homology to SwfA were found to include the characteristic QCALVEL motif (see Appendix , Figure 11), which is unique to SwfA-AT domains (Della Sala et al., 2013). Taken together, these findings support and confirm the phylogenetic KS-classification of the mWGS PKS genes as members of either the *sup* or *swf* groups.

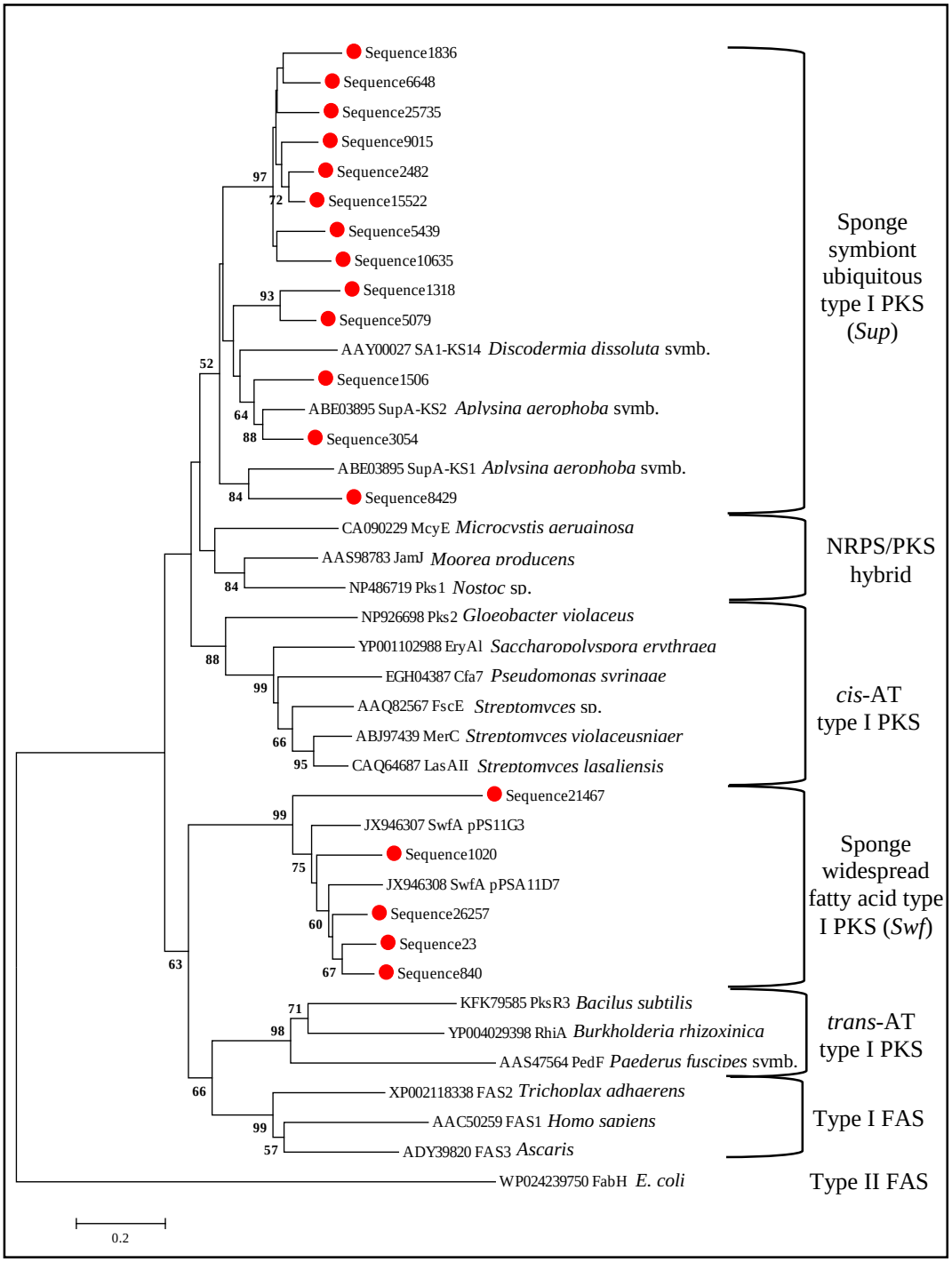

Figure 6.6 Phylogenetic analysis of KS amino acid sequences from type I PKS clusters encoded by mWGS contigs. Whole KS amino acid sequences from mWGS contigs were aligned with characterised KS sequences from various PKS and FAS enzymes. The Neighbour-Joining method (Saitou and Nei, 1987) was used to construct the tree shown. The labels of known KS sequences retrieved from the GenBank database are shown with accession numbers, and the PKS types from which they originated are labelled as groups on the far right. KS sequences discovered from *I. ramosa* are highlighted with a red circle. The percentage of replicate trees in which the associated sequences clustered together in the bootstrap test (1000 replicates) are shown next to the branches (Felsenstein 1985). The evolutionary distances were computed using the Poisson correction method (Zuckerlandl and Pauling, 1965) and are in the units of the number of amino acid substitutions per site, also shown by the scale bar.

6.4 Discussion

The aim of this chapter was clone and sequence PKS/NRPS genes from the metagenome of *I. ramosa* that could be compared with the predicted model of 73-DOC biosynthesis (Figure 6.1 B). To this end, two different strategies were employed in order to clone PKS/NRPS sequences. The first involved a KS-guided, hybridisation-based screen of a metagenomic fosmid library constructed from *I. ramosa* DNA, followed by screening for adenylation domains. The second strategy involved using bioinformatic tools to annotate genomic sequences for PKS/NRPS genes, obtained from mWGS of metagenomic *I. ramosa* DNA.

The first strategy employed was unsuccessful in isolating PKS/NRPS genes as none of the fully sequenced fosmids were found to contain a KS domain, nor any other common protein showing homology to KS domains. This result implied that the hybridisation screening conditions may not have been fully effective and resulted in the detection of sequences unrelated to KS domains and the identification of false-positive fosmids. The KS1 sequence used as a probe in hybridisation screening was certainly a suitable choice as, out of all the KS sequences obtained from *I. ramosa*, this particular sequence was the only one found to show phylogenetic similarities with KS domains typical of hybrid PKS/NRPS systems (Figure 6.4). Positive and negative controls were also used during the colony screening, the positive represented by *E. coli* DNA containing the KS1 plasmid, the negative by host *E. coli* DNA, and each membrane screened with the KS1 probe showed positive detection of positive control cell DNA. However, this experiment could perhaps have included additional controls, such as clones containing entire, characterised PKS clusters, which would have confirmed the conditions were suitable for the detection of KS-containing PKS clusters.

The method used to screen the fosmid library could, perhaps, also be improved. With metagenomic studies, due to the uncertainty in total genome size, the decision of how many clones to screen is difficult to predict. During the current work, a total of 1200 colonies were screened, a number calculated based on achieving suitable coverage of a typical cyanobacterial genome size of 10 Mb, as cyanobacteria were previously shown to be abundant in *I. ramosa* (Dunlap et al., 2007). However, since NGS technologies have been utilised for sponge microbial diversity studies, estimates for symbiont diversity have been extended into the hundreds (Schmitt et al., 2012) and even thousands (Lee et al., 2011). One study involving deep pyrosequencing of 16S rRNA sequences amongst 3 Australian sponge species found a total of over 5,000 OTUs (operational taxonomic units) (Webster et al., 2010). *I. ramosa* was included in this study and was reported to be host to 1199 OTUs.

Whilst it is possible that these numbers are inflated due to the low similarity threshold (97 % or 99 % usually used instead of 95 %) or from potential sequencing and PCR artefacts (Quince et al., 2009, Kunin et al., 2010), these findings fit with the generally accepted underestimation of microbial diversity in marine environments and invertebrate hosts (Sogin et al., 2006, Sunagawa et al., 2010, Behrendt et al., 2012, White et al., 2012). Considering the seemingly high level of bacterial diversity in *I. ramosa*, the number of clones screened in the current work was likely an underestimate of the total number that required screening. The combined genomes associated with *I. ramosa* would likely require screening many thousands of clones. Such a task would benefit from either using a robotic system with colonies in microplates, as used by Schirmer et al. (2005) for the sponge *Discodermia dissoluta* and by Parsley et al. (2011) for a soil metagenome, or by using a PCR based approach with pools of clone DNA such as that advocated by Gurgui and Piel (2010).

During the second round of screening, adenylation domains were amplified and sequenced from fosmids using degenerate PCR primers. Once sequenced however, neither adenylation domain genes, nor the complete sub-cloned PCR sequence were found from the fosmid insert sequence. The amplified sequences from fosmid templates were found to encode conserved motifs and residues consistent with adenylation domains, as shown by significant HMM alignments using the LSI software developed by Baranasic et al. (2014). However, the absence of the complete PCR sequences from the fosmid template DNA implies PCR errors occurred, such as primer-template mismatching or low fidelity extension. Such errors could be occurring due to the use of highly degenerate primers (total degeneracy of 224). The primer pair used for PCR screening of the KS-positive fosmids was chosen based on the previous success by Zhang et al. (2009) with sponge metagenomic DNA templates. Furthermore, the primers were initially tested by sequencing PCR products from *I. ramosa* metagenomic DNA which, when analysed using HMM alignments, showed homology to adenylation domains, indicating that the primers were suitable for screening purposes. An alternative approach to the adenylation domain screen could have involved designing novel PCR primers based on consensus sequences from characterised adenylation domains with substrate specificities for either leucine, threonine or 3-hydroxyaspartic acid. If successful, this would have enabled specific detection of adenylation domains that have activity consistent with the predictions of 73-DOC biosynthesis.

The second strategy used to capture PKS/NRPS sequences was successful, and resulted in the isolation of 18 PKS genes from the metagenome of *I. ramosa*, which were all characterised as belonging to the *sup* or *swf* groups. Only one other similar study has attempted to capture PKS/NRPS domains from sponges using mWGS, where deep sequencing was used to characterise the diversity of PKSs and NRPSs from 5 different sponge metagenomes (Woodhouse et al., 2013). For 4 out of the 5 sponges sampled

during this study, only 5 or less PKS sequences were found, which is over three-fold less than the number recovered during the current work. Of the 18 type I PKS genes sequenced from *I. ramosa*, 5 were annotated as showing homology to *swf* gene clusters. *Swf* gene clusters are the second example (after *sup*) of PKS/FAS genes found only from sponge symbionts and were first described by Della Sala et al. (2013) following a metagenomic investigation into the PKS genes of the sponge *P. simplex*. The results presented here therefore extend the occurrence of the *swf* genes to the sponge *I. ramosa*. The authors characterised the *swf* operon as composed of *swfA*, a gene encoding for a single PKS module with unique features such as a characteristic QCALVEL motif only found in AT domains from SwfA, also found in all 5 *swf* homologues from *I. ramosa.* Downstream of *swfA* is *swfB*, which encodes a predicted fusion of a thioester reductase domain with a sulfotransferase domain, and *swfC*, which may or may not be present, but shows homology to enzymes that act as methyltransferases. The association of *swfB* and *swfC* with *swfA* suggests a product that could be expected to be a methylated alkyl sulphate, but no such metabolites are found in sponges and so the actual biosynthetic function of the *swf* cluster remains to be established (Della Sala et al., 2013).

The KS sequences cloned from *I. ramosa* during the current study using either PCR or mWGS were found to be dominated (72-89 %) by *sup* sequences, which is consistent with the original discovery of *sup* genes by Fieseler et al. (2007), as well as other studies that have also reported the widespread occurrence and dominance of this group amongst sponge KS sequences (Piel et al., 2004, Schirmer et al., 2005, Kim and Fuerst, 2006, Fieseler et al., 2007, Hochmuth and Piel, 2009b, Hochmuth et al., 2010, Woodhouse et al., 2013, Della Sala et al., 2014, Wilson et al., 2014). The *sup* operon contains the *supA* gene, which encodes a single PKS module composed of an unusual domain architecture that terminates with KS and AT domains. The C-terminal AT domain of SupA was also reported to lack a conserved serine residue considered crucial

for activity, having a glycine instead (Fieseler et al., 2007). All 13 of the mWGS PKS sequences that were annotated as *sup* systems were shown to have PKS genes homologous to *supA* and most had the C-terminal AT domains bearing the reported amino acid substitution, indicating this domain may be non-functional. Additional non-functional ER and KR domains in the *supA* homologues were also predicted by ClustScan.

The predicted domain architecture of SupA is almost identical to type I mammalian FAS systems, but includes an active methyltransferase domain which is non-functional in the mammalian FAS (Fieseler et al., 2007, Maier et al., 2008), and C-terminal KS/AT domains instead of a TE domain (Figure 6.7). Amongst the few cases of type I FAS in bacteria are the enzymes from pathogenic mycobacteria, which are involved in the biosynthesis of methyl-branched fatty acids for cell walls (Minnikin et al., 2002). The architectural similarities of SupA to the mammalian FAS and the presence of an active methyltransferase domain implied that the products of this protein are also methyl-branched fatty acids, which are present in numerous sponges containing

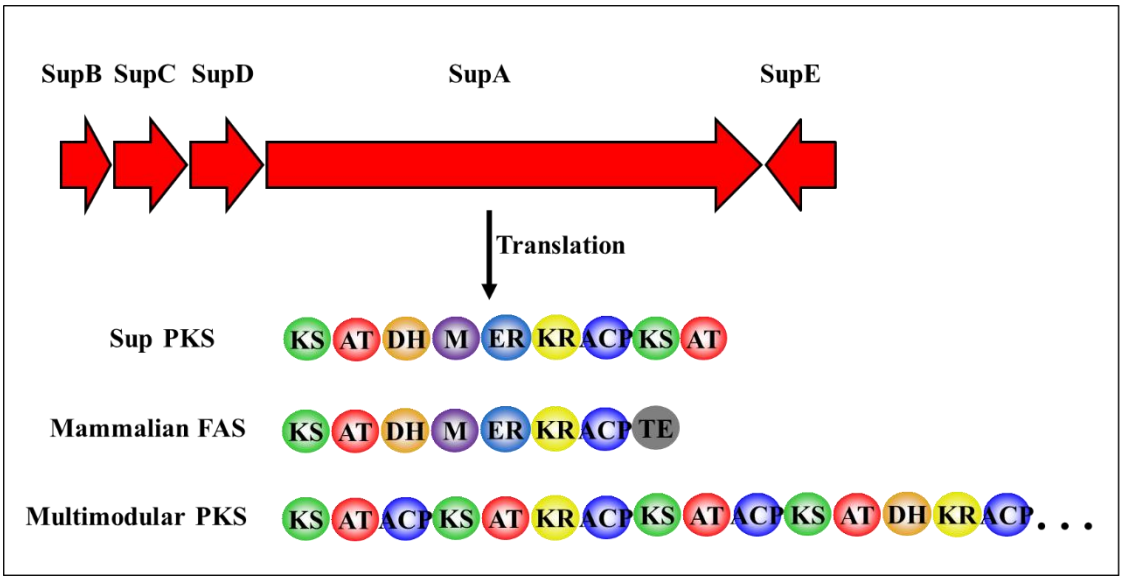

Figure 6.7 Schematic of the *sup* operon. The 5 genes (SupA-E) constituting the *sup* operon are shown (Fieseler et al., 2007). The domain organisation of the SupA PKS is also shown for comparison with the mammalian FAS and a hypothetical multimodular PKS. Adapted from Hochmuth et al. (2010)

symbiotic microorganisms (Gillan et al., 1988, Thiel et al., 1999, Robainac et al., 2002, Thiel et al., 2002, Hochmuth et al., 2010). As methylated fatty acids are common in fossil sediments and fuels, an interesting hypothesis has suggested that microbial producers of methyl-branched fatty acids were once widespread but are now rare, with sponges representing one of the last extant habitats for such microorganisms (Thiel et al., 1999, Fieseler et al., 2007).

Clearly the majority of PKS sequences found from *I. ramosa* share high levels of similarity with the *sup* systems but it is also possible that these genes may be involved in the biosynthesis of 73-DOC. Considering the role of *sup* in the biosynthesis of methylated fatty acids, it is interesting to note that the chemical structure of 73-DOC was reported as containing numerous methyl branches, particularly on the polyketide backbone at locations corresponding to the predicted starter and first 2 extender units (Figure 6.1 A) (Rashid et al., 2001b). Whilst the model for 73-DOC biosynthesis shown in Figure 6.1 does not have domain architecture consistent with SupA, this was a purely hypothetical model based on the paradigm of type I PKS structure and organisation that emerged following intense investigation of DEBS and many other *cis*-AT PKSs (Katz, 2009). However, when non-canonical PKS organisation is taken into account, along with the predicted inactivity of the ER, KR and C-terminal AT domains of SupA, a potential role of a SupA homologue in 73-DOC biosynthesis can be considered.

Type I PKS modules are a convenient way to organise enzymatic domains but have no reality in terms of protein structure and ultimately the executed biochemical sequence of a PKS determines the product structure. Accordingly, there are instances of split modules where module domains are found on different polypetides. For example, in the disorazole PKS system, the 4th module is split between the DH domain of DsxA and the KR domain of DsxB (Carvalho et al., 2005), and there are other similar examples in the PKS systems for myxalamid (Silakowski et al., 2001), bacillaene (Butcher et al.,

2007) and etnangien (Menche et al., 2008). If a similar situation is applied with modules 2 and 3 from the putative 73-DOC model, the resulting active domain architecture is similar to that of SupA (Figure 6.8). The remaining differences are biosynthetic order, the lack of a second active AT domain and contrasting AT specificities, all of which can be accounted for (see below).

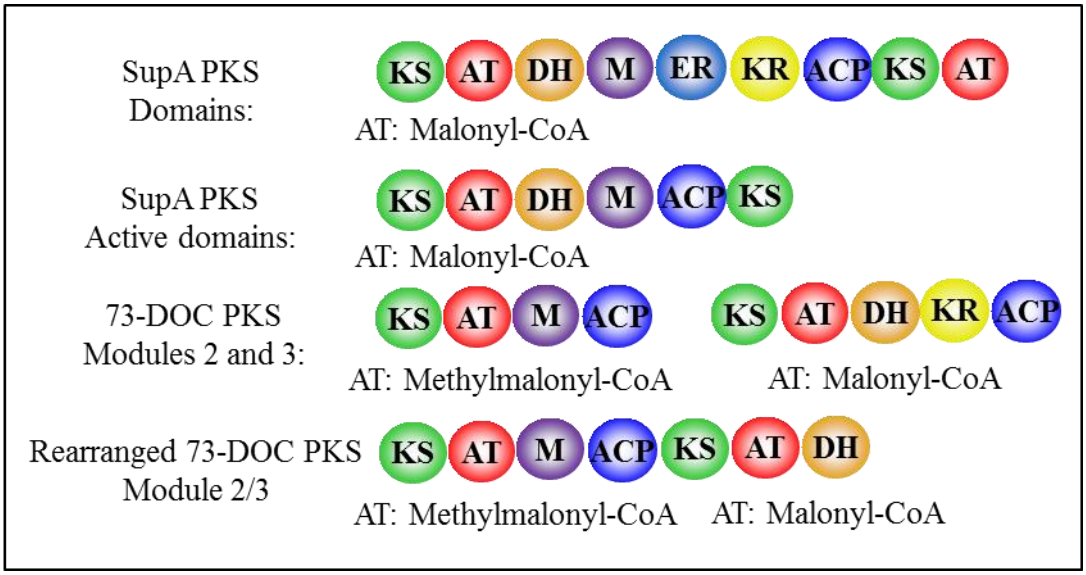

Figure 6.8 Comparison of SupA active domain architecture with a hypothetical rearrangement of the 73-DOC domain model of biosynthesis

In regards to AT domain specificity, the first AT region in SupA was shown to catalyse malonyl-CoA extender units (Hochmuth et al., 2010), which was consistently predicted for all SupA homologues from *I. ramosa* (Appendix I, Figure 7). In the original architectural domain model of 73-DOC, module 2 was predicted to incorporate methylmalonyl-CoA due to the presence of a geminal dimethyl group in the 73-DOC structure. However, characterised PKS gene clusters for bryostatin (Sudek et al., 2007) and onnamide (Piel et al., 2004), which produce similar dimethyl groups, imply methyltransferase enzymes catalysing malonyl-CoA substrates. This has also been empirically demonstrated by Miller et al. (2002) using radiolabelled isotope feeding studies and the yersinabactin synthase, where the AT domain involved in the biosynthesis of a gem dimethyl group exhibited a 500-fold preference for malonyl-CoA

over methylmalonyl-CoA. A similar mechanism could also occur with 73-DOC biosynthesis, allowing the predicted AT specificity of modules 2/3 to be consistent with SupA.

In regards to the contrasting biosynthetic order of the rearranged module 2/3 and that of SupA, recent crystal structures for both the PikAIII type I PKS (Dutta et al., 2014) and mammalian type I FAS (Maier et al., 2008) systems show a homodimeric quaternary structure, where monomers are arranged head-to-head (Figure 6.9 A). Whilst furthermore, during fatty acid synthesis (Joshi et al., 1997, Witkowski et al., 2004) and polyketide synthesis (Kao et al., 1996, Staunton et al., 1996, Gokhale et al., 1998), the domains of either monomer have been demonstrated as functional. Currently, it is unknown whether SupA has structure similar to the type I FAS or PKS but with either situation, the likely homodimeric, head-to head arrangement of the enzyme subunits would allow the domain organisation of SupA to be reconciled with the biosynthetic order of the rearranged module 2/3, as both AT monomers could be used during chain extension. If SupA has mammalian FAS structure, this situation could involve the iterative use of the same ACP domain, via a process that has been shown to include rotation of the lower portion of the FAS structure relative to the upper portion, providing access for a flexible, mobile ACP to all domains (Figure 6.9 B) (Maier et al., 2008). If SupA has PKS structural similarities, the arrangement of the domain active sites around a single, arch-shaped reaction chamber would also permit the biosynthetic order of the rearranged module 2/3 due to the use of either monomer, the close proximity of the opposing subunits around a single reaction chamber and a highly mobile ACP domain (Figure 6.9 A) (Dutta et al., 2014).

Non-canonical iterative polyketide biosynthesis may also help resolve SupA activity with the biosynthetic sequence of 73-DOC. Iterative type I PKS biosynthesis is

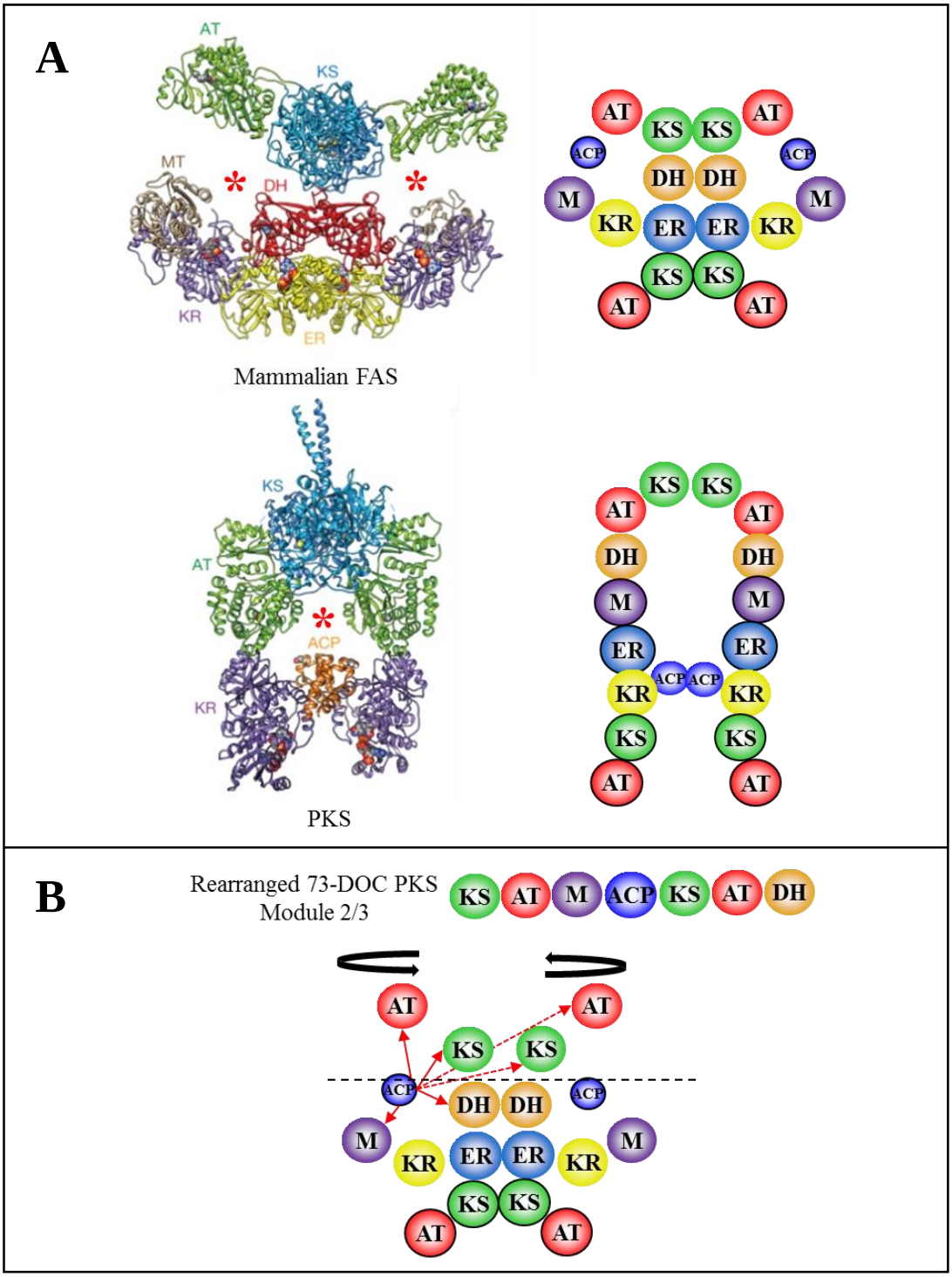

Figure 6.9 Schematics of proposed SupA structure and mechanism. The potential 3D structures of SupA are shown, following structural models of the mammalian FAS and the PikAIII PKS module from Maier et al. (2008) and Dutta et al. (2014) respectively **(A)**. Red stars indicate reaction chambers. Positions of domains with a black border are purely hypothetical and not based on crystal structure knowledge. Assuming a mammalian FAS structure, a proposed biosynthetic route for the rearranged module 2/3 from the 73-DOC gene cluster is shown **(B)**. This route shows the iterative use of the ACP domain, which is provided access to both AT monomers following rotation of the upper portion of the FAS (above black dotted line) relative to the lower portion.

well known from fungal systems but has also been reported in bacteria (Moss et al., 2004, Cox and Simpson, 2009). Described as stuttering and involving the repeated use of a single module or domain, this phenomenon is usually implicated when the number of modules present in a PKS is fewer than the number of condensation cycles needed for the corresponding polyketide. For example, stigmatellin is assembled from 10 condensations by a PKS with 9 modules, leading to the prediction that either one of two identical modules in the stigmatellin PKS are used twice (Gaitatzis et al., 2002). The most unusual example of stuttering is found from the biosynthesis of lankacidin, where 5 out of 8 rounds of condensation are carried out iteratively by a single module, but involving a different set of reductive domains in each cycle (Tatsuno et al., 2007). This implied that, for this PKS, the reductive domain use by a particular module can be optional during repeated cycles (Hertweck, 2009). The biochemical basis of stuttering is not completely understood but considering the similarity of SupA to the iteratively acting type I FAS, and the lack of a terminal TE domain, it is tempting to speculate that SupA may also function iteratively. If, like the lankacidin PKS, the reductive domains are optionally used during each extension, this would also support a role of SupA domain architecture in the predicted 73-DOC biosynthetic sequence of the loading module up to module 3, where additional KR activities were predicted. However, a more rigorous examination of reductive domain functionality in SupA would be required to establish whether this is possible.

In summary, whilst the exact function of the *sup* or *swf* operon has yet to be demonstrated, it is possible that the potential chemistry produced by SupA could be reconciled with the activities of modules 2 and 3 from the hypothetical 73-DOC biosynthetic model. Methyltransferase activity from SupA could presumably also be responsible for additional branching patterns seen in the unusual loading unit and the extension unit attributed to module 1. This suggests a possible role of SupA in supplying

methylated fatty acid extension units or perhaps a precursor for 73-DOC biosynthesis. Hybrid FAS-PKS systems have previously been described, such as in aflatoxin biosynthesis in *Aspergillus* spp., where an unusual hexanoyl starter unit is formed by a dedicated FAS and then extended by a PKS (Watanabe et al., 1996, Hitchman et al., 2001). Here, the C_6 fatty acid is selected and transferred to the PKS ACP via a specialised starter-unit AT domain (Crawford et al., 2006, Foulke-Abel and Townsend, 2012). Similarly in mycobacteria, several complex cell-wall lipids are produced by the combined actions of FASs and PKSs (Kolattukudy et al., 1997, Sirakova et al., 2001). Long-chain fatty acids in these systems are transferred to PKSs for further extension by fatty acyl-AMP ligases, which activate fatty acids as adenylates then transfer them to carrier proteins that show homology with the thiolation domain of NRPSs (Trivedi et al., 2004, Gokhale et al., 2007). These studies show a precedent for chain-transfer mechanisms between FAS and PKS biosynthetic systems which could also be occurring between SupA and the main 73-DOC-producing synthase. This would implicate an intriguing role of SupA in providing for primary and secondary metabolism, which could lead to future research directions exploring sponge holobiome physiology.

To confirm the ideas presented above, future work could focus on the heterologous expression and protein purification of SupA which, in tandem with site-directed mutagenesis, could ultimately allow determination of products and functional reductive domain activities, as well as the opportunity to obtain a crystal structure which could lead to establishing SupA protein structure. Additionally, once expression and protein purification of SupA is achieved, intersubunit domain interactions could be examined to test the proposed biosynthetic mechanisms of SupA. These could mirror the cross-linking and mutated subunit complementation experiments that were applied for the study of type I FAS/PKS subunit organisation (Kao et al., 1996, Joshi et al., 1997, Gokhale et al., 1998, Weissman and Müller, 2008). The origin of the *sup* genes has not

been conclusively demonstrated but the *Poribacteria*, a sponge-specific bacterial phylum, have been implicated (Fieseler et al., 2004, Siegl et al., 2011, Della Sala et al., 2014). Taxonomic classification of the *sup* sequences was beyond the aims of this thesis, but future work involving further phylogenetic examination of these sequences and surrounding genes could be one additional direction for future work that may support or contradict the hypothetical involvement of the *Poribacteria*.

Clearly there are parts of the 73-DOC gene cluster that were not isolated during the current work. This was especially noticeable as no NRPS genes were annotated following mWGS, despite the predicted role in 73-DOC biosynthesis and the frequent occurrence of these genes in other sponge holobiomes (Schirmer et al., 2005, Siegl and Hentschel, 2009, Zhang et al., 2009, Pimentel-Elardo et al., 2012). The PKS genes responsible for bioactive metabolites from sponge metagenomes are known to be rare (Fieseler et al., 2007, Hochmuth and Piel, 2009b). Between 2001 and 2010, 30 bioactive polyketides have been discovered from sponges (Mehbub et al., 2014) but during this time, only 3 sponge-derived PKSs responsible for bioactive polyketides (pysmmberin, onnamide and theopederin) have had their gene clusters successfully mapped (Piel et al., 2004, Fisch et al., 2009), and all from one research group working with compounds that share structural and biosynthetic similarities. Capturing the biosynthetic genes for compounds known to be present in sponges is thus not a straightforward task, even when that compound is known to be present in large amounts (Della Sala et al., 2014).

In conclusion, this chapter detailed the first ever investigation of biosynthetic genes from *I. ramosa*. PKS genes were successfully cloned, sequenced and annotated using a metagenomic sequencing approach, with many showing homology to the *sup* group of single module PKSs. A potential role for SupA homologues in the biosynthesis of 73-DOC was proposed but cloning and sequencing additional 73-DOC biosynthetic genes remains a goal for future work. Intriguingly, all the PKS clusters mapped from

sponges to date belong to the non-canonical *trans*-AT group and there are certain indicators that are highly suggestive of such a system being responsible for the biosynthesis of 73-DOC. First, all known enzymes generating complex polyketides from non-actinomycete symbionts belong to the *trans*-AT group (Hochmuth and Piel, 2009b, Piel, 2010), indicating the relevance of such systems in the secondary metabolism of sponge symbionts. Second, a β-branch was also predicted for the 73-DOC chemical structure (C-37) and most *trans*-AT PKSs contain unusual domains or external components, such as the β-branching cassette; a groups of genes encoding enzymes that convert β-keto groups to carbon branches (Piel, 2010). Finally, the *I. ramosa*-sourced compound irciniastain A (Pettit et al., 2004), was found to be identical to pysmberin (Jiang et al., 2005), the complete biosynthetic pathway of which utilises a *trans*-AT PKS (Fisch et al., 2009). This indicates that *trans*-AT PKS systems are present in *I. ramosa* and could also be involved in the biosynthesis of 73-DOC. Consideration of a *trans*-AT PKS is particularly interesting as it would enable the application of strategies that could greatly facilitate the future characterisation of 73-DOC biosynthesis. This and other strategies for proposed further research into 73-DOC biosynthesis are discussed in the following final chapter.

Chapter 7: General Discussion and Future Work

The work presented in this thesis detailed studies conducted with 73-DOC, a sponge-derived marine natural product. Following demonstrated antiproliferative activity in cancer cells (Rashid et al., 2001b), as well as suggested V-ATPase inhibitory activity (Bowman et al., 2003), work with 73-DOC ceased due to an exhausted supply of the compound in collections (Bowman and Bowman, 2005). Since the V-ATPase is critical for bone resorption, this thesis sought to determine whether a putative V-ATPase inhibitor could inhibit the function of osteoclasts, ultimately leading to further research into developing this compound as a novel therapeutic to treat diseases characterised by excessive bone resorption. Considering the importance of natural product leads in developing valuable pharmaceuticals, and the supply problems that often impede such development, research into a method of supplying these novel compounds is certainly needed alongside investigating the biological activity of the compound itself. This led to the multidisciplinary work presented in this thesis: One aim dedicated to evaluating the *in vitro* activity of 73-DOC, the other aim directed at cloning the biosynthetic pathway to eventually provide a sustainable supply of the compound.

Prior to the commencement of *in vitro* testing, a stock of 73-DOC was first extracted from sponge tissues, achieved using procedures detailed in Chapter 3. A yield of 73-DOC (19.5 mg) equating to 0.013 % g dry wt^{-1} and with an estimated 91 % purity was successfully obtained, consistent with, or superior to other published reports of 73-DOC extractions (Rashid et al., 2001b, Chevallier et al., 2004). The purified 73-DOC was tested on osteosarcoma cells and antiproliferative effects confirmed its activity. The extraction and purification procedure therefore yielded sufficient material for small scale *in vitro* testing, and possibly even for larger scale *in vivo* work. However, any

commercial production using this approach would be economically unfeasible and ethically controversial due to the amounts of sponges that would need to be harvested from the natural environment. This therefore highlights the need for an alternative method of 73-DOC production, the principle behind the work presented in Chapter 6.

Another option for generating a sustainable supply of 73-DOC lies in chemically synthesising the compound. Whole or semi-chemical synthesis was previously considered to be economically nonviable in producing sufficient quantities of bioactive natural products due to the complex structures of the compounds (Munro et al., 1999, Sipkema et al., 2005). However, as improvements in synthetic chemistry have been constantly evolving, this approach is much more feasible than it has been in the past (Kuttruff et al., 2014, Woerly et al., 2014). Indeed, there have been successes with marine natural products such as the sponge metabolites discodermolide (Florence et al., 2008) and eribulin (Yu et al., 2013), as well as the ascidian metabolite trabectabin (Cuevas and Francesch, 2009). The synthesis of natural products is usually not attempted until after there is preclinical or clinical evidence to support its exploitation, but considering the promising potential of 73-DOC shown in Chapters 4 and 5, such work may now be worth expediting (Carballo et al., 2010). This work could also involve research into testing synthetic structural analogues in structure-activity relationships studies that may lead to a simpler compound that retains the biological activity of 73-DOC (Smith et al., 2011). Synthetic derivatives of 73-DOC could also be further investigated in photoaffinity or fluorescent labelling studies (Gonçalves, 2008, Bockelmann et al., 2010, Carballo et al., 2010, Osteresch et al., 2012). Photoaffinity labelling of synthetic derivatives of V-ATPase inhibitors has previously been used to determine V-ATPase binding sites, so similar experiments using 73-DOC could ultimately facilitate *in vitro* and *in vivo* identification of targets and mechanisms (discussed in Chapters 4 and 5). There are still uncertainties regarding the

stereochemistry and absolute configuration of 73-DOC that require resolution. Obtaining absolute 3D structure is not only a necessity for pharmaceutical development but would also enable structure-activity relationships to be probed using virtual screening and docking models before synthesis is attempted, which could also help predict targets and binding sites on V-ATPase subunits (Ma et al., 2011). Application of single crystal x-ray crystallography is typically used to determine the relative stereochemistry of natural products and attempts to generate crystals of 73-DOC have already commenced (Albright and White, 2013).

The work in this thesis described a novel biological application for 73-DOC through inhibition of the osteoclast V-ATPase, representing a potential opportunity for developing a new therapeutic to treat osteolytic diseases. Comparisons with other compounds that target V-ATPases, including bafilomycin, or novel compounds such as enoxacin, diphyllin and luteolin, show that whilst 73-DOC shares some overlapping properties, it also appears to have unique effects on bone cells and, other than bafilomycin, has superior potency (Karsdal et al., 2005, Sorensen et al., 2007, Toro et al., 2012a, Toro et al., 2012b, Crasto et al., 2013). As both osteoclasts and osteoblasts are involved in bone remodeling and are tightly coupled as a result of catabolic and anabolic signals that occur between the two cell types, characterisation of the effects of a potential resorption inhibitor on both cell types was required for demonstrating therapeutic potential. Work presented in Chapter 4 showed that 73-DOC exhibited similar inhibitory effects towards precursor proliferation, differentiation and viability of both cell types, but dose-response proliferation analyses revealed a greater sensitivity of osteoclast lineage cells to 73-DOC compared to osteoblasts. Furthermore, the viability of mature osteoclasts was found to be 10-fold less sensitive to the effects of 73-DOC than precursor cells, demonstrating specificity and tolerance by some cell-types and contrasting with the results of bafilomycin treatment.

In Chapter 5, 73-DOC was found to inhibit both osteoclastic bone resorption and osteoblastic bone formation. However, it was also shown that the compound could significantly reduce bone resorption at concentrations 5-10 fold lower than those causing functional impairment of osteoblasts, as well as the inhibitory effects seen in Chapter 4. Taken together, these exciting *in vitro* observations show differential activity between osteoclasts and osteoblasts and imply that 73-DOC may represent an ideal novel bone resorption inhibitor that can functionally attenuate the resorptive activity of osteoclasts whilst having no impact on the generation and viability of new osteoclasts/osteoblasts, as well as the bone forming capabilities of osteoblasts. In an *in vivo* situation, this should theoretically translate into the uncoupling of bone resorption, leading to a net gain in bone tissue as normal numbers of functionally attenuated osteoclasts can be maintained, providing anabolic signals to osteoblasts. This is the ideal therapeutic outcome for osteolytic diseases such as osteoporosis. However, in order to fully satisfy these criteria, it remains to be seen what effects 73-DOC has on the putative anabolic factors produced by osteoclasts, such as glucocorticoids (Kim et al., 2006), ephrin-B2 (Zhao et al., 2006) and sphingosine 1-phosphate (Pederson et al., 2008). For example, it may be possible that conditioned media from 73-DOC-treated osteoclasts retains the capability of stimulating bone formation by osteoblasts, as was previously demonstrated in a similar experiment by Karsdal et al. (2008) using conditioned media from resorbing and non-resorbing osteoclasts. Further future work will be necessary to firmly establish whether 73-DOC can regulate potential cross-talk between osteoblasts and osteoclasts.

The exact mechanism by which 73-DOC inhibits resorption in osteoclasts is still to be determined. Decreased overall and localised acidification in osteoclasts treated with 73-DOC does imply V-ATPase inhibition, as the V-ATPase is primarily responsible for intracellular pH regulation. However, the reduction in localised acidification at the osteoclast ruffled border could be attributed to either direct inhibition

of the ruffled border-bound V-ATPases, or it may be an indirect effect, caused by ineffective trafficking of the V-ATPase complex to the ruffled border during activation of resorption, or indeed, the absence of the ruffled border itself. In comparing the *in vitro* effects of 73-DOC with V-ATPase subunit isoform knockdowns/knockouts, it was of great interest that similarities were seen with the knockdown of *Ac45*, which include normal actin ring formation and decreased osteoclast precursor proliferation, differentiation and resorption (Qin et al., 2011, Yang et al., 2012). The effects of *Ac45* knockdown were attributed to ineffective vesicular trafficking, potentially mediated by a V-ATPase interaction with Rab7 GTPases. It is therefore tempting to speculate that the *Ac45* V-ATPase subunit could be the target of 73-DOC, though further work will be necessary to verify this.

Other possible explanations for the observed effects of 73-DOC include mTOR signalling, a key pathway involved in the proliferation and growth of cells, or the endocytotic pathway, which is crucial for intracellular signalling and trafficking events. There was also the suggestion that the inhibition of autophagy may be occurring, as the autophagy proteins Atg5, Atg7, Atg4B and LC3 have been shown to be essential for ruffled border formation as well as effective osteoclast resorption *in vitro* and *in vivo* (DeSelm et al., 2011). More work remains in conclusively determining the exact roles of V-ATPases in both mTOR signalling and autophagy, but the potential involvement of 73-DOC in these cellular processes is particularly intriguing. Considering the roles of lysosomal pH in both the mTOR and autophagy pathways, as well as endosomal trafficking, future work examining the specific magnitude of lysosomal acidification in response to 73-DOC using modern pH-sensitive probes would aid clarification of the effects of 73-DOC on these processes (Vegesna et al., 2014, Aldrich et al., 2015, Shen et al., 2015). Determining the response of autophagy, mTOR and osteoclast/osteoblast

differentiation markers to 73-DOC would also be very informative and would help resolve outstanding questions related to mechanism of action.

Work presented in this thesis also showed clear effects on osteoblasts. The viability of proliferating precursors was inhibited by 73-DOC, confirming initial work with osteosarcoma cells, but differentiation and mineralisation were also impaired, demonstrating another novel aspect of 73-DOC. Previous studies using V-ATPase inhibitors and knockouts have suggested that some subunit isoforms are unimportant in osteoblasts (*a3*, *d2*, *B2*) and whilst bafilomycin has been reported to inhibit osteoblastic bone mineralisation, consistent with the work presented in this thesis, other inhibitors such as diphyllin and enoxacin do not cause inhibitory effects in osteoblasts (Lee et al., 2006, Sorensen et al., 2007, Ostrov et al., 2009, Ochotny et al., 2011). This suggests that 73-DOC and bafilomycin have a common V-ATPase target in both osteoclasts and osteoblasts but additional work is needed to clarify the subunit composition and function of osteoblast V-ATPases. Interestingly, vesicular trafficking is known to be important for the mineralisation process of osteoblasts and autophagy has recently been identified as contributing to both mineralisation (Nollet et al., 2014) and osteoblast differentiation (Pantovic et al., 2013). These processes may indicate a common 73-DOC-induced mechanism of action between osteoclast and osteoblast V-ATPases, explaining the observed effects on both cell types. However, further work is required to address this proposal and to also elucidate the complex interactions between V-ATPases, autophagy and mTOR signalling.

Ultimately the next step in the goal of developing 73-DOC as an osteoclast resorption inhibitor therapeutic should be to commence *in vivo* testing. The use of an osteoporotic animal model such as ovariectomised rodents (Kalu, 1991), would conclusively demonstrate the efficacy of using 73-DOC as an osteoporosis therapeutic through quantification of bone density using x-ray computed tomography, before and

after administration of 73-DOC. This experiment would provide unambiguous answers regarding the potential off-target effects of the compound, as well as characterising direct effects on osteoclasts and osteoblasts *in vivo*. Preliminary work in this direction has already started, where a small pilot toxicity study was conducted involving intravenous injection of mice with 73-DOC to achieve an estimated blood concentration of 2.5 μM. The treated mice, alongside untreated controls, were monitored and then sacrificed after 24 hours and 7 days, with multiple organ and bone marrow samples taken in order to ascertain any biological effects from 73-DOC. Interestingly, despite a comparatively high dose compared with that eliciting *in vitro* effects with osteoclasts and osteoblasts, the administration of 73-DOC caused no mortalities at either time point and, additionally, there were no observable gross morphological defects in any of the organs sampled, including kidney, spleen, liver, heart, lungs and brain. These initial observations therefore suggest 73-DOC is safe to use *in vivo* and that the compound does not cause any noticeable toxicity that would be expected if the compound was a universal V-ATPase inhibitor, as has been observed for bafilomycin (Keeling et al. 1998). These promising initial observations justify further extensive *in vivo* experimentation that could include a full pharmacokinetic assessment of the compound, as well as an investigation using the animal model of osteoporosis.

Having established a biological effect of 73-DOC, the final aim of this thesis concerned the cloning and sequencing of biosynthetic genes from in *I. ramosa.* As the biogenic origin of 73-DOC is likely microbial, and specifically via a PKS, work conducted in Chapter 6 was undertaken as a first step towards a goal of providing a sustainable supply of 73-DOC through expression of the biosynthetic genes in a fermentable host. The mWGS strategy led to the isolation of 18 unique PKS gene sequences, which showed homology to 1 of 2 groups of sponge-specific PKS, named *sup* and *swf*. Whilst the function of the *swf* group are still under investigation, putatively

involved in alkyl sulphate biosynthesis (Della Sala et al., 2013), the *sup* group of PKSs have been suggested to have roles in the biosynthesis of methyl-branched fatty acids. In Chapter 6, the speculative involvement of SupA in supplying methyl-branched precursors for 73-DOC biosynthesis was suggested. Examining the structure and biosynthetic mechanisms of SupA is one potential direction for future research.

Another direction concerns cloning additional genes involved in 73-DOC biosynthesis that were not isolated during the course of the current study. One approach to this goal could adopt similar methods utilised in this thesis but with important modifications. The use of degenerate KS primers has been successful in isolating several PKS gene clusters from sponge metagenomes, but crucially, these are used to sequence large numbers of KS domains from a holobiome, from which sequences of interest can then be selected based on phylogenetic clustering (Piel et al., 2004, Schirmer et al., 2005, Fisch et al., 2009). The KS domains involved in the biosynthesis of bioactive sponge metabolites are typically rare in sponge metagenomes, representing ~2 % of KS amplicons containing hundreds of sequences (Fieseler et al., 2007, Hochmuth and Piel, 2009b), but the study by Woodhouse et al. (2013) demonstrated that amplicon-based NGS strategies are particularly successful in detecting rare, novel KS sequences that are undetected when deep sequencing techniques are not applied (Della Sala et al., 2014). If KS sequences indicative of a *trans*-AT mode of biosynthesis are sequenced, these could be directly related to the chemical structure of 73-DOC as Nguyen et al. (2008) demonstrated that the phylogeny of KS domains from *trans*-AT PKSs directly correlates with the structural moieties incorporated during biosynthesis. There are also other biosynthetic components implied by the 73-DOC chemical structure that could be worth targeting, such as the methyltransferase domains responsible for geminal dimethyl groups in other sponge-derived PKS clusters such as onnamide or psymberrin (Piel et al., 2004, Fisch et al., 2009), or the β-branching cassette. Degenerate primers for the

latter were recently used by Grindberg et al. (2011) to clone the PKS/NRPS apratoxin biosynthetic pathway from a cyanobacterial metagenomic library. Once suitable targets are sequenced and identified, the loci of these targets of interest can then be isolated by screening a fosmid library with specific primers and the application of a 3D colony screening/PCR method using pools of clone DNA (Hrvatin and Piel, 2007, Gurgui and Piel, 2010). This strategy would lead to the isolation of clones with rare biosynthetic genes likely involved in complex polyketide/non-ribosomal peptide biosynthesis and would thus dramatically increase the chances of capturing the 73-DOC biosynthetic gene cluster.

An alternative approach could involve examination of *Entotheonella* spp. from *I. ramosa*. Two members of this bacterial phylotype were recently found to be responsible for the biosynthesis of almost all of the many bioactive polyketides and non-ribosomal peptides found in the sponge, *T. swinhoei* (Wilson et al., 2014). These species were suggested as belonging to a distinct, biosynthetically-rich novel candidate phylum called the Tectomicrobia that are also widespread in sponges (Wilson et al., 2014). The relevance of these bacteria as sources of bioactive polyketides/non-ribosomal peptides in sponges was recently supported by Ueoka et al. (2015), where the misakinolide gene cluster was isolated following screening of a fosmid library and was shown to originate from *Entotheonella* spp., demonstrated using fluorescent sorting of *Entotheonella* cells and whole genome amplification. On the basis of such rich secondary metabolism in a sponge symbiont, investigation of similar species in *I. ramosa* would be of great interest in isolating the biosynthetic genes responsible for 73-DOC. Intriguingly, this idea is given additional weight as sequences flanking a *supA* homologue showed homology to genes from *Entotheonella* spp. If confirmed present in *I. ramosa*, isolation of *Entotheonella* cells using fluorescent cell-sorting, or the enrichment techniques detailed

in Wilson et al. (2014), could then be followed by whole genome amplification and sequencing, or fosmid library screening.

In conclusion, the inhibition of osteoclast-mediated resorption by 73-DOC was demonstrated for the first time, thereby establishing a novel application for this compound and confirming the hypothesis of this thesis. Differential functional activity between osteoclasts and osteoblasts was also shown, suggesting that 73-DOC could represent a novel candidate for therapeutic use in osteolytic diseases to inhibit bone resorption whilst maintaining bone formation. Future *in vivo* work using an osteoporotic animal model is planned, which will enable further verification of the therapeutic potential of 73-DOC. Concurrent work further examining the role of SupA in 73-DOC biosynthesis was recommended, in addition to deep sequencing of *I. ramosa* KS domains for specific-PCR screening targets. This work should inevitably lead to cloning of the 73-DOC biosynthetic genes, perhaps eventually leading to an inexhaustible supply of a novel and potentially highly valuable osteolytic therapeutic.

Appendix

Sequence	Query coverage (%)	% identity	E value	Match description	GenBank accession number
KS1	95	89	0.0	Uncultured sponge bacterium clone, partial KS gene	AY897156
KS2	93	92	0.0	Uncultured sponge bacterium clone, partial KS gene	DQ996325
KS3	98	95	0.0	Uncultured sponge bacterium clone, partial KS gene	DQ996336
KS4	97	75	1×10^{-124}	Uncultured sponge bacterium clone, partial KS gene	DQ996363
KS5	97	91	0.0	Uncultured sponge bacterium clone, partial KS gene	DQ227684
KS6	97	75	1×10^{-130}	Uncultured sponge bacterium clone, partial KS gene	DQ996326
KS7	97	75	4×10^{-130}	Uncultured sponge bacterium clone, partial KS gene	AY897163
KS8	95	91	0.0	Uncultured sponge bacterium clone, partial KS gene	DQ227684
KS9	95	85	0.0	Uncultured sponge bacterium clone, partial KS gene	DQ438988
KS10	95	82	0.0	Uncultured sponge bacterium clone, partial KS gene	AY897152
KS11	97	75	8×10^{-127}	Uncultured sponge bacterium clone, partial KS gene	DQ996363
KS12	95	91	0.0	Uncultured sponge bacterium clone, partial KS gene	DQ227684
KS13	97	75	4×10^{-130}	Uncultured sponge bacterium clone, partial KS gene	DQ996363
KS14	95	92	0.0	Uncultured sponge bacterium clone, partial KS gene	AY897169

Table 9 KS sequences amplified from the metagenome of I. ramosa share identity with KS domain sequences from uncultured sponge symbionts. PCR-amplified partial KS domain sequences from *I. ramosa* were subjected to BLASTn searches against the NCBI non-redundant nucleotide database (Camacho et al., 2009). The top match description for each sequence is shown along with % coverage, % identity and the accession number for that match. The E-value for that match is also shown, where a value of 0.0 indicates a highly significant match.

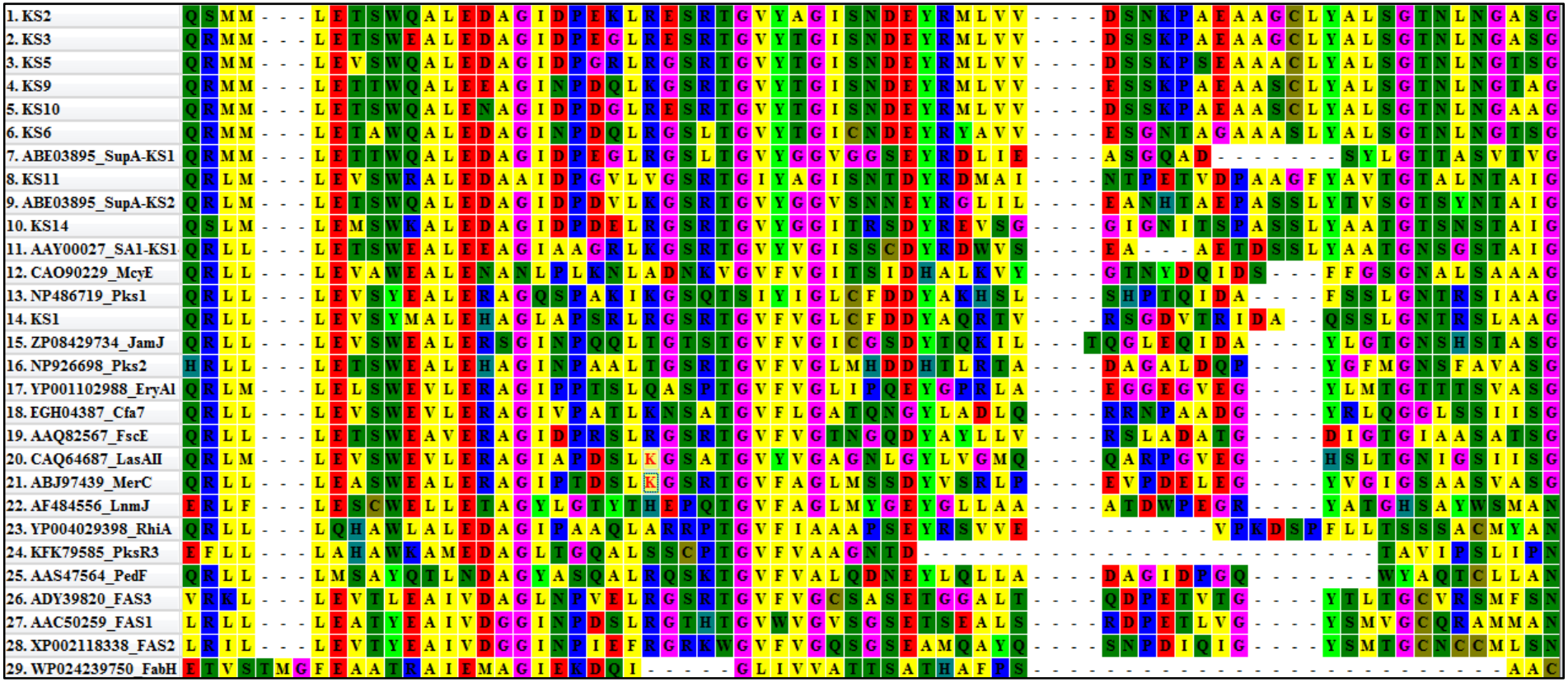

Figure 1 Multiple alignment of uncharacterised KS amino acid sequences from *I. ramosa*. The 9 unique, partial KS sequences found from *I. ramosa* were aligned with characterised KS domains from various type I PKS and FAS enzymes. The characterised KS sequences were retrieved from the GenBank database with the accession numbers shown in brackets. See Figure 6.4 and text in section 6.3.2 for details of the known KS sequences. Uncharacterised KS sequences found from *I. ramosa* are given the prefix KS-. The sequences were aligned using the MEGA software (Tamura et al., 2013) and the ClustalW algorithm (Larkin et al., 2007).

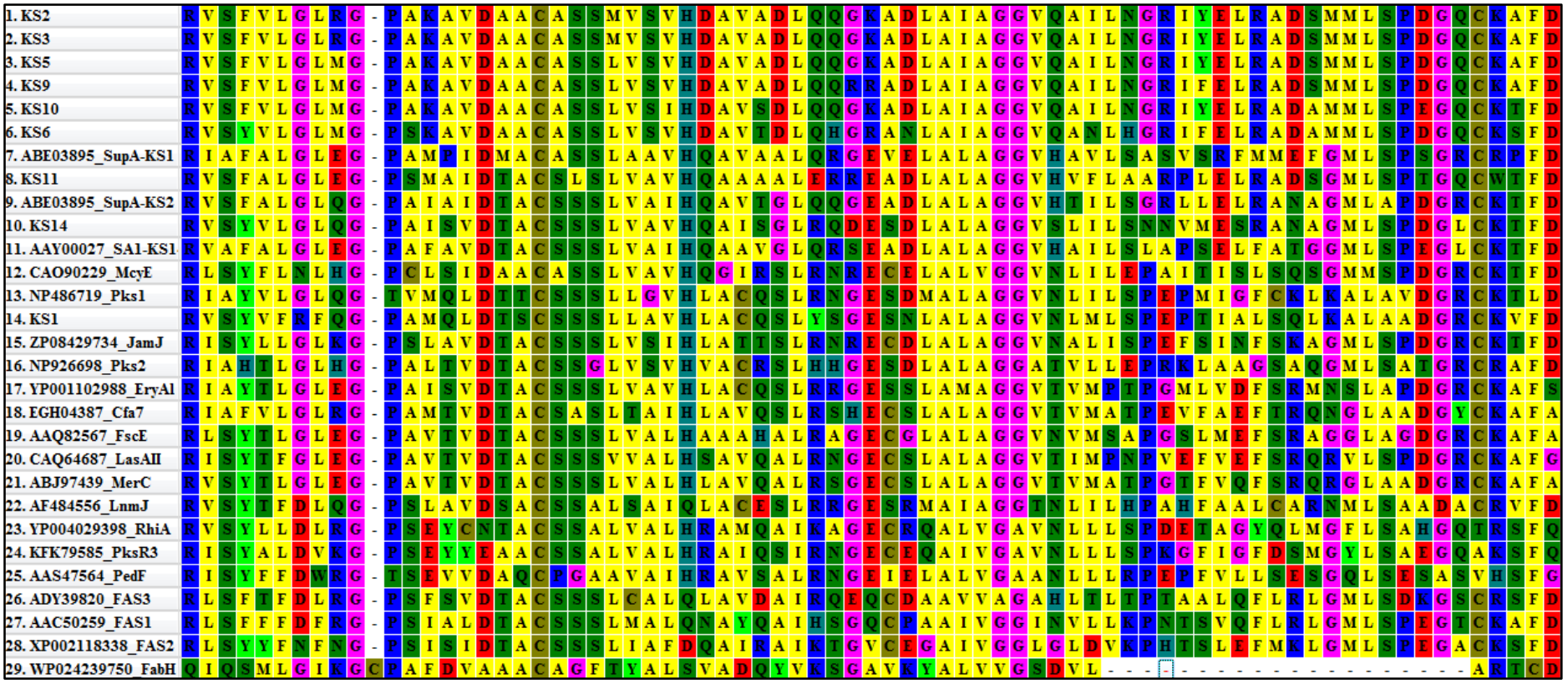
1. KS2
2. KS3
3. KS5
4. KS9
5. KS10
6. KS6
7. ABE03895_SupA-KS1
8. KS11
9. ABE03895_SupA-KS2
10. KS14
11. AAY00027_SA1-KS1
12. CAO90229_McyE
13. NP486719_Pks1
14. KS1
15. ZP08429734_JamJ
16. NP926698_Pks2
17. YP001102988_EryAI
18. EGH04387_Cfa7
19. AAQ82567_FscE
20. CAQ64687_LasAII
21. ABJ97439_MerC
22. AF484556_LnmJ
23. YP004029398_RhiA
24. KFK79585_PksR3
25. AAS47564_PedF
26. ADY39820_FAS3
27. AAC50259_FAS1
28. XP002118338_FAS2
29. WP024239750_FabH

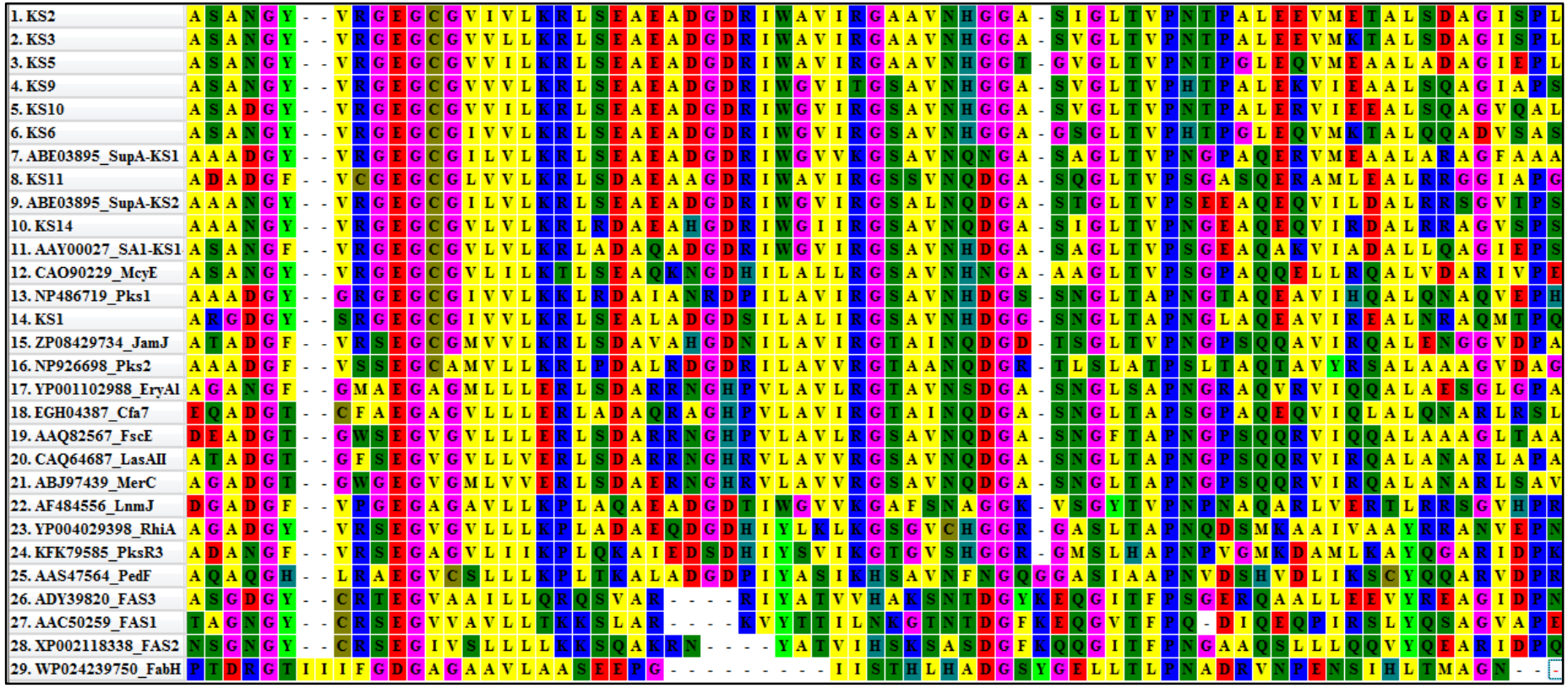
1. KS2
2. KS3
3. KS5
4. KS9
5. KS10
6. KS6
7. ABE03895_SupA-KS1
8. KS11
9. ABE03895_SupA-KS2
10. KS14
11. AAY00027_SA1-KS1
12. CAO90229_McyE
13. NP486719_Pks1
14. KS1
15. ZP08429734_JamJ
16. NP926698_Pks2
17. YP001102988_EryAI
18. EGH04387_Cfa7
19. AAQ82567_FscE
20. CAQ64687_LasAII
21. ABJ97439_MerC
22. AF484556_LnmJ
23. YP004029398_RhiA
24. KFK79585_PksR3
25. AAS47564_PedF
26. ADY39820_FAS3
27. AAC50259_FAS1
28. XP002118338_FAS2
29. WP024239750_FabH

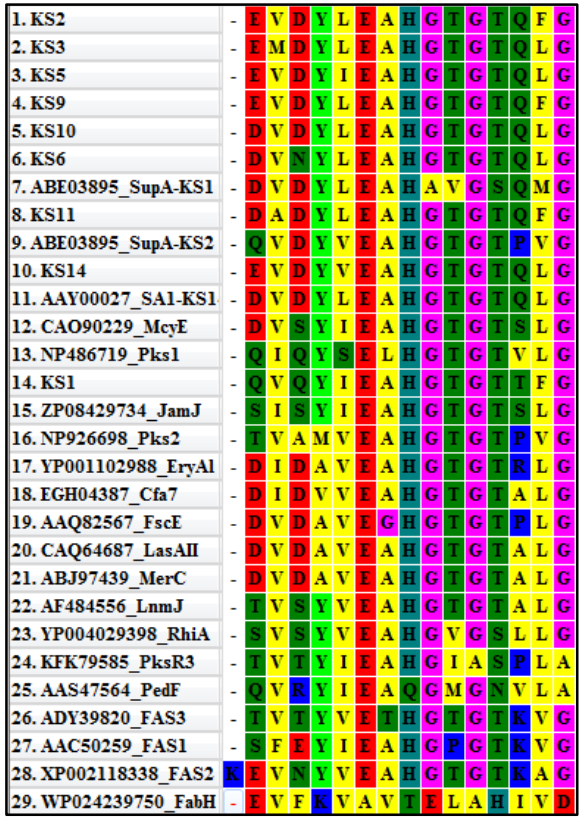
1. KS2 - E V D Y L E A H G T G T Q F G
2. KS3 - E M D Y L E A H G T G T Q L G
3. KS5 - E V D Y I E A H G T G T Q L G
4. KS9 - E V D Y L E A H G T G T Q F G
5. KS10 - D V D Y L E A H G T G T Q L G
6. KS6 - D V N Y L E A H G T G T Q L G
7. ABE03895_SupA-KS1 - D V D Y L E A H A V G S Q M G
8. KS11 - D A D Y L E A H G T G T Q F G
9. ABE03895_SupA-KS2 - Q V D Y V E A H G T G T P V G
10. KS14 - E V D Y V E A H G T G T Q L G
11. AAY00027_SA1-KS1 - D V D Y L E A H G T G T Q L G
12. CAO90229_McyE - D V S Y I E A H G T G T S L G
13. NP486719_Pks1 - Q I Q Y S E L H G T G T V L G
14. KS1 - Q V Q Y I E A H G T G T T F G
15. ZP08429734_JamJ - S I S Y I E A H G T G T S L G
16. NP926698_Pks2 - T V A M V E A H G T G T P V G
17. YP001102988_EryAI - D I D A V E A H G T G T R L G
18. EGH04387_Cfa7 - D I D V V E A H G T G T A L G
19. AAQ82567_FscE - D V D A V E G H G T G T P L G
20. CAQ64687_LasAII - D V D A V E A H G T G T A L G
21. ABJ97439_MerC - D V D A V E A H G T G T A L G
22. AF484556_LnmJ - T V S Y V E A H G T G T A L G
23. YP004029398_RhiA - S V S Y V E A H G V G S L L G
24. KFK79585_PksR3 - T V T Y I E A H G I A S P L A
25. AAS47564_PedF - Q V R Y I E A Q G M G N V L A
26. ADY39820_FAS3 - T V T Y V E T H G T G T K V G
27. AAC50259_FAS1 - S F E Y I E A H G P G T K V G
28. XP002118338_FAS2 K E V N Y V E A H G T G T K A G
29. WP024239750_FabH - E V F K V A V T E L A H I V D

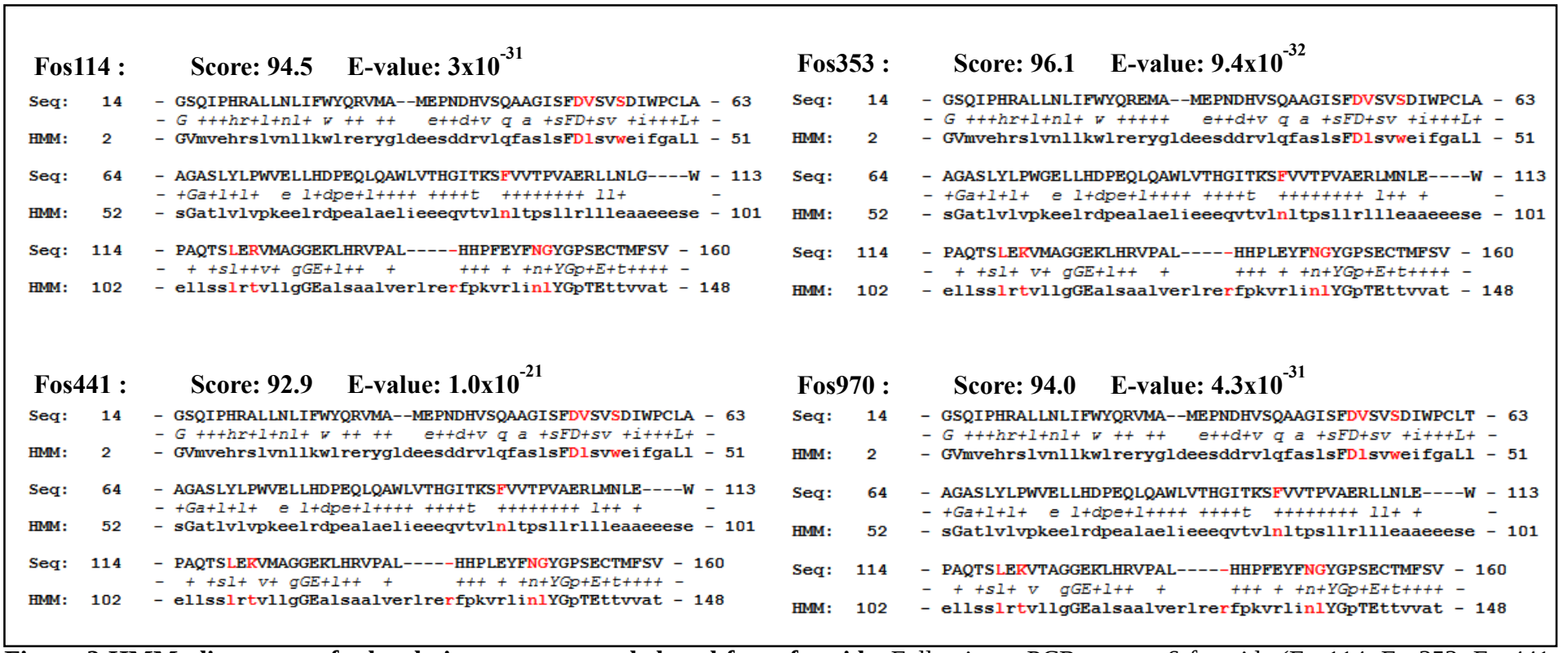

Figure 2 HMM alignments of adenylation sequences subcloned from fosmids. Following a PCR screen, 6 fosmids (Fos114, Fos353, Fos441, Fos970, Fos1118 and Fos1207) were shown to be produce a PCR band of the correct size using degenerate primers for adenylation domains. The PCR products from each of the 6 fosmids were subcloned into *E. coli* and sequenced. Amino acid sequences were then analysed using the LSI software (Baranasic et al., 2014) for *in silico* prediction of adenylation domain substrate specificity. The alignment of sequences (Seq) from each of the 6 fosmids against an HMM profile specific for the adenylation domain binding pocket is shown. Fos1118 was found to encode two unique sequences whilst a single sequence was found from the remaining fosmids. Scores and E-values for each alignment are also given where an E-value below $1x10^{-10}$ is considered reliable (Baranasic et al., 2014). Residues highlighted in red correspond to the amino acids used to determine substrate specificity by the software, which is shown in Table 6.1.

Fos1118 (1/2): Score: 66.8 E-value: 1.0×10^{-22}

```
Seq:   14   - GSQIPHRALLNLIFWYQRVMA--MEPNDHVSQAAGISFDVSVSDIWPCLA - 63
            - G +++hr+l+nl+ w ++ ++   e++d+v q a +sFD+sv +i+++L+ -
HMM:    2   - GVmvehrslvnllkwlrerygldeesddrvlqfaslsFDlsvweifgaLl - 51

Seq:   64   - AGASLYLPWVELLHDPEQLQAWLVTHGITKSFVVTPVAERLMNLEWP--- - 113
            - +Ga+l+l+  e l+dpe+l++++ ++++t  ++++++++ l++ +     -
HMM:   52   - sGatlvlvpkeelrdpealaelieeeqvtvlnltpsllrllleaaeeese - 101

Seq:  114   - -AQTSLEEV - 122
            -  + +sl++v -
HMM:  102   - ellsslrtv - 110
```

Fos1118 (2/2): Score: 94.5 E-value: 3×10^{-31}

```
Seq:   14   - GSQIPHRALLNLIFWYQRVMA--MEPNDHVSQAAGISFDVSVSDIWPCLA - 63
            - G +++hr+l+nl+ w ++ ++   e++d+v q a +sFD+sv +i+++L+ -
HMM:    2   - GVmvehrslvnllkwlrerygldeesddrvlqfaslsFDlsvweifgaLl - 51

Seq:   64   - AGASLYLPWVELLHDPEQLQAWLVTHGITKSFVVTPVAERLMNLE----W - 113
            - +Ga+l+l+  e l+dpe+l++++ ++++t  ++++++++ l++ +     -
HMM:   52   - sGatlvlvpkeelrdpealaelieeeqvtvlnltpsllrllleaaeeese - 101

Seq:  114   - PAQTSLEKVMAGGEKLHRVPAL-----HHPLEYFNGYGPSECTMFSV - 160
            -  + +sl+ v+ gGE+l++  +      +++ + +n+YGp+E+t++++ -
HMM:  102   - ellsslrtvllgGEalsaalverlrerfpkvrlinlYGpTEttvvat - 148
```

Fos1207: Score: 94.9 E-value: 2.2×10^{-22}

```
Seq:   14   - GSQIPHRALLNLIFWYQRVMA--MEPNDHVSQAAGISFDVSVSDIWPCLA - 63
            - G +++hr+l+nl+ w ++ ++   e++d+v q a +sFD+sv +i+++L+ -
HMM:    2   - GVmvehrslvnllkwlrerygldeesddrvlqfaslsFDlsvweifgaLl - 51

Seq:   64   - AGASLYLPWVELLHDPEQLQAWLVTHGITKSFVVTPVAERLMNLE----W - 113
            - +Ga+l+l+  e l+dpe+l++++ ++++t  ++++++++ l++ +     -
HMM:   52   - sGatlvlvpkeelrdpealaelieeeqvtvlnltpsllrllleaaeeese - 101

Seq:  114   - PAQTSLEKVMAGGEKLHRVPAL-----HHPLEYFNGYGPSECTMFSV - 160
            -  + +sl+ v+ gGE+l++  +      +++ + +n+YGp+E+t++++ -
HMM:  102   - ellsslrtvllgGEalsaalverlrerfpkvrlinlYGpTEttvvat - 148
```

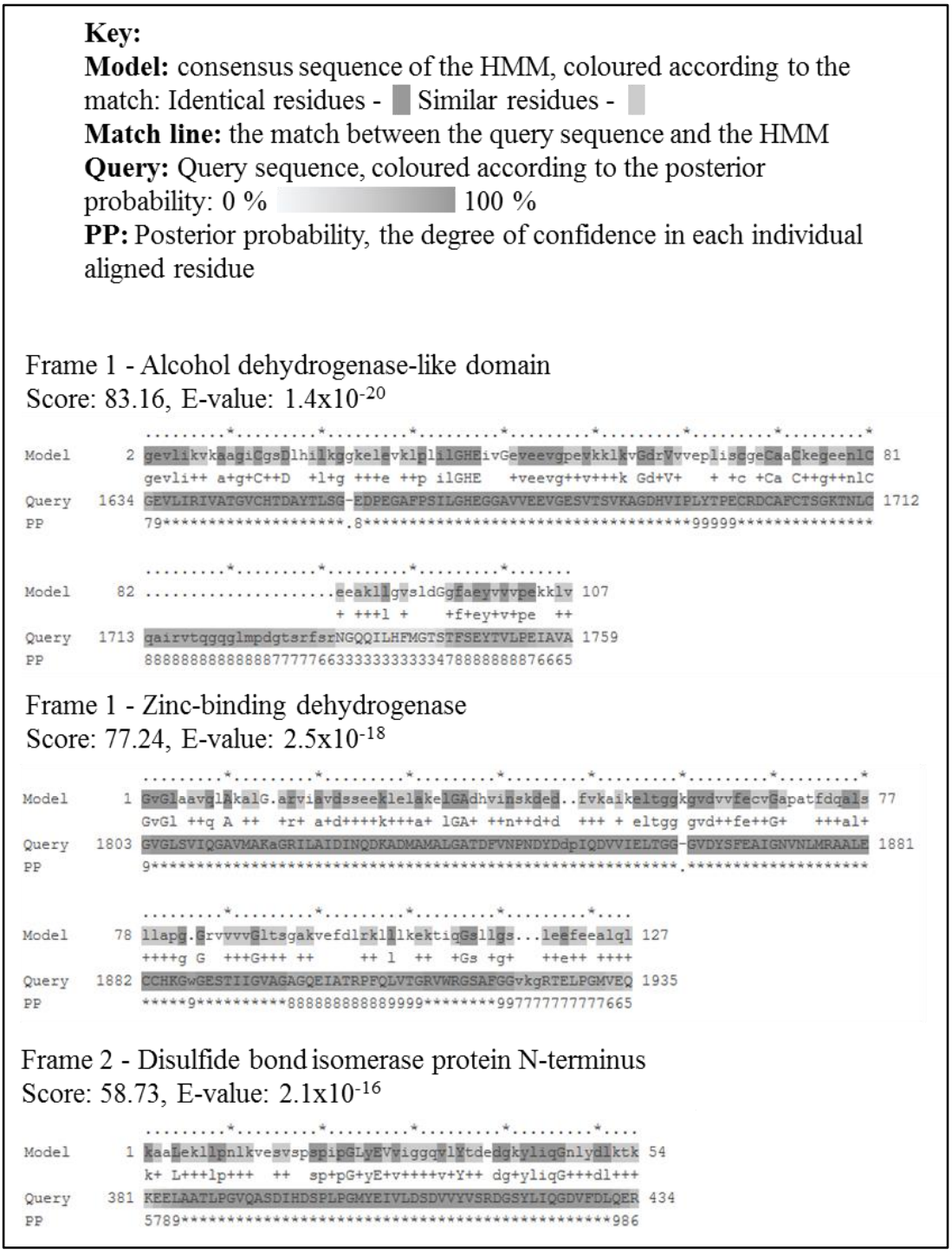

Figure 3 Alignments of proteins identified following a HMM search of the sequence obtained from Fos1118. The DNA sequence found following primer walking of Fos1118 was translated into all 6 reading frames and searched against the Pfam protein families database (Finn et al., 2011). Alignments for each protein match found are shown along with scores and E-values for that alignment. See key at top of figure for details on interpreting the alignment.

Frame 2 - Thioredoxin-like domain
Score: 79.36, E-value: 5.8×10^{-16}

Frame 2 - Flavin adenine dinucleotide binding domain
Score: 104.26, E-value: 4.3×10^{-30}

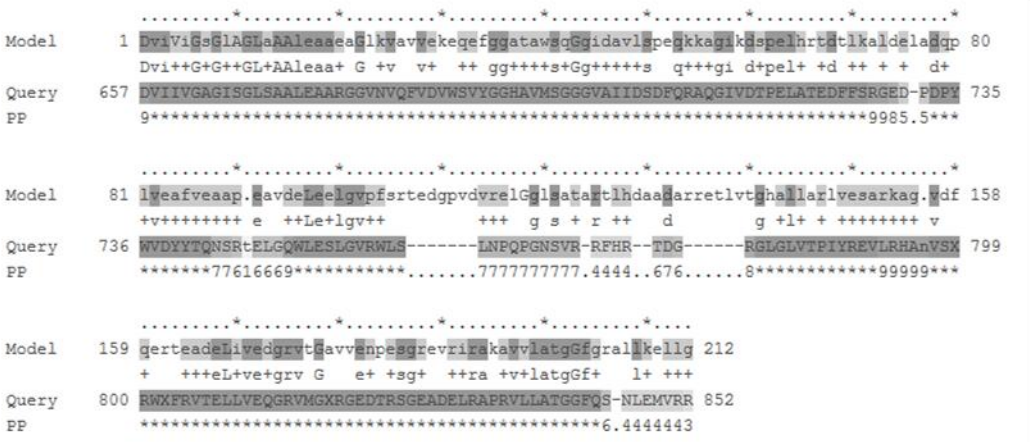

Frame 3 - Flavin adenine dinucleotide binding domain
Score: 66.25, E-value: 2.2×10^{-25}

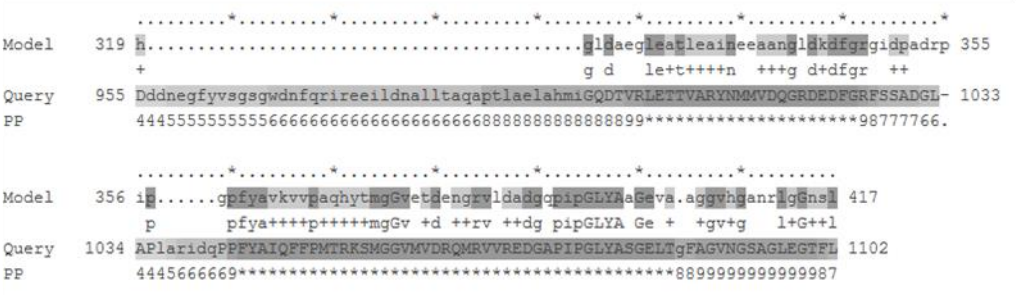

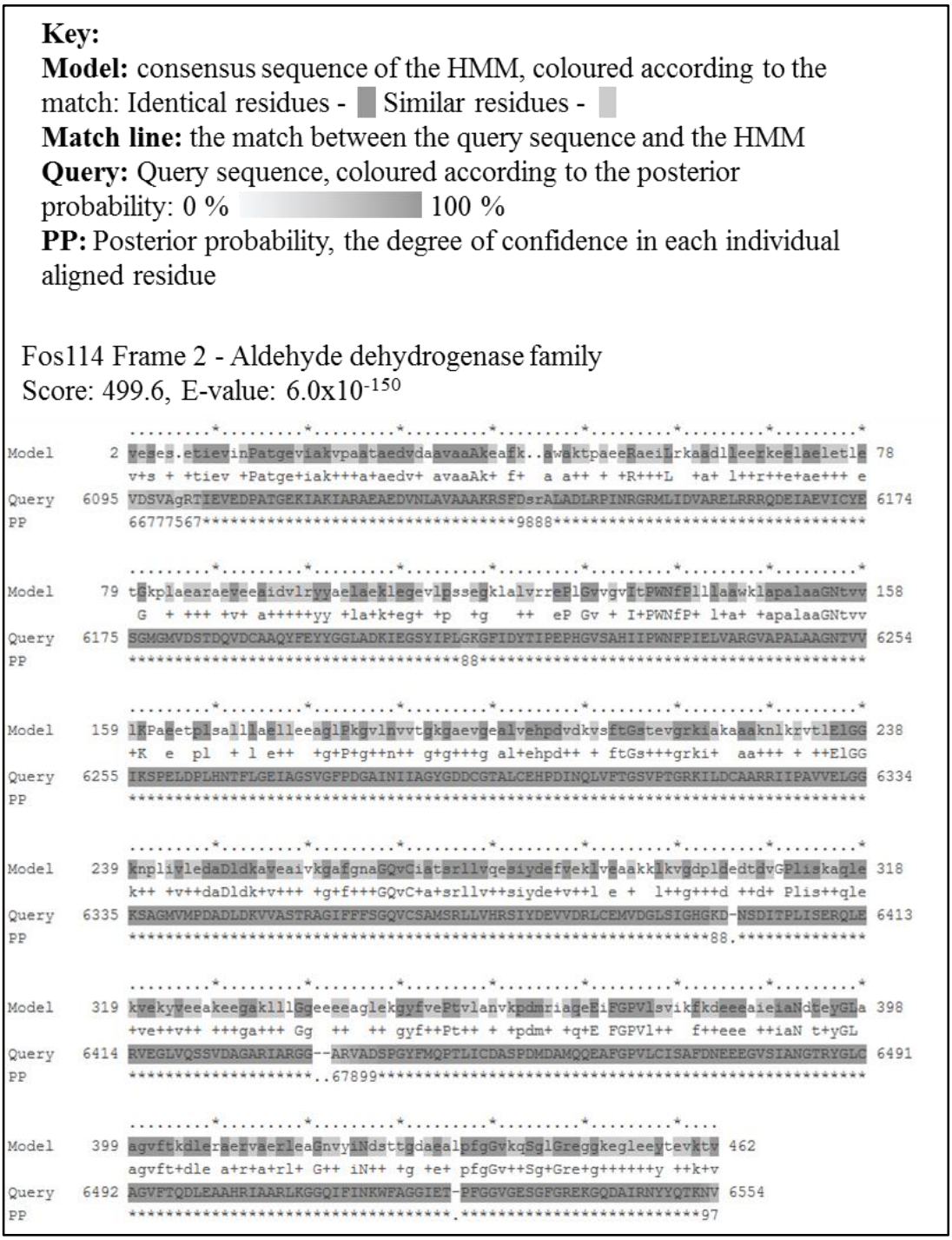

Figure 4 Alignments of proteins identified following a HMM search of the candidate fosmid insert sequences. The DNA sequences of all 5 of the candidate fosmids were translated into all 6 reading frames and searched against the Pfam protein database (Finn et al., 2011). The output alignments from Pfam for the top 3 matches based on score are shown along with scores and E-values for that alignment. See key at top of figure for details on interpreting the alignment.

Fos114 Frame 3 - Prolyl oligopeptidase, N-terminal
Score: 374.7, E-value: 4.7×10^{-112}

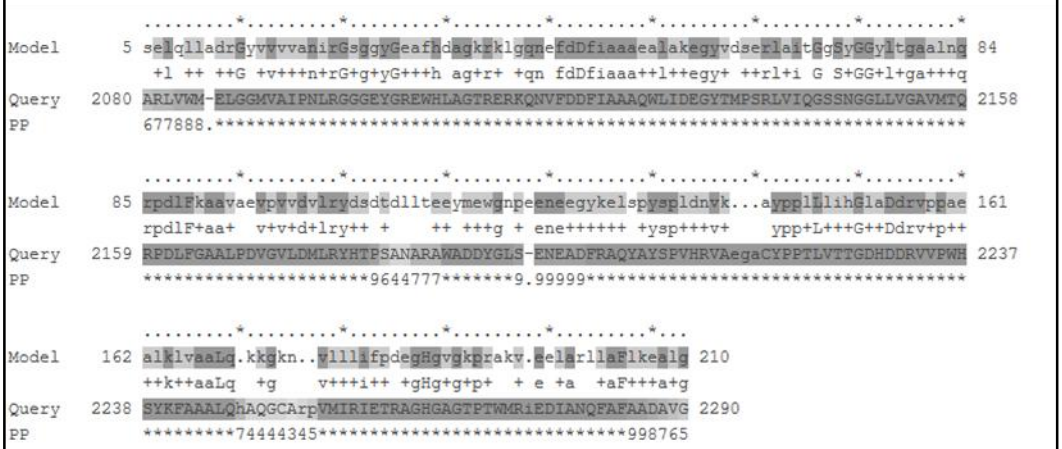

Fos114 Frame 3 - Aminotransferase class-III
Score: 326.2, E-value: 1.8×10^{-97}

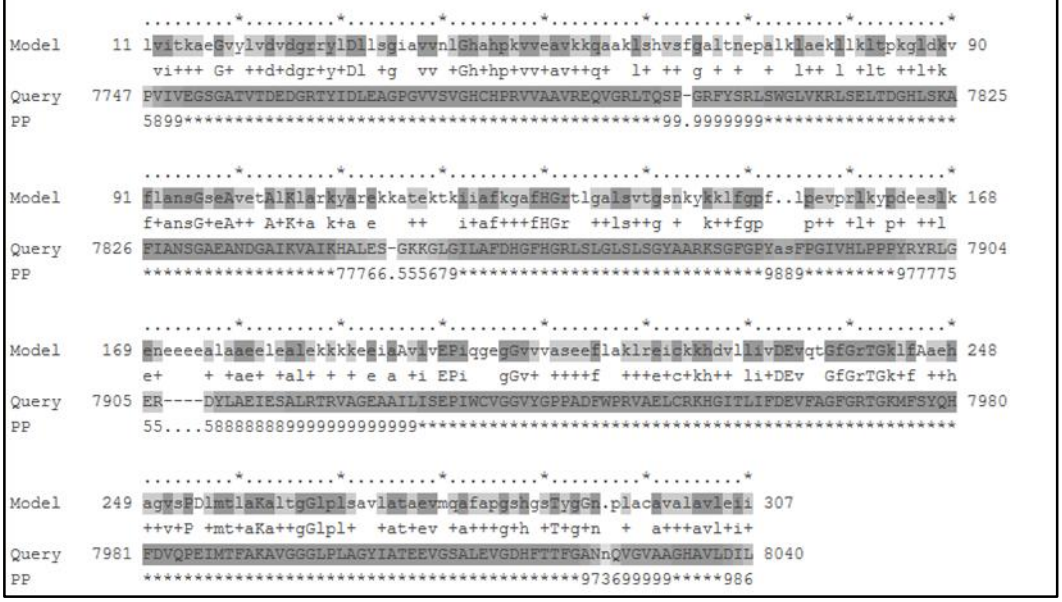

Fos353 Frame 2 - Phage terminase subunit
Score: 530.4, E-value: $5.4x10^{-159}$

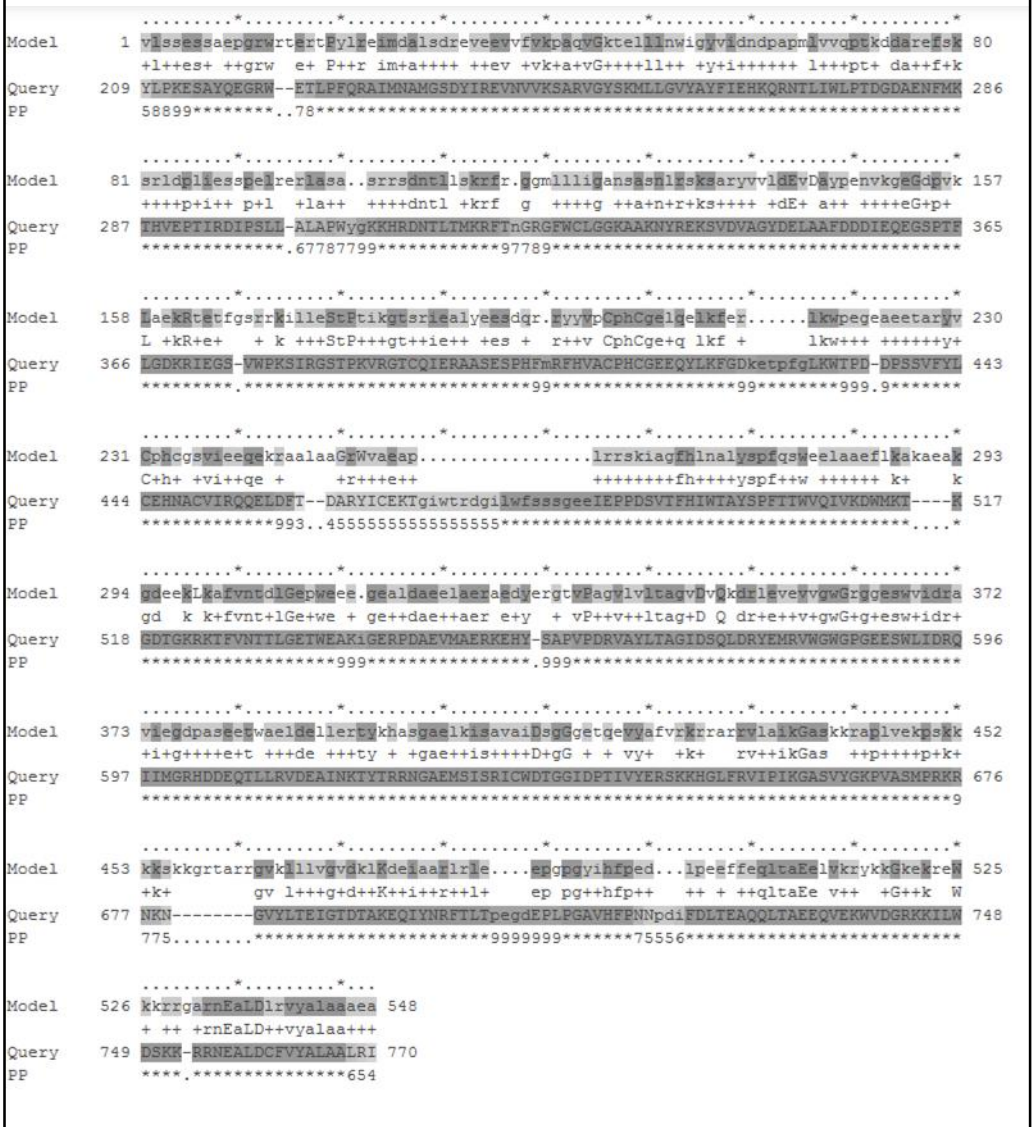

Fos353 Frame 3 - Phage minor tail protein
Score: 322.9, E-value: $5.4x10^{-97}$

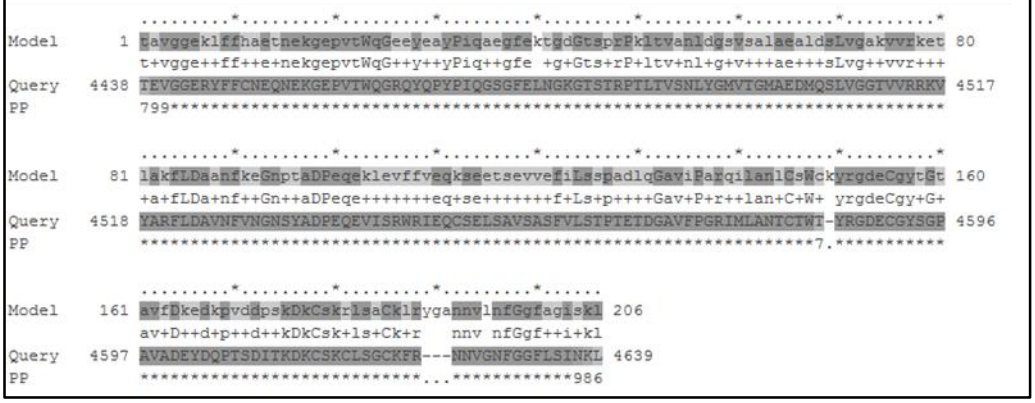

Fos353 Frame 6 - Aminotransferase class-III
Score: 437.6, E-value: 3.3×10^{-131}

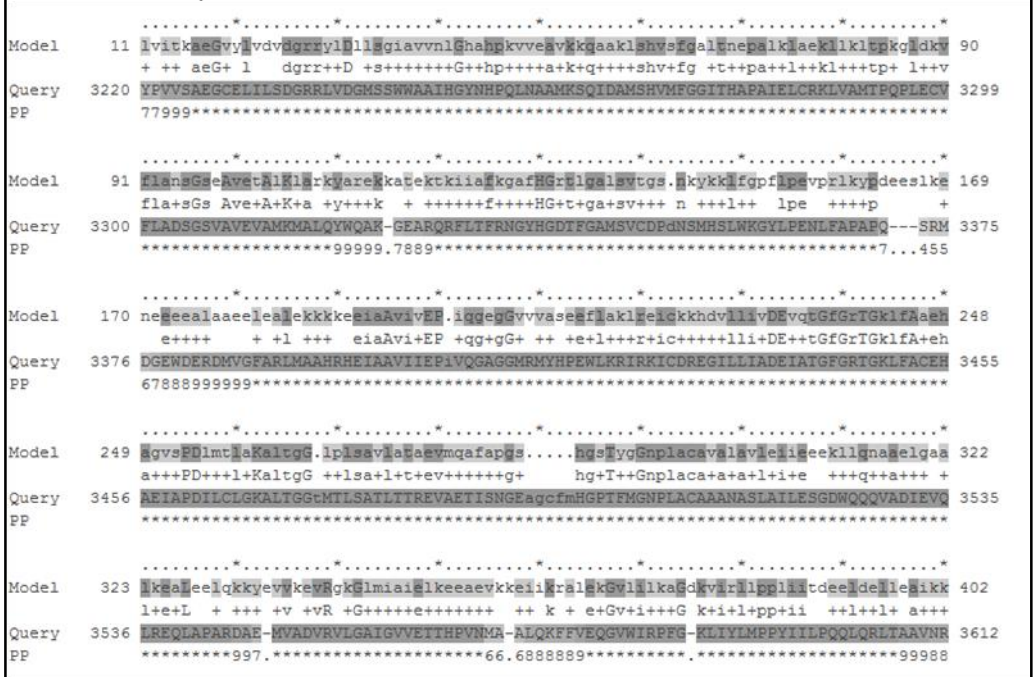

Fos441 Frame 1 - CoA-transferase family III
Score: 463.7, E-value: 4.0×10^{-139}

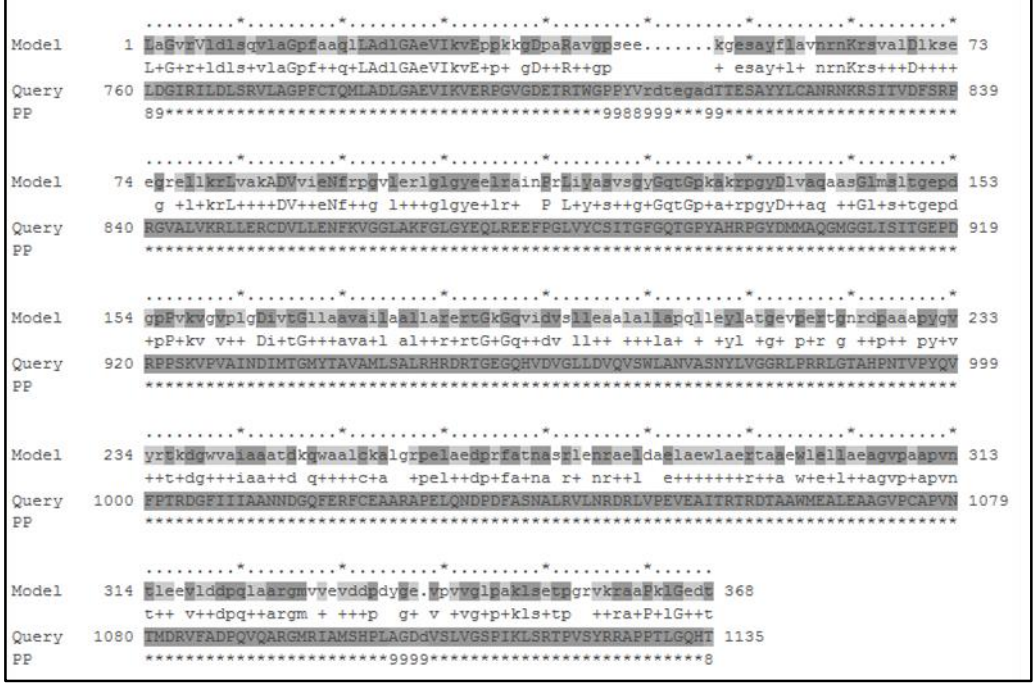

Fos441 Frame 6 - Aminotransferase class-V
Score: 171.8, E-value: $1.9x10^{-50}$

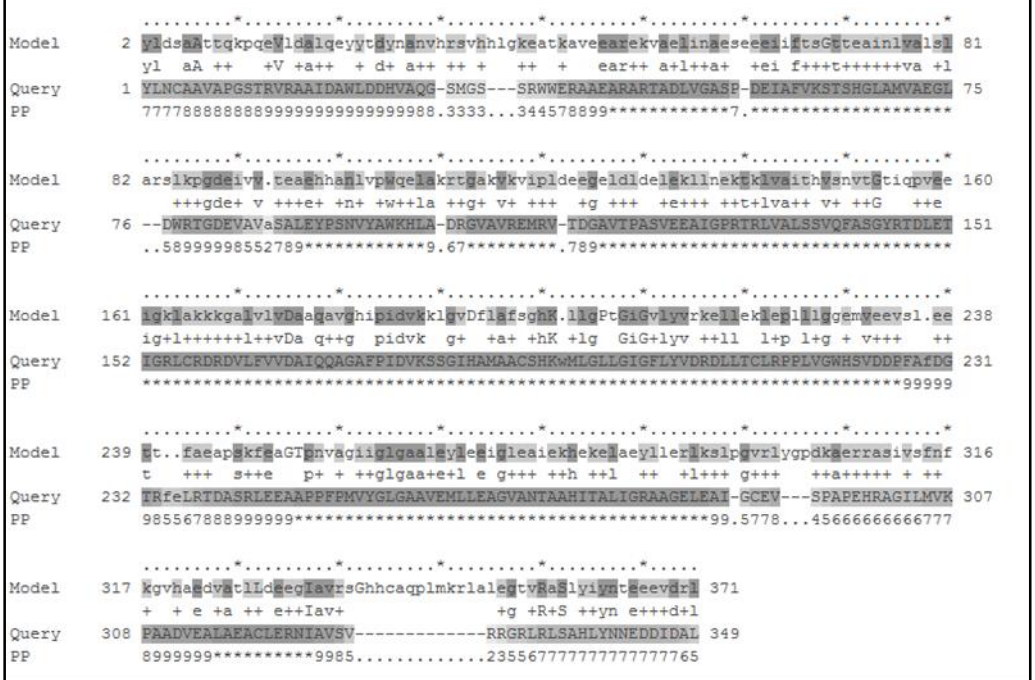

Fos441 Frame 6 - Bacterial type II and III secretion system protein
Score: 128.9, E-value: $1.3x10^{-37}$

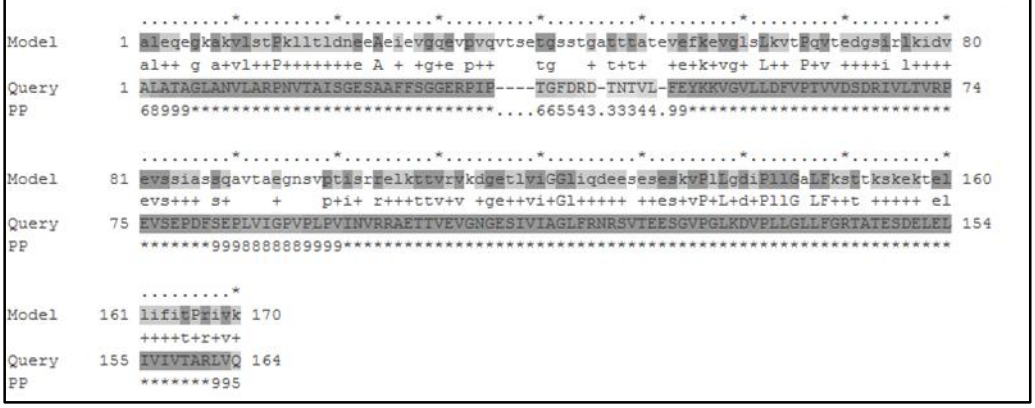

Fos970 Frame 6 - tRNA synthetase class I
Score: 643.6, E-value: 2.3×10^{-193}

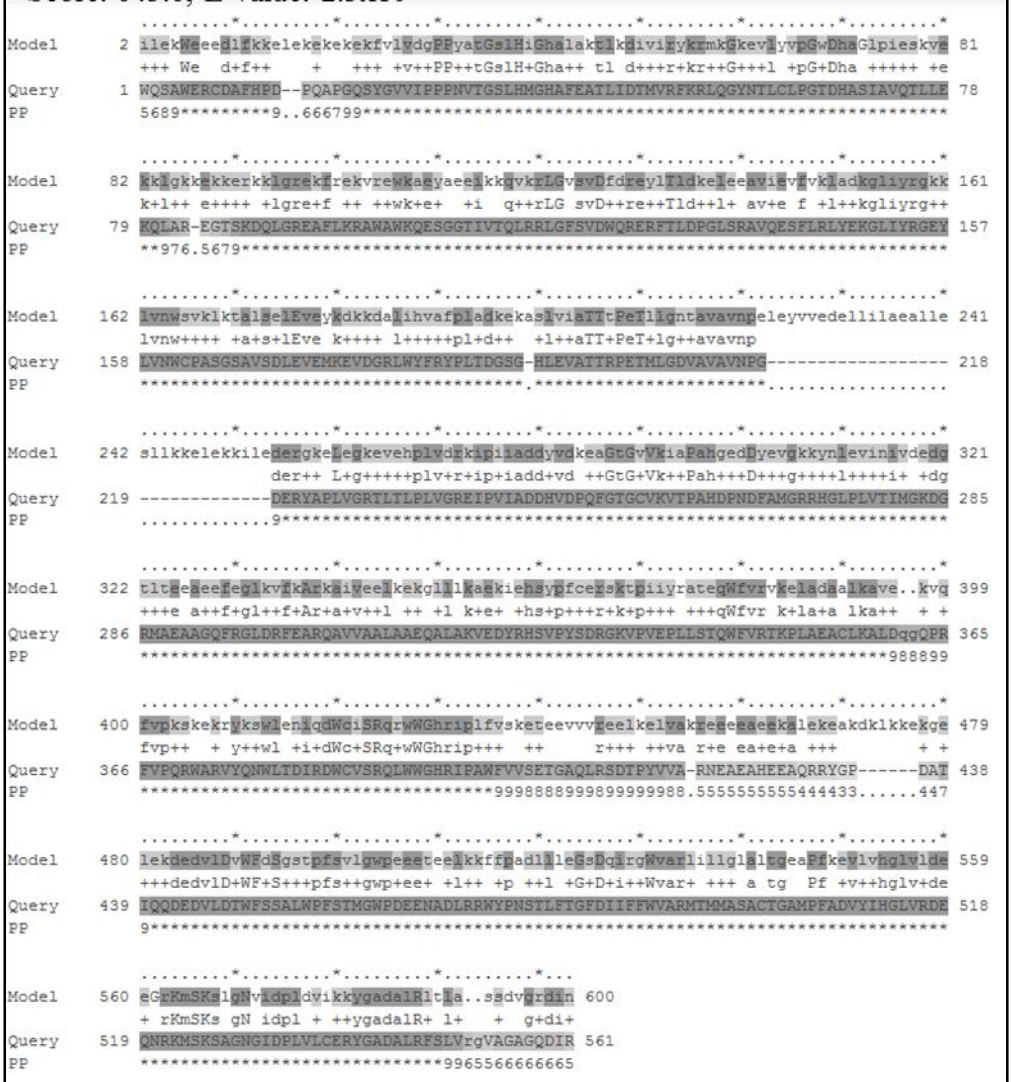

Fos970 Frame 3 - Tryptophan synthase alpha chain
Score: 276.9, E-value: 9.0×10^{-83}

Fos970 Frame 4 - Transposase
Score: 227.1, E-value: 2.7×10^{-67}

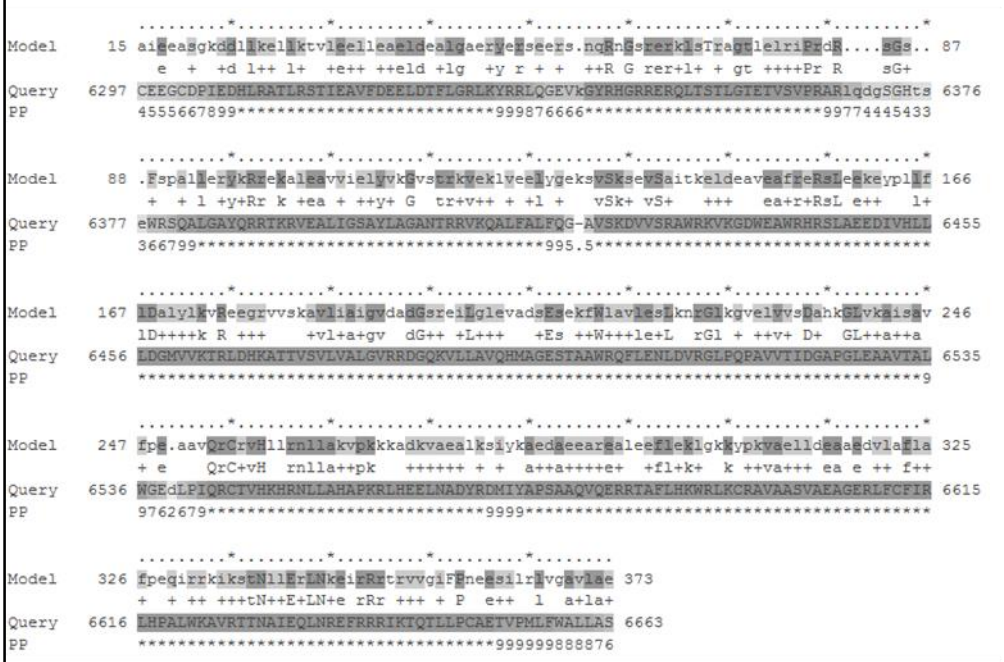

Fos1118 Frame 4 -Tripartite ATP-independent periplasmic transporter
Score: 301.2, E-value: 8.8×10^{-90}

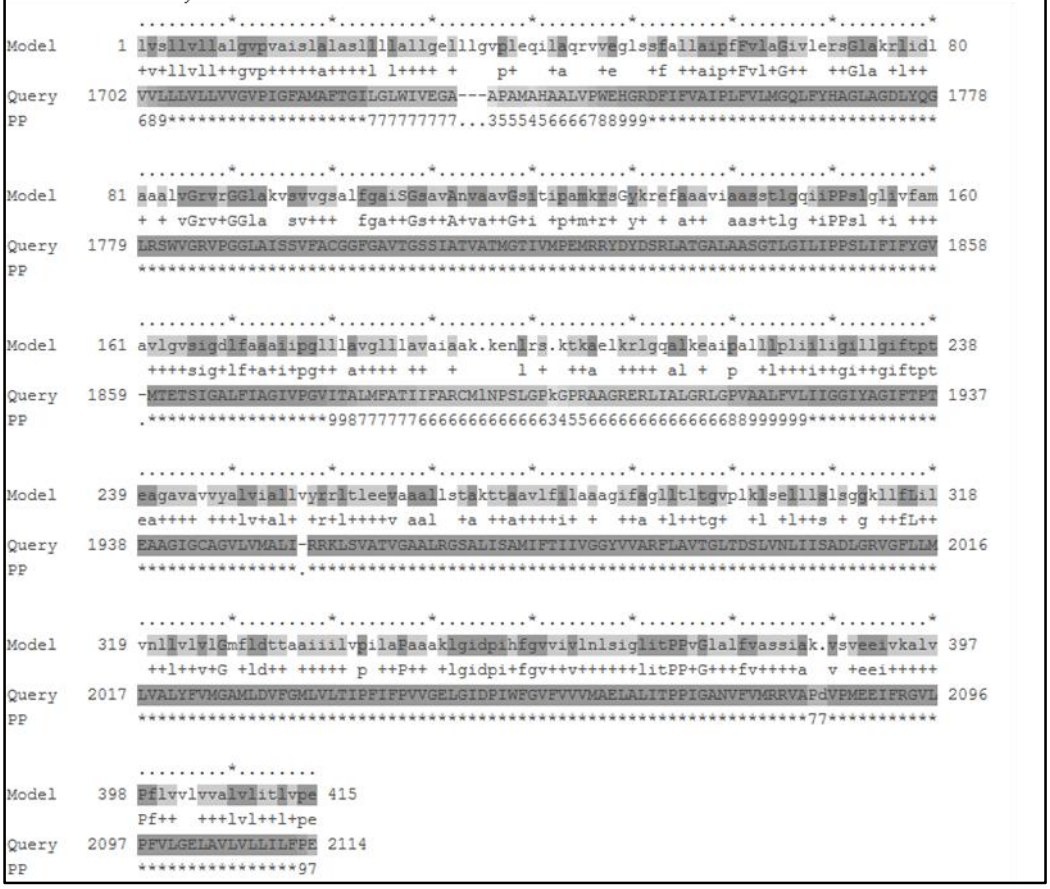

Fos1118 Frame 2 -Flavin adenine dinucleotide binding domain
Score: 217.9, E-value: 2.3×10^{-64}

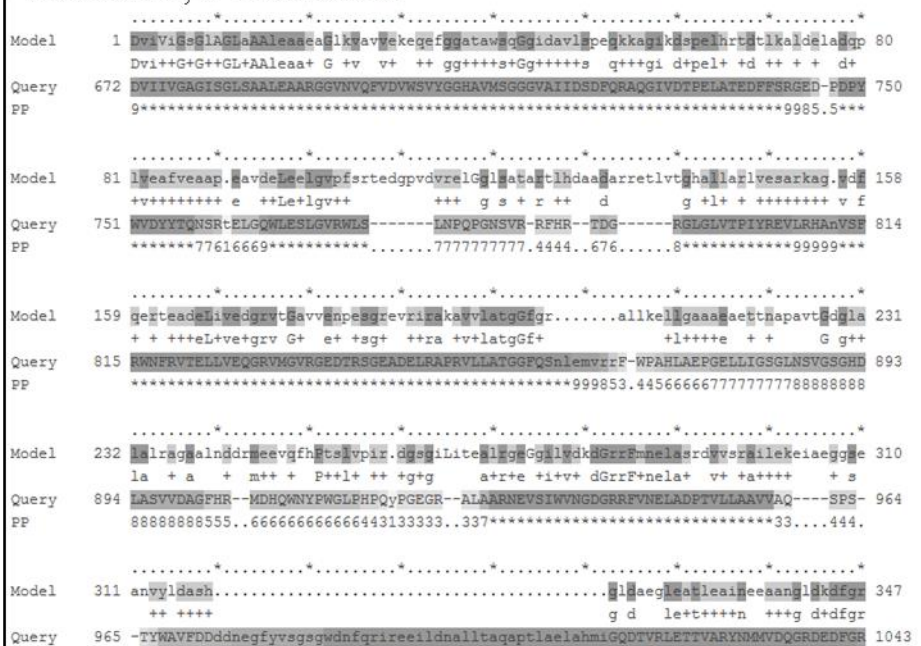

Fos1118 Frame 3 - Sulfatase
Score: 169.9, E-value: 7.5×10^{-50}

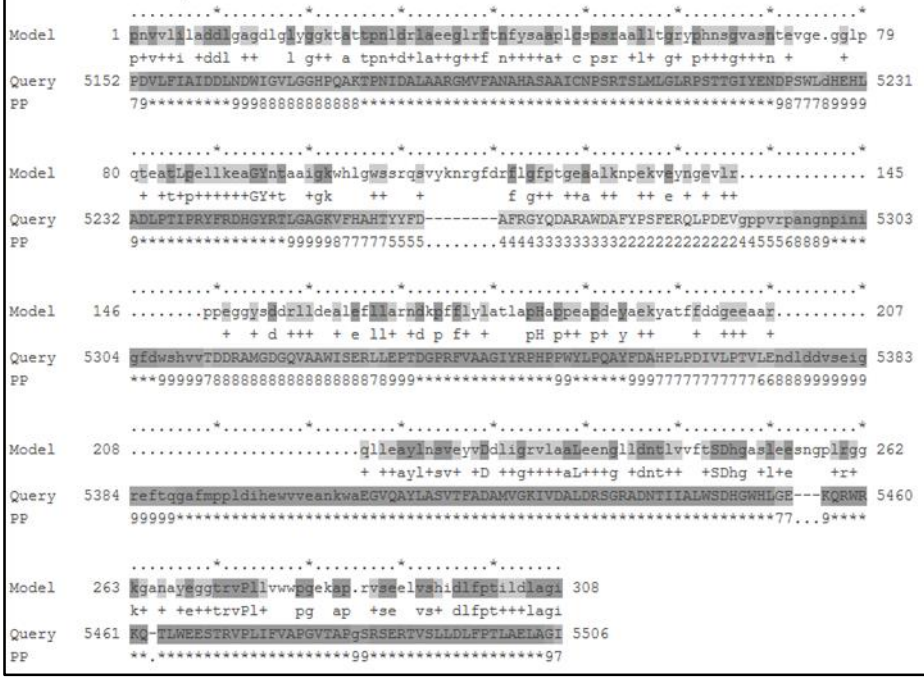

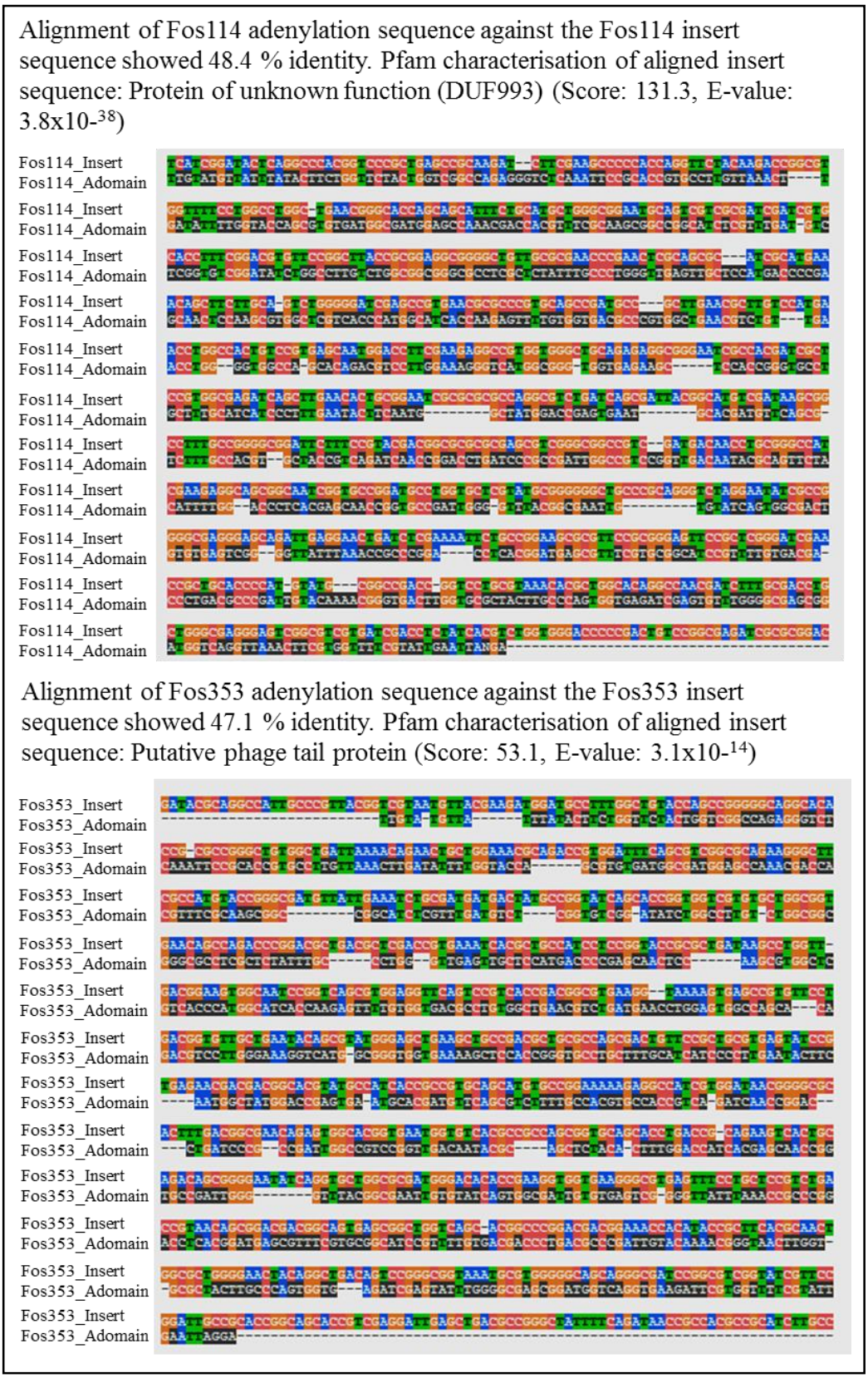

Figure 5 Pairwise DNA alignments of putative adenylation domain sequences and fosmid insert sequences. The sequences were aligned using the EMBOSS Needle tool for pairwise alignements (Rice et al., 2000). Nucleotides with matching identities have matching colours. The aligned sequence from the fosmid insert was characterised by searching the DNA sequence against the Pfam protein families database (Finn et al., 2011).

Alignment of Fos441 adenylation sequence against the Fos441 insert sequence, showed 41.1 % identity. Pfam characterisation of aligned insert sequence: No matches detected

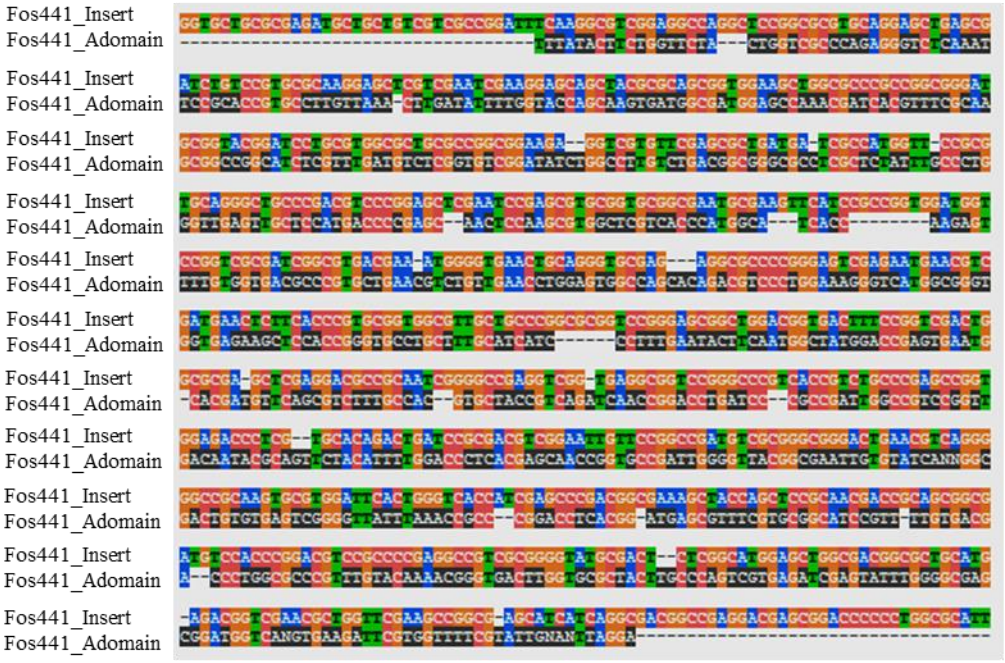

Alignment of Fos970 adenylation sequence against the Fos970 insert sequence showed 39.9 % identity. Pfam characterisation of aligned insert sequence: Transposase (Score: 169.4, E-value: 9.5×10^{-50})

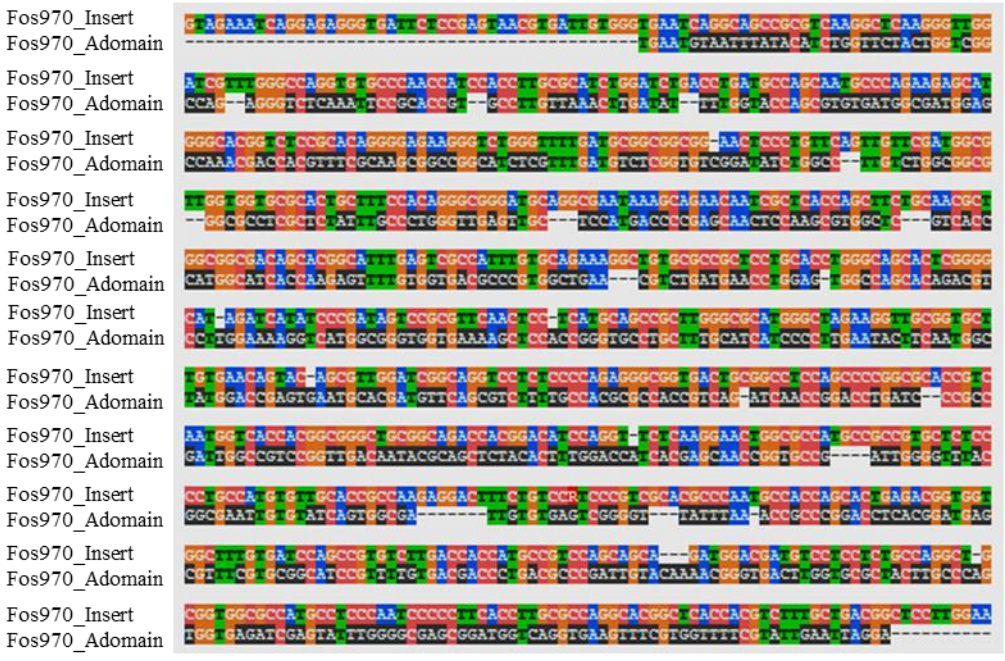

Alignment of Fos1118 adenylation sequences against the Fos1118 insert sequence showed 42.1 and 41.9 % identity for Adomain1 and Adomain2 respectively. Pfam characterisation of aligned insert sequence:
No matches detected

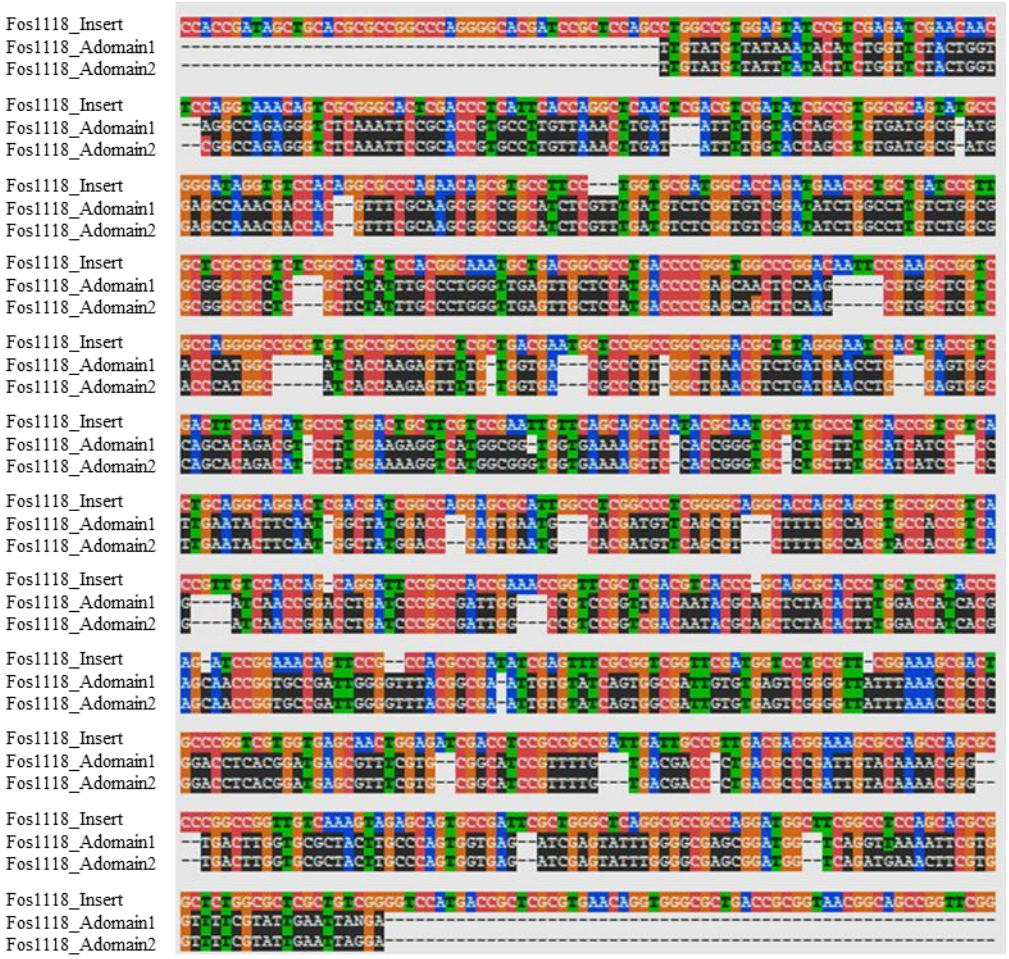

Alignment of Fos114 insert sequence against the KS1 sequence showed 41.5 % identity. Pfam characterisation of aligned insert sequence: CoA binding domain (Score: 67.4, E-value: $1.3x10^{-18}$)

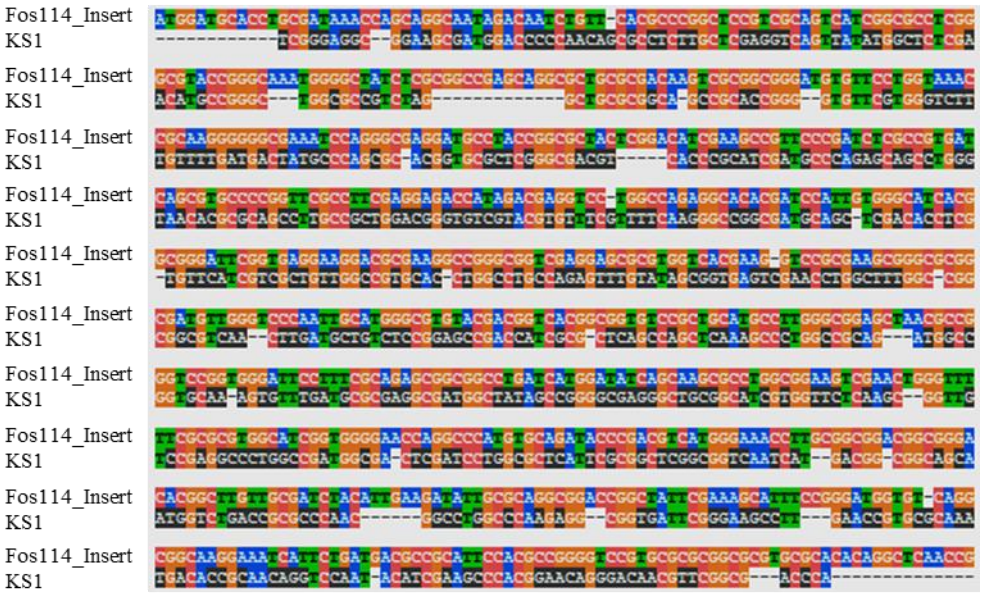

Alignment of Fos353 insert sequence against the KS1 sequence showed 46.1 % identity. Pfam characterisation of aligned insert sequence: Phage tail protein (Score: 163.2, E-value: $3.5x10^{-48}$)

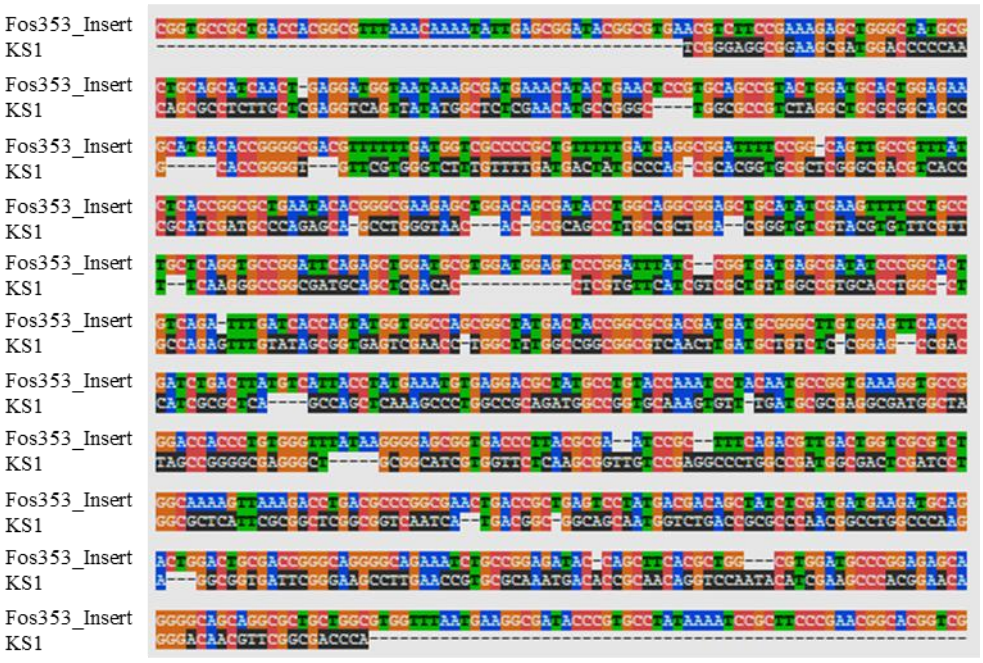

Figure 6 Pairwise DNA alignments of KS1 sequence and fosmid insert sequences. The sequences were aligned using the EMBOSS Needle tool for pairwise alignements (Rice et al., 2000). Nucleotides with matching identities have matching colours. The aligned sequence from the fosmid insert was characterised by searching against the Pfam protein database (Finn et al., 2011).

Alignment of Fos441 insert sequence against the KS1 sequence showed 49.8 % identity. Pfam characterisation of aligned insert sequence: No matches detected

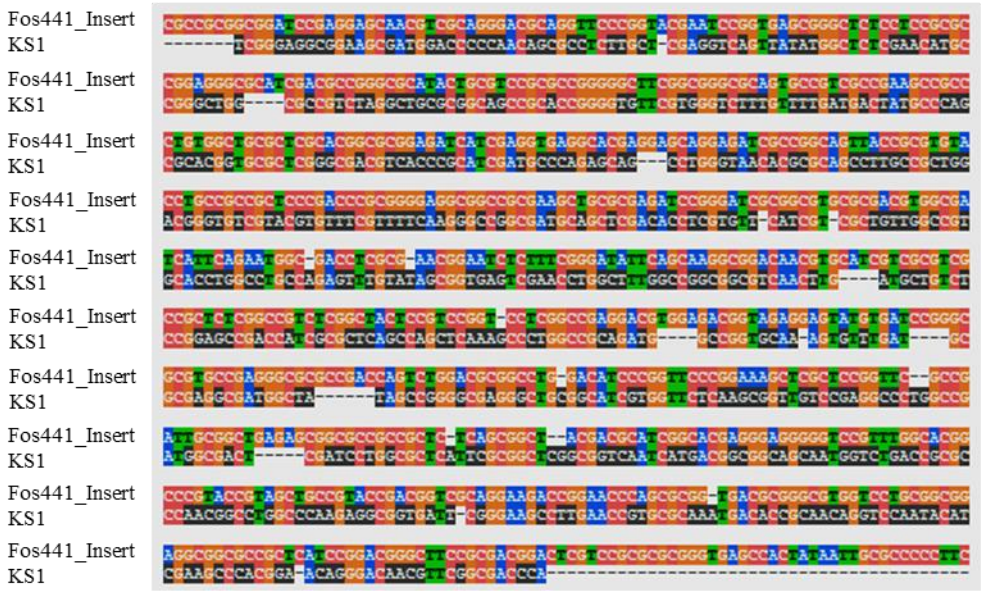

Alignment of Fos970 insert sequence against the KS1 sequence showed 46.4 % identity. Pfam characterisation of aligned insert sequence: No matches detected

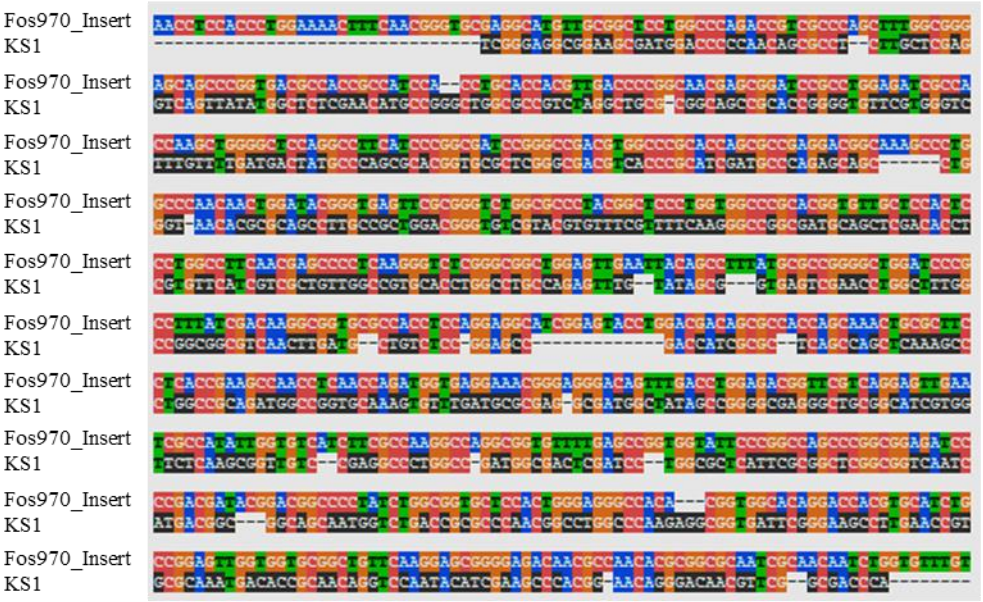

Alignment of Fos1118 insert sequence against the KS1 sequence showed 46.1 % identity. Pfam characterisation of aligned insert sequence: FAD binding domain (Score: 77.1, E-value: $1.3x10^{-21}$)

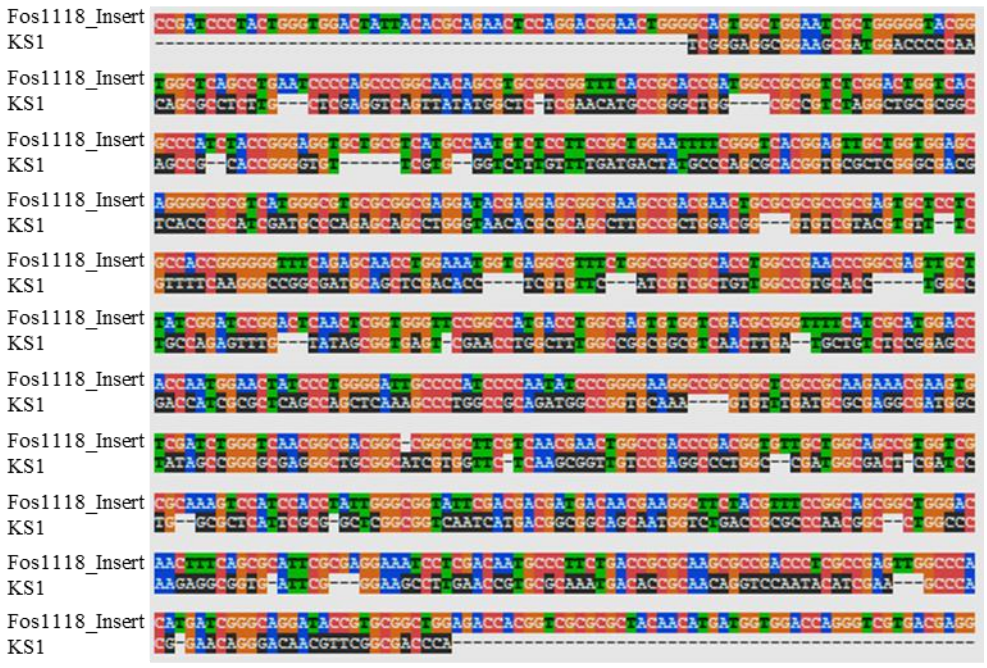

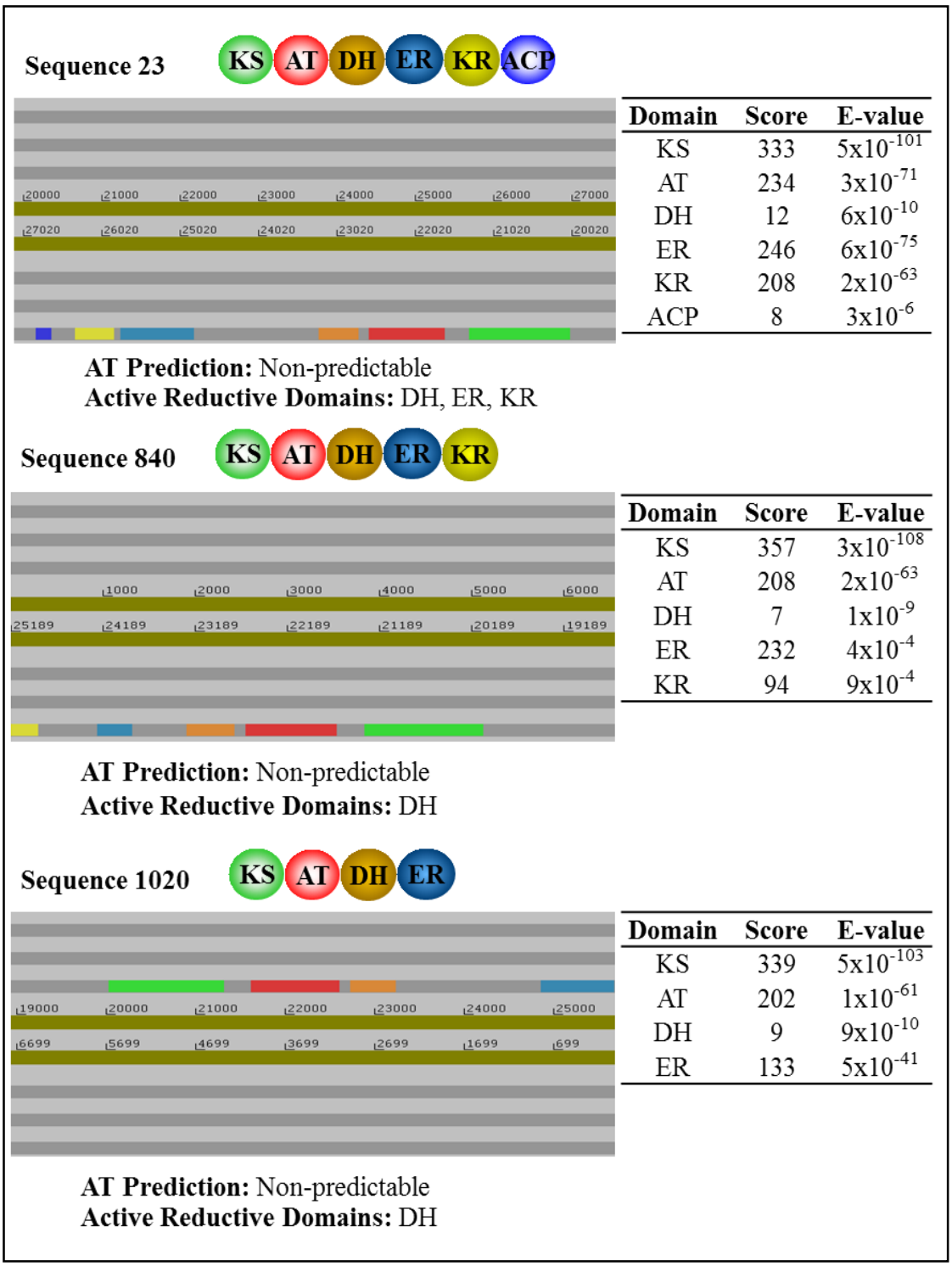

Domain	Score	E-value
KS	333	$5x10^{-101}$
AT	234	$3x10^{-71}$
DH	12	$6x10^{-10}$
ER	246	$6x10^{-75}$
KR	208	$2x10^{-63}$
ACP	8	$3x10^{-6}$

Domain	Score	E-value
KS	357	$3x10^{-108}$
AT	208	$2x10^{-63}$
DH	7	$1x10^{-9}$
ER	232	$4x10^{-4}$
KR	94	$9x10^{-4}$

Domain	Score	E-value
KS	339	$5x10^{-103}$
AT	202	$1x10^{-61}$
DH	9	$9x10^{-10}$
ER	133	$5x10^{-41}$

Figure 7 Domain annotation of type I PKS sequences identified by antiSMASH. A total of 18 type I PKS sequences were identified following screening of mWGS contigs using antiSMASH. To confirm the automatic domain annotation of antiSMASH, each sequence was also manually annotated using ClustScan (Starcevic et al., 2008) with the output shown for each sequence. This included a schematic showing the colour-coded locations of each domain encoded by that sequence, a table showing the scores and E-values from HMM profile alignments, and a prediction of AT domain specificity and active reductive domains, as determined by the program.

Sequence 1318 KS AT DH M ER KR ACP KS

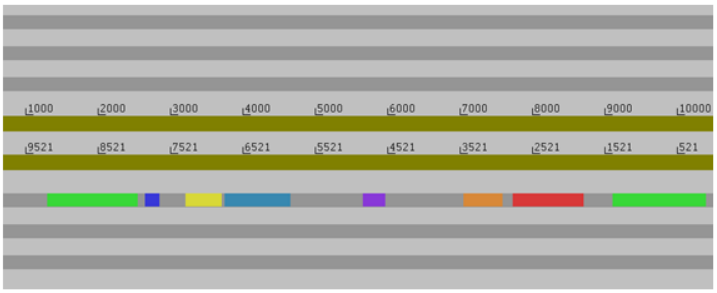

Domain	Score	E-value
KS 1	729	$3x10^{-220}$
KS 2	701	$5x10^{-212}$
AT	178	$1x10^{-54}$
DH	52	$2x10^{-16}$
M	91	$4x10^{-28}$
ER	293	$7x10^{-89}$
KR	280	$3x10^{-85}$
ACP	45	$2x10^{-14}$

AT Prediction: Malonyl
Active Reductive Domains: DH

Sequence 1506 KS AT DH M ER KR ACP KS AT

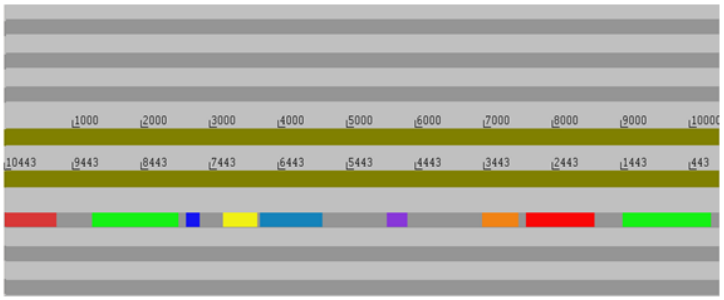

Domain	Score	E-value
KS 1	799	$2x10^{-243}$
KS 2	742	$2x10^{-242}$
AT1	210	$3x10^{-64}$
AT2	89	$3x10^{-26}$
DH	52	$1x10^{-16}$
M	87	$3x10^{-27}$
ER	343	$2x10^{-104}$
KR	258	$1x10^{-78}$
ACP	43	$6x10^{-14}$

AT Prediction: Malonyl (1) & Non-predictable (2)
Active Reductive Domains: DH

Sequence 1836 KS AT DH M ER KR ACP KS AT

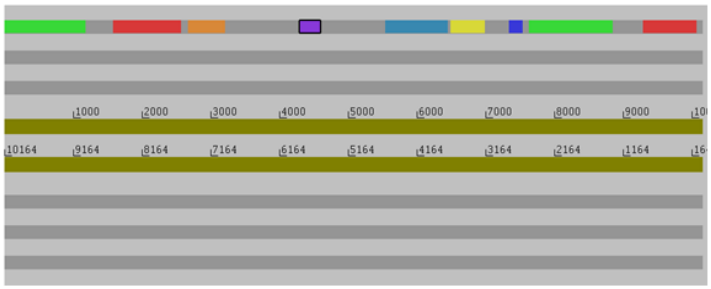

Domain	Score	E-value
KS 1	625	$4x10^{-189}$
KS 2	723	$2x10^{-218}$
AT 1	207	$3x10^{-63}$
AT 2	29	$2x10^{-17}$
DH	57	$8x10^{-18}$
M	98	$3x10^{-30}$
ER	303	$5x10^{-92}$
KR	247	$3x10^{-75}$
ACP	44	$4x10^{-14}$

AT Prediction: Malonyl (1) & Non-predictable (2)
Active Reductive Domains: DH

Sequence 2482 KS AT DH M ER KR ACP KS AT

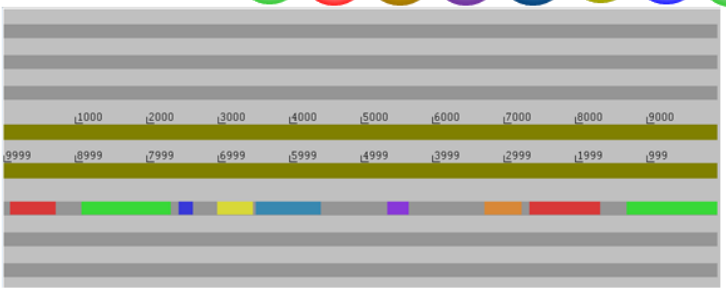

AT Prediction: Malonyl (1) & Non-predictable (2)
Active Reductive Domains: DH

Domain	Score	E-value
KS 1	697	$1x10^{-210}$
KS 2	745	$2x10^{-225}$
AT 1	206	$6x10^{-63}$
AT 2	11	$3x10^{-16}$
DH	65	$3x10^{-20}$
M	90	$6x10^{-28}$
ER	302	$7x10^{-92}$
KR	268	$2x10^{-81}$
ACP	47	$7x10^{-15}$

Sequence 3054 KS AT DH M ER KR ACP KS

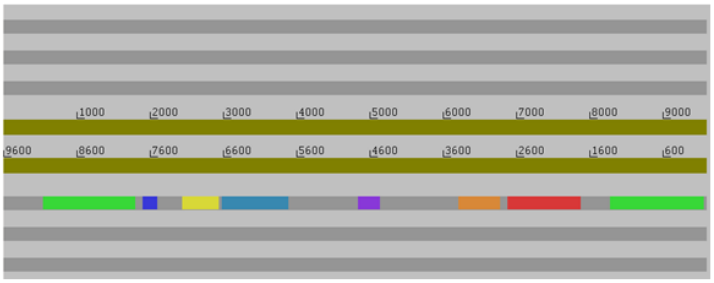

AT Prediction: Malonyl
Active Reductive Domains: DH

Domain	Score	E-value
KS 1	809	$2x10^{-244}$
KS 2	698	$8x10^{-211}$
AT	210	$5x10^{-64}$
DH	56	$1x10^{-17}$
M	101	$2x10^{-31}$
ER	297	$3x10^{-90}$
KR	271	$2x10^{-82}$
ACP	32	$3x10^{-10}$

Sequence 5079 KS AT DH M ER KR ACP KS AT

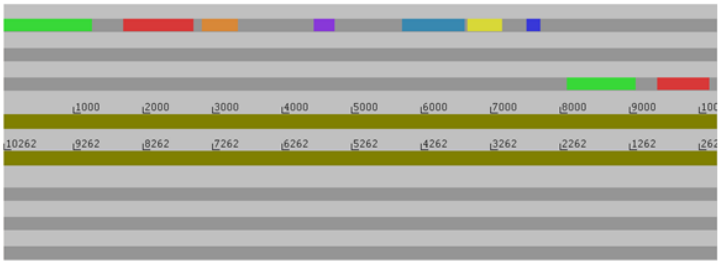

AT Prediction: Malonyl (1) & Non-predictable(2)
Active Reductive Domains: DH

Domain	Score	E-value
KS 1	709	$4x10^{-214}$
KS 2	406	$5x10^{-4}$
AT 1	197	$3x10^{-60}$
AT 2	56	$3x10^{-12}$
DH	31	$4x10^{-11}$
M	101	$3x10^{-31}$
ER	324	$2x10^{-98}$
KR	278	$3x10^{-84}$
ACP	36	$1x10^{-11}$

Sequence 5439 

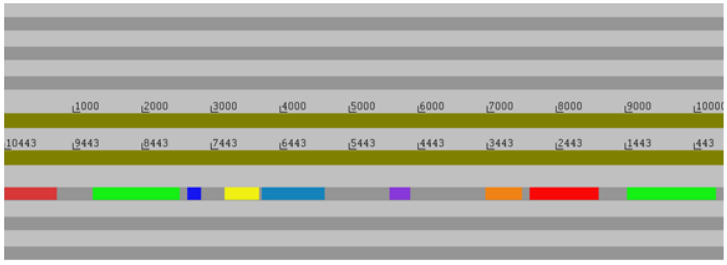

AT Prediction: Malonyl (1) & Non-predictable (2)
Active Reductive Domains: DH

Domain	Score	E-value
KS 1	725	$3x10^{-219}$
KS 2	770	$1x10^{-232}$
AT 1	183	$8x10^{-56}$
AT 2	90	$4x10^{-30}$
DH	60	$9x10^{-19}$
M	95	$2x10^{-29}$
ER	327	$4x10^{-99}$
KR	253	$6x10^{-77}$
ACP	43	$1x10^{-13}$

Sequence 6648 

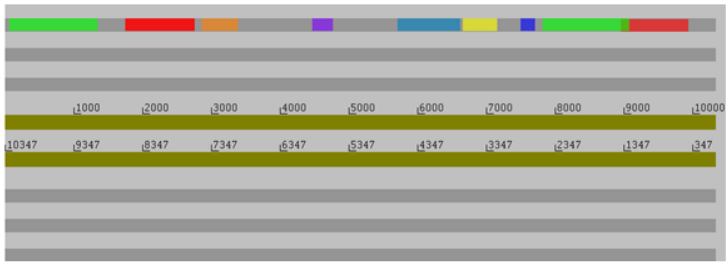

AT Prediction: Malonyl (1) & Non-predictable (2)
Active Reductive Domains: DH

Domain	Score	E-value
KS 1	719	$3x10^{-217}$
KS 2	748	$3x10^{-226}$
AT 1	218	$2x10^{-66}$
AT 2	103	$1x10^{-30}$
DH	53	$1x10^{-16}$
M	93	$1x10^{-28}$
ER	316	$5x10^{-96}$
KR	258	$2x10^{-78}$
ACP	48	$3x10^{-15}$

Sequence 8429 

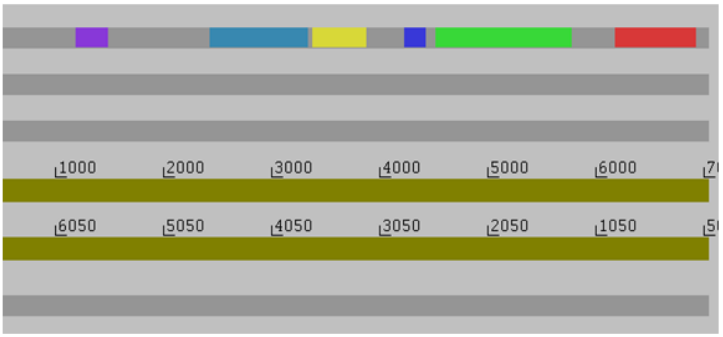

AT Prediction: Non-predictable
Active Reductive Domains:

Domain	Score	E-value
KS 2	747	$8x10^{-226}$
AT	62	$2x10^{-19}$
M	96	$1x10^{-29}$
ER	304	$3x10^{-92}$
KR	252	$1x10^{-76}$
ACP	46	$8x10^{-15}$

Sequence 9015 KS AT DH M ER KR ACP KS

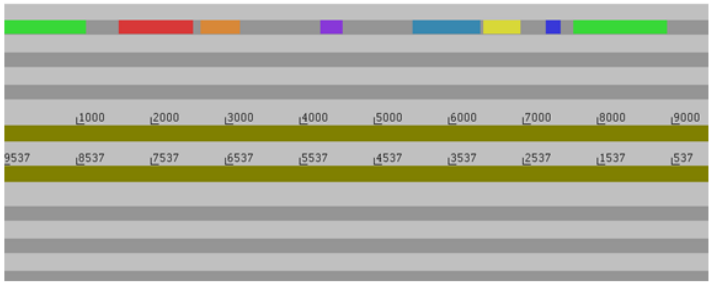

AT Prediction: Malonyl

Active Reductive Domains: DH

Domain	Score	E-value
KS 1	641	$7x10^{-194}$
KS 2	723	$1x10^{-218}$
AT	193	$4x10^{-59}$
DH	95	$2x10^{-29}$
M	103	$9x10^{-32}$
ER	297	$2x10^{-90}$
KR	261	$2x10^{-79}$
ACP	40	$9x10^{-13}$

Sequence 10635 KS AT DH M ER KR ACP KS AT

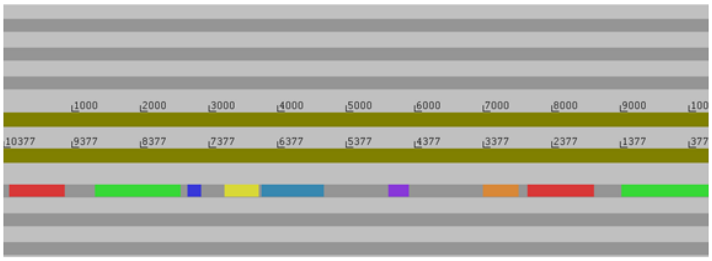

AT Prediction: Malonyl (1) & Non-predictable (2)

Active Reductive Domains: DH

Domain	Score	E-value
KS 1	690	$2x10^{-208}$
KS 2	714	$8x10^{-216}$
AT 1	195	$1x10^{-59}$
AT 2	107	$2x10^{-32}$
DH	66	$9x10^{-21}$
M	95	$2x10^{-29}$
ER	314	$3x10^{-95}$
KR	257	$3x10^{-78}$
ACP	44	$7x10^{-14}$

Sequence 15522 KS AT DH M ER KR ACP KS AT

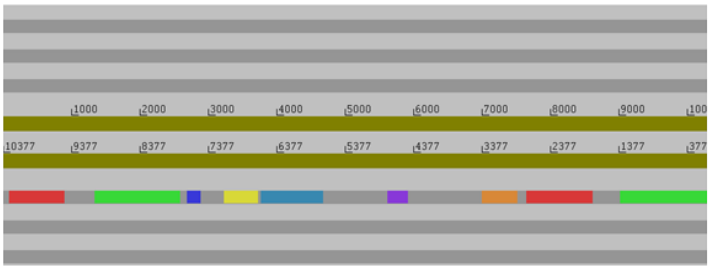

AT Prediction: Malonyl (1) & Non Predictable (2)

Active Reductive Domains: DH

Domain	Score	E-value
KS 1	733	$1x10^{-221}$
KS 2	757	$8x10^{-229}$
AT 1	214	$5x10^{-64}$
AT 2	46	$2x10^{-18}$
DH	54	$7x10^{-17}$
M	96	$1x10^{-29}$
ER	306	$9x10^{-93}$
KR	262	$2x10^{-79}$
ACP	41	$5x10^{-13}$

Sequence 21467 KS AT DH ER KR ACP

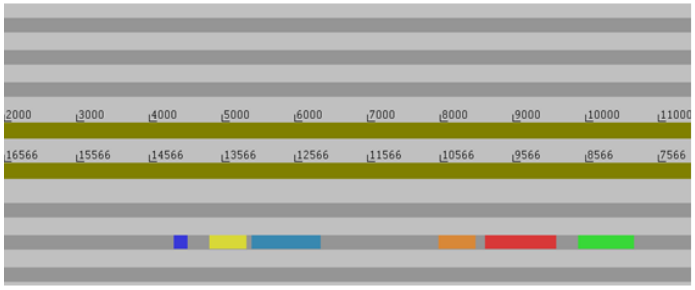

Domain	Score	E-value
KS	333	$5x10^{-101}$
AT	234	$3x10^{-71}$
DH	12	$6x10^{-10}$
ER	246	$6x10^{-75}$
KR	208	$2x10^{-63}$
ACP	8	$3x10^{-6}$

AT Prediction: Non-predictable
Active Reductive Domains: DH, ER, KR

Sequence 25735 KS AT DH M ER KR ACP

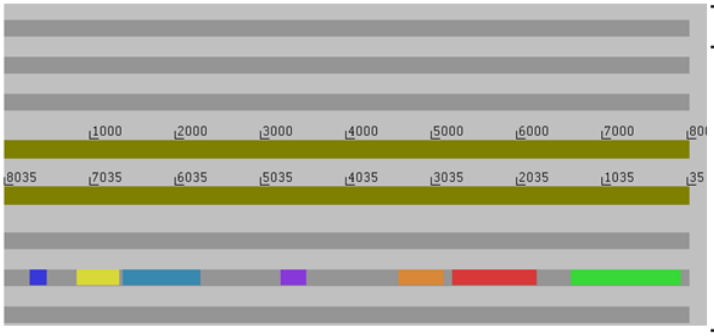

Domain	Score	E-value
KS	740	$1x10^{-223}$
AT	184	$3x10^{-56}$
DH	79	$1x10^{-24}$
M	91	$5x10^{-28}$
ER	325	$1x10^{-98}$
KR	257	$5x10^{-78}$
ACP	49	$2x10^{-15}$

AT Prediction: Malonyl
Active Reductive Domains: DH

Sequence 26257 KS AT DH ER KR ACP

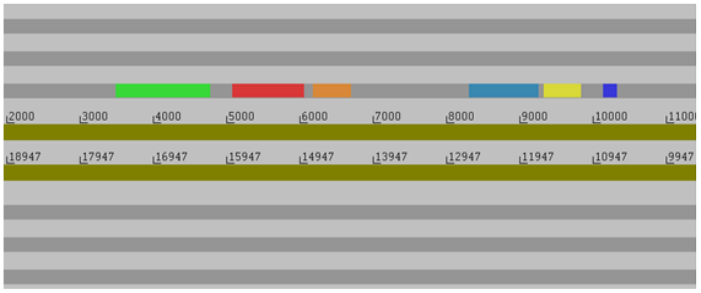

Domain	Score	E-value
KS	371	$2x10^{-112}$
AT	212	$2x10^{-64}$
DH	10	$8x10^{-10}$
ER	267	$5x10^{-81}$
KR	207	$4x10^{-63}$
ACP	8	$3x10^{-6}$

AT Prediction: Non-predictable
Active Reductive Domains: DH, ER, KR

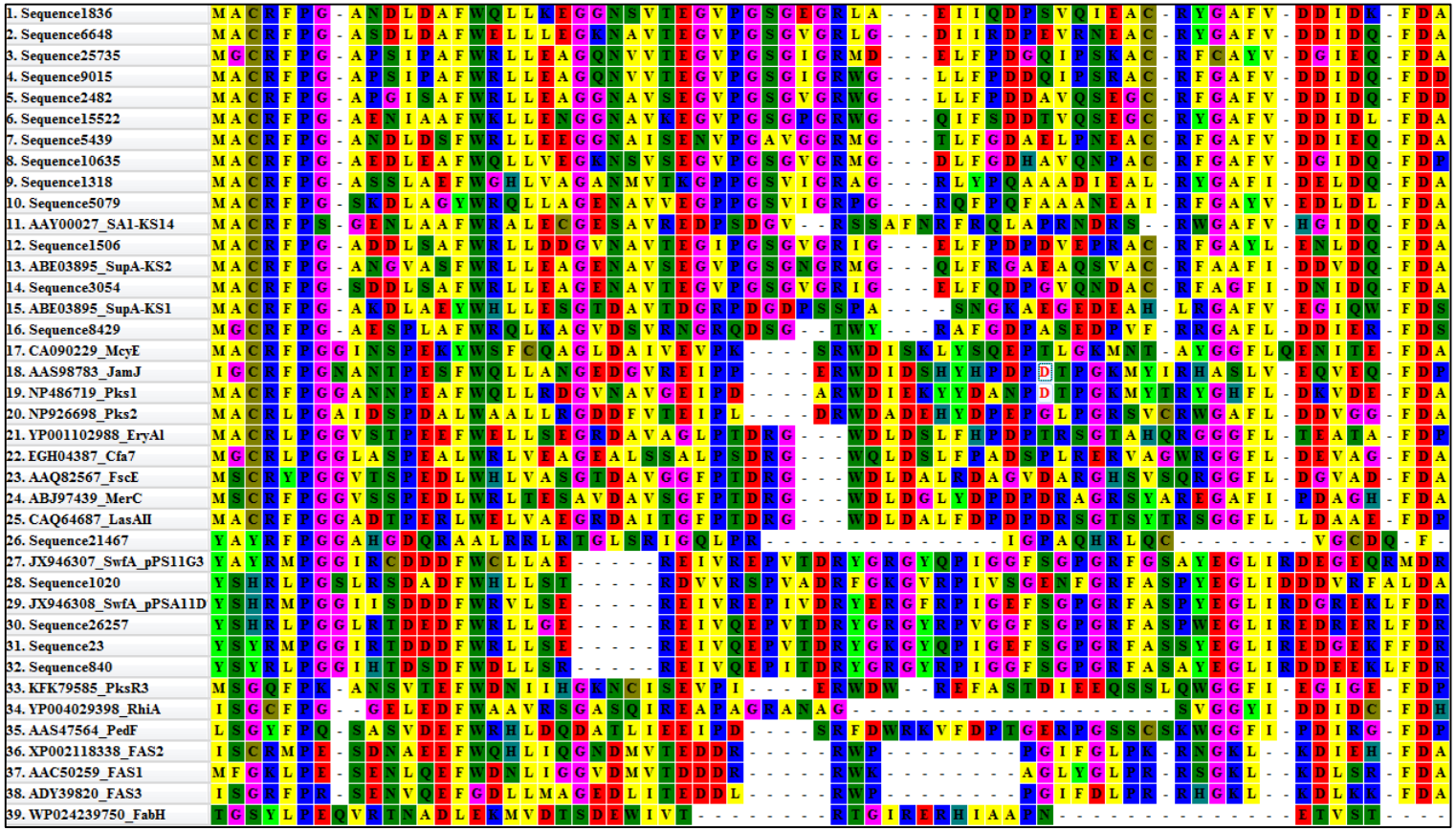

Figure 8 Multiple alignment of KS amino acid sequences from type I PKS clusters encoded by mWGS contigs. Whole KS sequences from mWGS contigs were aligned with characterised KS sequences from various type I PKS and FAS groups. The characterised KS sequences were retrieved from the GenBank database with the accession numbers shown. See Figure 6.6 and text in section 6.3.5 for details of the characterised KS sequences. The sequences were aligned using the MEGA software, v.6.06 (Tamura et al., 2013) and the ClustalW algorithm (Larkin et al., 2007).

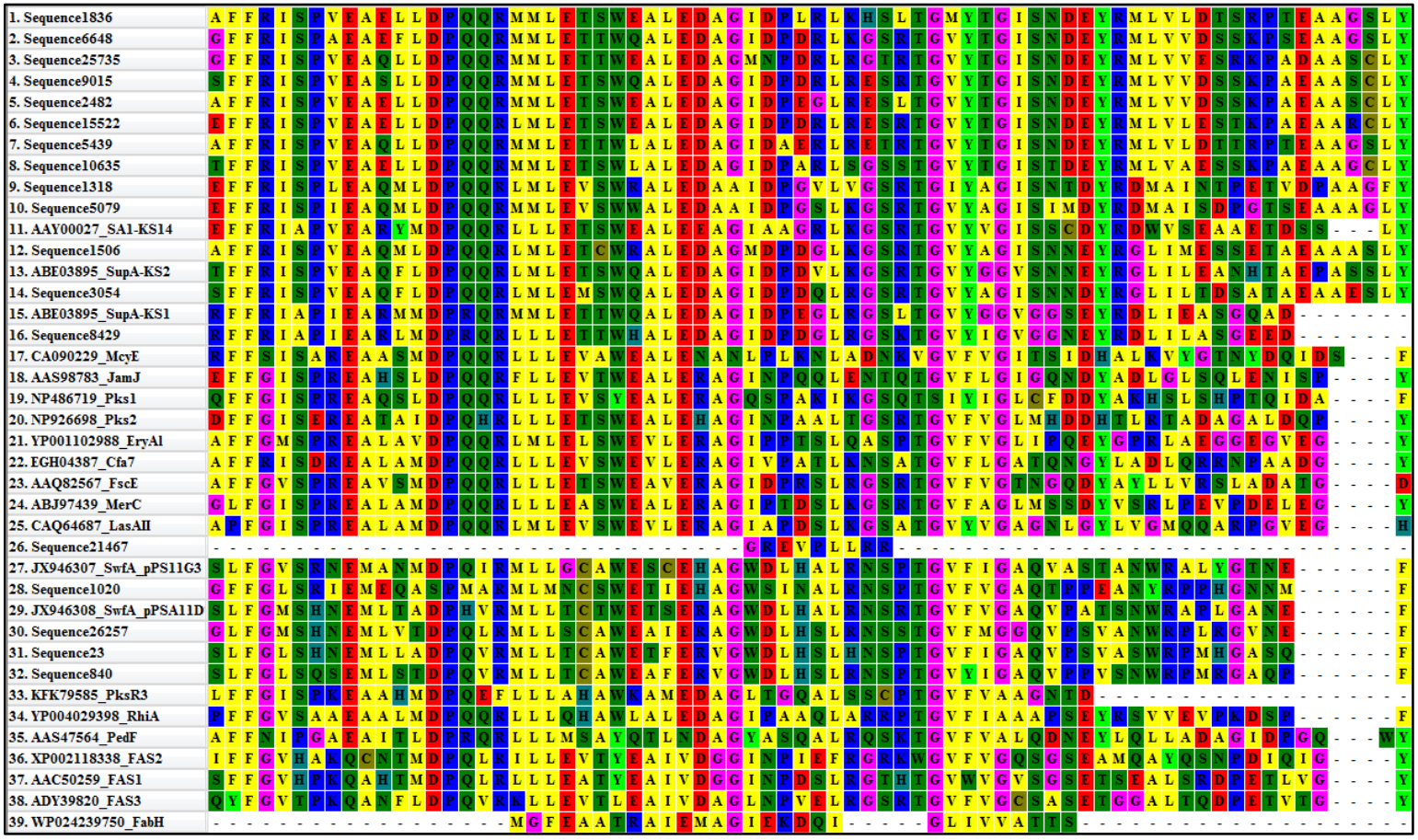
1. Sequence1836
2. Sequence6648
3. Sequence25735
4. Sequence9015
5. Sequence2482
6. Sequence15522
7. Sequence5439
8. Sequence10635
9. Sequence1318
10. Sequence5079
11. AAY00027_SA1-KS14
12. Sequence1506
13. ABE03895_SupA-KS2
14. Sequence3054
15. ABE03895_SupA-KS1
16. Sequence8429
17. CA090229_McyE
18. AAS98783_JamJ
19. NP486719_Pks1
20. NP926698_Pks2
21. YP001102988_EryAI
22. EGH04387_Cfa7
23. AAQ82567_FscE
24. ABJ97439_MerC
25. CAQ64687_LasAII
26. Sequence21467
27. JX946307_SwfA_pPS11G3
28. Sequence1020
29. JX946308_SwfA_pPSA11D
30. Sequence26257
31. Sequence23
32. Sequence840
33. KFK79585_PksR3
34. YP004029398_RhiA
35. AAS47564_PedF
36. XP002118338_FAS2
37. AAC50259_FAS1
38. ADY39820_FAS3
39. WP024239750_FabH

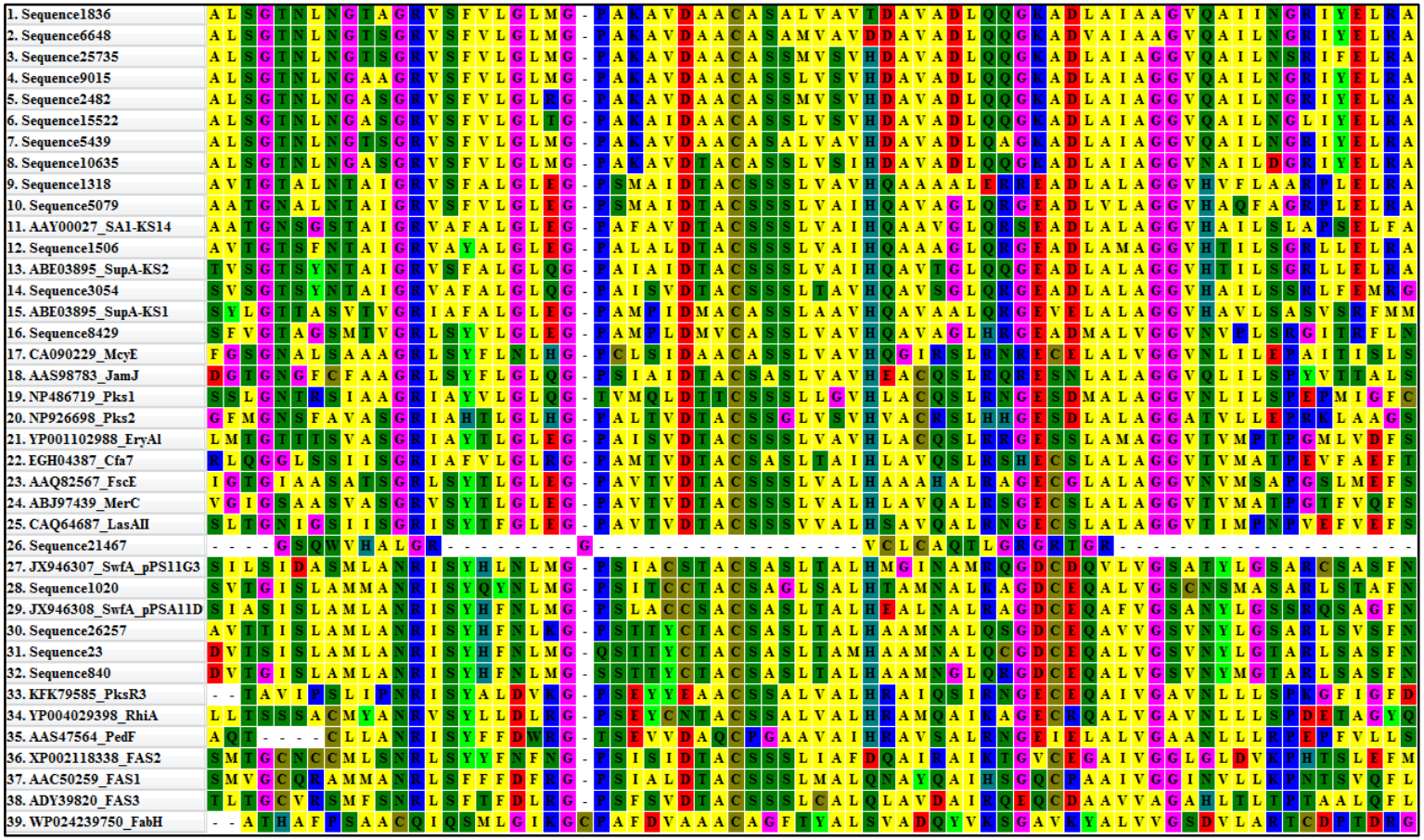
1. Sequence1836
2. Sequence6648
3. Sequence25735
4. Sequence9015
5. Sequence2482
6. Sequence15522
7. Sequence5439
8. Sequence10635
9. Sequence1318
10. Sequence5079
11. AAY00027_SA1-KS14
12. Sequence1506
13. ABE03895_SupA-KS2
14. Sequence3054
15. ABE03895_SupA-KS1
16. Sequence8429
17. CA090229_McyE
18. AAS98783_JamJ
19. NP486719_Pks1
20. NP926698_Pks2
21. YP001102988_EryAI
22. EGH04387_Cfa7
23. AAQ82567_FscE
24. ABJ97439_MerC
25. CAQ64687_LasAII
26. Sequence21467
27. JX946307_SwfA_pPS11G3
28. Sequence1020
29. JX946308_SwfA_pPSA11D
30. Sequence26257
31. Sequence23
32. Sequence840
33. KFK79585_PksR3
34. YP004029398_RhiA
35. AAS47564_PedF
36. XP002118338_FAS2
37. AAC50259_FAS1
38. ADY39820_FAS3
39. WP024239750_FabH

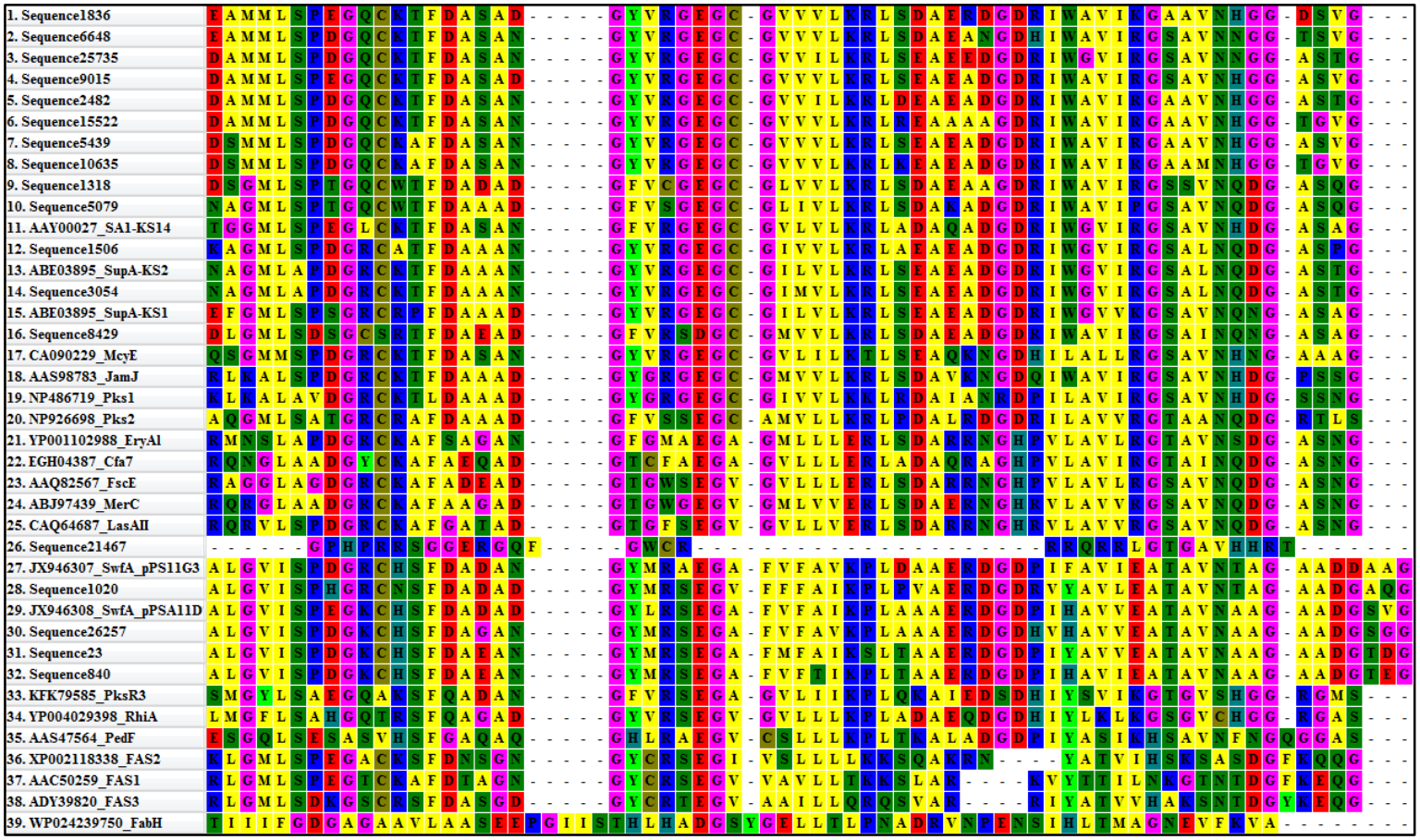
1. Sequence1836
2. Sequence6648
3. Sequence25735
4. Sequence9015
5. Sequence2482
6. Sequence15522
7. Sequence5439
8. Sequence10635
9. Sequence1318
10. Sequence5079
11. AAY00027_SA1-KS14
12. Sequence1506
13. ABE03895_SupA-KS2
14. Sequence3054
15. ABE03895_SupA-KS1
16. Sequence8429
17. CA090229_McyE
18. AAS98783_JamJ
19. NP486719_Pks1
20. NP926698_Pks2
21. YP001102988_EryAI
22. EGH04387_Cfa7
23. AAQ82567_FscE
24. ABJ97439_MerC
25. CAQ64687_LasAII
26. Sequence21467
27. JX946307_SwfA_pPS11G3
28. Sequence1020
29. JX946308_SwfA_pPSA11D
30. Sequence26257
31. Sequence23
32. Sequence840
33. KFK79585_PksR3
34. YP004029398_RhiA
35. AAS47564_PedF
36. XP002118338_FAS2
37. AAC50259_FAS1
38. ADY39820_FAS3
39. WP024239750_FabH

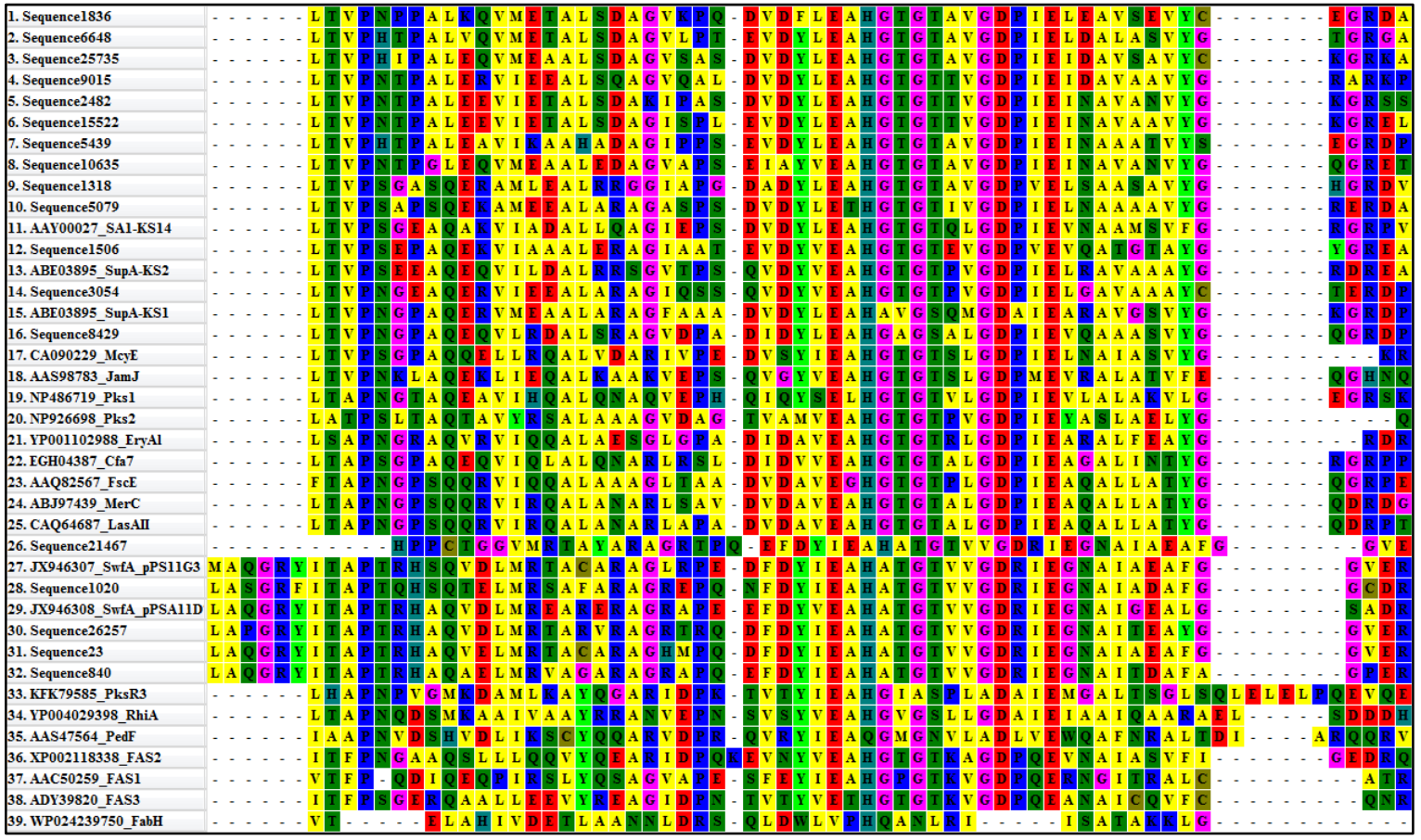
1. Sequence1836
2. Sequence6648
3. Sequence25735
4. Sequence9015
5. Sequence2482
6. Sequence15522
7. Sequence5439
8. Sequence10635
9. Sequence1318
10. Sequence5079
11. AAY00027_SA1-KS14
12. Sequence1506
13. ABE03895_SupA-KS2
14. Sequence3054
15. ABE03895_SupA-KS1
16. Sequence8429
17. CA090229_McyE
18. AAS98783_JamJ
19. NP486719_Pks1
20. NP926698_Pks2
21. YP001102988_EryAI
22. EGH04387_Cfa7
23. AAQ82567_FscE
24. ABJ97439_MerC
25. CAQ64687_LasAII
26. Sequence21467
27. JX946307_SwfA_pPS11G3
28. Sequence1020
29. JX946308_SwfA_pPSA11D
30. Sequence26257
31. Sequence23
32. Sequence840
33. KFK79585_PksR3
34. YP004029398_RhiA
35. AAS47564_PedF
36. XP002118338_FAS2
37. AAC50259_FAS1
38. ADY39820_FAS3
39. WP024239750_FabH

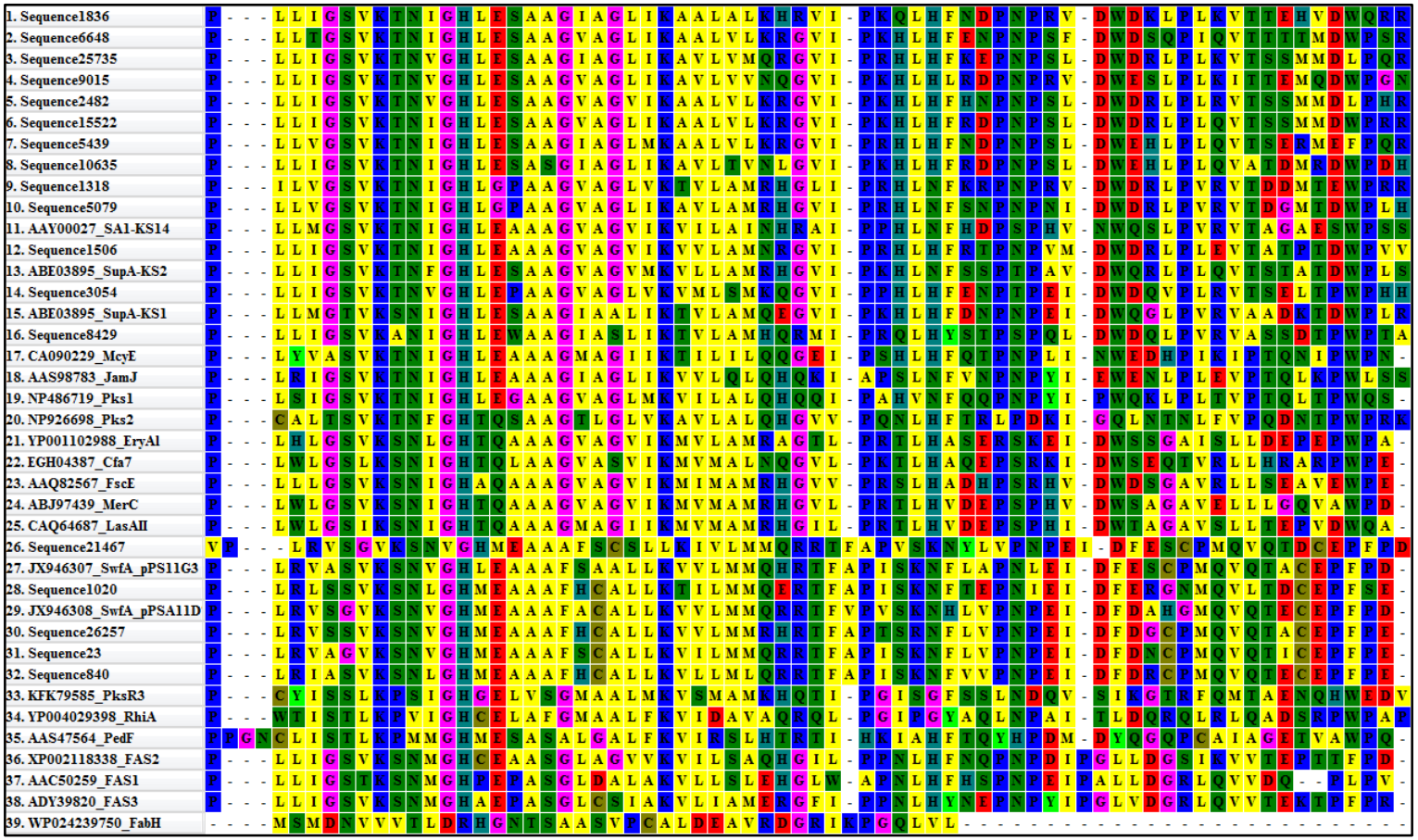
1. Sequence1836
2. Sequence6648
3. Sequence25735
4. Sequence9015
5. Sequence2482
6. Sequence15522
7. Sequence5439
8. Sequence10635
9. Sequence1318
10. Sequence5079
11. AAY00027_SA1-KS14
12. Sequence1506
13. ABE03895_SupA-KS2
14. Sequence3054
15. ABE03895_SupA-KS1
16. Sequence8429
17. CA090229_McyE
18. AAS98783_JamJ
19. NP486719_Pks1
20. NP926698_Pks2
21. YP001102988_EryAI
22. EGH04387_Cfa7
23. AAQ82567_FscE
24. ABJ97439_MerC
25. CAQ64687_LasAII
26. Sequence21467
27. JX946307_SwfA_pPS11G3
28. Sequence1020
29. JX946308_SwfA_pPSA11D
30. Sequence26257
31. Sequence23
32. Sequence840
33. KFK79585_PksR3
34. YP004029398_RhiA
35. AAS47564_PedF
36. XP002118338_FAS2
37. AAC50259_FAS1
38. ADY39820_FAS3
39. WP024239750_FabH

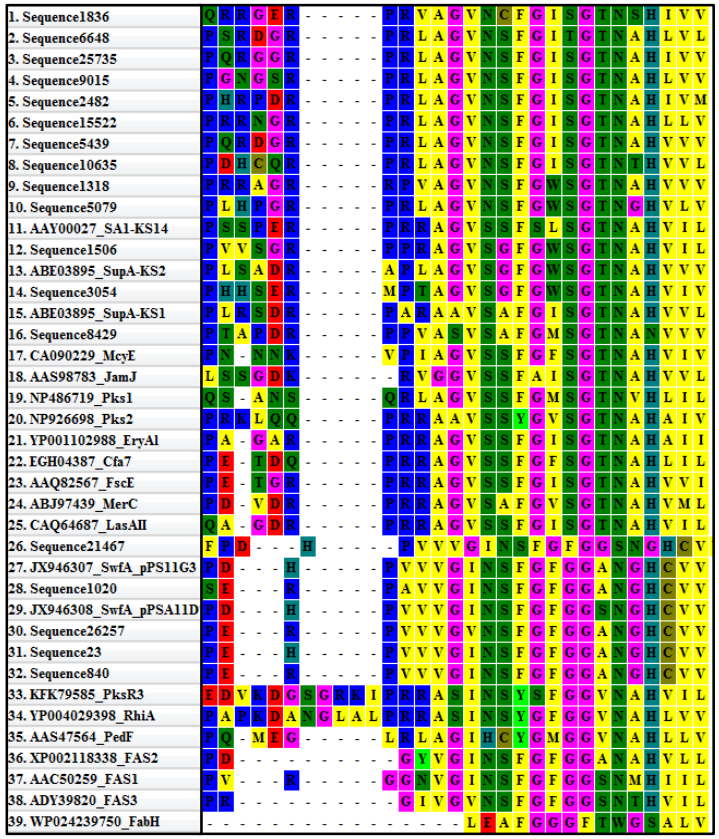
1. Sequence1836
2. Sequence6648
3. Sequence25735
4. Sequence9015
5. Sequence2482
6. Sequence15522
7. Sequence5439
8. Sequence10635
9. Sequence1318
10. Sequence5079
11. AAY00027_SA1-KS14
12. Sequence1506
13. ABE03895_SupA-KS2
14. Sequence3054
15. ABE03895_SupA-KS1
16. Sequence8429
17. CA090229_McyE
18. AAS98783_JamJ
19. NP486719_Pks1
20. NP926698_Pks2
21. YP001102988_EryAI
22. EGH04387_Cfa7
23. AAQ82567_FscE
24. ABJ97439_MerC
25. CAQ64687_LasAII
26. Sequence21467
27. JX946307_SwfA_pPS11G3
28. Sequence1020
29. JX946308_SwfA_pPSA11D
30. Sequence26257
31. Sequence23
32. Sequence840
33. KFK79585_PksR3
34. YP004029398_RhiA
35. AAS47564_PedF
36. XP002118338_FAS2
37. AAC50259_FAS1
38. ADY39820_FAS3
39. WP024239750_FabH

Sequence 23

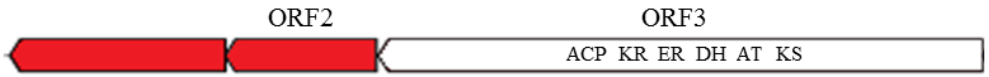

ORF	Size (aa)	Closest homologue (accession no.)	Organism	Identity (%)	Coverage (%)	E-value	Putative function
1	835	SwfB (AGH13591)	*Plakortis simplex* bacterial symbiont	58	98	0	Thioester reductase and sulfotransferase
2	571	SwfC (AGH13579)	*P. Simplex* bacterial symbiont	65	100	0	Radical S-Adenosyl methionine (SAM) domain
3	2330	SwfA (AGH13590)	*P. Simplex* bacterial symbiont	69	99	0	Type I PKS/FAS

Figure 9 BLASTp results of PKS proteins identified from mWGS contigs. Following screening of assembled mWGS contigs using antiSMASH, 18 sequences were identified as encoding a type I PKS. Open reading frames (ORF) for each of contigs were annotated using the Gimmer3 (Delcher et al., 2007) software within antiSMASH, and then subjected to BLASTp searches against all non-redundant protein databases. For each sequence, the closest homologue to the encoded PKS sequence is shown in the tables, along with the GenBank accession number in brackets. Identified homologues for genes reported from the *sup* (Fieseler et al., 2007) and *swf* (Della Sala et al., 2013) operons are also shown. Above each table is a schematic showing the annotated flanking genes (red) and the PKS gene (white), which also shows putative PKS domain annotation.

Sequence 840

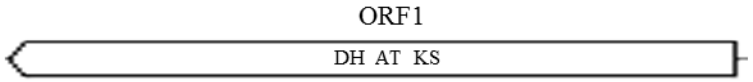

ORF	Size (aa)	Closest homologue (accession no.)	Organism	Identity (%)	Coverage (%)	E-value	Putative function
1	1729	SwfA (AGH13590)	*P. Simplex* bacterial symbiont	66	99	0	Type I PKS/FAS

Sequence 1020

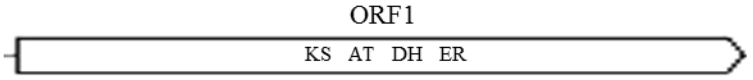

ORF	Size (aa)	Closest homologue (accession no.)	Organism	Identity (%)	Coverage (%)	E-value	Putative function
1	1729	SwfA (AGH13590)	*P. Simplex* bacterial symbiont	66	99	0	Type I PKS/FAS

Sequence 1318

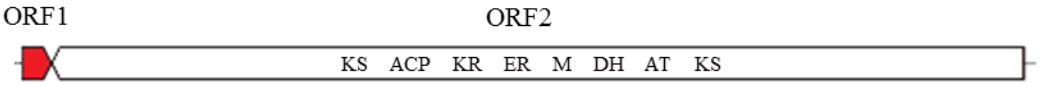

ORF	Size (aa)	Closest homologue (accession no.)	Organism	Identity (%)	Coverage (%)	E-value	Putative function
1	106	SupD (ABE03934)	*T. swinhoei* bacterial symbiont	64	71	$1x10^{-39}$	αβ-hydrolase
2	3506	SupA (ABE03935)	*T. swinhoei* bacterial symbiont	55	99	0	Methyl branched FAS

Sequence 1506

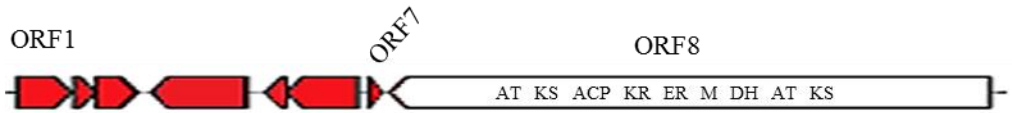

ORF	Size (aa)	Closest homologue (accession no.)	Organism	Identity (%)	Coverage (%)	E-value	Putative function
1	239	SupC (ABE03913)	*A. aerophoba* bacterial symbiont	63	97	$2x10^{-96}$	Phosphopantetheinyl transferase
7	76	SupB (ABE03911)	*A. aerophoba* bacterial symbiont	55	100	$6x10^{-23}$	Acyl carrier protein
8	3480	SupA (ABE03915)	*A. aerophoba* bacterial symbiont	68	99	0	Methyl branched FAS

Sequence 1836

ORF	Size (aa)	Closest homologue (accession no.)	Organism	Identity (%)	Coverage (%)	E-value	Putative function
1	3417	SupA (ABE03935)	*T. swinhoei* bacterial symbiont	67	100	0	Methyl branched FAS
2	80	SupB (ABE03933)	*A. aerophoba* bacterial symbiont	39	100	$3x10^{-14}$	Acyl carrier protein

Sequence 2482

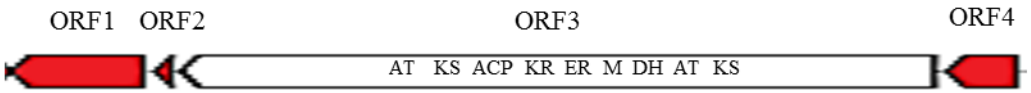

ORF	Size (aa)	Closest homologue (accession no.)	Organism	Identity (%)	Coverage (%)	E-value	Putative function
1	583	SupE (ABE03914)	*A. aerophoba* bacterial symbiont	63	96	0	Permease
2	80	SupB (ABE03911)	*A. aerophoba* bacterial symbiont	40	96	$2x10^{-10}$	Acyl carrier protein
3	3332	SupA (ABE03935)	*T. swinhoei* bacterial symbiont	73	100	0	Methyl branched FAS
4	308	SupD (ABE03934)	*T. swinhoei* bacterial symbiont	72	97	$6x10^{-163}$	αβ-hydrolase

Sequence 3054

ORF	Size (aa)	Closest homologue (accession no.)	Organism	Identity (%)	Coverage (%)	E-value	Putative function
1	301	SupD (ABE03934)	*T. swinhoei* bacterial symbiont	54	98	$6x10^{-116}$	αβ-hydrolase
2	156	SupC (ABE03932)	*T. swinhoei* bacterial symbiont	57	98	$2x10^{-55}$	Phosphopantetheinyl transferase
3	80	SupB (ABE03911)	*A. aerophoba* bacterial symbiont	34	96	$3x10^{-7}$	Acyl carrier protein
4	3199	SupA (ABE03935)	*T. swinhoei* bacterial symbiont	64	99	0	Methyl branched FAS
5	578	SupE (ABE03914)	*A. aerophoba* bacterial symbiont	44	98	$3x10^{-137}$	Permease

Sequence 5079

ORF	Size (aa)	Closest homologue (accession no.)	Organism	Identity (%)	Coverage (%)	E-value	Putative function
1	3360	SupA (ABE03935)	*T. swinhoei* bacterial symbiont	56	98	0	Methyl branched FAS
2	288	SupD (ABE03916)	*A. aerophoba* bacterial symbiont	67	97	$1x10^{-134}$	αβ-hydrolase
3	122	SupC (ABE03932)	*T. swinhoei* bacterial symbiont	58	93	$9x10^{-38}$	Phosphopantetheinyl transferase
4	76	SupB (ABE03933)	*T. swinhoei* bacterial symbiont	45	98	$1x10^{-17}$	Acyl carrier protein

Sequence 5439

ORF	Size (aa)	Closest homologue (accession no.)	Organism	Identity (%)	Coverage (%)	E-value	Putative function
1	3360	SupA (ABE03935)	*T. swinhoei* bacterial symbiont	69	97	0	Methyl branched FAS

Sequence 6648

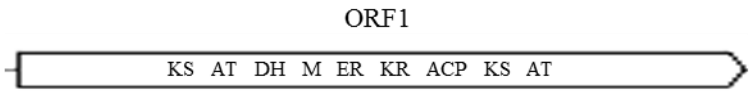

ORF	Size (aa)	Closest homologue (accession no.)	Organism	Identity (%)	Coverage (%)	E-value	Putative function
1	3448	SupA (ABE03935)	*T. swinhoei* bacterial symbiont	69	99	0	Methyl branched FAS

Sequence 8429

ORF	Size (aa)	Closest homologue (accession no.)	Organism	Identity (%)	Coverage (%)	E-value	Putative function
1	2331	SupA (ABE03935)	*T. swinhoei* bacterial symbiont	68	100	0	Methyl branched FAS
2	81	SupB (ABE03911)	*A. aerophoba* bacterial symbiont	41	100	$3x10^{-12}$	Acyl carrier protein
3	223	SupC (ABE03932)	*T. swinhoei* bacterial symbiont	55	96	$2x10^{-78}$	Phosphopantetheinyl transferase
4	296	SupD (ABE03916)	*A. aerophoba* bacterial symbiont	64	99	$2x10^{-131}$	αβ-hydrolase
5	609	SupE (ABE03914)	*A. aerophoba* bacterial symbiont	42	94	$4x10^{-122}$	Permease

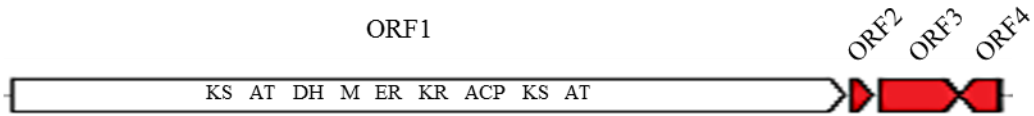

Sequence 9015

ORF	Size (aa)	Closest homologue (accession no.)	Organism	Identity (%)	Coverage (%)	E-value	Putative function
1	3178	SupA (ABE03935)	*T. swinhoei* bacterial symbiont	69	99	0	Methyl branched FAS
2	81	SupB (ABE03911)	*A. aerophoba* bacterial symbiont	35	100	$6x10^{-7}$	Acyl carrier protein
3	310	SupD (ABE03916)	*A. aerophoba* bacterial symbiont	56	95	$4x10^{-118}$	αβ-hydrolase
4	155	SupC (ABE03932)	*T. swinhoei* bacterial symbiont	55	100	$4x10^{-52}$	Phosphopantetheinyl transferase

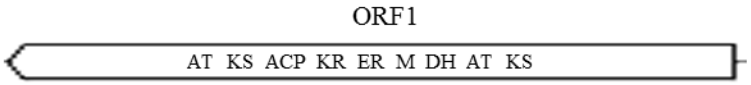

Sequence 10635

ORF	Size (aa)	Closest homologue (accession no.)	Organism	Identity (%)	Coverage (%)	E-value	Putative function
1	3417	SupA (ABE03935)	*T. swinhoei* bacterial symbiont	66	99	0	Methyl branched FAS

Sequence 15522

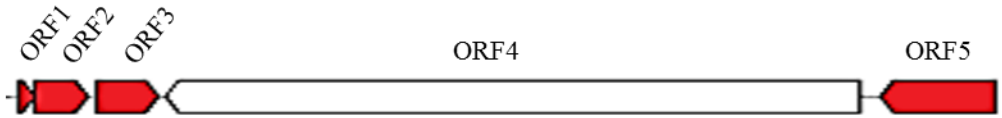

ORF	Size (aa)	Closest homologue (accession no.)	Organism	Identity (%)	Coverage (%)	E-value	Putative function
1	76	SupB (ABE03933)	*T. swinhoei* bacterial symbiont	54	100	$1x10^{-21}$	Acyl carrier protein
2	266	SupC (ABE03932)	*T. swinhoei* bacterial symbiont	66	90	$2x10^{-110}$	Phosphopantetheinyl transferase
3	305	SupD (ABE03934)	*T. swinhoei* bacterial symbiont	64	97	$2x10^{-143}$	αβ-hydrolase
4	3458	SupA (ABE03935)	*T. swinhoei* bacterial symbiont	72	99	0	Methyl branched FAS
5	577	SupE (ABE03914)	*A. aerophoba* bacterial symbiont	62	98	0	Permease

Sequence 21467

ORF	Size (aa)	Closest homologue (accession no.)	Organism	Identity (%)	Coverage (%)	E-value	Putative function
1	533	SwfC (AGH13579)	*P. Simplex* bacterial symbiont	63	99	0	Radical S-Adenosyl methionine (SAM) domain
2	2127	SwfA (AGH13590)	*P. Simplex* bacterial symbiont	76	96	0	Type I PKS/FAS

Sequence 25735

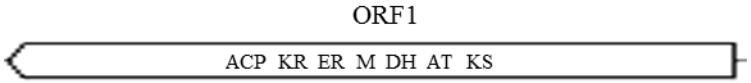

ORF	Size (aa)	Closest homologue (accession no.)	Organism	Identity (%)	Coverage (%)	E-value	Putative function
1	2678	SupA (ABE03935)	*T. swinhoei* bacterial symbiont	80	99	0	Methyl branched FAS

Sequence 26257

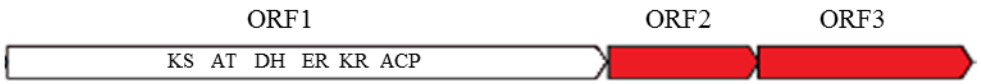

ORF	Size (aa)	Closest homologue (accession no.)	Organism	Identity (%)	Coverage (%)	E-value	Putative function
1	2361	SwfA (AGH13590)	*P. Simplex* bacterial symbiont	66	99	0	Type I PKS/FAS
2	592	SwfC (AGH13579)	*P. Simplex* bacterial symbiont	62	95	0	Radical S-Adenosyl methionine (SAM) domain
3	842	SwfB (AGH13591)	*P. Simplex* bacterial symbiont	57	97	0	Thioester reductase and sulfotransferase

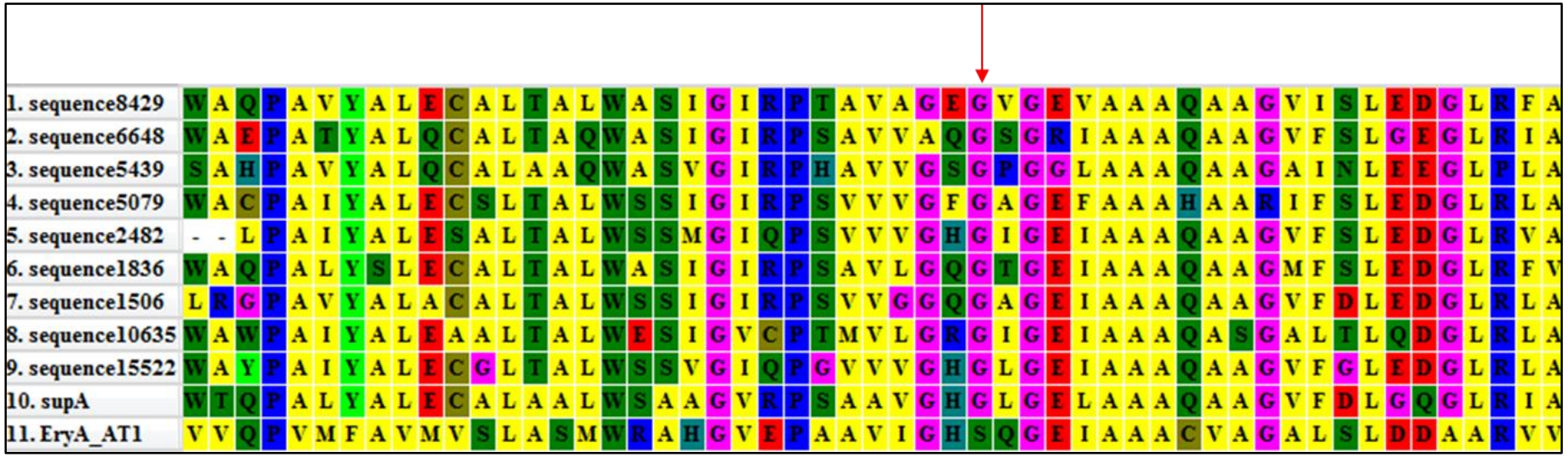

Figure 10 Multiple amino acid alignment of C-terminal AT domains from PKS genes showing homology to SupA. Out of the 18 type I PKS sequences detected by antiSMASH, 13 were shown to be homologues of SupA, of which, 9 were found to have a C-terminal AT domain. These 9 whole AT domains were aligned with the SupA C-terminal AT domain from *T. swinhoei* (accession number: ABE03935) with the red arrow showing the presence of a glycine residue instead of a conserved serine residue considered crucial for activity (ref). An AT domain from the eryA gene of the erythromycin gene cluster (accession number: Q03131) was also included for comparison. The sequences were aligned using the MEGA software (Tamura et al., 2013) and the ClustalW algorithm (Larkin et al., 2007).

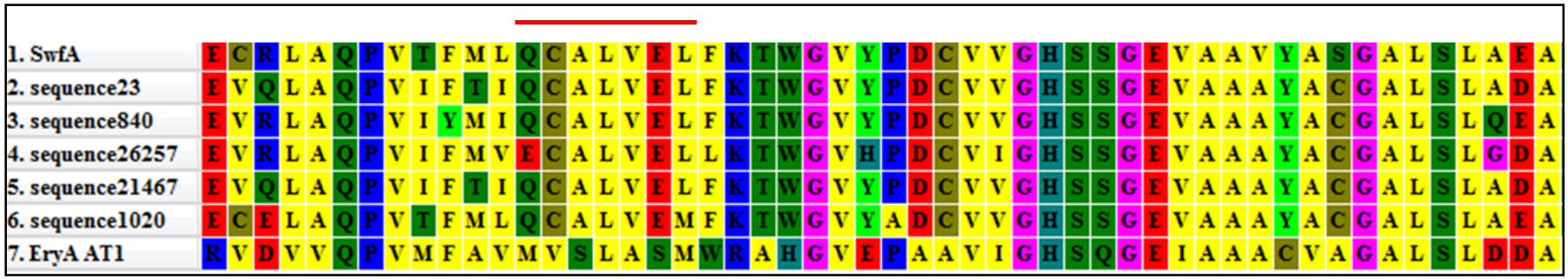

Figure 11 Multiple amino acid alignment of AT domains from PKS genes showing homology to SwfA. Out of the 18 type I PKS sequences detected by antiSMASH, 5 were shown to be homologues of SwfA, of which. Whole AT domains from the 5 sequences were aligned with the SwfA AT domain from *P. simplex* (accession number: AGH13590). The red line indicates the location of the QCALVEL motif shown to be unique to SwfA AT domains, though with some variation in the first and last amino acid (ref). An AT domain from the *eryA* gene of the erythromycin gene cluster (accession number: Q03131) was also included for comparison. The sequences were aligned using the MEGA software (Tamura et al., 2013) and the ClustalW algorithm (Larkin et al., 2007).

References

Albright, A. L. & White, J. M. 2013. Determination of absolute configuration using single crystal x-ray diffraction. *Metabolomics tools for natural product discovery.* Springer.

Aldrich, L. N., Kuo, S.Y., Castoreno, A. B., Goel, G., Kuballa, P., Rees, M. G., Seashore-Ludlow, B. A., Cheah, J. H., Latorre, I. J. & Schreiber, S. L. 2015. Discovery of a small-molecule probe for V-ATPase function. *Journal of the American chemical society,* 137**,** 5563-5568.

Ali, S. Y., Sajdera, S. W. & Anderson, H. C. 1970. Isolation and characterization of calcifying matrix vesicles from epiphyseal cartilage. *Proceedings of the national academy of sciences of the United States of America,* 67**,** 1513-1520.

Andersen, T. L., Sondergaard, T. E., Skorzynska, K. E., Dagnaes-Hansen, F., Plesner, T. L., Hauge, E. M., Plesner, T. & Delaisse, J.-M. 2009. A physical mechanism for coupling bone resorption and formation in adult human bone. *The American journal of pathology,* 174**,** 239-247.

Anderson, D. M., Maraskovsky, E., Billingsley, W. L., Dougall, W. C., Tometsko, M. E., Roux, E. R., Teepe, M. C., Dubose, R. F., Cosman, D. & Galibert, L. 1997. A homologue of the TNF receptor and its ligand enhance T-cell growth and dendritic-cell function. *Nature,* 390**,** 175-179.

Anderson, H. C. 1995. Molecular biology of matrix vesicles. *Clinical orthopaedics and related research,* 314**,** 266-280.

Aparicio, J. F., Molnár, I., Schwecke, T., König, A., Haydock, S. F., Khaw, L. E., Staunton, J. & Leadlay, P. F. 1996. Organization of the biosynthetic gene cluster for rapamycin in *Streptomyces hygroscopicus*: Analysis of the enzymatic domains in the modular polyketide synthase. *Gene,* 169**,** 9-16.

Appeltans, W., Ahyong, S. T., Anderson, G., Angel, M. V., Artois, T., Bailly, N., Bamber, R., Barber, A., Bartsch, I. & Berta, A. 2012. The magnitude of global marine species diversity. *Current biology,* 22**,** 2189-2202.

Arai, F., Miyamoto, T., Ohneda, O., Inada, T., Sudo, T., Brasel, K., Miyata, T., Anderson, D. M. & Suda, T. 1999. Commitment and differentiation of osteoclast precursor cells by the sequential expression of c-Fms and receptor activator of nuclear factor kappaB (RANK) receptors. *The Journal of experimental medicine,* 190**,** 1741-1754.

Asagiri, M. & Takayanagi, H. 2007. The molecular understanding of osteoclast differentiation. *Bone,* 40**,** 251-264.

Atta-Ur-Rahman 2000. *New advances in analytical chemistry,* Taylor & Francis.

Balgi, A. D., Diering, G. H., Donohue, E., Lam, K. K. Y., Fonseca, B. D., Zimmerman, C., Numata, M. & Roberge, M. 2011. Regulation of mTORC1 signaling by pH. *Public library of science one,* 6**,** e21549.

Bandyopadhyay, A., Tsuji, K., Cox, K., Harfe, B. D., Rosen, V. & Tabin, C. J. 2006. Genetic analysis of the roles of BMP2, BMP4, and BMP7 in limb patterning and skeletogenesis. *Public library of science: genetics,* 2**,** e216.

Baranasic, D., Zucko, J., Diminic, J., Gacesa, R., Long, P. F., Cullum, J., Hranueli, D. & Starcevic, A. 2014. Predicting substrate specificity of adenylation domains of nonribosomal peptide synthetases and other protein properties by latent semantic indexing. *Journal of industrial microbiology & biotechnology,* 41**,** 461-467.

Baron, R., Neff, L., Louvard, D. & Courtoy, P. J. 1985. Cell-mediated extracellular acidification and bone resorption: Evidence for a low pH in resorbing lacunae and localization of a 100-kD lysosomal membrane protein at the osteoclast ruffled border. *The journal of cell biology,* 101**,** 2210-2222.

Bartkiewicz, M., Hernando, N., Reddy, S. V., Roodman, G. D. & Baron, R. 1995. Characterization of the osteoclast vacuolar H+-ATPase B-subunit. *Gene,* 160**,** 157-164.

Behrendt, L., Larkum, A. W. D., Trampe, E., Norman, A., Sorensen, S. J. & Kuhl, M. 2012. Microbial diversity of biofilm communities in microniches associated with the didemnid ascidian *Lissoclinum patella*. *The ISME journal,* 6**,** 1222-1237.

Bendall, A. J. & Abate-Shen, C. 2000. Roles for Msx and Dlx homeoproteins in vertebrate development. *Gene,* 247**,** 17-31.

Benson, D. A., Cavanaugh, M., Clark, K., Karsch-Mizrachi, I., Lipman, D. J., Ostell, J. & Sayers, E. W. 2013. Genbank. *Nucleic acids research,* 41**,** D36-42.

Bergmann, W. & Burke, D. C. 1955. Contributions to the study of marine products. XXXIX. The nucleosides of sponges. III. Spongothymidine and spongouridine. *The Journal of organic chemistry,* 20**,** 1501-1507.

Beyenbach, K. W. & Wieczorek, H. 2006. The V-type H+ ATPase: Molecular structure and function, physiological roles and regulation. *The Journal of experimental biology,* 209**,** 577-589.

Bhatnagar, I. & Kim, S.K. 2010. Immense essence of excellence: Marine microbial bioactive compounds. *Marine drugs,* 8**,** 2673-2701.

Bialek, P., Kern, B., Yang, X., Schrock, M., Sosic, D., Hong, N., Wu, H., Yu, K., Ornitz, D. M. & Olson, E. N. 2004. A twist code determines the onset of osteoblast differentiation. *Developmental cell,* 6**,** 423-435.

Blair, H. C., Teitelbaum, S. L., Ghiselli, R. & Gluck, S. 1989. Osteoclastic bone resorption by a polarized vacuolar proton pump. *Science,* 245**,** 855-857.

Blin, K., Medema, M. H., Kazempour, D., Fischbach, M. A., Breitling, R., Takano, E. & Weber, T. 2013. antiSMASH 2.0—a versatile platform for genome mining of secondary metabolite producers. *Nucleic acids research,* 41**,** W204-W212.

Blomqvist, S. R., Vidarsson, H., Söder, O. & Enerbäck, S. 2006. Epididymal expression of the forkhead transcription factor Foxi1 is required for male fertility. *The EMBO journal,* 25**,** 4131-4141.

Blunt, J. W., Copp, B. R., Hu, W.P., Munro, M. H. G., Northcote, P. T. & Prinsep, M. R. 2009. Marine natural products. *Natural product reports,* 26**,** 170-244.

Blunt, J. W., Copp, B. R., Keyzers, R. A., Munro, M. H. & Prinsep, M. R. 2014. Marine natural products. *Natural product reports,* 31**,** 160-258.

Blunt, J. W., Copp, B. R., Munro, M. H. G., Northcote, P. T. & Prinsep, M. R. 2004. Marine natural products. *Natural product reports,* 21**,** 1-49.

Blunt, J. W., Copp, B. R., Munro, M. H. G., Northcote, P. T. & Prinsep, M. R. 2005. Marine natural products. *Natural product reports,* 22**,** 15-61.

Bockelmann, S., Menche, D., Rudolph, S., Bender, T., Grond, S., Von Zezschwitz, P., Muench, S. P., Wieczorek, H. & Huss, M. 2010. Archazolid A binds to the equatorial region of the c-ring of the vacuolar H+-ATPase. *Journal of biological chemistry,* 285**,** 38304-38314.

Bollerslev, J., Marks, S., Pockwinse, S., Kassem, M., Brixen, K., Steiniche, T. & Mosekilde, L. 1993. Ultrastructural investigations of bone resorptive cells in two types of autosomal dominant osteopetrosis. *Bone,* 14**,** 865-869.

Bonet, B., Teufel, R., Crusemann, M., Ziemert, N. & Moore, B. S. 2014. Direct capture and heterologous expression of *Salinispora* natural product genes for the biosynthesis of enterocin. *Journal of natural products,* 22, 539-542.

Bonewald, L. F. 2011. The amazing osteocyte. *Journal of bone and mineral research,* 26**,** 229-238.

Bonifacino, J. S. & Glick, B. S. 2004. The mechanisms of vesicle budding and fusion. *Cell,* 116**,** 153-166.

Boskey, A., Gadaleta, S., Gundberg, C., Doty, S., Ducy, P. & Karsenty, G. 1998. Fourier transform infrared microspectroscopic analysis of bones of osteocalcin-deficient mice provides insight into the function of osteocalcin. *Bone,* 23**,** 187-196.

Bowman, B. J. & Bowman, E. J. 2002. Mutations in subunit c of the vacuolar ATPase confer resistance to bafilomycin and identify a conserved antibiotic binding site. *Journal of biological chemistry,* 277**,** 3965-3972.

Bowman, B. J., Mccall, M. E., Baertsch, R. & Bowman, E. J. 2006. A model for the proteolipid ring and bafilomycin/concanamycin-binding site in the vacuolar ATPase of *Neurospora crassa*. *The Journal of biological chemistry,* 281**,** 31885-31893.

Bowman, E. J. & Bowman, B. J. 1988. Purification of vacuolar membranes, mitochondria, and plasma membranes from *Neurospora crassa* and modes of discriminating among the different H+-ATPases. *Methods in enzymology,* 157**,** 562.

Bowman, E. J. & Bowman, B. J. 2005. V-ATPases as drug targets. *Journal of bioenergetics and biomembranes,* 37**,** 431-435.

Bowman, E. J., Gustafson, K. R., Bowman, B. J. & Boyd, M. R. 2003. Identification of a new chondropsin class of antitumor compound that selectively inhibits V-ATPases. *The Journal of biological chemistry,* 278**,** 44147-44152.

Bowman, E. J., Siebers, A. & Altendorf, K. 1988. Bafilomycins: A class of inhibitors of membrane atpases from microorganisms, animal cells, and plant cells. *Proceedings of the national academy of sciences of the United States of America,* 85**,** 7972-7976.

Boyd, M. R., Farina, C., Belfiore, P., Gagliardi, S., Kim, J. W., Hayakawa, Y., Beutler, J. A., Mckee, T. C., Bowman, B. J. & Bowman, E. J. 2001. Discovery of a novel antitumor benzolactone enamide class that selectively inhibits mammalian vacuolar-type (H+)-ATPases. *Journal of pharmacology and experimental therapeutics,* 297**,** 114-120.

Boyd, M. R. & Paull, K. D. 1995. Some practical considerations and applications of the national cancer institute *in vitro* anticancer drug discovery screen. *Drug development research,* 34**,** 91-109.

Boyle, W. J., Simonet, W. S. & Lacey, D. L. 2003. Osteoclast differentiation and activation. *Nature,* 423**,** 337-342.

Brown, D., Paunescu, T. G., Breton, S. & Marshansky, V. 2009. Regulation of the V-ATPase in kidney epithelial cells: Dual role in acid–base homeostasis and vesicle trafficking. *Journal of experimental biology,* 212**,** 1762-1772.

Bruder, E., Stallmach, T., Peier, K., Superti-Furga, A. & Vezzoni, P. 2003. Osteoclast morphology in autosomal recessive malignant osteopetrosis due to a TCIRG1 gene mutation. *Fetal & pediatric pathology,* 22**,** 3-9.

Burr, D. B. & Allen, M. R. 2013. *Basic and applied bone biology, 1st edition,* Academic Press.

Burres, N. S. & Clement, J. J. 1989. Antitumor activity and mechanism of action of the novel marine natural products mycalamide-A and -B and onnamide. *Cancer research,* 49**,** 2935-2940.

Butcher, R. A., Schroeder, F. C., Fischbach, M. A., Straight, P. D., Kolter, R., Walsh, C. T. & Clardy, J. 2007. The identification of bacillaene, the product of the PksX megacomplex in *Bacillus subtilis*. *Proceedings of the national academy of sciences,* 104**,** 1506-1509.

Camacho, C., Coulouris, G., Avagyan, V., Ma, N., Papadopoulos, J., Bealer, K. & Madden, T. L. 2009. BLAST+: Architecture and applications. *BMC Bioinformatics,* 10**,** 421-428.

Cane, D. E. & Walsh, C. T. 1999. The parallel and convergent universes of polyketide synthases and nonribosomal peptide synthetases. *Chemistry & biology,* 6**,** R319-325.

Cane, D. E., Walsh, C. T. & Khosla, C. 1998. Harnessing the biosynthetic code: Combinations, permutations, and mutations. *Science,* 282**,** 63-68.

Cantrell, C. L., Gustafson, K. R., Cecere, M. R., Pannell, L. K. & Boyd, M. R. 2000. Chondropsins A and B: Novel tumor cell growth-inhibitory macrolide lactams from the marine sponge *Chondropsis* sp. *Journal of the American chemical society,* 122**,** 8825-8829.

Carballo, J. L., Yanez, B., Zubia, E., Ortega, M. J. & Vega, C. 2010. Culture of explants from the sponge *Mycale cecilia* to obtain bioactive mycalazal-type metabolites. *Marine biotechnology,* 12**,** 516-525.

Carvalho, R., Reid, R., Viswanathan, N., Gramajo, H. & Julien, B. 2005. The biosynthetic genes for disorazoles, potent cytotoxic compounds that disrupt microtubule formation. *Gene,* 359**,** 91-98.

Cejka, D., Hayer, S., Niederreiter, B., Sieghart, W., Fuereder, T., Zwerina, J. & Schett, G. 2010. Mammalian target of rapamycin signaling is crucial for joint destruction in experimental arthritis and is activated in osteoclasts from patients with rheumatoid arthritis. *Arthritis and rheumatism,* 62**,** 2294-2302.

Chamoux, E., Couture, J., Bisson, M., Morissette, J., Brown, J. P. & Roux, S. 2009. The p62 p392l mutation linked to Paget's disease induces activation of human osteoclasts. *Molecular endocrinology,* 23**,** 1668-1680.

Chen, J. S. & Sambrook, P. N. 2012. Antiresorptive therapies for osteoporosis: A clinical overview. *Nature reviews endocrinology,* 8**,** 81-91.

Chen, S. H., Bubb, M. R., Yarmola, E. G., Zuo, J., Jiang, J., Lee, B. S., Lu, M., Gluck, S. L., Hurst, I. R. & Holliday, L. S. 2004. Vacuolar H+-ATPase binding to microfilaments: Regulation in response to phosphatidylinositol 3-kinase activity and detailed characterization of the actin-binding site in subunit B. *The Journal of biological chemistry,* 279**,** 7988-7998.

Chevallier, C., Laprevote, O., Bignon, J., Debitus, C., Guenard, D. & Sevenet, T. 2004. Isolation of cytotoxic chondropsins, macrolide lactams from the new-caledonian marine sponge *Psammoclemma* sp. and electrospray ion trap multiple stage MS study of these macrolides. *Natural product research,* 18**,** 479-484.

Cichewicz, R. H., Valeriote, F. A. & Crews, P. 2004. Psymberin, a potent sponge-derived cytotoxin from *psammocinia* distantly related to the pederin family. *Organic letters,* 6**,** 1951-1954.

Clague, M. J., Urbé, S., Aniento, F. & Gruenberg, J. 1994. Vacuolar ATPase activity is required for endosomal carrier vesicle formation. *Journal of biological chemistry,* 269**,** 21-24.

Clark, R. J., Akcan, M., Kaas, Q., Daly, N. L. & Craik, D. J. 2012. Cyclization of conotoxins to improve their biopharmaceutical properties. *Toxicon,* 59**,** 446-455.

Cleiren, E., Bénichou, O., Van Hul, E., Gram, J., Bollerslev, J., Singer, F. R., Beaverson, K., Aledo, A., Whyte, M. P. & Yoneyama, T. 2001. Albers-Schönberg disease (autosomal dominant osteopetrosis, type II) results from mutations in the ClCN7 chloride channel gene. *Human molecular genetics,* 10**,** 2861-2867.

Conti, E., Stachelhaus, T., Marahiel, M. A. & Brick, P. 1997. Structural basis for the activation of phenylalanine in the non-ribosomal biosynthesis of gramicidin S. *The EMBO journal,* 16**,** 4174-4183.

Corey, E. J., Gin, D. Y. & Kania, R. S. 1996. Enantioselective total synthesis of Ecteinascidin 743. *Journal of the american chemical society,* 118**,** 9202-9203.

Cortes, J., O'shaughnessy, J., Loesch, D., Blum, J. L., Vahdat, L. T., Petrakova, K., Chollet, P., Manikas, A., Dieras, V., Delozier, T., Vladimirov, V., Cardoso, F., Koh, H., Bougnoux, P., Dutcus, C. E., Seegobin, S., Mir, D., Meneses, N., Wanders, J. & Twelves, C. 2011. Eribulin monotherapy versus treatment of physician's choice in patients with metastatic breast cancer (embrace): A phase 3 open-label randomised study. *Lancet,* 377**,** 914-923.

Costello, M. J., Coll, M., Danovaro, R., Halpin, P., Ojaveer, H. & Miloslavich, P. 2010. A census of marine biodiversity knowledge, resources, and future challenges. *Public library of science one,* 5**,** e12110.

Cox, R. J. & Simpson, T. J. 2009. Fungal type I polyketide synthases. *Methods in enzymology,* 459**,** 49-78.

Coxon, F. P. & Taylor, A. 2008. Vesicular trafficking in osteoclasts. *Seminars in cell & developmental biology,* 19**,** 424-433.

Coxon, F. P., Thompson, K. & Rogers, M. J. 2006. Recent advances in understanding the mechanism of action of bisphosphonates. *Current opinion in pharmacology,* 6**,** 307-312.

Cragg, G. M. & Newman, D. J. 2013. Natural products: A continuing source of novel drug leads. *Biochimica et biophysica acta - general subjects,* 1830**,** 3670-3695.

Crasto, G. J., Kartner, N., Yao, Y., Li, K., Bullock, L., Datti, A. & Manolson, M. F. 2013. Luteolin inhibition of V-ATPase a3-d2 interaction decreases osteoclast resorptive activity. *Journal of cellular biochemistry,* 114**,** 929-941.

Crawford, J. M., Dancy, B. C. R., Hill, E. A., Udwary, D. W. & Townsend, C. A. 2006. Identification of a starter unit acyl-carrier protein transacylase domain in an iterative type I polyketide synthase. *Proceedings of the national academy of sciences of the United States of America,* 103**,** 16728-16733.

Cruciat, C.M., Ohkawara, B., Acebron, S. P., Karaulanov, E., Reinhard, C., Ingelfinger, D., Boutros, M. & Niehrs, C. 2010. Requirement of prorenin receptor and vacuolar H+-ATPase–mediated acidification for Wnt signaling. *Science,* 327**,** 459-463.

Cuevas, C. & Francesch, A. 2009. Development of Yondelis (trabectedin, ET-743). A semisynthetic process solves the supply problem. *Natural product reports,* 26**,** 322-337.

Cuevas, C., Perez, M., Martin, M. J., Chicharro, J. L., Fernandez-Rivas, C., Flores, M., Francesch, A., Gallego, P., Zarzuelo, M., De La Calle, F., Garcia, J., Polanco, C., Rodriguez, I. & Manzanares, I. 2000. Synthesis of ecteinascidin ET-743 and phthalascidin Pt-650 from cyanosafracin B. *Organic letters,* 2**,** 2545-2548.

Cummings, M., Breitling, R. & Takano, E. 2014. Steps towards the synthetic biology of polyketide biosynthesis. *Fems microbiology letters,* 351**,** 116-125.

D'incalci, M. & Galmarini, C. M. 2010. A review of trabectedin (ET-743): A unique mechanism of action. *Molecular cancer therapeutics,* 9**,** 2157-2163.

Dai, X. M., Zong, X. H., Akhter, M. P. & Stanley, E. R. 2004. Osteoclast deficiency results in disorganized matrix, reduced mineralization, and abnormal osteoblast behavior in developing bone. *Journal of bone and mineral research,* 19**,** 1441-1451.

Dechant, R., Binda, M., Lee, S. S., Pelet, S., Winderickx, J. & Peter, M. 2010. Cytosolic pH is a second messenger for glucose and regulates the PKA pathway through V-ATPase. *The EMBO journal,* 29**,** 2515-2526.

Del Fattore, A., Cappariello, A. & Teti, A. 2008. Genetics, pathogenesis and complications of osteopetrosis. *Bone,* 42**,** 19-29.

Del Fattore, A., Peruzzi, B., Rucci, N., Recchia, I., Cappariello, A., Longo, M., Fortunati, D., Ballanti, P., Iacobini, M. & Luciani, M. 2006. Clinical, genetic, and cellular analysis of 49 osteopetrotic patients: Implications for diagnosis and treatment. *Journal of medical genetics,* 43**,** 315-325.

Delcher, A. L., Bratke, K. A., Powers, E. C. & Salzberg, S. L. 2007. Identifying bacterial genes and endosymbiont DNA with glimmer. *Bioinformatics,* 23**,** 673-679.

Della Sala, G., Hochmuth, T., Costantino, V., Teta, R., Gerwick, W., Gerwick, L., Piel, J. & Mangoni, A. 2013. Polyketide genes in the marine sponge *Plakortis simplex*: A new group of mono-modular type I polyketide synthases from sponge symbionts. *Environmental microbiology reports,* 5**,** 809-818.

Della Sala, G., Hochmuth, T., Teta, R., Costantino, V. & Mangoni, A. 2014. Polyketide synthases in the microbiome of the marine sponge *Plakortis halichondrioides*: A metagenomic update. *Marine drugs,* 12**,** 5425-5440.

Delmas, P. D., Vergnaud, P., Arlot, M. E., Pastoureau, P., Meunier, P. J. & Nilssen, M. H. L. 1995. The anabolic effect of human PTH (1-34) on bone formation is blunted when bone resorption is inhibited by the bisphosphonate tiludronate-is activated resorption a prerequisite for the *in vivo* effect of PTH on formation in a remodeling system? *Bone,* 16**,** 603-610.

Demain, A. & Fang, A. 2000. The natural functions of secondary metabolites. *In:* Fiechter, A. (ed.) *History of modern biotechnology.* Springer Berlin Heidelberg.

Deselm, C. J., Miller, B. C., Zou, W., Beatty, W. L., Van Meel, E., Takahata, Y., Klumperman, J., Tooze, S. A., Teitelbaum, S. L. & Virgin, H. W. 2011. Autophagy proteins regulate the secretory component of osteoclastic bone resorption. *Developmental cell,* 21**,** 966-974.

Dewick, P. M. 2002. *Medicinal natural products: A biosynthetic approach*, John Wiley & Sons.

Diakov, T. T. & Kane, P. M. 2010. Regulation of vacuolar proton-translocating ATPase activity and assembly by extracellular pH. *The Journal of biological chemistry,* 285**,** 23771-23778.

Dobbins, D. E., Sood, R., Hashiramoto, A., Hansen, C. T., Wilder, R. L. & Remmers, E. F. 2002. Mutation of macrophage colony stimulating factor (Csf1) causes osteopetrosis in the tl rat. *Biochemical and biophysical research communications,* 294**,** 1114-1120.

Dobnig, H. & Turner, R. T. 1995. Evidence that intermittent treatment with parathyroid hormone increases bone formation in adult rats by activation of bone lining cells. *Endocrinology,* 136**,** 3632-3638.

Dougall, W. C., Glaccum, M., Charrier, K., Rohrbach, K., Brasel, K., De Smedt, T., Daro, E., Smith, J., Tometsko, M. E. & Maliszewski, C. R. 1999. RANK is essential for osteoclast and lymph node development. *Genes & development,* 13**,** 2412-2424.

Droese, S., Bindseil, K. U., Bowman, E. J., Siebers, A., Zeeck, A. & Altendorf, K. 1993. Inhibitory effect of modified bafilomycins and concanamycins on P- and V-type adenosinetriphosphatases. *Biochemistry,* 32**,** 3902-3906.

Du, L., Sanchez, C. & Shen, B. 2001. Hybrid peptide-polyketide natural products: Biosynthesis and prospects toward engineering novel molecules. *Metabolic engineering,* 3**,** 78-95.

Ducy, P., Zhang, R., Geoffroy, V., Ridall, A. L. & Karsenty, G. 1997. Osf2/Cbfa1: A transcriptional activator of osteoblast differentiation. *Cell,* 89**,** 747-754.

Dunlap, W. C., Battershill, C. N., Liptrot, C. H., Cobb, R. E., Bourne, D. G., Jaspars, M., Long, P. F. & Newman, D. J. 2007. Biomedicinals from the phytosymbionts of marine invertebrates: A molecular approach. *Methods,* 42**,** 358-376.

Dunlap, W. C., Jaspars, M., Hranueli, D., Battershill, C. N., Peric-Concha, N., Zucko, J., Wright, S. H. & Long, P. F. 2006. New methods for medicinal chemistry-universal gene cloning and expression systems for production of marine bioactive metabolites. *Current medicinal chemistry,* 13**,** 697-710.

Dutta, S., Whicher, J. R., Hansen, D. A., Hale, W. A., Chemler, J. A., Congdon, G. R., Narayan, A. R. H., Hakansson, K., Sherman, D. H., Smith, J. L. & Skiniotis, G. 2014. Structure of a modular polyketide synthase. *Nature,* 510**,** 512-517.

Edgar, R. C. 2004. MUSCLE: Multiple sequence alignment with high accuracy and high throughput. *Nucleic acids research,* 32**,** 1792-1797.

Eghbali-Fatourechi, G., Khosla, S., Sanyal, A., Boyle, W. J., Lacey, D. L. & Riggs, B. L. 2003. Role of RANK ligand in mediating increased bone resorption in early postmenopausal women. *Journal of clinical investigation,* 111**,** 1221.

Einhorn, Z., Trapani, J. G., Liu, Q. & Nicolson, T. 2012. Rabconnectin3α promotes stable activity of the H+ pump on synaptic vesicles in hair cells. *The Journal of neuroscience,* 32**,** 11144-11156.

Ekkers, D. M., Cretoiu, M. S., Kielak, A. M. & Elsas, J. D. 2012. The great screen anomaly--a new frontier in product discovery through functional metagenomics. *Applied microbiology biotechnology,* 93**,** 1005-1020.

Everts, V., Delaisse, J. M., Korper, W., Jansen, D. C., Tigchelaar-Gutter, W., Saftig, P. & Beertsen, W. 2002. The bone lining cell: Its role in cleaning howship's lacunae and initiating bone formation. *Journal of bone and mineral research,* 17**,** 77-90.

Everts, V., Korper, W., Hoeben, K. A., Jansen, I. D. C., Bromme, D., Cleutjens, K. B. J. M., Heeneman, S., Peters, C., Reinheckel, T., Saftig, P. & Beertsen, W. 2006. Osteoclastic bone degradation and the role of different cysteine proteinases and matrix metalloproteinases: Differences between calvaria and long bone. *Journal of bone and mineral research,* 21**,** 1399-1408.

Faulkner, D. J. 1986. Natural product reports. *Natural product reports,* 3**,** 1-33.

Felsenstein, J. 1985. Confidence limits on phylogenies: An approach using the bootstrap. *Evolution***,** 783-791.

Feng, H., Cheng, T., Pavlos, N. J., Yip, K. H., Carrello, A., Seeber, R., Eidne, K., Zheng, M. H. & Xu, J. 2008. Cytoplasmic terminus of vacuolar type proton pump accessory subunit Ac45 is required for proper interaction with V(0) domain subunits and efficient osteoclastic bone resorption. *The Journal of biological chemistry,* 283**,** 13194-13204.

Feng, H., Cheng, T., Steer, J. H., Joyce, D. A., Pavlos, N. J., Leong, C., Kular, J., Liu, J., Feng, X., Zheng, M. H. & Xu, J. 2009a. Myocyte enhancer factor 2 and microphthalmia-associated transcription factor cooperate with NFATc1 to transactivate the V-ATPase d2 promoter during RANKL-induced osteoclastogenesis. *The Journal of biological chemistry,* 284**,** 14667-14676.

Feng, S., Deng, L., Chen, W., Shao, J., Xu, G. & Li, Y. P. 2009b. Atp6v1c1 is an essential component of the osteoclast proton pump and in F-actin ring formation in osteoclasts. *The Biochemical journal,* 417**,** 195-203.

Fenical, W., Jensen, P. R., Palladino, M. A., Lam, K. S., Lloyd, G. K. & Potts, B. C. 2009. Discovery and development of the anticancer agent salinosporamide A (NPI-0052). *Bioorganic & Medicinal Chemistry,* 17**,** 2175-2180.

Fieseler, L., Hentschel, U., Grozdanov, L., Schirmer, A., Wen, G., Platzer, M., Hrvatin, S., Butzke, D., Zimmermann, K. & Piel, J. 2007. Widespread occurrence and genomic context of unusually small polyketide synthase genes in microbial consortia associated with marine sponges. *Applied and environmental microbiology,* 73**,** 2144-2155.

Fieseler, L., Horn, M., Wagner, M. & Hentschel, U. 2004. Discovery of the novel candidate phylum "Poribacteria" in marine sponges. *Applied and environmental microbiology,* 70**,** 3724-3732.

Finking, R. & Marahiel, M. A. 2004. Biosynthesis of nonribosomal peptides. *Annual review of microbiology,* 58**,** 453-488.

Finn, R. D., Bateman, A., Clements, J., Coggill, P., Eberhardt, R. Y., Eddy, S. R., Heger, A., Hetherington, K., Holm, L., Mistry, J., Sonnhammer, E. L. L., Tate, J. & Punta, M. 2014. Pfam: The protein families database. *Nucleic acids research,* 42**,** D222-D230.

Finn, R. D., Clements, J. & Eddy, S. R. 2011. HMMer web server: Interactive sequence similarity searching. *Nucleic acids research,* 39**,** W29-W37.

Fisch, K. M., Gurgui, C., Heycke, N., Van Der Sar, S. A., Anderson, S. A., Webb, V. L., Taudien, S., Platzer, M., Rubio, B. K., Robinson, S. J., Crews, P. & Piel, J. 2009. Polyketide assembly lines of uncultivated sponge symbionts from structure-based gene targeting. *Nature chemical biology,* 5**,** 494-501.

Fischbach, M. A. & Walsh, C. T. 2006. Assembly-line enzymology for polyketide and nonribosomal peptide antibiotics: Logic, machinery, and mechanisms. *Chemical reviews,* 106**,** 3468-3496.

Flanagan, A. M., Sarma, U., Steward, C. G., Vellodi, A. & Horton, M. A. 2000. Study of the nonresorptive phenotype of osteoclast-like cells from patients with malignant osteopetrosis: A new approach to investigating pathogenesis. *Journal of bone and mineral research,* 15**,** 352-360.

Florence, G. J., Gardner, N. M. & Paterson, I. 2008. Development of practical syntheses of the marine anticancer agents discodermolide and dictyostatin. *Natural product reports,* 25**,** 342-375.

Fonseca, B. D., Diering, G. H., Bidinosti, M. A., Dalal, K., Alain, T., Balgi, A. D., Forestieri, R., Nodwell, M., Rajadurai, C. V., Gunaratnam, C., Tee, A. R., Duong, F., Andersen, R. J., Orlowski, J., Numata, M., Sonenberg, N. & Roberge, M. 2012. Structure-activity analysis of niclosamide reveals potential role for cytoplasmic pH in control of mammalian target of rapamycin complex 1 (MTORC1) signaling. *The Journal of biological chemistry,* 287**,** 17530-17545.

Forgac, M. 2007. Vacuolar atpases: Rotary proton pumps in physiology and pathophysiology. *Nature reviews molecular cell biology,* 8**,** 917-929.

Foulke-Abel, J. & Townsend, C. A. 2012. Demonstration of starter unit inter-protein transfer from a fatty acid synthase to a multidomain, non-reducing polyketide synthase. *Chembiochem,* 13**,** 1880-1884.

Frattini, A., Orchard, P. J., Sobacchi, C., Giliani, S., Abinun, M., Mattsson, J. P., Keeling, D. J., Andersson, A. K., Wallbrandt, P., Zecca, L., Notarangelo, L. D., Vezzoni, P. & Villa, A. 2000. Defects in TCIRG1 subunit of the vacuolar proton pump are responsible for a subset of human autosomal recessive osteopetrosis. *Nature genetics,* 25**,** 343-346.

Frattini, A., Pangrazio, A., Susani, L., Sobacchi, C., Mirolo, M., Abinun, M., Andolina, M., Flanagan, A., Horwitz, E. M. & Mihci, E. 2003. Chloride channel ClCN7

mutations are responsible for severe recessive, dominant, and intermediate osteopetrosis. *Journal of bone and mineral research,* 18**,** 1740-1747.

Frost, H. M. 1964. *Bone remodeling dynamics*, Thomas, Springfield.

Fu, Q., Jilka, R. L., Manolagas, S. C. & O'brien, C. A. 2002. Parathyroid hormone stimulates receptor activator of NFκB ligand and inhibits osteoprotegerin expression via protein kinase a activation of camp-response element-binding protein. *Journal of biological chemistry,* 277**,** 48868-48875.

Fusetani, N., Sugawara, T. & Matsunaga, S. 1992. Bioactive marine metabolites. 41. Theopederins A-E, potent antitumor metabolites from a marine sponge, *Theonella* sp. *The Journal of organic chemistry,* 57**,** 3828-3832.

Gaitatzis, N., Silakowski, B., Kunze, B., Nordsiek, G., Blöcker, H., Höfle, G. & Müller, R. 2002. The biosynthesis of the aromatic myxobacterial electron transport inhibitor stigmatellin is directed by a novel type of modular polyketide synthase. *Journal of biological chemistry,* 277**,** 13082-13090.

Galli, C., Passeri, G. & Macaluso, G. M. 2010. Osteocytes and Wnt: The mechanical control of bone formation. *Journal of dental research,* 89**,** 331-343.

Geng, W., Hill, K., Zerwekh, J. E., Kohler, T., Muller, R. & Moe, O. W. 2009. Inhibition of osteoclast formation and function by bicarbonate: Role of soluble adenylyl cyclase. *Journal of cellular physiology,* 220**,** 332-340.

Geng, W., Wang, Z., Zhang, J., Reed, B. Y., Pak, C. Y. & Moe, O. W. 2005. Cloning and characterization of the human soluble adenylyl cyclase. *American journal of physiology. Cell Physiology,* 288**,** C1305-1316.

Gerwick, W. H. & Moore, B. S. 2012. Lessons from the past and charting the future of marine natural products drug discovery and chemical biology. *Chemistry & biology,* 19**,** 85-98.

Gillan, F., Stoilov, I., Thompson, J., Hogg, R., Wilkinson, C. & Djerassi, C. 1988. Fatty acids as biological markers for bacterial symbionts in sponges. *Lipids,* 23**,** 1139-1145.

Gillespie, D. E., Brady, S. F., Bettermann, A. D., Cianciotto, N. P., Liles, M. R., Rondon, M. R., Clardy, J., Goodman, R. M. & Handelsman, J. 2002. Isolation of antibiotics turbomycin A and B from a metagenomic library of soil microbial DNA. *Applied and environmental microbiology,* 68**,** 4301-4306.

Glimcher, M. & Muir, H. 1984. Recent studies of the mineral phase in bone and its possible linkage to the organic matrix by protein-bound phosphate bonds [and discussion]. *Philosophical transactions of the Royal Society of London. B, biological sciences,* 304**,** 479-508.

Gokhale, R. S., Lau, J., Cane, D. E. & Khosla, C. 1998. Functional orientation of the acyltransferase domain in a module of the erythromycin polyketide synthase. *Biochemistry,* 37**,** 2524-2528.

Gokhale, R. S., Saxena, P., Chopra, T. & Mohanty, D. 2007. Versatile polyketide enzymatic machinery for the biosynthesis of complex mycobacterial lipids. *Natural product reports,* 24**,** 267-277.

Goltzman, D. 2001. Osteolysis and cancer. *Journal of clinical investigation,* 107**,** 1219-1220.

Gonçalves, M. S. T. 2008. Fluorescent labeling of biomolecules with organic probes. *Chemical reviews,* 109**,** 190-212.

Gowen, M., Lazner, F., Dodds, R., Kapadia, R., Feild, J., Tavaria, M., Bertoncello, I., Drake, F., Zavarselk, S. & Tellis, I. 1999. Cathepsin K knockout mice develop osteopetrosis due to a deficit in matrix degradation but not demineralization. *Journal of bone and mineral research,* 14**,** 1654-1663.

Graham, L. A., Flannery, A. R. & Stevens, T. H. 2003. Structure and assembly of the yeast V-ATPase. *Journal of bioenergetics and biomembranes,* 35**,** 301-312.

Grigoriadis, A. E., Wang, Z. Q., Cecchini, M. G., Hofstetter, W., Felix, R., Fleisch, H. A. & Wagner, E. F. 1994. C-fos: A key regulator of osteoclast-macrophage lineage determination and bone remodeling. *Science,* 266**,** 443-448.

Grindberg, R. V., Ishoey, T., Brinza, D., Esquenazi, E., Coates, R. C., Liu, W.-T., Gerwick, L., Dorrestein, P. C., Pevzner, P., Lasken, R. & Gerwick, W. H. 2011. Single cell genome amplification accelerates identification of the apratoxin biosynthetic pathway from a complex microbial assemblage. *Public library of science one,* 6**,** e18565.

Guerrini, M. M., Sobacchi, C., Cassani, B., Abinun, M., Kilic, S. S., Pangrazio, A., Moratto, D., Mazzolari, E., Clayton-Smith, J. & Orchard, P. 2008. Human osteoclast-poor osteopetrosis with hypogammaglobulinemia due to TNFRSF11A (RANK) mutations. *The American journal of human genetics,* 83**,** 64-76.

Guise, T. A., Mohammad, K. S., Clines, G., Stebbins, E. G., Wong, D. H., Higgins, L. S., Vessella, R., Corey, E., Padalecki, S. & Suva, L. 2006. Basic mechanisms responsible for osteolytic and osteoblastic bone metastases. *Clinical cancer research,* 12**,** 6213s-6216s.

Gullberg, B., Johnell, O. & Kanis, J. 1997. World-wide projections for hip fracture. *Osteoporosis international,* 7**,** 407-413.

Gurgui, C. & Piel, J. 2010. Metagenomic approaches to identify and isolate bioactive natural products from microbiota of marine sponges. *Methods in molecular biology,* 668**,** 247-264.

Hadas, E., Shpigel, M. & Ilan, M. 2005. Sea ranching of the marine sponge *Negombata magnifica* (Demospongiae, Latrunculiidae) as a first step for latrunculin B mass production. *Aquaculture,* 244**,** 159-169.

Hadjidakis, D. J. & Androulakis, Ii 2006. Bone remodeling. *Annals of the New York academy of sciences,* 1092**,** 385-396.

Haefner, B. 2003. Drugs from the deep: Marine natural products as drug candidates. *Drug discovery today,* 8**,** 536-544.

Hall, G. E. & Kenny, A. D. 1987. Role of carbonic anhydrase in bone resorption: Effect of acetazolamide on basal and parathyroid hormone-induced bone metabolism. *Calcified Tissue International,* 40**,** 212-218.

Hall, N. 2007. Advanced sequencing technologies and their wider impact in microbiology. *The Journal of experimental biology,* 210**,** 1518-1525.

Halleen, J. M., Räisänen, S., Salo, J. J., Reddy, S. V., Roodman, G. D., Hentunen, T. A., Lehenkari, P. P., Kaija, H., Vihko, P. & Väänänen, H. K. 1999. Intracellular fragmentation of bone resorption products by reactive oxygen species generated by osteoclastic tartrate-resistant acid phosphatase. *Journal of biological chemistry,* 274**,** 22907-22910.

Handelsman, J., Rondon, M. R., Brady, S. F., Clardy, J. & Goodman, R. M. 1998. Molecular biological access to the chemistry of unknown soil microbes: A new frontier for natural products. *Chemistry & biology,* 5**,** R245-249.

Harmey, D., Stenbeck, G., Nobes, C. D., Lax, A. J. & Grigoriadis, A. E. 2004. Regulation of osteoblast differentiation by pasteurella multocida toxin (PMT): A role for Rho GTPase in bone formation. *Journal of bone and mineral research,* 19**,** 661-670.

Hayden, J. M., Mohan, S. & Baylink, D. J. 1995. The insulin-like growth factor system and the coupling of formation to resorption. *Bone,* 17**,** 93S-98S.

Hayman, A. R. & Cox, T. M. 2003. Tartrate-resistant acid phosphatase knockout mice. *Journal of bone and mineral research,* 18**,** 1905-1907.

Heino, T. J., Hentunen, T. A. & Väänänen, H. K. 2002. Osteocytes inhibit osteoclastic bone resorption through transforming growth factor-β: Enhancement by estrogen. *Journal of cellular biochemistry,* 85**,** 185-197.

Helfrich, M. H. & Hocking, L. J. 2008. Genetics and aetiology of pagetic disorders of bone. *Archives of biochemistry and biophysics,* 473**,** 172-182.

Henriksen, K., Andreassen, K. V., Thudium, C. S., Gudmann, K. N. S., Moscatelli, I., Crüger-Hansen, C. E., Schulz, A. S., Dziegiel, M. H., Richter, J., Karsdal, M. A. & Neutzsky-Wulff, A. V. 2012a. A specific subtype of osteoclasts secretes factors inducing nodule formation by osteoblasts. *Bone,* 51**,** 353-361.

Henriksen, K., Bollerslev, J., Everts, V. & Karsdal, M. A. 2011a. Osteoclast activity and subtypes as a function of physiology and pathology--implications for future treatments of osteoporosis. *Endocrine reviews,* 32**,** 31-63.

Henriksen, K., Flores, C., Thomsen, J. S., Brüel, A.-M., Thudium, C. S., Neutzsky-Wulff, A. V., Langenbach, G. E. J., Sims, N., Askmyr, M., Martin, T. J., Everts, V., Karsdal, M. A. & Richter, J. 2011b. Dissociation of bone resorption and bone formation in adult mice with a non-functional V-ATPase in osteoclasts leads to increased bone strength. *Public library of scienc one,* 6**,** e27482.

Henriksen, K., Karsdal, M., Taylor, A., Tosh, D. & Coxon, F. 2012b. Generation of human osteoclasts from peripheral blood. *In:* Helfrich, M. H. & Ralston, S. H. (eds.) *Bone research protocols.* Humana Press.

Hentschel, U., Usher, K. M. & Taylor, M. W. 2006. Marine sponges as microbial fermenters. *FEMS microbiology ecology,* 55**,** 167-177.

Hertweck, C. 2009. The biosynthetic logic of polyketide diversity. *Angewandte chemie international edition,* 48**,** 4688-4716.

Heymann, D., Fortun, Y., Redini, F. & Padrines, M. 2005. Osteolytic bone diseases: Physiological analogues of bone resorption effectors as alternative therapeutic tools. *Drug discovery today,* 10**,** 242-247.

Hiesinger, P. R., Fayyazuddin, A., Mehta, S. Q., Rosenmund, T., Schulze, K. L., Zhai, R. G., Verstreken, P., Cao, Y., Zhou, Y., Kunz, J. & Bellen, H. J. 2005. The V-ATPase V0 subunit a1 is required for a late step in synaptic vesicle exocytosis in drosophila. *Cell,* 121**,** 607-620.

Hildebrand, M., Waggoner, L. E., Lim, G. E., Sharp, K. H., Ridley, C. P. & Haygood, M. G. 2004. Approaches to identify, clone, and express symbiont bioactive metabolite genes. *Natural product reports,* 21**,** 122-142.

Hill, R. T. & Fenical, W. 2010. Pharmaceuticals from marine natural products: Surge or ebb? *Current opinion in biotechnology,* 21**,** 777-779.

Hilton, M. J., Tu, X., Wu, X., Bai, S., Zhao, H., Kobayashi, T., Kronenberg, H. M., Teitelbaum, S. L., Ross, F. P. & Kopan, R. 2008. Notch signaling maintains bone marrow mesenchymal progenitors by suppressing osteoblast differentiation. *Nature medicine,* 14**,** 306-314.

Hinton, A., Bond, S. & Forgac, M. 2009. V-ATPase functions in normal and disease processes. *Pflügers archiv-European journal of physiology,* 457**,** 589-598.

Hitchman, T. S., Schmidt, E. W., Trail, F., Rarick, M. D., Linz, J. E. & Townsend, C. A. 2001. Hexanoate synthase, a specialized type I fatty acid synthase in aflatoxin B1 biosynthesis. *Bioorganic chemistry,* 29**,** 293-307.

Hochmuth, T., Niederkruger, H., Gernert, C., Siegl, A., Taudien, S., Platzer, M., Crews, P., Hentschel, U. & Piel, J. 2010. Linking chemical and microbial diversity in marine sponges: Possible role for Poribacteria as producers of methyl-branched fatty acids. *Chembiochem,* 11**,** 2572-2578.

Hochmuth, T. & Piel, J. 2009. Polyketide synthases of bacterial symbionts in sponges--evolution-based applications in natural products research. *Phytochemistry,* 70**,** 1841-1849.

Hocking, L. J., Whitehouse, C. & Helfrich, M. H. 2012. Autophagy: A new player in skeletal maintenance? *Journal of bone and mineral research,* 27**,** 1439-1447.

Hofbauer, L. C., Gori, F., Riggs, B. L., Lacey, D. L., Dunstan, C. R., Spelsberg, T. C. & Khosla, S. 1999. Stimulation of osteoprotegerin ligand and inhibition of osteoprotegerin production by glucocorticoids in human osteoblastic lineage cells: Potential paracrine mechanisms of glucocorticoid-induced osteoporosis 1. *Endocrinology,* 140**,** 4382-4389.

Hofbauer, L. C., Khosla, S., Dunstan, C. R., Lacey, D. L., Boyle, W. J. & Riggs, B. L. 2000. The roles of osteoprotegerin and osteoprotegerin ligand in the paracrine regulation of bone resorption. *Journal of bone and mineral research,* 15**,** 2-12.

Hollberg, K., Hultenby, K., Hayman, A., Cox, T. & Andersson, G. 2002. Osteoclasts from mice deficient in tartrate-resistant acid phosphatase have altered ruffled borders and disturbed intracellular vesicular transport. *Experimental cell research,* 279**,** 227-238.

Holliday, L. S. 2014. Vacuolar H+-ATPase: An essential multitasking enzyme in physiology and pathophysiology. *New journal of science,* 2014**,** 21-29.

Holliday, L. S., Lu, M., Lee, B. S., Nelson, R. D., Solivan, S., Zhang, L. & Gluck, S. L. 2000. The amino-terminal domain of the B subunit of vacuolar H+-ATPase contains a filamentous actin binding site. *The Journal of biological chemistry,* 275**,** 32331-32337.

Hrvatin, S. & Piel, J. 2007. Rapid isolation of rare clones from highly complex DNA libraries by PCR analysis of liquid gel pools. *Journal of microbiological methods,* 68**,** 434-436.

Hu, G.P., Yuan, J., Sun, L., She, Z.G., Wu, J.H., Lan, X.J., Zhu, X., Lin, Y.C. & Chen, S.P. 2011. Statistical research on marine natural products based on data obtained between 1985 and 2008. *Marine drugs,* 9**,** 514-525.

Hu, H., Hilton, M. J., Tu, X., Yu, K., Ornitz, D. M. & Long, F. 2005a. Sequential roles of hedgehog and Wnt signaling in osteoblast development. *Development,* 132**,** 49-60.

Hu, Y., Nyman, J., Muhonen, P., Vaananen, H. K. & Laitala-Leinonen, T. 2005b. Inhibition of the osteoclast V-ATPase by small interfering RNAs. *FEBS letters,* 579**,** 4937-4942.

Hughes, C. C. & Fenical, W. 2010. Antibacterials from the sea. *Chemistry,* 16**,** 12512-12525.

Humphrey, M. B., Lanier, L. L. & Nakamura, M. C. 2005. Role of ITAM-containing adapter proteins and their receptors in the immune system and bone. *Immunological reviews,* 208**,** 50-65.

Hurtado-Lorenzo, A., Skinner, M., El Annan, J., Futai, M., Sun-Wada, G. H., Bourgoin, S., Casanova, J., Wildeman, A., Bechoua, S., Ausiello, D. A., Brown, D. & Marshansky, V. 2006. V-ATPase interacts with ARNO and Arf6 in early endosomes and regulates the protein degradative pathway. *Nature cell biology,* 8**,** 124-136.

Husheem, M., Nyman, J. K. E., Vääräniemi, J., Vaananen, H. K. & Hentunen, T. A. 2005. Characterization of circulating human osteoclast progenitors: Development of *in vitro* resorption assay. *Calcified tissue international,* 76**,** 222-230.

Huss, M., Ingenhorst, G., Konig, S., Gassel, M., Drose, S., Zeeck, A., Altendorf, K. & Wieczorek, H. 2002. Concanamycin A, the specific inhibitor of V-ATPases, binds to the V(o) subunit c. *The Journal of biological chemistry,* 277**,** 40544-40548.

Huss, M., Sasse, F., Kunze, B., Jansen, R., Steinmetz, H., Ingenhorst, G., Zeeck, A. & Wieczorek, H. 2005. Archazolid and apicularen: Novel specific V-ATPase inhibitors. *BMC Biochemistry,* 6**,** 13.

Huss, M. & Wieczorek, H. 2009. Inhibitors of V-ATPases: Old and new players. *Journal of experimental biology,* 212**,** 341-346.

Huyck, T. K., Gradishar, W., Manuguid, F. & Kirkpatrick, P. 2011. Eribulin mesylate. *Nature reviews drug discovery,* 10**,** 173-174.

Imamura, H., Nakano, M., Noji, H., Muneyuki, E., Ohkuma, S., Yoshida, M. & Yokoyama, K. 2003. Evidence for rotation of V1-ATPase. *Proceedings of the national academy of sciences of the United States of America,* 100**,** 2312-2315.

Indo, Y., Takeshita, S., Ishii, K.A., Hoshii, T., Aburatani, H., Hirao, A. & Ikeda, K. 2013. Metabolic regulation of osteoclast differentiation and function. *Journal of bone and mineral research,* 28**,** 2392-2399.

Inoue, J.I., Ishida, T., Tsukamoto, N., Kobayashi, N., Naito, A., Azuma, S. & Yamamoto, T. 2000. Tumor necrosis factor receptor-associated factor (TRAF) family: Adapter proteins that mediate cytokine signaling. *Experimental cell research,* 254**,** 14-24.

Ishida, N., Hayashi, K., Hoshijima, M., Ogawa, T., Koga, S., Miyatake, Y., Kumegawa, M., Kimura, T. & Takeya, T. 2002. Large scale gene expression analysis of osteoclastogenesis *in vitro* and elucidation of NFAT2 as a key regulator. *Journal of biological chemistry,* 277**,** 41147-41156.

Ishii, M., Egen, J. G., Klauschen, F., Meier-Schellersheim, M., Saeki, Y., Vacher, J., Proia, R. L. & Germain, R. N. 2009. Sphingosine-1-phosphate mobilizes osteoclast precursors and regulates bone homeostasis. *Nature,* 458**,** 524-528.

Itzstein, C., Coxon, F. P. & Rogers, M. J. 2011. The regulation of osteoclast function and bone resorption by small GTPases. *Small GTPases,* 2**,** 117-130.

Jackson, K. L., Henderson, J. A. & Phillips, A. J. 2009. The halichondrins and E7389. *Chemical reviews,* 109**,** 3044-3079.

Jewell, J. L., Russell, R. C. & Guan, K.L. 2013. Amino acid signalling upstream of MTOR. *Nature reviews molecular cell biology,* 14**,** 133-139.

Jiang, X., García-Fortanet, J. & De Brabander, J. K. 2005. Synthesis and complete stereochemical assignment of psymberin/irciniastatin A. *Journal of the American chemical society,* 127**,** 11254-11255.

Jilka, R. L., Weinstein, R. S., Bellido, T., Roberson, P., Parfitt, A. M. & Manolagas, S. C. 1999. Increased bone formation by prevention of osteoblast apoptosis with parathyroid hormone. *The Journal of clinical investigation,* 104**,** 439-446.

Jimi, E., Nakamura, I., Amano, H., Taguchi, Y., Tsurukai, T., Tamura, M., Takahashi, N. & Suda, T. 1996. Osteoclast function is activated by osteoblastic cells through a mechanism involving cell-to-cell contact. *Endocrinology,* 137**,** 2187-2190.

Johnell, O. 1997. The socioeconomic burden of fractures: Today and in the 21st century. *American journal of medicine,* 103**,** 20S-25S; discussion 25S-26S.

Johnell, O. & Kanis, J. 2005. Epidemiology of osteoporotic fractures. *Osteoporosis international,* 16**,** S3-S7.

Joint, I., Muhling, M. & Querellou, J. 2010. Culturing marine bacteria - an essential prerequisite for biodiscovery. *Microbial biotechnology,* 3**,** 564-575.

Joshi, A. K., Witkowski, A. & Smith, S. 1997. Mapping of functional interactions between domains of the animal fatty acid synthase by mutant complementation *in vitro*. *Biochemistry,* 36**,** 2316-2322.

Jouret, F., Auzanneau, C., Debaix, H., Wada, G.H. S., Pretto, C., Marbaix, E., Karet, F. E., Courtoy, P. J. & Devuyst, O. 2005. Ubiquitous and kidney-specific subunits of vacuolar H+-ATPase are differentially expressed during nephrogenesis. *Journal of the American society of nephrology,* 16**,** 3235-3246.

Junge, W. & Nelson, N. 2005. Nature's rotary electromotors. *Science,* 308**,** 642-644.

Kallifatidis, G., Hoepfner, D., Jaeg, T., Guzman, E. A. & Wright, A. E. 2013. The marine natural product manzamine A targets vacuolar ATPases and inhibits autophagy in pancreatic cancer cells. *Marine drugs,* 11**,** 3500-3516.

Kalu, D. N. 1991. The ovariectomized rat model of postmenopausal bone loss. *Bone and mineral,* 15**,** 175-191.

Kameda, T., Mano, H., Yuasa, T., Mori, Y., Miyazawa, K., Shiokawa, M., Nakamaru, Y., Hiroi, E., Hiura, K. & Kameda, A. 1997. Estrogen inhibits bone resorption by directly inducing apoptosis of the bone-resorbing osteoclasts. *The Journal of experimental medicine,* 186**,** 489-495.

Kane, P. M. 1995. Disassembly and reassembly of the yeast vacuolar H(+)-ATPase *in vivo*. *The Journal of biological chemistry,* 270**,** 17025-17032.

Kane, P. M. 2006. The where, when, and how of organelle acidification by the yeast vacuolar H+-ATPase. *Microbiology and molecular biology reviews,* 70**,** 177-191.

Kane, P. M. & Parra, K. J. 2000. Assembly and regulation of the yeast vacuolar H (+)-ATPase. *Journal of experimental biology,* 203**,** 81-87.

Kanehisa, J., Yamanaka, T., Doi, S., Turksen, K., Heersche, J. N., Aubin, J. E. & Takeuchi, H. 1990. A band of F-actin containing podosomes is involved in bone resorption by osteoclasts. *Bone,* 11**,** 287-293.

Kao, C. M., Pieper, R., Cane, D. E. & Khosla, C. 1996. Evidence for two catalytically independent clusters of active sites in a functional modular polyketide synthase. *Biochemistry,* 35**,** 12363-12368.

Karsdal, M. A., Henriksen, K., Sorensen, M. G., Gram, J., Schaller, S., Dziegiel, M. H., Heegaard, A. M., Christophersen, P., Martin, T. J., Christiansen, C. & Bollerslev, J. 2005. Acidification of the osteoclastic resorption compartment provides insight into the coupling of bone formation to bone resorption. *The American journal of pathology,* 166**,** 467-476.

Karsdal, M. A., Martin, T. J., Bollerslev, J., Christiansen, C. & Henriksen, K. 2007. Are nonresorbing osteoclasts sources of bone anabolic activity? *Journal of bone and mineral research,* 22**,** 487-494.

Karsdal, M. A., Neutzsky-Wulff, A. V., Dziegiel, M. H., Christiansen, C. & Henriksen, K. 2008. Osteoclasts secrete non-bone derived signals that induce bone formation. *Biochemical and biophysical research communications,* 366**,** 483-488.

Kartner, N., Yao, Y., Li, K., Crasto, G. J., Datti, A. & Manolson, M. F. 2010. Inhibition of osteoclast bone resorption by disrupting vacuolar H+-ATPase a3-B2 subunit interaction. *The Journal of biological chemistry,* 285**,** 37476-37490.

Katz, L. 2009. The DEBS paradigm for type I modular polyketide synthases and beyond. *Methods in enzymology,* 459**,** 113-142.

Kawasaki-Nishi, S., Bowers, K., Nishi, T., Forgac, M. & Stevens, T. H. 2001a. The amino-terminal domain of the vacuolar proton-translocating ATPase a subunit controls targeting and *in vivo* dissociation, and the carboxyl-terminal domain affects coupling of proton transport and ATP hydrolysis. *The Journal of biological chemistry,* 276**,** 47411-47420.

Kawasaki-Nishi, S., Nishi, T. & Forgac, M. 2001b. Arg-735 of the 100-kDa subunit a of the yeast V-ATPase is essential for proton translocation. *Proceedings of the national academy of sciences of the United States of America,* 98**,** 12397-12402.

Kawasaki-Nishi, S., Nishi, T. & Forgac, M. 2001c. Yeast V-ATPase complexes containing different isoforms of the 100-kDa a-subunit differ in coupling efficiency and *in vivo* dissociation. *The Journal of biological chemistry,* 276**,** 17941-17948.

Keatinge-Clay, A. T. 2012. The structures of type I polyketide synthases. *Natural product reports,* 29**,** 1050-1073.

Keeling, D. J., Herslof, M., Mattsson, J. P. & Ryberg, B. 1998. Tissue-selective inhibition of vacuolar acid pumps. *Acta physiologica Scandinavica. supplementum,* 643**,** 195-201.

Keller, H. & Kneissel, M. 2005. SOST is a target gene for PTH in bone. *Bone,* 37**,** 148-158.

Kellner, R. L. & Dettner, K. 1996. Differential efficacy of toxic pederin in deterring potential arthropod predators of *Paederus* (Coleoptera: Staphylinidae) offspring. *Oecologia,* 107**,** 293-300.

Kennedy, J. 2008. Mutasynthesis, chemobiosynthesis, and back to semi-synthesis: Combining synthetic chemistry and biosynthetic engineering for diversifying natural products. *Natural product reports,* 25**,** 25-34.

Khosla, C., Gokhale, R. S., Jacobsen, J. R. & Cane, D. E. 1999. Tolerance and specificity of polyketide synthases. *Annual review of biochemistry,* 68**,** 219-253.

Khosla, C., Tang, Y., Chen, A. Y., Schnarr, N. A. & Cane, D. E. 2007. Structure and mechanism of the 6-deoxyerythronolide B synthase. *Annual review of biochemistry,* 76**,** 195-221.

Kim, E. J., Lee, J. H., Choi, H., Pereira, A. R., Ban, Y. H., Yoo, Y. J., Kim, E., Park, J. W., Sherman, D. H., Gerwick, W. H. & Yoon, Y. J. 2012. Heterologous production of 4-O-demethylbarbamide, a marine cyanobacterial natural product. *Organic letters,* 14**,** 5824-5827.

Kim, H. J., Zhao, H., Kitaura, H., Bhattacharyya, S., Brewer, J. A., Muglia, L. J., Ross, F. P. & Teitelbaum, S. L. 2006. Glucocorticoids suppress bone formation via the osteoclast. *Journal of clinical investigation,* 116**,** 2152-2160.

Kim, K., Lee, S.H., Ha Kim, J., Choi, Y. & Kim, N. 2008. NFATc1 induces osteoclast fusion via up-regulation of Atp6v0d2 and the dendritic cell-specific transmembrane protein (DC-STAMP). *Molecular endocrinology,* 22**,** 176-185.

Kim, T. K. & Fuerst, J. A. 2006. Diversity of polyketide synthase genes from bacteria associated with the marine sponge *Pseudoceratina clavata*: Culture-dependent and culture-independent approaches. *Environmental microbiology,* 8**,** 1460-1470.

Kim, U. J., Shizuya, H., De Jong, P. J., Birren, B. & Simon, M. I. 1992. Stable propagation of cosmid sized human DNA inserts in an F factor based vector. *Nucleic acids research,* 20**,** 1083-1085.

Kinashi, H., Someno, K. & Sakaguchi, K. 1984. Isolation and characterization of concanamycins A, B and C. *The Journal of antibiotics,* 37**,** 1333-1343.

Kircher, M. & Kelso, J. 2010. High-throughput DNA sequencing--concepts and limitations. *Bioessays,* 32**,** 524-536.

Klionsky, D. J., Elazar, Z., Seglen, P. O. & Rubinsztein, D. C. 2008. Does bafilomycin A1 block the fusion of autophagosomes with lysosomes? *Autophagy,* 4**,** 849-850.

Kobayashi, J. & Ishibashi, M. 1993. Bioactive metabolites of symbiotic marine microorganisms. *Chemical reviews,* 93**,** 1753-1769.

Kobayashi, J. I., Itagaki, F., Shigemori, H. & Sasaki, T. 1993. Three new onnamide congeners from the okinawan marine sponge *Theonella* sp. *Journal of natural products,* 56**,** 976-981.

Kobayashi, N., Kadono, Y., Naito, A., Matsumoto, K., Yamamoto, T., Tanaka, S. & Inoue, J. I. 2001. Segregation of TRAF6-mediated signaling pathways clarifies its role in osteoclastogenesis. *The EMBO journal,* 20**,** 1271-1280.

Koh, A. J., Demiralp, B., Neiva, K. G., Hooten, J., Nohutcu, R. M., Shim, H., Datta, N. S., Taichman, R. S. & Mccauley, L. K. 2005. Cells of the osteoclast lineage as

mediators of the anabolic actions of parathyroid hormone in bone. *Endocrinology,* 146**,** 4584-4596.

Kolattukudy, P. E., Fernandes, N. D., Azad, A. K., Fitzmaurice, A. M. & Sirakova, T. D. 1997. Biochemistry and molecular genetics of cell-wall lipid biosynthesis in mycobacteria. *Molecular microbiology,* 24**,** 263-270.

Komori, T., Yagi, H., Nomura, S., Yamaguchi, A., Sasaki, K., Deguchi, K., Shimizu, Y., Bronson, R. T., Gao, Y. H., Inada, M., Sato, M., Okamoto, R., Kitamura, Y., Yoshiki, S. & Kishimoto, T. 1997. Targeted disruption of Cbfa1 results in a complete lack of bone formation owing to maturational arrest of osteoblasts. *Cell,* 89**,** 755-764.

Kong, Y. Y., Yoshida, H., Sarosi, I., Tan, H. L., Timms, E., Capparelli, C., Morony, S., Oliveira-Dos-Santos, A. J., Van, G., Itie, A., Khoo, W., Wakeham, A., Dunstan, C. R., Lacey, D. L., Mak, T. W., Boyle, W. J. & Penninger, J. M. 1999. OPGL is a key regulator of osteoclastogenesis, lymphocyte development and lymph-node organogenesis. *Nature,* 397**,** 315-323.

Kornak, U., Kasper, D., Bösl, M. R., Kaiser, E., Schweizer, M., Schulz, A., Friedrich, W., Delling, G. & Jentsch, T. J. 2001. Loss of the ClC-7 chloride channel leads to osteopetrosis in mice and man. *Cell,* 104**,** 205-215.

Kornak, U., Schulz, A., Friedrich, W., Uhlhaas, S., Kremens, B., Voit, T., Hasan, C., Bode, U., Jentsch, T. J. & Kubisch, C. 2000. Mutations in the a3 subunit of the vacuolar H(+)-ATPPase cause infantile malignant osteopetrosis. *Human molecular genetics,* 9**,** 2059-2063.

Kukita, T., Wada, N., Kukita, A., Kakimoto, T., Sandra, F., Toh, K., Nagata, K., Iijima, T., Horiuchi, M. & Matsusaki, H. 2004. RANKL-induced DC-STAMP is essential for osteoclastogenesis. *The Journal of experimental medicine,* 200**,** 941-946.

Kunin, V., Engelbrektson, A., Ochman, H. & Hugenholtz, P. 2010. Wrinkles in the rare biosphere: Pyrosequencing errors can lead to artificial inflation of diversity estimates. *Environmental microbiology,* 12**,** 118-123.

Kuttruff, C. A., Eastgate, M. D. & Baran, P. S. 2014. Natural product synthesis in the age of scalability. *Natural product reports,* 31**,** 419-432.

Kwan, D. H. & Schulz, F. 2011. The stereochemistry of complex polyketide biosynthesis by modular polyketide synthases. *Molecules,* 16**,** 6092-6115.

Kwan, J. C., Donia, M. S., Han, A. W., Hirose, E., Haygood, M. G. & Schmidt, E. W. 2012. Genome streamlining and chemical defense in a coral reef symbiosis. *Proceedings of the national academy of sciences of the United States of America,* 109**,** 20655-20660.

Lacey, D., Timms, E., Tan, H.-L., Kelley, M., Dunstan, C., Burgess, T., Elliott, R., Colombero, A., Elliott, G. & Scully, S. 1998. Osteoprotegerin ligand is a cytokine that regulates osteoclast differentiation and activation. *Cell,* 93**,** 165-176.

Laitala-Leinonen, T. & Vaananen, H. K. 1999. Decreased bone resorption, osteoclast differentiation, and expression of vacuolar H+-ATPase in antisense DNA-treated mouse metacarpal and calvaria cultures *ex vivo*. *Antisense & nucleic acid drug development,* 9**,** 155-169.

Lakkakorpi, P., Tuukkanen, J., Hentunen, T., Järvelin, K. & Väänänen, K. 1989. Organization of osteoclast microfilaments during the attachment to bone surface *in vitro*. *Journal of bone and mineral research,* 4**,** 817-825.

Lakkakorpi, P. T. & Väänänen, H. K. 1996. Cytoskeletal changes in osteoclasts during the resorption cycle. *Microscopy research and technique,* 33**,** 171-181.

Lane, A. L. & Moore, B. S. 2011. A sea of biosynthesis: Marine natural products meet the molecular age. *Natural product reports,* 28**,** 411-428.

Larkin, M. A., Blackshields, G., Brown, N., Chenna, R., Mcgettigan, P. A., Mcwilliam, H., Valentin, F., Wallace, I. M., Wilm, A. & Lopez, R. 2007. Clustal W and clustal X version 2.0. *Bioinformatics,* 23**,** 2947-2948.

Leal, M. C., Puga, J., Serôdio, J., Gomes, N. C. M. & Calado, R. 2012. Trends in the discovery of new marine natural products from invertebrates over the last two decades – where and what are we bioprospecting? *Public library of science one,* 7**,** e30580.

Lee, B. S., Gluck, S. L. & Holliday, L. S. 1999. Interaction between vacuolar H(+)-ATPase and microfilaments during osteoclast activation. *The Journal of biological chemistry,* 274**,** 29164-29171.

Lee, B. S., Holliday, L., Ojikutu, B., Krits, I. & Gluck, S. L. 1996. Osteoclasts express the B2 isoform of vacuolar H(+)-ATPase intracellularly and on their plasma membranes. *American journal of physiology-cell physiology,* 270**,** C382-C388.

Lee, B. S., Krits, I., Crane-Zelkovic, M. K. & Gluck, S. L. 1997. A novel transcription factor regulates expression of the vacuolar H+-ATPase B2 subunit through AP-2 sites during monocytic differentiation. *Journal of biological chemistry,* 272**,** 174-181.

Lee, O. O., Wang, Y., Yang, J., Lafi, F. F., Al-Suwailem, A. & Qian, P.Y. 2011. Pyrosequencing reveals highly diverse and species-specific microbial communities in sponges from the red sea. *The ISME journal,* 5**,** 650-664.

Lee, S.H., Kim, T.S., Choi, Y. & Lorenzo, J. 2008. Osteoimmunology: Cytokines and the skeletal system. *BMB reports,* 41**,** 495-510.

Lee, S., Goldring, S. & Lorenzo, J. A. 1995. Expression of the calcitonin receptor in bone marrow cell cultures and in bone: A specific marker of the differentiated osteoclast that is regulated by calcitonin. *Endocrinology,* 136**,** 4572-4581.

Lee, S. H., Rho, J., Jeong, D., Sul, J. Y., Kim, T., Kim, N., Kang, J. S., Miyamoto, T., Suda, T., Lee, S. K., Pignolo, R. J., Koczon-Jaremko, B., Lorenzo, J. & Choi, Y. 2006. V-ATPase V0 subunit d2-deficient mice exhibit impaired osteoclast fusion and increased bone formation. *Nature medicine,* 12**,** 1403-1409.

Lenart, B. A., Lorich, D. G. & Lane, J. M. 2008. Atypical fractures of the femoral diaphysis in postmenopausal women taking alendronate. *New England journal of medicine,* 358**,** 1304-1306.

Li, J., Sarosi, I., Yan, X.Q., Morony, S., Capparelli, C., Tan, H.L., Mccabe, S., Elliott, R., Scully, S. & Van, G. 2000. RANK is the intrinsic hematopoietic cell surface receptor that controls osteoclastogenesis and regulation of bone mass and calcium metabolism. *Proceedings of the national academy of sciences,* 97**,** 1566-1571.

Li, Y. P., Chen, W., Liang, Y., Li, E. & Stashenko, P. 1999. Atp6i-deficient mice exhibit severe osteopetrosis due to loss of osteoclast-mediated extracellular acidification. *Nature genetics,* 23**,** 447-451.

Lin, N. Y., Beyer, C., Giessl, A., Kireva, T., Scholtysek, C., Uderhardt, S., Munoz, L. E., Dees, C., Distler, A., Wirtz, S., Kronke, G., Spencer, B., Distler, O., Schett, G. & Distler, J. H. 2013. Autophagy regulates TNF alpha-mediated joint destruction in experimental arthritis. *Annals of the rheumatic diseases,* 72**,** 761-768.

Liou, G. F., Lau, J., Cane, D. E. & Khosla, C. 2003. Quantitative analysis of loading and extender acyltransferases of modular polyketide synthases. *Biochemistry,* 42**,** 200-207.

Liu, X.H., Kirschenbaum, A., Yao, S. & Levine, A. C. 2005. Cross-talk between the interleukin-6 and prostaglandin E2 signaling systems results in enhancement of osteoclastogenesis through effects on the osteoprotegerin/receptor activator of nuclear factor-κB (RANK) ligand/RANK system. *Endocrinology,* 146**,** 1991-1998.

Lomaga, M. A., Yeh, W.C., Sarosi, I., Duncan, G. S., Furlonger, C., Ho, A., Morony, S., Capparelli, C., Van, G., Kaufman, S., Van Der Heiden, A., Itie, A., Wakeham, A., Khoo, W., Sasaki, T., Cao, Z., Penninger, J. M., Paige, C. J., Lacey, D. L., Dunstan, C. R., Boyle, W. J., Goeddel, D. V. & Mak, T. W. 1999. TRAF6 deficiency results in osteopetrosis and defective interleukin-1, CD40, and LPS signaling. *Genes & Development,* 13**,** 1015-1024.

Long, F. 2012. Building strong bones: Molecular regulation of the osteoblast lineage. *Nature reviews molecular cell biology,* 13**,** 27-38.

Long, F., Chung, U.I., Ohba, S., Mcmahon, J., Kronenberg, H. M. & Mcmahon, A. P. 2004. Ihh signaling is directly required for the osteoblast lineage in the endochondral skeleton. *Development,* 131**,** 1309-1318.

Long, P. F., Dunlap, W. C., Battershill, C. N. & Jaspars, M. 2005. Shotgun cloning and heterologous expression of the patellamide gene cluster as a strategy to achieving sustained metabolite production. *ChemBioChem,* 6**,** 1760-1765.

Lu, M., Sautin, Y. Y., Holliday, L. S. & Gluck, S. L. 2004. The glycolytic enzyme aldolase mediates assembly, expression, and activity of vacuolar H+-ATPase. *The Journal of biological chemistry,* 279**,** 8732-8739.

Ma, D.L., Chan, D. S.H. & Leung, C.H. 2011. Molecular docking for virtual screening of natural product databases. *Chemical science,* 2**,** 1656-1665.

Ma, Y. L., Cain, R. L., Halladay, D. L., Yang, X., Zeng, Q., Miles, R. R., Chandrasekhar, S., Martin, T. J. & Onyia, J. E. 2001. Catabolic effects of continuous human PTH (1–38) *in vivo* is associated with sustained stimulation of RANKL and inhibition of osteoprotegerin and gene-associated bone formation. *Endocrinology,* 142**,** 4047-4054.

Mahamid, J., Sharir, A., Gur, D., Zelzer, E., Addadi, L. & Weiner, S. 2011. Bone mineralization proceeds through intracellular calcium phosphate loaded vesicles: A cryo-electron microscopy study. *Journal of structural biology,* 174**,** 527-535.

Maier, T., Leibundgut, M. & Ban, N. 2008. The crystal structure of a mammalian fatty acid synthase. *Science,* 321**,** 1315-1322.

Malkus, P., Graham, L. A., Stevens, T. H. & Schekman, R. 2004. Role of Vma21p in assembly and transport of the yeast vacuolar ATPase. *Molecular biology of the cell,* 15**,** 5075-5091.

Maloof, A. C., Rose, C. V., Beach, R., Samuels, B. M., Calmet, C. C., Erwin, D. H., Poirier, G. R., Yao, N. & Simons, F. J. 2010. Possible animal-body fossils in pre-marinoan limestones from South Australia. *Nature geosciences,* 3**,** 653-659.

Manabe, T., Yoshimori, T., Henomatsu, N. & Tashiro, Y. 1993. Inhibitors of vacuolar-type H(+)-ATPase suppresses proliferation of cultured cells. *Journal of cellular physiology,* 157**,** 445-452.

Manolson, M. F., Yu, H., Chen, W., Yao, Y., Li, K., Lees, R. L. & Heersche, J. N. 2003. The a3 isoform of the 100-kDa V-ATPase subunit is highly but differentially expressed in large (≥10 nuclei) and small (≤ 5 nuclei) osteoclasts. *The Journal of biological chemistry,* 278**,** 49271-49278.

Marahiel, M. A. & Essen, L. O. 2009. Chapter 13: Nonribosomal peptide synthetases: Mechanistic and structural aspects of essential domains. *Methods in enzymology.* Academic Press.

Marahiel, M. A., Stachelhaus, T. & Mootz, H. D. 1997. Modular peptide synthetases involved in nonribosomal peptide synthesis. *Chemical reviews,* 97**,** 2651-2674.

Marchisio, P. C., Bergui, L., Corbascio, G. C., Cremona, O., D'urso, N., Schena, M., Tesio, L. & Caligaris-Cappio, F. 1988. Vinculin, talin, and integrins are localized at specific adhesion sites of malignant B lymphocytes. *Blood,* 72**,** 830-833.

Marieb, E. N., Wilhelm, P. B. & Mallatt, J. 2014. *Human anatomy, 7th edition,* Pearson USA.

Marshansky, V., Ausiello, D. A. & Brown, D. 2002. Physiological importance of endosomal acidification: Potential role in proximal tubulopathies. *Current opinion in nephrology and hypertension,* 11**,** 527-537.

Marshansky, V. & Futai, M. 2008. The V-type H+-ATPase in vesicular trafficking: Targeting, regulation and function. *Current opinion in cell biology,* 20**,** 415-426.

Marshansky, V., Rubinstein, J. L. & Gruber, G. 2014. Eukaryotic V-ATPase: Novel structural findings and functional insights. *Biochimica et biophysica acta (BBA) - general subjects,* 1837**,** 857-879.

Martin, T. 2004. Paracrine regulation of osteoclast formation and activity: Milestones in discovery. *Journal of musculoskeletal and neuronal interactions,* 4**,** 243.

Martinez-Lopez, N., Athonvarangkul, D., Mishall, P., Sahu, S. & Singh, R. 2013. Autophagy proteins regulate ERK phosphorylation. *Nature communications,* 4.

Martinez, A., Kolvek, S. J., Yip, C. L. T., Hopke, J., Brown, K. A., Macneil, I. A. & Osburne, M. S. 2004. Genetically modified bacterial strains and novel bacterial artificial chromosome shuttle vectors for constructing environmental libraries and detecting heterologous natural products in multiple expression hosts. *Applied and environmental microbiology,* 70**,** 2452-2463.

Martini, F. H. & Martini, F. 1992. *Fundamentals of anatomy and physiology, 5th edition,* Prentice Hall USA.

Martins, A., Vieira, H., Gaspar, H. & Santos, S. 2014. Marketed marine natural products in the pharmaceutical and cosmeceutical industries: Tips for success. *Marine drugs,* 12**,** 1066-1101.

Mayer, A., Rodríguez, A., Taglialatela-Scafati, O. & Fusetani, N. 2013. Marine pharmacology in 2009–2011: Marine compounds with antibacterial, antidiabetic, antifungal, anti-inflammatory, antiprotozoal, antituberculosis, and antiviral activities; affecting the immune and nervous systems, and other miscellaneous mechanisms of action. *Marine drugs,* 11**,** 2510-2573.

Mayer, A. M. S. 2014. *Marine pharmaceuticals: The clinical pipeline* [Online]. Available: from http://marinepharmacology.midwestern.edu/clinPipeline.htm [Accessed Last accessed: March 2015 2015].

McClung, M. R., Lewiecki, E. M., Cohen, S. B., Bolognese, M. A., Woodson, G. C., Moffett, A. H., Peacock, M., Miller, P. D., Lederman, S. N. & Chesnut, C. H. 2006. Denosumab in postmenopausal women with low bone mineral density. *New England journal of medicine,* 354**,** 821-831.

McEwan, D G., Popovic, D., Gubas, A., Terawaki, S., Suzuki, H., Stadel, D., Coxon, F. P., de stegmann, M. D., Bhogaraju, S., Maddi, K., Kirchof, A., Gatti, E., Helfrich, M. H., Wakatsuki, S., Behrends, C., Pierre, P. & Dikic, I. 2015. PLEKHM1 regulates autophagosome-lysosome fusion through HOPS complex and LC3/GABARAP proteins. *Molecular cell,* 57**,** 39-54.

McGill, G. G., Horstmann, M., Widlund, H. R., Du, J., Motyckova, G., Nishimura, E. K., Lin, Y.L., Ramaswamy, S., Avery, W. & Ding, H.F. 2002. Bcl2 regulation by the melanocyte master regulator Mitf modulates lineage survival and melanoma cell viability. *Cell,* 109**,** 707-718.

McGivern, J. G. 2006. Targeting N-type and T-type calcium channels for the treatment of pain. *Drug discovery today,* 11**,** 245-253.

McHenry, P., Wang, W. L., Devitt, E., Kluesner, N., Davisson, V. J., Mckee, E., Schweitzer, D., Helquist, P. & Tenniswood, M. 2010. Iejimalides A and B inhibit lysosomal vacuolar H+-ATPase (V-ATPase) activity and induce S-phase arrest and apoptosis in MCF-7 cells. *Journal of cell biochemistry,* 109**,** 634-642.

McHugh, K. P., Hodivala-Dilke, K., Zheng, M. H., Namba, N., Lam, J., Novack, D., Feng, X., Ross, F. P., Hynes, R. O. & Teitelbaum, S. L. 2000. Mice lacking beta3 integrins are osteosclerotic because of dysfunctional osteoclasts. *The Journal of clinical investigation,* 105**,** 433-440.

Mehbub, M. F., Lei, J., Franco, C. & Zhang, W. 2014. Marine sponge derived natural products between 2001 and 2010: Trends and opportunities for discovery of bioactives. *Marine drugs,* 12**,** 4539-4577.

Meier, J. L. & Burkart, M. D. 2009. The chemical biology of modular biosynthetic enzymes. *Chemical society reviews,* 38**,** 2012-2045.

Mellman, I. 1992. The importance of being acid: The role of acidification in intracellular membrane traffic. *The Journal of experimental biology,* 172**,** 39-45.

Menche, D., Arikan, F., Perlova, O., Horstmann, N., Ahlbrecht, W., Wenzel, S. C., Jansen, R., Irschik, H. & MüLler, R. 2008. Stereochemical determination and complex biosynthetic assembly of etnangien, a highly potent RNA polymerase inhibitor from the myxobacterium *Sorangium cellulosum*. *Journal of the American chemical society,* 130**,** 14234-14243.

Menzella, H. G., Reid, R., Carney, J. R., Chandran, S. S., Reisinger, S. J., Patel, K. G., Hopwood, D. A. & Santi, D. V. 2005. Combinatorial polyketide biosynthesis by *de novo* design and rearrangement of modular polyketide synthase genes. *Nature biotechnology,* 23**,** 1171-1176.

Michigami, T., Kageyama, T., Satomura, K., Shima, M., Yamaoka, K., Nakayama, M. & Ozono, K. 2002. Novel mutations in the a3 subunit of vacuolar H+-adenosine triphosphatase in a Japanese patient with infantile malignant osteopetrosis. *Bone,* 30**,** 436-439.

Milat, F. & Ng, K. W. 2009. Is Wnt signalling the final common pathway leading to bone formation? *Molecular and cellular endocrinology,* 310**,** 52-62.

Miller, D. A., Luo, L., Hillson, N., Keating, T. A. & Walsh, C. T. 2002. Yersiniabactin synthetase: A four-protein assembly line producing the nonribosomal peptide/polyketide hybrid siderophore of *Yersinia pestis*. *Chemistry & biology,* 9**,** 333-344.

Miller, S. C., De Saint-Georges, L., Bowman, B. M. & Jee, W. S. 1989. Bone lining cells: Structure and function. *Scanning microscopy,* 3**,** 953-960; discussion 960-951.

Minnikin, D. E., Kremer, L., Dover, L. G. & Besra, G. S. 2002. The methyl-branched fortifications of mycobacterium tuberculosis. *Chemistry & biology,* 9**,** 545-553.

Moffitt, M. C. & Neilan, B. A. 2003. Evolutionary affiliations within the superfamily of ketosynthases reflect complex pathway associations. *Journal of molecular evolution,* 56**,** 446-457.

Montaser, R. & Luesch, H. 2011. Marine natural products: A new wave of drugs? *Future medicinal chemistry,* 3**,** 1475-1489.

Montero, A., Okada, Y., Tomita, M., Ito, M., Tsurukami, H., Nakamura, T., Doetschman, T., Coffin, J. D. & Hurley, M. M. 2000. Disruption of the fibroblast growth factor-2 gene results in decreased bone mass and bone formation. *Journal of clinical investigation,* 105**,** 1085.

Moore, B. S. & Hertweck, C. 2002. Biosynthesis and attachment of novel bacterial polyketide synthase starter units. *Natural product reports,* 19**,** 70-99.

Moss, S. J., Martin, C. J. & Wilkinson, B. 2004. Loss of co-linearity by modular polyketide synthases: A mechanism for the evolution of chemical diversity. *Natural product reports,* 21**,** 575-593.

Mossadegh-Keller, N., Sarrazin, S., Kandalla, P. K., Espinosa, L., Stanley, E. R., Nutt, S. L., Moore, J. & Sieweke, M. H. 2013. M-CSF instructs myeloid lineage fate in single haematopoietic stem cells. *Nature,* 497**,** 239-243.

Munro, M. H., Blunt, J. W., Dumdei, E. J., Hickford, S. J., Lill, R. E., Li, S., Battershill, C. N. & Duckworth, A. R. 1999. The discovery and development of marine compounds with pharmaceutical potential. *Journal of biotechnology,* 70**,** 15-25.

Nakamura, H., Sato, G., Hirata, A. & Yamamoto, T. 2004. Immunolocalization of matrix metalloproteinase-13 on bone surface under osteoclasts in rat tibia. *Bone,* 34**,** 48-56.

Nakamura, I., Takahashi, N., Udagawa, N., Moriyama, Y., Kurokawa, T., Jimi, E., Sasaki, T. & Suda, T. 1997. Lack of vacuolar proton atpase association with the cytoskeleton in osteoclasts of osteosclerotic (*oc/oc*) mice. *FEBS Letters,* 401**,** 207-212.

Nakamura, T., Imai, Y., Matsumoto, T., Sato, S., Takeuchi, K., Igarashi, K., Harada, Y., Azuma, Y., Krust, A. & Yamamoto, Y. 2007. Estrogen prevents bone loss via estrogen receptor α and induction of Fas ligand in osteoclasts. *Cell,* 130**,** 811-823.

Nakashima, K., Zhou, X., Kunkel, G., Zhang, Z., Deng, J. M., Behringer, R. R. & De Crombrugghe, B. 2002. The novel zinc finger-containing transcription factor osterix is required for osteoblast differentiation and bone formation. *Cell,* 108**,** 17-29.

Nakashima, T., Hayashi, M., Fukunaga, T., Kurata, K., Oh-Hora, M., Feng, J. Q., Bonewald, L. F., Kodama, T., Wutz, A. & Wagner, E. F. 2011. Evidence for osteocyte regulation of bone homeostasis through RANKL expression. *Nature medicine,* 17**,** 1231-1234.

NCI 2006. NCI-CRADA opportunity for the development of chondropsin V-ATPase inhibitors. *NCI Technology Transfer Branch*.

Neer, R. M., Arnaud, C. D., Zanchetta, J. R., Prince, R., Gaich, G. A., Reginster, J.Y., Hodsman, A. B., Eriksen, E. F., Ish-Shalom, S., Genant, H. K., Wang, O., Mellström, D., Oefjord, E. S., Marcinowska-Suchowierska, E., Salmi, J., Mulder, H., Halse, J., Sawicki, A. Z. & Mitlak, B. H. 2001. Effect of parathyroid hormone (1-34) on fractures and bone mineral density in postmenopausal women with osteoporosis. *New England journal of medicine,* 344**,** 1434-1441.

Negishi-Koga, T., Shinohara, M., Komatsu, N., Bito, H., Kodama, T., Friedel, R. H. & Takayanagi, H. 2011. Suppression of bone formation by osteoclastic expression of semaphorin 4D. *Nature medicine,* 17**,** 1473-1480.

Nesbitt, S., Nesbit, A., Helfrich, M. & Horton, M. 1993. Biochemical characterization of human osteoclast integrins. Osteoclasts express $\alpha_V\beta_3$, $\alpha_2\beta_1$, and $\alpha v\beta_1$ integrins. *Journal of biological chemistry,* 268**,** 16737-16745.

Nesbitt, S. A. & Horton, M. A. 1997. Trafficking of matrix collagens through bone-resorbing osteoclasts. *Science,* 276**,** 266-269.

Newman, D. & Hill, R. 2006. New drugs from marine microbes: The tide is turning. *Journal of industrial microbiology and biotechnology,* 33**,** 539-544.

Newman, D. J. & Cragg, G. M. 2004. Marine natural products and related compounds in clinical and advanced preclinical trials. *Journal of natural products,* 67**,** 1216-1238.

Newman, D. J. & Cragg, G. M. 2012. Natural products as sources of new drugs over the 30 years from 1981 to 2010. *Journal of natural products,* 75**,** 311-335.

Nguyen, T., Ishida, K., Jenke-Kodama, H., Dittmann, E., Gurgui, C., Hochmuth, T., Taudien, S., Platzer, M., Hertweck, C. & Piel, J. 2008. Exploiting the mosaic structure of trans-acyltransferase polyketide synthases for natural product discovery and pathway dissection. *Nature biotechnololgy,* 26**,** 225-233.

Niikura, K., Nakajima, S., Takano, M. & Yamazaki, H. 2007. FR177995, a novel vacuolar ATPase inhibitor, exerts not only an inhibitory effect on bone destruction but also anti-immunoinflammatory effects in adjuvant-induced arthritic rats. *Bone,* 40**,** 888-894.

Niikura, K., Takano, M. & Sawada, M. 2004. A novel inhibitor of vacuolar ATPase, FR167356, which can discriminate between osteoclast vacuolarATPase and lysosomal vacuolar ATPase. *British journal of pharmacology,* 142**,** 558-566.

Niikura, K., Takeshita, N. & Takano, M. 2005. A vacuolar atpase inhibitor, FR167356, prevents bone resorption in ovariectomized rats with high potency and specificity: Potential for clinical application. *Journal of bone and mineral research,* 20**,** 1579-1588.

Nishi, T. & Forgac, M. 2002. The vacuolar (H+)-ATPases — nature's most versatile proton pumps. *Nature reviews molecular cell biology,* 3**,** 94-103.

Nollet, M., Santucci-Darmanin, S., Breuil, V., Al-Sahlanee, R., Cros, C., Topi, M., Momier, D., Samson, M., Pagnotta, S., Cailleteau, L., Battaglia, S., Farlay, D., Dacquin, R., Barois, N., Jurdic, P., Boivin, G., Heymann, D., Lafont, F., Lu, S. S., Dempster, D. W., Carle, G. F. & Pierrefite-Carle, V. 2014. Autophagy in osteoblasts is involved in mineralization and bone homeostasis. *Autophagy,* 10**,** 1965-1977.

Nyman, J. K. & Vaananen, H. K. 2010. A rationale for osteoclast selectivity of inhibiting the lysosomal V-ATPase a3 isoform. *Calcified tissue international,* 87**,** 273-283.

O'callaghan, K. M., Ayllon, V., O'keeffe, J., Wang, Y., Cox, O. T., Loughran, G., Forgac, M. & O'connor, R. 2010. Heme-binding protein HRG-1 is induced by insulin-like growth factor I and associates with the vacuolar H+-ATPase to control endosomal pH and receptor trafficking. *Journal of biological chemistry,* 285**,** 381-391.

Ochotny, N., Flenniken, A. M., Owen, C., Voronov, I., Zirngibl, R. A., Osborne, L. R., Henderson, J. E., Adamson, S. L., Rossant, J. & Manolson, M. F. 2011. The V–ATPase a3 subunit mutation R740S is dominant negative and results in osteopetrosis in mice. *Journal of bone and mineral research,* 26**,** 1484-1493.

Ochotny, N., Voronov, I., Owen, C., Aubin, J. E. & Manolson, M. F. 2013. The R740S mutation in the V-ATPase a3 subunit results in osteoclast apoptosis and defective early-stage autophagy. *Journal of cellular biochemistry,* 114**,** 2823-2833.

Odvina, C. V., Zerwekh, J. E., Rao, D. S., Maalouf, N., Gottschalk, F. A. & Pak, C. Y. 2005. Severely suppressed bone turnover: A potential complication of alendronate therapy. *Journal of clinical endocrinology and metabolism,* 90**,** 1294-1301.

Ögmundsdóttir, M. H., Heublein, S., Kazi, S., Reynolds, B., Visvalingam, S. M., Shaw, M. K. & Goberdhan, D. C. I. 2012. Proton-assisted amino acid transporter PAT1 complexes with Rag GTPases and activates TORC1 on late endosomal and lysosomal membranes. *Public library of science one,* 7**,** e36616.

Olivera, B. M. 2000. Conotoxin MVIIa: From marine snail venom to analgesic drug. *In:* Fusetani, N. (ed.) *Drugs from the sea.* Karger, Basel.

Orriss, I. R. & Arnett, T. R. 2012. Rodent osteoclast cultures. *Methods in molecular biology,* 816**,** 103-117.

Osteresch, C., Bender, T., Grond, S., Von Zezschwitz, P., Kunze, B., Jansen, R., Huss, M. & Wieczorek, H. 2012. The binding site of the V-ATPase inhibitor apicularen is in the vicinity of those for bafilomycin and archazolid. *The Journal of biological chemistry,* 287**,** 31866-31876.

Ostrov, D. A., Magis, A. T., Wronski, T. J., Chan, E. K., Toro, E. J., Donatelli, R. E., Sajek, K., Haroun, I. N., Nagib, M. I., Piedrahita, A., Harris, A. & Holliday, L. S. 2009. Identification of enoxacin as an inhibitor of osteoclast formation and bone resorption by structure-based virtual screening. *Journal of medicinal chemistry,* 52**,** 5144-5151.

Ott, S. M., Oleksik, A., Lu, Y., Harper, K. & Lips, P. 2002. Bone histomorphometric and biochemical marker results of a 2-year placebo-controlled trial of raloxifene in postmenopausal women. *Journal of bone and mineral research,* 17**,** 341-348.

Otto, F., Thornell, A. P., Crompton, T., Denzel, A., Gilmour, K. C., Rosewell, I. R., Stamp, G. W., Beddington, R. S., Mundlos, S., Olsen, B. R., Selby, P. B. & Owen, M. J. 1997. Cbfa1, a candidate gene for cleidocranial dysplasia syndrome, is essential for osteoblast differentiation and bone development. *Cell,* 89**,** 765-771.

Owegi, M. A., Pappas, D. L., Finch, M. W., Jr., Bilbo, S. A., Resendiz, C. A., Jacquemin, L. J., Warrier, A., Trombley, J. D., Mcculloch, K. M., Margalef, K. L., Mertz,

M. J., Storms, J. M., Damin, C. A. & Parra, K. J. 2006. Identification of a domain in the V0 subunit d that is critical for coupling of the yeast vacuolar proton-translocating ATPase. *The Journal of biological chemistry,* 281**,** 30001-30014.

Page, M. J., Northcote, P. T., Webb, V. L., Mackey, S. & Handley, S. J. 2005. Aquaculture trials for the production of biologically active metabolites in the new zealand sponge *Mycale hentscheli* (Demospongiae: Poecilosclerida). *Aquaculture,* 250**,** 256-269.

Palokangas, H., Mulari, M. & Vaananen, H. 1997. Endocytic pathway from the basal plasma membrane to the ruffled border membrane in bone-resorbing osteoclasts. *Journal of cell science,* 110**,** 1767-1780.

Pantovic, A., Krstic, A., Janjetovic, K., Kocic, J., Harhaji-Trajkovic, L., Bugarski, D. & Trajkovic, V. 2013. Coordinated time-dependent modulation of AMPK/Akt/mTOR signaling and autophagy controls osteogenic differentiation of human mesenchymal stem cells. *Bone,* 52**,** 524-531.

Parfitt, A. 1982. The coupling of bone formation to bone resorption: A critical analysis of the concept and of its relevance to the pathogenesis of osteoporosis. *Metabolic bone disease and related research,* 4**,** 1-6.

Parfitt, A. M. 2000. The mechanism of coupling: A role for the vasculature. *Bone,* 26**,** 319-323.

Parsley, L. C., Linneman, J., Goode, A. M., Becklund, K., George, I., Goodman, R. M., Lopanik, N. B. & Liles, M. R. 2011. Polyketide synthase pathways identified from a metagenomic library are derived from soil *Acidobacteria*. *FEMS Microbiology ecology,* 78**,** 176-187.

Pastor-Soler, N., Beaulieu, V., Litvin, T. N., Da Silva, N., Chen, Y., Brown, D., Buck, J., Levin, L. R. & Breton, S. 2003. Bicarbonate-regulated adenylyl cyclase (sAC) is a sensor that regulates pH-dependent V-ATPase recycling. *The Journal of biological chemistry,* 278**,** 49523-49529.

Paul, V. J., Ritson-Williams, R. & Sharp, K. 2011. Marine chemical ecology in benthic environments. *Natural product reports,* 28**,** 345-387.

Pawlik, J. R., Mcfall, G. & Zea, S. 2002. Does the odor from sponges of the genus ircinia protect them from fish predators? *Journal of chemical ecology,* 28**,** 1103-1115.

Pederson, L., Ruan, M., Westendorf, J. J., Khosla, S. & Oursler, M. J. 2008. Regulation of bone formation by osteoclasts involves Wnt/Bmp signaling and the chemokine sphingosine-1-phosphate. *Proceedings of the national academy of sciences of the United States of America,* 105**,** 20764-20769.

Pérez-Sayáns, M., Somoza-Martín, J. M., Barros-Angueira, F., Rey, J. M. G. & García-García, A. 2009. V-ATPase inhibitors and implication in cancer treatment. *Cancer treatment reviews,* 35**,** 707-713.

Perry, N. B., Blunt, J. W., Munro, M. H. G. & Pannell, L. K. 1988. Mycalamide A, an antiviral compound from a New Zealand sponge of the genus *Mycale*. *Journal of the American chemical society,* 110**,** 4850-4851.

Peters, C., Bayer, M. J., Buhler, S., Andersen, J. S., Mann, M. & Mayer, A. 2001. Trans-complex formation by proteolipid channels in the terminal phase of membrane fusion. *Nature,* 409**,** 581-588.

Pettit, G. R., Xu, J. P., Chapuis, J. C., Pettit, R. K., Tackett, L. P., Doubek, D. L., Hooper, J. N. & Schmidt, J. M. 2004. Antineoplastic agents. 520. Isolation and structure of irciniastatins A and B from the Indo-Pacific marine sponge *Ircinia ramosa*. *Journal of medical chemistry,* 47**,** 1149-1152.

Piel, J. 2002. A polyketide synthase-peptide synthetase gene cluster from an uncultured bacterial symbiont of *Paederus* beetles. *Proceedings of the national academy of sciences of the United States of America,* 99**,** 14002-14007.

Piel, J. 2006. Bacterial symbionts: Prospects for the sustainable production of invertebrate-derived pharmaceuticals. *Current medicinal chemistry,* 13**,** 39-50.

Piel, J. 2010. Biosynthesis of polyketides by *trans*-AT polyketide synthases. *Natural product reports,* 27**,** 996-1047.

Piel, J. 2011. Approaches to capturing and designing biologically active small molecules produced by uncultured microbes. *Annual review of microbiology,* 65**,** 431-453.

Piel, J., Hui, D., Wen, G., Butzke, D., Platzer, M., Fusetani, N. & Matsunaga, S. 2004. Antitumor polyketide biosynthesis by an uncultivated bacterial symbiont of the marine sponge *Theonella swinhoei*. *Proceedings of the national academy of sciences of the United States of America,* 101**,** 16222-16227.

Pietrement, C., Sun-Wada, G., Da Silva, N., Mckee, M., Marshansky, V., Brown, D., Futai, M. & Breton, S. 2006. Distinct expression patterns of different subunit isoforms of the V-ATPase in the rat epididymis. *Biology of reproduction,* 74**,** 185-194.

Pimentel-Elardo, S. M., Grozdanov, L., Proksch, S. & Hentschel, U. 2012. Diversity of nonribosomal peptide synthetase genes in the microbial metagenomes of marine sponges. *Marine drugs,* 10**,** 1192-1202.

Pixley, F. J. & Stanley, E. R. 2004. Csf-1 regulation of the wandering macrophage: Complexity in action. *Trends in cell biology,* 14**,** 628-638.

Poole, K. E., Van Bezooijen, R. L., Loveridge, N., Hamersma, H., Papapoulos, S. E., Lowik, C. W. & Reeve, J. 2005. Sclerostin is a delayed secreted product of osteocytes that inhibits bone formation. The *FASEB journal,* 19**,** 1842-1844.

Proksch, P. 1994. Defensive roles for secondary metabolites from marine sponges and sponge-feeding nudibranchs. *Toxicon,* 32**,** 639-655.

Proksch, P., Ebel, R., Edrada, R., Wray, V. & Steube, K. 2003a. Bioactive natural products from marine invertebrates and associated fungi. *Sponges (porifera).* Springer, USA.

Proksch, P., Edrada-Ebel, R. & Ebel, R. 2003b. Drugs from the sea - opportunities and obstacles. *Marine drugs,* 1**,** 5-17.

Proksch, P., Edrada, R. & Ebel, R. 2002. Drugs from the seas – current status and microbiological implications. *Applied microbiology and biotechnology,* 59**,** 125-134.

Qin, A., Cheng, T. S., Lin, Z., Cao, L., Chim, S. M., Pavlos, N. J., Xu, J., Zheng, M. H. & Dai, K. R. 2012a. Prevention of wear particle-induced osteolysis by a novel V-ATPase inhibitor saliphenylhalamide through inhibition of osteoclast bone resorption. *Public library of science one,* 7**,** e34132.

Qin, A., Cheng, T. S., Lin, Z., Pavlos, N. J., Jiang, Q., Xu, J., Dai, K. R. & Zheng, M. H. 2011. Versatile roles of V-ATPases accessory subunit Ac45 in osteoclast formation and function. *Public library of science one,* 6**,** e27155.

Qin, A., Cheng, T. S., Pavlos, N. J., Lin, Z., Dai, K. R. & Zheng, M. H. 2012b. V-ATPases in osteoclasts: Structure, function and potential inhibitors of bone resorption. *The International journal of biochemistry & cell biology,* 44**,** 1422-1435.

Quince, C., Lanzen, A., Curtis, T. P., Davenport, R. J., Hall, N., Head, I. M., Read, L. F. & Sloan, W. T. 2009. Accurate determination of microbial diversity from 454 pyrosequencing data. *Nature methods,* 6**,** 639-641.

Rashid, M. A., Cantrell, C. L., Gustafson, K. R. & Boyd, M. R. 2001a. Chondropsin D, a new 37-membered-ring macrolide lactam from the marine sponge *Chondropsis* species. *Journal of natural products,* 64**,** 1341-1344.

Rashid, M. A., Gustafson, K. R. & Boyd, M. R. 2001b. New chondropsin macrolide lactams from marine sponges in the genus *Ircinia*. *Tetrahedron letters,* 42**,** 1623-1626.

Rath, C. M., Janto, B., Earl, J., Ahmed, A., Hu, F. Z., Hiller, L., Dahlgren, M., Kreft, R., Yu, F., Wolff, J. J., Kweon, H. K., Christiansen, M. A., Håkansson, K., Williams, R. M., Ehrlich, G. D. & Sherman, D. H. 2011. Meta-omic characterization of the

marine invertebrate microbial consortium that produces the chemotherapeutic natural product ET-743. *ACS Chemical Biology,* 6**,** 1244-1256.

Rath, S., Liebl, J., Fürst, R., Vollmar, A. & Zahler, S. 2014. Regulation of endothelial signaling and migration by V-ATPase. *Angiogenesis,* 17**,** 587-601.

Rawlings, B. J. 1998. Biosynthesis of fatty acids and related metabolites. *Natural product reports,* 15**,** 275-308.

Ricciardi, A. & Bourget, E. 1998. Weight-to-weight conversion factors for marine benthic macroinvertebrates. *Marine ecology progress series,* 163**,** 245-251.

Rice, P., Longden, I. & Bleasby, A. 2000. EMBOSS: The European molecular biology open software suite. *Trends in genetics,* 16**,** 276-277.

Robainac, R., De Diegoc, F., Popova, S. & Stefanova, K. 2002. Lipid composition of the sponge *Verongia aerophoba* from the canary islands. *European journal of lipid science and technology,* 104**,** 800-807.

Robledo, R. F., Rajan, L., Li, X. & Lufkin, T. 2002. The Dlx5 and Dlx6 homeobox genes are essential for craniofacial, axial, and appendicular skeletal development. *Genes and development,* 16**,** 1089-1101.

Robling, A. G., Castillo, A. B. & Turner, C. H. 2006. Biomechanical and molecular regulation of bone remodeling. *Annual review of biomedical engineering,* 8**,** 455-498.

Rodriguez, E., Menzella, H. G. & Gramajo, H. 2009. Heterologous production of polyketides in bacteria. *Methods in enzymology,* 459**,** 339-365.

Rondon, M. R., August, P. R., Bettermann, A. D., Brady, S. F., Grossman, T. H., Liles, M. R., Loiacono, K. A., Lynch, B. A., Macneil, I. A., Minor, C., Tiong, C. L., Gilman, M., Osburne, M. S., Clardy, J., Handelsman, J. & Goodman, R. M. 2000. Cloning the soil metagenome: A strategy for accessing the genetic and functional diversity of uncultured microorganisms. *Applied and environmental microbiology,* 66**,** 2541-2547.

Ross, A. C., Gulland, L. E. S., Dorrestein, P. C. & Moore, B. S. 2014. Targeted capture and heterologous expression of the *Pseudoalteromonas* alterochromide gene cluster in *Escherichia coli* represents a promising natural product exploratory platform. *ACS Synthetic Biology,* 4, 414-420

Ross, F. P. & Teitelbaum, S. L. 2005. Avβ3 and macrophage colony-stimulating factor: Partners in osteoclast biology. *Immunological reviews,* 208**,** 88-105.

Ruiz, C., Valderrama, K., Zea, S. & Castellanos, L. 2013. Mariculture and natural production of the antitumoural (+)-discodermolide by the caribbean marine sponge *Discodermia dissoluta*. *Marine biotechnology,* 15**,** 571-583.

Ryu, J., Kim, H., Lee, S. K., Chang, E. J., Kim, H. J. & Kim, H. H. 2005. Proteomic identification of the TRAF6 regulation of vacuolar ATPase for osteoclast function. *Proteomics,* 5**,** 4152-4160.

Ryu, J., Kim, H. J., Chang, E. J., Huang, H., Banno, Y. & Kim, H. H. 2006. Sphingosine 1-phosphate as a regulator of osteoclast differentiation and osteoclast–osteoblast coupling. *The EMBO journal,* 25**,** 5840-5851.

Sahara, T., Itoh, K., Debari, K. & Sasaki, T. 2003. Specific biological functions of vacuolar-type H+-ATPase and lysosomal cysteine proteinase, cathepsin K, in osteoclasts. *The Anatomical record part A: Discoveries in molecular, cellular, and evolutionary biology,* 270A**,** 152-161.

Sahara, T. & Sasaki, T. 2001. Effects of brefeldin-A: Potent inhibitor of intracellular protein transport on ultrastructure and resorptive function of cultured osteoclasts. *The Anatomical record,* 263**,** 127-138.

Saika, M., Inoue, D., Kido, S. & Matsumoto, T. 2001. 17beta-estradiol stimulates expression of osteoprotegerin by a mouse stromal cell line, ST-2, via estrogen receptor-alpha. *Endocrinology,* 142**,** 2205-2212.

Saitou, N. & Nei, M. 1987. The Neighbor-Joining method: A new method for reconstructing phylogenetic trees. *Molecular biology and evolution,* 4**,** 406-425.

Sakagami, N., Amizuka, N., Li, M., Takeuchi, K., Hoshino, M., Nakamura, M., Nozawa-Inoue, K., Udagawa, N. & Maeda, T. 2005. Reduced osteoblastic population and defective mineralization in osteopetrotic (*op/op*) mice. *Micron,* 36**,** 688-695.

Salo, J., Lehenkari, P., Mulari, M., Metsikko, K. & Vaananen, H. K. 1997. Removal of osteoclast bone resorption products by transcytosis. *Science,* 276**,** 270-273.

Sambrook, J. 2001. *Molecular cloning : A laboratory manual, 3rd edition*, Cold Spring Harbor Laboratory, New York.

Sanchez, C. P. & He, Y. Z. 2009. Bone growth during rapamycin therapy in young rats. *BMC pediatrics,* 9**,** 3.

Sanger, F., Nicklen, S. & Coulson, A. R. 1977. DNA sequencing with chain-terminating inhibitors. *Proceedings of the national academy of sciences of the United States of America,* 74**,** 5463-5467.

Schirmer, A., Gadkari, R., Reeves, C. D., Ibrahim, F., Delong, E. F. & Hutchinson, C. R. 2005. Metagenomic analysis reveals diverse polyketide synthase gene clusters in microorganisms associated with the marine sponge *Discodermia dissoluta*. *Applied environmental microbiology,* 71**,** 4840-4849.

Schmidt, E. W., Nelson, J. T., Rasko, D. A., Sudek, S., Eisen, J. A., Haygood, M. G. & Ravel, J. 2005. Patellamide A and C biosynthesis by a microcin-like pathway in *Prochloron didemni*, the cyanobacterial symbiont of *Lissoclinum patella*. *Proceedings of the national academy of sciences of the United States of America,* 102**,** 7315-7320.

Schmitt, S., Tsai, P., Bell, J., Fromont, J., Ilan, M., Lindquist, N., Perez, T., Rodrigo, A., Schupp, P. J., Vacelet, J., Webster, N., Hentschel, U. & Taylor, M. W. 2012. Assessing the complex sponge microbiota: Core, variable and species-specific bacterial communities in marine sponges. *The ISME journal,* 6**,** 564-576.

Schofield, M. M. & Sherman, D. H. 2013. Meta-omic characterization of prokaryotic gene clusters for natural product biosynthesis. *Current opinion in biotechnology,* 24**,** 1151-1158.

Schwarzer, D., Finking, R. & Marahiel, M. A. 2003. Nonribosomal peptides: From genes to products. *Natural product reports,* 20**,** 275-287.

Scimeca, J. C., Franchi, A., Trojani, C., Parrinello, H., Grosgeorge, J., Robert, C., Jaillon, O., Poirier, C., Gaudray, P. & Carle, G. F. 2000. The gene encoding the mouse homologue of the human osteoclast-specific 116-kDa V-ATPase subunit bears a deletion in osteosclerotic (*oc/oc*) mutants. *Bone,* 26**,** 207-213.

Scott, B. B. & Chapman, C. G. 1998. The putative 116 kDa osteoclast specific vacuolar proton pump subunit has ubiquitous tissue distribution. *European journal of pharmacology,* 346**,** R3-R4.

Seeman, E. 2003. Invited review: Pathogenesis of osteoporosis. *Journal of applied physiology,* 95**,** 2142-2151.

Seeman, E. & Delmas, P. D. 2006. Bone quality — the material and structural basis of bone strength and fragility. *New England journal of medicine,* 354**,** 2250-2261.

Segovia-Silvestre, T., Neutzsky-Wulff, A. V., Sorensen, M. G., Christiansen, C., Bollerslev, J., Karsdal, M. A. & Henriksen, K. 2009. Advances in osteoclast biology resulting from the study of osteopetrotic mutations. *Human genetics,* 124**,** 561-577.

Seifert, M. F. & Marks, S. C., Jr. 1985. Morphological evidence of reduced bone resorption in the osteosclerotic (oc) mouse. *The American journal of anatomy,* 172**,** 141-153.

Seletsky, B. M., Wang, Y., Hawkins, L. D., Palme, M. H., Habgood, G. J., Dipietro, L. V., Towle, M. J., Salvato, K. A., Wels, B. F., Aalfs, K. K., Kishi, Y., Littlefield, B. A. & Yu, M. J. 2004. Structurally simplified macrolactone analogues of halichondrin B. *Bioorganic & medicinal chemistry letters,* 14**,** 5547-5550.

Sennoune, S. R., Bakunts, K., Martínez, G. M., Chua-Tuan, J. L., Kebir, Y., Attaya, M. N. & Martínez-Zaguilán, R. 2004. Vacuolar H+-ATPase in human breast cancer cells with distinct metastatic potential: Distribution and functional activity. *American journal of physiology-cell physiology,* 286**,** C1443-C1452.

Sethi, N., Yan, Y., Quek, D., Schupbach, T. & Kang, Y. 2010. Rabconnectin-3 is a functional regulator of mammalian Notch signaling. *Journal of biological chemistry,* 285**,** 34757-34764.

Settembre, C., Zoncu, R., Medina, D. L., Vetrini, F., Erdin, S., Erdin, S., Huynh, T., Ferron, M., Karsenty, G., Vellard, M. C., Facchinetti, V., Sabatini, D. M. & Ballabio, A. 2012. A lysosome-to-nucleus signalling mechanism senses and regulates the lysosome via mTOR and TFEB. *The EMBO journal,* 31, 1095-1108

Shao, E., Nishi, T., Kawasaki-Nishi, S. & Forgac, M. 2003. Mutational analysis of the non-homologous region of subunit a of the yeast V-ATPase. *The Journal of biological chemistry,* 278**,** 12985-12991.

Shen, B., Du, L., Sanchez, C., Chen, M. & Edwards, D. J. 1999. Bleomycin biosynthesis in *Streptomyces verticillus*: A model of hybrid peptide and polyketide biosynthesis. *Bioorganic chemistry,* 27**,** 155-171.

Shen, S.L., Chen, X.P., Zhang, X.F., Miao, J.Y. & Zhao, B.X. 2015. A rhodamine b-based lysosomal pH probe. *Journal of Materials Chemistry B,* 3**,** 919-925.

Shoemaker, R. H. 2006. The NCI60 human tumour cell line anticancer drug screen. *Nature reviews cancer,* 6**,** 813-823.

Shum, W. W., Da Silva, N., Brown, D. & Breton, S. 2009. Regulation of luminal acidification in the male reproductive tract via cell–cell crosstalk. *Journal of experimental biology,* 212**,** 1753-1761.

Siegl, A. & Hentschel, U. 2009. PKS and NRPS gene clusters from microbial symbiont cells of marine sponges by whole genome amplification. *Environmental Microbiology reports,* 2**,** 507-513.

Siegl, A., Kamke, J., Hochmuth, T., Piel, J., Richter, M., Liang, C., Dandekar, T. & Hentschel, U. 2011. Single-cell genomics reveals the lifestyle of *Poribacteria*, a candidate phylum symbiotically associated with marine sponges. *The ISME journal,* 5**,** 61-70.

Silakowski, B., Nordsiek, G., Kunze, B., Blöcker, H. & Müller, R. 2001. Novel features in a combined polyketide synthase/non-ribosomal peptide synthetase: The myxalamid biosynthetic gene cluster of the myxobacterium *Stigmatella aurantiaca*. *Chemistry & biology,* 8**,** 59-69.

Simmons, T. L., Coates, R. C., Clark, B. R., Engene, N., Gonzalez, D., Esquenazi, E., Dorrestein, P. C. & Gerwick, W. H. 2008. Biosynthetic origin of natural products

isolated from marine microorganism–invertebrate assemblages. *Proceedings of the national academy of sciences of the United States of America,* 105**,** 4587-4594.

Simonet, W., Lacey, D., Dunstan, C., Kelley, M., Chang, M.-S., Lüthy, R., Nguyen, H., Wooden, S., Bennett, L. & Boone, T. 1997. Osteoprotegerin: A novel secreted protein involved in the regulation of bone density. *Cell,* 89**,** 309-319.

Sims, N. A. 2010. Ephs and ephrins: Many pathways to regulate osteoblasts and osteoclasts. *IBMS BoneKEy,* 7**,** 304-313.

Sims, N. A. & Gooi, J. H. 2008. Bone remodeling: Multiple cellular interactions required for coupling of bone formation and resorption. *Seminars in cell & developmental biology,* 19**,** 444-451.

Sims, N. A. & Martin, T. J. 2014. Coupling the activities of bone formation and resorption: A multitude of signals within the basic multicellular unit. *BoneKEy Reports,* 3.

Sipkema, D., Osinga, R., Schatton, W., Mendola, D., Tramper, J. & Wijffels, R. H. 2005. Large-scale production of pharmaceuticals by marine sponges: Sea, cell, or synthesis? *Biotechnology and bioengineering,* 90**,** 201-222.

Sirakova, T. D., Thirumala, A. K., Dubey, V. S., Sprecher, H. & Kolattukudy, P. E. 2001. The mycobacterium tuberculosis Pks2 gene encodes the synthase for the hepta- and octamethyl-branched fatty acids required for sulfolipid synthesis. *The Journal of biological chemistry,* 276**,** 16833-16839.

Smardon, A. M., Diab, H. I., Tarsio, M., Diakov, T. T., Nasab, N. D., West, R. W. & Kane, P. M. 2014. The RAVE complex is an isoform-specific V-ATPase assembly factor in yeast. *Molecular biology of the cell,* 25**,** 356-367.

Smink, J. J., Tunn, P. U. & Leutz, A. 2012. Rapamycin inhibits osteoclast formation in giant cell tumor of bone through the C/EBPβ - MafB axis. *Journal of molecular medicine (Berlin, Germany),* 90**,** 25-30.

Smith, A. B., 3rd, Risatti, C. A., Atasoylu, O., Bennett, C. S., Liu, J., Cheng, H., Tendyke, K. & Xu, Q. 2011. Design, synthesis, and biological evaluation of diminutive forms of (+)-spongistatin 1: Lessons learned. *Journal of the American chemical society,* 133**,** 14042-14053.

Smith, A. N., Borthwick, K. J. & Karet, F. E. 2002. Molecular cloning and characterization of novel tissue-specific isoforms of the human vacuolar H+-ATPase C, G and d subunits, and their evaluation in autosomal recessive distal renal tubular acidosis. *Gene,* 297**,** 169-177.

Smith, A. N., Jouret, F., Bord, S., Borthwick, K. J., Al-Lamki, R. S., Wagner, C. A., Ireland, D. C., Cormier-Daire, V., Frattini, A. & Villa, A. 2005. Vacuolar H+-

ATPase d2 subunit: Molecular characterization, developmental regulation, and localization to specialized proton pumps in kidney and bone. *Journal of the American society of nephrology,* 16**,** 1245-1256.

Smith, A. N., Skaug, J., Choate, K. A., Nayir, A., Bakkaloglu, A., Ozen, S., Hulton, S. A., Sanjad, S. A., Al-Sabban, E. A. & Lifton, R. P. 2000. Mutations in Atp6n1b, encoding a new kidney vacuolar proton pump 116-kDa subunit, cause recessive distal renal tubular acidosis with preserved hearing. *Nature genetics,* 26**,** 71-75.

Smith, S. & Tsai, S.C. 2007. The type I fatty acid and polyketide synthases: A tale of two megasynthases. *Natural product reports,* 24**,** 1041-1072.

Sobacchi, C., Frattini, A., Guerrini, M. M., Abinun, M., Pangrazio, A., Susani, L., Bredius, R., Mancini, G., Cant, A. & Bishop, N. 2007. Osteoclast-poor human osteopetrosis due to mutations in the gene encoding RANKL. *Nature genetics,* 39**,** 960-962.

Sogin, M. L., Morrison, H. G., Huber, J. A., Welch, D. M., Huse, S. M., Neal, P. R., Arrieta, J. M. & Herndl, G. J. 2006. Microbial diversity in the deep sea and the underexplored "rare biosphere". *Proceedings of the national academy of sciences of the United States of America,* 103**,** 12115-12120.

Sørensen, H. P. & Mortensen, K. K. 2005. Advanced genetic strategies for recombinant protein expression in escherichia coli. *Journal of biotechnology,* 115**,** 113-128.

Sorensen, M. G., Henriksen, K., Neutzsky-Wulff, A. V., Dziegiel, M. H. & Karsdal, M. A. 2007. Diphyllin, a novel and naturally potent V-ATPase inhibitor, abrogates acidification of the osteoclastic resorption lacunae and bone resorption. *Journal of bone and mineral research,* 22**,** 1640-1648.

Soriano, P., Montgomery, C., Geske, R. & Bradley, A. 1991. Targeted disruption of the *c-src* proto-oncogene leads to osteopetrosis in mice. *Cell,* 64**,** 693-702.

Srivastava, S., Toraldo, G., Weitzmann, M. N., Cenci, S., Ross, F. P. & Pacifici, R. 2001. Estrogen decreases osteoclast formation by down-regulating receptor activator of NF-κB ligand (RANKL)-induced JNK activation. *Journal of biological chemistry,* 276**,** 8836-8840.

Stachelhaus, T., Mootz, H. D. & Marahiel, M. A. 1999. The specificity-conferring code of adenylation domains in nonribosomal peptide synthetases. *Chemistry & biology,* 6**,** 493-505.

Stanislaus, D., Yang, X., Liang, J. D., Wolfe, J., Cain, R. L., Onyia, J. E., Falla, N., Marder, P., Bidwell, J. P., Queener, S. W. & Hock, J. M. 2000. *In vivo* regulation of apoptosis in metaphyseal trabecular bone of young rats by synthetic human parathyroid hormone (1-34) fragment. *Bone,* 27**,** 209-218.

Starcevic, A., Zucko, J., Simunkovic, J., Long, P. F., Cullum, J. & Hranueli, D. 2008. Clustscan: An integrated program package for the semi-automatic annotation of modular biosynthetic gene clusters and *in silico* prediction of novel chemical structures. *Nucleic acids research,* 36**,** 6882-6892.

Staunton, J., Caffrey, P., Aparicio, J. F., Roberts, G. A., Bethell, S. S. & Leadlay, P. F. 1996. Evidence for a double-helical structure for modular polyketide synthases. *Nature Structural & Molecular Biology,* 3**,** 188-192.

Staunton, J. & Weissman, K. J. 2001. Polyketide biosynthesis: A millennium review. *Natural product reports,* 18**,** 380-416.

Strasser, B., Iwaszkiewicz, J., Michielin, O. & Mayer, A. 2011. The V-ATPase proteolipid cylinder promotes the lipid-mixing stage of SNARE-dependent fusion of yeast vacuoles. *The EMBO journal,* 30**,** 4126-4141.

Suda, T., Takahashi, N., Udagawa, N., Jimi, E., Gillespie, M. T. & Martin, T. J. 1999. Modulation of osteoclast differentiation and function by the new members of the tumor necrosis factor receptor and ligand families. *Endocrine Reviews,* 20**,** 345-357.

Sudek, S., Lopanik, N. B., Waggoner, L. E., Hildebrand, M., Anderson, C., Liu, H., Patel, A., Sherman, D. H. & Haygood, M. G. 2007. Identification of the putative bryostatin polyketide synthase gene cluster from "*Candidatus Endobugula sertula*", the uncultivated microbial symbiont of the marine bryozoan *Bugula neritina*. *Jouranal of natural products,* 70**,** 67-74.

Sun-Wada, G.H., Tabata, H., Kawamura, N., Futai, M. & Wada, Y. 2007. Differential expression of a subunit isoforms of the vacuolar-type proton pump ATPase in mouse endocrine tissues. *Cell and Tissue Research,* 329**,** 239-248.

Sun-Wada, G. H., Imai-Senga, Y., Yamamoto, A., Murata, Y., Hirata, T., Wada, Y. & Futai, M. 2002. A proton pump atpase with testis-specific E1-subunit isoform required for acrosome acidification. *The Journal of biological chemistry,* 277**,** 18098-18105.

Sun-Wada, G. H., Murata, Y., Namba, M., Yamamoto, A., Wada, Y. & Futai, M. 2003. Mouse proton pump ATPase C subunit isoforms (C2-a and C2-b) specifically expressed in kidney and lung. *The Journal of biological chemistry,* 278**,** 44843-44851.

Sun-Wada, G. H., Toyomura, T., Murata, Y., Yamamoto, A., Futai, M. & Wada, Y. 2006. The a3 isoform of V-ATPase regulates insulin secretion from pancreatic beta-cells. *Journal of cell Science,* 119**,** 4531-4540.

Sunagawa, S., Woodley, C. M. & Medina, M. 2010. Threatened corals provide underexplored microbial habitats. *Public library of science one,* 5**,** e9554.

Sundquist, K., Lakkakorpi, P., Wallmark, B. & Vaananen, K. 1990. Inhibition of osteoclast proton transport by bafilomycin A1 abolishes bone resorption. *Biochemical and biophysical research communications,* 168**,** 309-313.

Sundquist, K. T. & Marks, S. C., Jr. 1994. Bafilomycin A1 inhibits bone resorption and tooth eruption *in vivo*. *Journal of bone and mineral research,* 9**,** 1575-1582.

Takayanagi, H., Kim, S., Koga, T., Nishina, H., Isshiki, M., Yoshida, H., Saiura, A., Isobe, M., Yokochi, T., Inoue, J., Wagner, E. F., Mak, T. W., Kodama, T. & Taniguchi, T. 2002. Induction and activation of the transcription factor NFATc1 (NFAT2) integrate RANKL signaling in terminal differentiation of osteoclasts. *Developmental cell,* 3**,** 889-901.

Takeshita, S., Fumoto, T., Matsuoka, K., Park, K.A., Aburatani, H., Kato, S., Ito, M. & Ikeda, K. 2013. Osteoclast-secreted CTHRC1 in the coupling of bone resorption to formation. *The Journal of clinical investigation,* 123**,** 3914-3924.

Tamura, K., Stecher, G., Peterson, D., Filipski, A. & Kumar, S. 2013. MEGA6: Molecular evolutionary genetics analysis version 6.0. *Molecular biology and evolution,* 30**,** 2725-2729.

Tang, Y., Kim, C. Y., Mathews, Ii, Cane, D. E. & Khosla, C. 2006. The 2.7-angstrom crystal structure of a 194-kDa homodimeric fragment of the 6-deoxyerythronolide B synthase. *Proceedings of the national academy of sciences of the United States of America,* 103**,** 11124-11129.

Tang, Y., Wu, X., Lei, W., Pang, L., Wan, C., Shi, Z., Zhao, L., Nagy, T. R., Peng, X., Hu, J., Feng, X., Van Hul, W., Wan, M. & Cao, X. 2009. TGF-β1-induced migration of bone mesenchymal stem cells couples bone resorption with formation. *Nature medicine,* 15**,** 757-765.

Tatsuno, S., Arakawa, K. & Kinashi, H. 2007. Analysis of modular-iterative mixed biosynthesis of lankacidin by heterologous expression and gene fusion. *Journal of antibiotics,* 60**,** 700-708.

Taylor, M. W., Radax, R., Steger, D. & Wagner, M. 2007a. Sponge-associated microorganisms: Evolution, ecology, and biotechnological potential. *Microbiology and molecular biology reviews,* 71**,** 295-347.

Teitelbaum, S. L. & Ross, F. P. 2003. Genetic regulation of osteoclast development and function. *Nature reviews genetics,* 4**,** 638-649.

Terlau, H. & Olivera, B. M. 2004. Conus venoms: A rich source of novel ion channel-targeted peptides. *Physiological reviews,* 84**,** 41-68.

Tesch, W., Vandenbos, T., Roschgr, P., Fratzl-Zelman, N., Klaushofer, K., Beertsen, W. & Fratzl, P. 2003. Orientation of mineral crystallites and mineral density during

skeletal development in mice deficient in tissue nonspecific alkaline phosphatase. *Journal of bone and mineral research,* 18**,** 117-125.

Teti, A., Blair, H., Teitelbaum, S., Kahn, J., Carano, A., Grano, M., Santacroce, G., Schlesinger, P. & Zambonin, Z. A. 1989. Cytoplasmic pH is regulated in isolated avian osteoclasts by a Cl-/HCO3-exchanger. *Bollettino della societa Italiana di biologia sperimentale,* 65**,** 589-595.

Thiel, V., Blumenberg, M., Hefter, J., Pape, T., Pomponi, S., Reed, J., Reitner, J., Wörheide, G. & Michaelis, W. 2002. A chemical view of the most ancient metazoa–biomarker chemotaxonomy of Hexactinellid sponges. *Naturwissenschaften,* 89**,** 60-66.

Thiel, V., Jenisch, A., Wörheide, G., Löwenberg, A., Reitner, J. & Michaelis, W. 1999. Mid-chain branched alkanoic acids from "living fossil" demosponges: A link to ancient sedimentary lipids? *Organic Geochemistry,* 30**,** 1-14.

Thomas, T., Rusch, D., Demaere, M. Z., Yung, P. Y., Lewis, M., Halpern, A., Heidelberg, K. B., Egan, S., Steinberg, P. D. & Kjelleberg, S. 2010. Functional genomic signatures of sponge bacteria reveal unique and shared features of symbiosis. *The ISME journal,* 4**,** 1557-1567.

Thudium, C. S., Jensen, V. K., Karsdal, M. A. & Henriksen, K. 2012. Disruption of the V-ATPase functionality as a way to uncouple bone formation and resorption - a novel target for treatment of osteoporosis. *Current protein & peptide science,* 13**,** 141-151.

Toei, M., Saum, R. & Forgac, M. 2010. Regulation and isoform function of the V-ATPases. *Biochemistry,* 49**,** 4715-4723.

Tolar, J., Teitelbaum, S. L. & Orchard, P. J. 2004. Osteopetrosis. *New England journal of medicine,* 351**,** 2839-2849.

Tondravi, M. M., Mckercher, S. R., Anderson, K., Erdmann, J. M., Quiroz, M., Maki, R. & Teitelbaum, S. L. 1997. Osteopetrosis in mice lacking haematopoietic transcription factor PU.1. *Nature,* 386**,** 81-84.

Toro, E. J., Ostrov, D. A., Wronski, T. J. & Holliday, L. S. 2012a. Rational identification of enoxacin as a novel V-ATPase-directed osteoclast inhibitor. *Current protein & peptide science,* 13**,** 180-191.

Toro, E. J., Zuo, J., Ostrov, D. A., Catalfamo, D., Bradaschia-Correa, V., Arana-Chavez, V., Caridad, A. R., Neubert, J. K., Wronski, T. J., Wallet, S. M. & Holliday, L. S. 2012b. Enoxacin directly inhibits osteoclastogenesis without inducing apoptosis. *The Journal of biological chemistry,* 287**,** 17894-17904.

Towle, M. J., Salvato, K. A., Budrow, J., Wels, B. F., Kuznetsov, G., Aalfs, K. K., Welsh, S., Zheng, W., Seletsky, B. M., Palme, M. H., Habgood, G. J., Singer, L.

A., Dipietro, L. V., Wang, Y., Chen, J. J., Quincy, D. A., Davis, A., Yoshimatsu, K., Kishi, Y., Yu, M. J. & Littlefield, B. A. 2001. *In vitro* and *in vivo* anticancer activities of synthetic macrocyclic ketone analogues of halichondrin B. *Cancer research,* 61**,** 1013-1021.

Toyomura, T., Murata, Y., Yamamoto, A., Oka, T., Sun-Wada, G. H., Wada, Y. & Futai, M. 2003. From lysosomes to the plasma membrane: Localization of vacuolar-type H+-ATPase with the a3 isoform during osteoclast differentiation. *The Journal of biological chemistry,* 278**,** 22023-22030.

Toyomura, T., Oka, T., Yamaguchi, C., Wada, Y. & Futai, M. 2000. Three subunit a isoforms of mouse vacuolar H+-ATPase: Preferential expression of the a3 isoform during osteoclast differentiation. *Journal of biological chemistry,* 275**,** 8760-8765.

Trincone, A. 2011. Marine biocatalysts: Enzymatic features and applications. *Marine drugs,* 9**,** 478-499.

Tringe, S. G., Von Mering, C., Kobayashi, A., Salamov, A. A., Chen, K., Chang, H. W., Podar, M., Short, J. M., Mathur, E. J., Detter, J. C., Bork, P., Hugenholtz, P. & Rubin, E. M. 2005. Comparative metagenomics of microbial communities. *Science,* 308**,** 554-557.

Trivedi, O. A., Arora, P., Sridharan, V., Tickoo, R., Mohanty, D. & Gokhale, R. S. 2004. Enzymic activation and transfer of fatty acids as acyl-adenylates in mycobacteria. *Nature,* 428**,** 441-445.

Ueoka, R., Uria, A. R., Reiter, S., Mori, T., Karbaum, P., Peters, E. E., Helfrich, E. J., Morinaka, B. I., Gugger, M., Takeyama, H., Matsunaga, S. & Piel, J. 2015. Metabolic and evolutionary origin of actin-binding polyketides from diverse organisms. *Nature chemical biology,* 11**,** 705-712.

Väänänen, H., Karhukorpi, E., Sundquist, K., Wallmark, B., Roininen, I., Hentunen, T., Tuukkanen, J. & Lakkakorpi, P. 1990. Evidence for the presence of a proton pump of the vacuolar H (+)-ATPase type in the ruffled borders of osteoclasts. *The Journal of cell biology,* 111**,** 1305-1311.

Väänänen, H. K. & Laitala-Leinonen, T. 2008. Osteoclast lineage and function. *Archives of biochemistry and biophysics,* 473**,** 132-138.

Vääräniemi, J., Halleen, J. M., Kaarlonen, K., Ylipahkala, H., Alatalo, S. L., Andersson, G., Kaija, H., Vihko, P. & Väänänen, H. K. 2004. Intracellular machinery for matrix degradation in bone-resorbing osteoclasts. *Journal of bone and mineral research,* 19**,** 1432-1440.

Vaccari, T., Duchi, S., Cortese, K., Tacchetti, C. & Bilder, D. 2010. The vacuolar ATPase is required for physiological as well as pathological activation of the Notch receptor. *Development,* 137**,** 1825-1832.

Vacelet, J. & Donadey, C. 1977. Electron microscope study of the association between some sponges and bacteria. *Journal of experimental marine biology and ecology,* 30**,** 301-314.

Van Deurs, B., Holm, P. & Sandvig, K. 1996. Inhibition of the vacuolar H (+)-ATPase with bafilomycin reduces delivery of internalized molecules from mature multivesicular endosomes to lysosomes in HEp-2 cells. *European journal of cell biology,* 69**,** 343-350.

Van Staa, T., Dennison, E., Leufkens, H. & Cooper, C. 2001. Epidemiology of fractures in England and Wales. *Bone,* 29**,** 517-522.

Van Wesenbeeck, L., Odgren, P. R., Coxon, F. P., Frattini, A., Moens, P., Perdu, B., Mackay, C. A., Van Hul, E., Timmermans, J. P., Vanhoenacker, F., Jacobs, R., Peruzzi, B., Teti, A., Helfrich, M. H., Rogers, M. J., Villa, A. & Van Hul, W. 2007. Involvement of PLEKHM1 in osteoclastic vesicular transport and osteopetrosis in incisors absent rats and humans. *The Journal of clinical investigation,* 117**,** 919-930.

Vegesna, G. K., Janjanam, J., Bi, J., Luo, F.T., Zhang, J., Olds, C., Tiwari, A. & Liu, H. 2014. pH-activatable near-infrared fluorescent probes for detection of lysosomal pH inside living cells. *Journal of Materials Chemistry B,* 2**,** 4500-4508.

Venter, J. C., Remington, K., Heidelberg, J. F., Halpern, A. L., Rusch, D., Eisen, J. A., Wu, D., Paulsen, I., Nelson, K. E., Nelson, W., Fouts, D. E., Levy, S., Knap, A. H., Lomas, M. W., Nealson, K., White, O., Peterson, J., Hoffman, J., Parsons, R., Baden-Tillson, H., Pfannkoch, C., Rogers, Y.H. & Smith, H. O. 2004. Environmental genome shotgun sequencing of the Sargasso Sea. *Science,* 304**,** 66-74.

Vidarsson, H., Westergren, R., Heglind, M., Blomqvist, S. R., Breton, S. & Enerback, S. 2009. The forkhead transcription factor Foxi1 is a master regulator of vacuolar H+-ATPase proton pump subunits in the inner ear, kidney and epididymis. *Public library of science one,* 4**,** e4471-e4471.

Visentin, L., Dodds, R. A., Valente, M., Misiano, P., Bradbeer, J. N., Oneta, S., Liang, X., Gowen, M. & Farina, C. 2000. A selective inhibitor of the osteoclastic V-H(+)-ATPase prevents bone loss in both thyroparathyroidectomized and ovariectomized rats. *Journal of clinical investigation,* 106**,** 309-318.

Vitavska, O., Wieczorek, H. & Merzendorfer, H. 2003. A novel role for subunit C in mediating binding of the H+-V-ATPase to the actin cytoskeleton. *Journal of biological chemistry,* 278**,** 18499-18505.

Von Schwarzenberg, K., Wiedmann, R. M., Oak, P., Schulz, S., Zischka, H., Wanner, G., Efferth, T., Trauner, D. & Vollmar, A. M. 2013. Mode of cell death induction by pharmacological vacuolar H+-ATPase (V-ATPase) inhibition. *The Journal of biological chemistry,* 288**,** 1385-1396.

Voronov, I., Ochotny, N., Jaumouille, V., Owen, C., Manolson, M. F. & Aubin, J. E. 2013. The R740S mutation in the V-ATPase a3 subunit increases lysosomal pH, impairs NFATc1 translocation, and decreases *in vitro* osteoclastogenesis. *Journal of bone and mineral research,* 28**,** 108-118.

Walker, E. C., Mcgregor, N. E., Poulton, I. J., Pompolo, S., Allan, E. H., Quinn, J. M. W., Gillespie, M. T., Martin, T. J. & Sims, N. A. 2008. Cardiotrophin-1 is an osteoclast-derived stimulus of bone formation required for normal bone remodeling. *Journal of bone and mineral research,* 23**,** 2025-2032.

Walsh, C. T. & Fischbach, M. A. 2010. Natural products version 2.0: Connecting genes to molecules. *Journal of the American chemical society,* 132**,** 2469-2493.

Wang, G.Y.S., Graziani, E., Waters, B., Pan, W., Li, X., Mcdermott, J., Meurer, G., Saxena, G., Andersen, R. J. & Davies, J. 2000. Novel natural products from soil DNA libraries in a *Streptomycete* host. *Organic letters,* 2**,** 2401-2404.

Wang, K., Niu, J., Kim, H. & Kolattukudy, P. E. 2011. Osteoclast precursor differentiation by MCPIP via oxidative stress, endoplasmic reticulum stress, and autophagy. *Journal of molecular cell biology,* 3**,** 360-368.

Wang, Z. Q., Ovitt, C., Grigoriadis, A. E., Mohle-Steinlein, U., Ruther, U. & Wagner, E. F. 1992. Bone and haematopoietic defects in mice lacking *c-fos. Nature,* 360**,** 741-745.

Wassmer, T., Kissmehl, R., Cohen, J. & Plattner, H. 2006. Seventeen a-subunit isoforms of paramecium V-ATPase provide high specialization in localization and function. *Molecular biology of the cell,* 17**,** 917-930.

Watanabe, C. M., Wilson, D., Linz, J. E. & Townsend, C. A. 1996. Demonstration of the catalytic roles and evidence for the physical association of type I fatty acid synthases and a polyketide synthase in the biosynthesis of aflatoxin B1. *Chemistry & biology,* 3**,** 463-469.

Weber, T., Rausch, C., Lopez, P., Hoof, I., Gaykova, V., Huson, D. H. & Wohlleben, W. 2009. Clusean: A computer-based framework for the automated analysis of bacterial secondary metabolite biosynthetic gene clusters. *Journal of biotechnology,* 140**,** 13-17.

Webster, N. & Hill, R. 2001. The culturable microbial community of the great barrier reef sponge *Rhopaloeides odorabile* is dominated by an α-Proteobacterium. *Marine biology,* 138**,** 843-851.

Webster, N. S., Taylor, M. W., Behnam, F., Lücker, S., Rattei, T., Whalan, S., Horn, M. & Wagner, M. 2010. Deep sequencing reveals exceptional diversity and modes of transmission for bacterial sponge symbionts. *Environmental microbiology,* 12**,** 2070-2082.

Weichhart, T. 2012. Mammalian target of rapamycin: A signaling kinase for every aspect of cellular life. *In:* Weichart, T. (ed.) *mTOR.* Humana Press.

Weilbaecher, K. N., Motyckova, G., Huber, W. E., Takemoto, C. M., Hemesath, T. J., Xu, Y., Hershey, C. L., Dowland, N. R., Wells, A. G. & Fisher, D. E. 2001. Linkage of M-CSF signaling to Mitf, TFE3, and the osteoclast defect in Mitf mi/mi mice. *Molecular cell,* 8**,** 749-758.

Weissman, K. J. & Leadlay, P. F. 2005. Combinatorial biosynthesis of reduced polyketides. *Nature reviews microbiology,* 3**,** 925-936.

Weissman, K. J. & Müller, R. 2008. Protein–protein interactions in multienzyme megasynthetases. *ChemBioChem,* 9**,** 826-848.

Wenzel, S. C. & Muller, R. 2005. Recent developments towards the heterologous expression of complex bacterial natural product biosynthetic pathways. *Current opinion in biotechnology,* 16**,** 594-606.

Werner, G., Hagenmaier, H., Drautz, H., Baumgartner, A. & Zahner, H. 1984. Bafilomycins, a new group of macrolide antibiotics. Production, isolation, chemical structure and biological activity. *The Journal of antibiotics,* 37**,** 110-117.

White, J. R., Patel, J., Ottesen, A., Arce, G., Blackwelder, P. & Lopez, J. V. 2012. Pyrosequencing of bacterial symbionts within *Axinella corrugata* sponges: Diversity and seasonal variability. *Public library of science one,* 7**,** e38204.

Wiktor-Jedrzejczak, W., Bartocci, A., Ferrante, A. W., Jr., Ahmed-Ansari, A., Sell, K. W., Pollard, J. W. & Stanley, E. R. 1990. Total absence of colony-stimulating factor 1 in the macrophage-deficient osteopetrotic (*op/op*) mouse. *Proceedings of the national academy of sciences of the United States of America,* 87**,** 4828-4832.

Wilkens, S. & Forgac, M. 2001. Three-dimensional structure of the vacuolar ATPase proton channel by electron microscopy. *Journal of biological chemistry,* 276**,** 44064-44068.

Wilkinson, C. R., Garrone, R. & Vacelet, J. 1984. Marine sponges discriminate between food bacteria and bacterial symbionts: Electron microscope radioautography and *in situ* evidence. *Proceedings of the royal society of London. Series B, biological sciences,* 220**,** 519-528.

Williams, G. J. 2013. Engineering polyketide synthases and nonribosomal peptide synthetases. *Current opinion in structural biology,* 23**,** 603-612.

Wilson, M. C., Mori, T., Ruckert, C., Uria, A. R., Helf, M. J., Takada, K., Gernert, C., Steffens, U. A., Heycke, N., Schmitt, S., Rinke, C., Helfrich, E. J., Brachmann, A. O., Gurgui, C., Wakimoto, T., Kracht, M., Crusemann, M., Hentschel, U.,

Abe, I., Matsunaga, S., Kalinowski, J., Takeyama, H. & Piel, J. 2014. An environmental bacterial taxon with a large and distinct metabolic repertoire. *Nature,* 506**,** 58-62.

Witkowski, A., Ghosal, A., Joshi, A. K., Witkowska, H. E., Asturias, F. J. & Smith, S. 2004. Head-to-head coiled arrangement of the subunits of the animal fatty acid synthase. *Chemistry & biology,* 11**,** 1667-1676.

Woerly, E. M., Roy, J. & Burke, M. D. 2014. Synthesis of most polyene natural product motifs using just 12 building blocks and one coupling reaction. *Nature chemistry,* 6**,** 484-491.

Woodhouse, J. N., Fan, L., Brown, M. V., Thomas, T. & Neilan, B. A. 2013. Deep sequencing of non-ribosomal peptide synthetases and polyketide synthases from the microbiomes of Australian marine sponges. *The ISME journal,* 7**,** 1842-1851.

Wu, H., Xu, G. & Li, Y. P. 2009a. Atp6v0d2 is an essential component of the osteoclast-specific proton pump that mediates extracellular acidification in bone resorption. *Journal of bone and mineral research,* 24**,** 871-885.

Wu, X., Peters, J., Gonzalez, F., Prasad, H., Rohrer, M. & Gimble, J. 2000. Frequency of stromal lineage colony forming units in bone marrow of peroxisome proliferator-activated receptor-α-null mice. *Bone,* 26**,** 21-26.

Wu, Y. C., Wu, W. K., Li, Y., Yu, L., Li, Z. J., Wong, C. C., Li, H. T., Sung, J. J. & Cho, C. H. 2009b. Inhibition of macroautophagy by bafilomycin A1 lowers proliferation and induces apoptosis in colon cancer cells. *Biochemical and biophysical research communications,* 382**,** 451-456.

Xie, X.S., Padron, D., Liao, X., Wang, J., Roth, M. G. & De Brabander, J. K. 2004. Salicylihalamide A inhibits the V0 sector of the V-ATPase through a mechanism distinct from bafilomycin A1. *Journal of biological chemistry,* 279**,** 19755-19763.

Xu, J., Feng, H. T., Wang, C., Yip, K. H., Pavlos, N., Papadimitriou, J. M., Wood, D. & Zheng, M. H. 2003. Effects of bafilomycin A1: An inhibitor of vacuolar H (+)-ATPases on endocytosis and apoptosis in raw cells and raw cell-derived osteoclasts. *Journal of cellular biochemistry,* 88**,** 1256-1264.

Xu, Y., Parmar, A., Roux, E., Balbis, A., Dumas, V., Chevalier, S. & Posner, B. I. 2012. Epidermal growth factor-induced vacuolar (H+)-ATPase assembly: A role in signaling via MTORC1 activation. *Journal of biological chemistry,* 287**,** 26409-26422.

Yagi, M., Miyamoto, T., Sawatani, Y., Iwamoto, K., Hosogane, N., Fujita, N., Morita, K., Ninomiya, K., Suzuki, T. & Miyamoto, K. 2005. DC-STAMP is essential for cell–cell fusion in osteoclasts and foreign body giant cells. *The Journal of experimental medicine,* 202**,** 345-351.

Yamamoto, A., Tagawa, Y., Yoshimori, T., Moriyama, Y., Masaki, R. & Tashiro, Y. 1998. Bafilomycin A1 prevents maturation of autophagic vacuoles by inhibiting fusion between autophagosomes and lysosomes in rat hepatoma cell line, H-4-II-E cells. *Cell structure and function,* 23**,** 33-42.

Yan, Y., Denef, N. & Schupbach, T. 2009. The vacuolar proton pump, V-ATPase, is required for Notch signaling and endosomal trafficking in drosophila. *Developmental cell,* 17**,** 387-402.

Yang, D. Q., Feng, S., Chen, W., Zhao, H., Paulson, C. & Li, Y. P. 2012. V-ATPase subunit ATP6AP1 (Ac45) regulates osteoclast differentiation, extracellular acidification, lysosomal trafficking, and protease exocytosis in osteoclast-mediated bone resorption. *Journal of bone and mineral research,* 27**,** 1695-1707.

Yang, X., Matsuda, K., Bialek, P., Jacquot, S., Masuoka, H. C., Schinke, T., Li, L., Brancorsini, S., Sassone-Corsi, P. & Townes, T. M. 2004. ATF4 is a substrate of RSK2 and an essential regulator of osteoblast biology: Implication for coffin-lowry syndrome. *Cell,* 117**,** 387-398.

Yasuda, H., Shima, N., Nakagawa, N., Yamaguchi, K., Kinosaki, M., Mochizuki, S.-I., Tomoyasu, A., Yano, K., Goto, M. & Murakami, A. 1998. Osteoclast differentiation factor is a ligand for osteoprotegerin/osteoclastogenesis-inhibitory factor and is identical to TRANCE/RANKL. *Proceedings of the national academy of sciences of the United States of America,* 95**,** 3597-3602.

Yoshida, H., Hayashi, S., Kunisada, T., Ogawa, M., Nishikawa, S., Okamura, H., Sudo, T., Shultz, L. D. & Nishikawa, S. 1990. The murine mutation osteopetrosis is in the coding region of the macrophage colony stimulating factor gene. *Nature,* 345**,** 442-444.

Yu, M. J., Zheng, W. & Seletsky, B. M. 2013. From micrograms to grams: Scale-up synthesis of eribulin mesylate. *Natural product reports,* 30**,** 1158-1164.

Yuan, F. L., Li, X., Lu, W. G., Li, C. W., Li, J. P. & Wang, Y. 2010. The vacuolar ATPase in bone cells: A potential therapeutic target in osteoporosis. *Molecular biology reports,* 37**,** 3561-3566.

Zaidi, M. 2007. Skeletal remodeling in health and disease. *Nature medicine,* 13**,** 791-801.

Zaidi, M., Inzerillo, A., Moonga, B., Bevis, P. & Huang, C.H. 2002. Forty years of calcitonin—where are we now? A tribute to the work of Iain MacIntyre, FRS. *Bone,* 30**,** 655-663.

Zerbino, D. R. & Birney, E. 2008. Velvet: Algorithms for *de novo* short read assembly using de bruijn graphs. *Genome Research,* 18**,** 821-829.

Zhang, C. 2010. Review transcriptional regulation of bone formation by the osteoblast-specific transcription factor Osx. *Journal of orthopaedic surgery and research, 5, 37*

Zhang, W., Li, Z., Miao, X. & Zhang, F. 2009. The screening of antimicrobial bacteria with diverse novel nonribosomal peptide synthetase (NRPS) genes from South China sea sponges. *Marine biotechnology,* 11**,** 346-355.

Zhao, C., Irie, N., Takada, Y., Shimoda, K., Miyamoto, T., Nishiwaki, T., Suda, T. & Matsuo, K. 2006. Bidirectional ephrinB2-EphB4 signaling controls bone homeostasis. *Cell metabolism,* 4**,** 111-121.

Zhao, H., Laitala-Leinonen, T., Parikka, V. & Väänänen, H. K. 2001. Downregulation of small GTPase Rab7 impairs osteoclast polarization and bone resorption. *Journal of biological chemistry,* 276**,** 39295-39302.

Zhao, Y., Chen, G., Zhang, W., Xu, N., Zhu, J.Y., Jia, J., Sun, Z.J., Wang, Y.N. & Zhao, Y.F. 2012. Autophagy regulates hypoxia-induced osteoclastogenesis through the HIF-1α/BNIP3 signaling pathway. *Journal of cellular physiology,* 227**,** 639-648.

Ziegler, A., Weihrauch, D., Hagedorn, M., Towle, D. W. & Bleher, R. 2004. Expression and polarity reversal of V-type H+-ATPase during the mineralization–demineralization cycle in *Porcellio scaber* sternal epithelial cells. *Journal of experimental biology,* 207**,** 1749-1756.

Zoncu, R., Bar-Peled, L., Efeyan, A., Wang, S., Sancak, Y. & Sabatini, D. M. 2011. MTORC1 senses lysosomal amino acids through an inside-out mechanism that requires the vacuolar H(+)-ATPase. *Science,* 334**,** 678-683.

Zuckerkandl, E. & Pauling, L. 1965. Evolutionary divergence and convergence in proteins. *Evolving genes and proteins,* 97**,** 97-166.

Zuo, J., Jiang, J., Chen, S. H., Vergara, S., Gong, Y., Xue, J., Huang, H., Kaku, M. & Holliday, L. S. 2006. Actin binding activity of subunit B of vacuolar H+-ATPase is involved in its targeting to ruffled membranes of osteoclasts. *Journal of bone and mineral research,* 21**,** 714-721.